

The Development of Non-Invasive Exo Muscular Assistive Devices

A thesis submitted to the University of Manchester for the
degree of Master of Philosophy (MPhil)
in the Faculty of Science and Engineering.

2023

Samuel D Edwards

School of Natural Sciences, Department of Materials

I. Contents

I.	Contents	2
II.	List of Tables	4
III.	List of Figures	5
IV.	List of Abbreviations	8
V.	List of Symbols	9
VI.	Abstract	10
VII.	Declaration	11
	Copyright Statement	11
VIII.	Acknowledgements	12
IX.	About the Author	13
1.	Introduction.....	14
1.1.	Applications of Assistive Devices	16
1.2.	Objectives.....	20
1.3.	Project Deliverables	21
2.	Literature Review	22
2.1.	Muscle Basics	22
2.2.	Control of muscles.....	25
2.3.	Neurological signals (neurons).....	27
2.4.	Stopping contraction	29
2.5.	Summation of muscle mechanics	29
2.6.	Artificial Muscles Currently Available	30
2.7.	Critical Analysis of Current Technologies	45
2.8.	Smart Material Properties	53
2.9.	Shape Memory Effect.....	54
2.10.	Smart Textiles/Fibres	58
2.11.	Passive smart textiles	58
2.12.	Active smart textiles	58
2.13.	Ultra-smart textiles	59
2.14.	Functions of Smart Textiles.....	59
2.15.	E-Fabrics	61
2.16.	Heat-storing fabrics	62
2.17.	Monofilaments	64
2.18.	Graphene Textiles	64
2.19.	Thermoelectric materials	65
2.20.	Seebeck Effect	66
2.21.	Critical Analysis	68
3.	Methodology	71
3.1.	Design Brief.....	71
3.2.	Biological Muscle and Skeletal structure	75

3.3.	Sensing Systems.....	81
3.4.	Development Test 1 - Heart Rate and Blood Oxygen Level monitoring	84
3.5.	Development Test 2 – Radiative (Wireless) Power Generation	88
3.6.	Development Test 3 – Accelerometer Motion Sensing.....	95
4.	Results and Discussions	113
4.1.	Test 1 - Heart Rate and Blood Oxygen Level Monitoring discussions.....	113
4.2.	Test 2 - Radiative (Wireless) Power Supply Results and discussions.....	119
4.3.	Test 3 – Motion Sensing Results and Discussions	126
5.	Conclusion.....	136
5.1.	Suggested Future Works	141
6.	References	142
7.	Appendix A	157
8.	Appendix B	162
9.	Appendix C.....	163

Total thesis word count is 38,329.

II. List of Tables

Table 1-1. Objective 1	20
Table 1-2. Objective 2	20
Table 2-1. Fluidic Muscle Data - Festo (2019).....	32
Table 2-2. VAMP Combination Table - Shuguang, et al (2017)	41
Table 2-3. Festo Fluidic Muscle DMSP Model Data Table – Festo Germany (2019).....	49
Table 3-1. Bending Moments Formula Table.....	77
Table 3-2. Bending Moments Results Table	78
Table 3-3. Sensing System GROW Model	81
Table 3-4. Exercise Operation Table	86
Table 3-5. Power Requirement Table	88
Table 3-6. Test Variant Table.....	90
Table 3-7. Hardware Description Table	97
Table 3-8. Voltage Offset Value	105
Table 3-9. Motion Test Variations	112
Table 4-1. Raw Data Table 1	118
Table 4-2. Radiative Power Supply Initial Testing data	121
Table 4-3. Radiative Power Supply Repeat 1 Testing data	121
Table 4-4. Radiative Power Supply Repeat 2 Testing data	121
Table 4-5. Radiance Testing Error Treatment Table	122
Table 4-6. Accelerometer Testing Error Treatment Table	130

III. List of Figures

Figure 1-1. Atlas Robot by Boston Dynamic USA (2022)	14
Figure 1-2. ASIMO Robot by American Honda Motor Co, INC (2022)	14
Figure 1-3. Hacksmith Industries Power Loader Testing. (Paleja 2021)	15
Figure 1-4 Number of trips per person per year, by main mode and disability status, The Department for Transport (2021)	16
Figure 1-5 (A) four-wheel walker, (B) non wheeled Zimmer frame, (C) walking stick, (D) Crutch, (E) Wheelchair, (F) motorised scooter. Provided by Jung and Ludden (2019)	17
Figure 1-6 ReWalk 6.0 assistive exoskeleton provided by Rewalk.com (2022)	18
Figure 2-1. Muscular Structures provided by ib.bioninja.au (2022)	23
Figure 2-2. Filament muscle theory diagram provided by Krans (2012)	23
Figure 2-3. Z band illustration provided by Krans (2012).....	24
Figure 2-4. Nervous system Diagram – Meenakshi and Gershon (2016)	26
Figure 2-5. Confocal microscopy image of a Neuron - Woodruff (2019)	27
Figure 2-6. Photoreceptor Diagram - thebrain.mcgill.ca. (2022).....	27
Figure 2-7. Neuron Diagram - Huang et al (2018)	28
Figure 2-8. Festo Fluidic Muscle - Festo Germany (2019)	30
Figure 2-9. Conveyor Application diagram - Festo Germany (2019)	31
Figure 2-10. Clamping Applications Diagram - Festo Germany (2019).....	31
Figure 2-11. Robo Thespian - www.engineeredarts.co.uk. (2022).....	31
Figure 2-12. Force Profile and Operating Range Graphic - Festo Germany (2019)	32
Figure 2-13. Linear Line graph of Muscle Contraction.....	33
Figure 2-14. Cucumber Tendrils - davidrhodes124. (2018).....	34
Figure 2-15. Strain Programmable Fibres – Chandler (2019)	34
Figure 2-16. Thermal Coiling Test Diagram – Kanik et al (2019)	35
Figure 2-17. Vertical Displacement Graph - Kanik et al (2019)	36
Figure 2-18. Generated Force vs Temperature Graph - Kanik et al (2019)	36
Figure 2-19. Programmable Fibre Bicep Actuation Test (on) – Chandler (2019)	37
Figure 2-20. Programmable Fibre Bicep Actuation Test (off) – Chandler (2019)	37
Figure 2-21. Fluid Driven Origami Muscle (FOAM) – Mandal (2017)	38
Figure 2-22. Miura-ori Fold - Magleby et al (2013)	38
Figure 2-23. (A) artificial muscle technology, (B) planetary explorers, (C) collapsible telescope glass lens, (D) foldable ballistic shield, (E) deep sea grabber. (Gent, 2018).....	39
Figure 2-24. Principle of VAMP operation - Shuguang et al (2017).....	40
Figure 2-25. Experimental Test for Zig Zag Actuator - Shuguang, et al (2017).....	41
Figure 2-26. Knitted Electronic Actuator - Puiu (2017)	43
Figure 2-27. Knitted and Weaved Structures – Edwin et al (2017).....	43
Figure 2-28. Fabric Structure - Edwin et al (2017).....	44
Figure 2-29. Spot the Dog - Boston Dynamics USA (2022)	47
Figure 2-30. Measure Isometric Force Graph - Edwin et al (2017)	50
Figure 2-31. Isotonic Strain Graph - Edwin et al (2017)	51
Figure 2-32. Smart Material Principles. Provided by Zhang (2019).....	53
Figure 2-33. Hydrogel Manufacturing Process. Chao (2017)	56
Figure 2-34. Photo responsive Categories. Zhaodi et al (2022)	56
Figure 2-35. Magnetic Filler Types. Thevenot et al (2013)	57
Figure 2-36. Smart Textiles Catagories. Celikel (2020)	58
Figure 2-37. Smart Textile Categories. Celikel (2020).....	59
Figure 2-38. E-textile Definitions. Maxey (2019).....	61
Figure 2-39. Schematic of Dual Mode Textile. Po-Chun et al (2017)	62
Figure 2-40. Artificial Skin Temperature Graph. Po-Chun et al (2017).....	63
Figure 2-41. WEST Monofilaments Test Strip. performancehealth.co.uk (2022)	64
Figure 2-42. Fabric TEG. Lund (2020)	65
Figure 2-43. Thermal Conversion Generator Diagram. Sault (2018)	66
Figure 2-44. PN Junction Diagram. James (2020)	67
Figure 2-45. Time/Cost/Scope Quality Triangle. Jacob, U & Ksenia, M. (2023)	69

Figure 3-1. Project Design Requirements Graphic	72
Figure 3-2. Project Mind Map	73
Figure 3-3. Schematic Bicep Curl Analysis	75
Figure 3-4. Bicep Operation Graphic	76
Figure 3-5. Tower Crane Schematic. Zeleny (2011)	76
Figure 3-6. Suspension Bridge Graphic. Fairclough, et al (2018)	76
Figure 3-7. Tendon Schematic. Jackson et al (2019)	76
Figure 3-8. Cantilever Beam Free Body Diagram. Mechanicalc (2022)	77
Figure 3-9. Bicep Free Body Diagram	78
Figure 3-10. Point R1 Bending Moment Force Map	79
Figure 3-11. Point R2 Bending Moment Force	79
Figure 3-12. Point R3 Bending Moment Force	79
Figure 3-13. Point R4 Bending Moment Force	79
Figure 3-14. Recommended age/maximum heart rate. American Heart Association (2021)	84
Figure 3-15. Oxyhaemoglobin and heart rate during exercise. Hüseyin et al (2018)	84
Figure 3-16. Contec CMS50D pulse oximeter	85
Figure 3-17. Testing Procedure Data Capture Sheet	85
Figure 3-18. Bicep Curl. Yeung (2022)	86
Figure 3-19. Hammer Curl. Yeung (2022)	86
Figure 3-20. Seated Preacher Curl (Barbell). Yeung (2022)	87
Figure 3-21. TEG Peltier Module. theplantbot.com (2019)	88
Figure 3-22. Body Heat Hot Spots. Lee (2019)	89
Figure 3-23. Fitted TEGs	90
Figure 3-24. TEG Series Wiring Schematic	91
Figure 3-25. TEG Parallel Wiring Schematic	91
Figure 3-26. Room Temperature Monitoring Unit	92
Figure 3-27. Granite Blocks Fixed in Place	92
Figure 3-28. Arm Position During Testing	94
Figure 3-29. Basic Motion Monitoring Schematic	95
Figure 3-30. Motion Monitoring Process Flow	96
Figure 3-31. Bicep Actuation Direction of Movement. Campbell (2022)	97
Figure 3-32. Accelerometer Graphic. Papoutsidakis (2016)	97
Figure 3-33. Raspberry Pi Graphic. Raspberrypi.org (2022)	97
Figure 3-34. Linear Actuator Graphic. Firgelli Automations Team (2020)	97
Figure 3-35. Bicep Actuation Direction of Movement. Campbell (2022)	98
Figure 3-36. Raspberry Pi Voice Module Graphic. Mahesh (2016)	98
Figure 3-37. Fall Detection. Wernhaur, Chia-Hwei and Hsin-Hun (2011)	98
Figure 3-38. Assistive Standing Device Schematic. Noritsugu et al (2007)	99
Figure 3-39. Robotic Arm. Jobbágy et al (2014)	100
Figure 3-40. Prototype Circuit Design	101
Figure 3-41. Capacitance Accelerometer. Venkatanarayanan and Spain (2014)	101
Figure 3-42. triaxial piezoelectric accelerometer. Montalvao (2015)	101
Figure 3-43. G Force to Gravity Line Graph. Analog Devices (2022)	102
Figure 3-44. ADXL335-BB Accelerometer	102
Figure 3-45. EasyLog EL-USB-3 Voltage Data Logger	103
Figure 3-46. Motion Sensing Prototype	104
Figure 3-47. Accelerometer Place in Equilibrium State	105
Figure 3-48. EasyLog Home Page	106
Figure 3-49. EasyLog Set up Page 1	107
Figure 3-50. EasyLog Set up Page 2	107
Figure 3-51. EasyLog Set up Page 3	108
Figure 3-52. EasyLog Set up Page 4	108
Figure 3-53. Hammer Curl. Stuart (2019)	109
Figure 3-54. Accelerometer Position Schematic	109
Figure 3-55. Wrist Mounted Accelerometer in position 3A	110
Figure 3-56. Arm in Default Position	110

Figure 3-57. Arm in Final Position.....	111
Figure 3-58 Arm in Simulated Struggle Point Position.....	111
Figure 4-1. Oxyhaemoglobin Standard Normal Distribution Graph	113
Figure 4-2. Exercise 1 – Recorded Heart Rate Graph.....	114
Figure 4-3. Exercise 2 – Recorded Heart Rate Graph.....	114
Figure 4-4. Exercise 3 – Recorded Heart Rate Graph.....	115
Figure 4-5. Exercise 4 – Recorded Heart Rate Graph.....	115
Figure 4-6. Exercise 5 – Recorded Heart Rate Graph.....	116
Figure 4-7. Exercise 6 – Recorded Heart Rate Graph.....	116
Figure 4-8. Exercise 7 – Recorded Heart Rate Graph.....	117
Figure 4-9. Measure Heart rate and SP02 level before activity	118
Figure 4-10. Measure Heart rate and SP02 level after activity	118
Figure 4-11. Results Graph Test 1 – Single TEG (No Granite Block)	122
Figure 4-12. Results Graph Test 2 – Three TEG’s, Series Wiring Method (No Granite Block).....	123
Figure 4-13. Results Graph Test 3 – Three TEG’s, Parallel Wiring Method (No Granite Block)....	123
Figure 4-14. Results Graph Test 4 – Single TEG, with Granite Block	124
Figure 4-15. Results Graph Test 5 – Three TEG’s, Series Wiring Method, with Granite Block	124
Figure 4-16. Results Graph Test 6 – Three TEG’s, Parallel Wiring Method, with Granite Block ...	125
Figure 4-17. Image Illustrating the Desired Graphical Shape.....	127
Figure 4-18. Processed Results of Accelerometer Testing	127
Figure 4-19 Accelerometer Position Schemati.....	129
Figure 4-20. Test MT-00-Y (Position 1A)	130
Figure 4-21. Test MT-01-Y (Position 1B)	131
Figure 4-22. Test MT-02-Y (Position 1C).....	131
Figure 4-23. Test MT-04-Y (Position 2A)	132
Figure 4-24. Test MT-05-Y (Position 2B)	132
Figure 4-25. Test MT-06-Y (Position 2C).....	133
Figure 4-26. Test MT-07-Y (Position 2D).....	133
Figure 4-27. Test MT-08-Y (Position 3A)	134
Figure 4-28. Test MT-09-Y (Position 3B)	134
Figure 4-29. Test MT-10-Y (Position 3C).....	135
Figure 4-30. Test MT-11-Y (Position 3D).....	135
Appendix A Figure 7-1. Hand Calculations for Bending Moments and Inertia	157
Appendix A Figure 7-2. Hand Calculations for Deflection at Points R1 and R2	158
Appendix A Figure 7-3. Hand Calculations for Deflection at points R3 and R4.....	159
Appendix A Figure 7-4. Deflection Calculation at R1 checked via Omnicalculator.com	160
Appendix A Figure 7-5. Deflection Calculation at R2 checked via Omnicalculator.com	160
Appendix A Figure 7-6. Deflection Calculation at R3 checked via Omnicalculator.com.	161
Appendix A Figure 7-7. Deflection Calculation at R4 checked via Omnicalculator.com	161
Appendix B Figure 8-1. Blood Oxygen Test Data Capture Sheet (Page 1).....	162
Appendix B Figure 8-2. Blood Oxygen Test Data Capture Sheet (Page 2).....	162
Appendix C Figure 9-1. ADXL335-BB Data Sheet Page 1	163
Appendix C Figure 9-2. ADXL335-BB Data Sheet Page 2	164
Appendix C Figure 9-3. ADXL335-BB Data Sheet Page 3	165
Appendix C Figure 9-4. ADXL335-BB Data Sheet Page 4	166
Appendix C Figure 9-5. ADXL335-BB Data Sheet Page 5	167
Appendix C Figure 9-6. ADXL335-BB Data Sheet Page 6	168
Appendix C Figure 9-7. ADXL335-BB Data Sheet Page 7	169
Appendix C Figure 9-8. ADXL335-BB Data Sheet Page 8	170
Appendix C Figure 9-9. ADXL335-BB Data Sheet Page 9	171
Appendix C Figure 9-10. ADXL335-BB Data Sheet Page 10.....	172
Appendix C Figure 9-11. ADXL335-BB Data Sheet Page 11	173
Appendix C Figure 9-12. ADXL335-BB Data Sheet Page 12.....	174
Appendix C Figure 9-13. ADXL335-BB Data Sheet Page 13.....	175
Appendix C Figure 9-14. ADXL335-BB Data Sheet Page 14.....	176

IV. List of Abbreviations

Abbreviation	Description
AC	Alternating Current
ALS	Amyotrophic Lateral Sclerosis
ANS	Autonomic Nervous System
BL	Bottom Left
BM	Bottom Middle
BPM	Beats Per Minute
BR	Bottom Right
CAD	Computer Aided Design
CNS	Central Nervous System
CP	Cerebral Palsy
DARPA	The Defense Advanced Research Projects AgencyThe Department of Defense
DC	Direct Current
FOAM	Fluid Operated Artificial Muscle
FWR	Force to Weight Ratio
GROW	Goal, Reality, Options, Will
LMN	Lower Motor Neuron
MIT	Massachusetts Institute of Technology
MND	Motor Neurone Disease
PCB	Printed Circuit Board
PE	Polyethylene
PEDOT	Poly Polystyrene Sulfonate
PHD	Doctor of Philosophy
PLC	Programmable Logic Controller
PMMA	Polymethyl Methacrylate
PNS	Peripheral Nervous System
PVA	Polyvinyl Acetate
PVC	Polyvinyl Chloride
QTY	Quantity
RAM	Random Access Memory
SF	Science Fiction
SKEM	Skeletal Materials
SKIM	Skin Materials
SMART	Specific, Measurable, Attainable, Relevant, Time
SNS	Somatic Nervous System
TEG	Thermoelectric Generator
TL	Top Left
TM	Top Middle
TPU	Thermoplastic Polyurethane
TR	Top Right
UK	United Kingdom
UMN	Upper Motor Neurons
USA	United States of America
US	United States
VAMP	Vacuum Actuated Muscle Pneumatic
VAT	Value Added Tax

V. List of Symbols

Symbol	Description	Unit
θ	Angle	Degrees ($^{\circ}$)
W	Applied Load	Newtons (N)
M	Bending Moment	Newton meters (N/M)
L_x	Contraction Length = % of Maximum Length	Percentage (%)
£	Currency	GBP
A	Current	Ampere
δ	Deflection	Millimetres (mm)
D	Diameter	Meters (m)
F	Force	Newtons (N)
N/g	Force to Weight Ratio	Newtons per gram
L	Length	Meters (m)
g	Mass	Grams
L_5	Maximum Length	Millimetres (mm)
L_1	Minimum Length	Millimetres (mm)
μ	Normal Distribution	N/A
τ	Radial Torque	Newton meters (N/M)
r	Radius	Millimetres (mm)
Ω	Resistance	Ohms
I_{NA}	Second Moment of Area (inertia)	Millimetres Biquadrate
$[\]l[\]ll$	Specific Resistor value	Kiloohms (K Ω)
SD	Standard Deviation	N/A
$^{\circ}\text{C}$	Temperature	Degrees Centigrade ($^{\circ}\text{C}$)
V	Voltage	Volts
E	Youngs Modulus of Elasticity	Giga pascals (GPa)
L_2	25% of Maximum Length	Millimetres (mm)
L_3	50% of Maximum Length	Millimetres (mm)
L_4	75% of Maximum Length	Millimetres (mm)

VI. Abstract

The following thesis provides insight into the undertakings of the research project “The Development of Non-Invasive Exo Muscular Assistive Devices”, investigating the current state of assistive muscular devices and how these can be improved through recent developments in electronics and materials engineering. The thesis incorporates a detailed literature review which provides insight into - and critique of - a multitude of elements such as: biological muscles, current available assistive devices, active and passive smart materials; identifying key areas of improvement in addition to characterising the requirements for such technologies.

Through practical experimentation performed, this research was able to demonstrate two areas of development within the field of artificial assistive devices. The first of which being the ability to integrate a low-cost motion sensing device such as an accelerometer into an artificial muscle. This research offers objective results which inform where the optimum location for an accelerometer monitoring arm movement should be placed. With the results showing a normal voltage distribution of 0.014V with a standard deviation of 0.002V, in addition to the graphical data visually being able to map the movement; including a simulated point of struggle. The second key area of development is with reference to a method of retrieving a renewable electrical signal local to the wearer, in this case human thermal radiance (body heat) converted via a thermoelectric generator. The testing performed illustrated that a 62% increase in output voltage could be achieved by employing an in series wiring methodology. Whilst a further 75% output voltage increase could be achieved by creating a large temperature differential within the thermoelectric generator.

VII. Declaration

No portion of the work referred to in the thesis has been submitted in support of an application for another degree or qualification of this or any other university or other institute of learning.

Copyright Statement

1. The author of this thesis (including any appendices and/or schedules to this thesis) owns certain copyright or related rights in it (the "Copyright") and s/he has given the University of Manchester certain rights to use such Copyright, including for administrative purposes.
2. Copies of this thesis, either in full or in extracts and whether in hard or electronic copy, may be made only in accordance with the Copyright, Designs and Patents Act 1988 (as amended) and regulations issued under it or, where appropriate, in accordance with licensing agreements which the University has from time to time. This page must form part of any such copies made.
3. Copies of this thesis, either in full or in extracts and whether in hard or electronic copy, may be made only in accordance with the Copyright, Designs and Patents Act 1988 (as amended) and regulations issued under it or, where appropriate, in accordance with licensing agreements which the University has from time to time. This page must form part of any such copies made.
4. Further information on the conditions under which disclosure, publication and commercialisation of this thesis, the Copyright and any Intellectual Property and/or Reproductions described in it may take place is available in the University IP Policy (see <http://documents.manchester.ac.uk/DocuInfo.aspx?DocID=24420>), in any relevant Thesis restriction declarations deposited in the University Library, the University Library's regulations (see <http://www.library.manchester.ac.uk/about/regulations/>) and in the University's policy on Presentation of Theses.

VIII. Acknowledgements

I would like to extend my gratitude to the following individuals for their continued and extensive support that they have provided to me for the duration of this project.

- My supervisor Dr Hugh Gong for his support and assistance with developing helping me to further develop my skills with research, in addition to his recognition flexibility due to my work commitments.
- My partner Aleksandra Tambor for her continued patience and support, in addition to lending her advanced skill of English grammar and spelling when checking the work produced.

IX. About the Author

Samuel David Edwards (Sam) is an apprentice-trained, professionally recognised mechanical engineer with over 10 years industrial experience, 3 years research experience and a first-class bachelor's degree in Mechanical Engineering. After leaving secondary school he has progressed rapidly through engineering, performing all educational activities on a part time basis whilst under full time employment within the pharmaceutical engineering industry. His primary focus is to continually fuse together the technical and practical elements of engineering based on his dual experience to provide the most effective outcomes of any task or projects he takes on. Throughout his professional career he has performed a multitude of employed roles such as: applications engineering, project management, manufacturing, onsite installation, onsite commissioning, and design engineering. Thanks to this versatile experience Mr Edwards has been responsible for the development of new products in addition to the creation and implementation of specific new technologies.

The author has been recognised for the research work undertaken for his final year dissertation entitled "Is there a deficit of engineering principle as a result of the UK skills gap?" - Mr Edwards was selected for publication through the FIELDS Journal of Huddersfield Student Research, with his work amassing to date over 700 accesses. Additionally, Mr Edwards is an approved STEM Ambassador that enjoys educating young people on the exciting opportunities within engineering; in this area his key aim is to vastly increase the availability, promotion, and employment of women within engineering with a specific focus on encouraging more women to undertake apprenticeships.

1. Introduction

As early as the 1960's assistive wearable exoskeletal systems have been physically present within engineering and science, with their existence first becoming widely hypothesised in the Lensmen series of science fiction literature produced in 1937 by E.E Smtih, (Sofge, 2010). However, it is commonly accepted that the 1959 novel Starship Troopers by Robert A Heinlein is the medium which popularised the idea of exoskeletal systems, (Sofge, 2010). Although often visualised in science fiction written works, it wasn't until the mid-1960's that an assistive wearable exoskeletal system was developed with commercial intent. It is widely accepted that the General Electric Hardiman manufactured and developed between 1965 and 1971 is the first iteration of transposing the previously hypothesised exoskeletal systems into and physical representation. The product used complex electronics and a bulky hydraulics system to provide the control and strength enhancements. Ultimately, this project was discontinued by General Electric, due to the system being too heavy and bulky to be of any use to the military, (Bellis, 2019). In 1992 Boston Dynamics formally a research program within the Massachusetts Institute of Technology (MIT) was founded by Marc Raiber, the company embarked on extensive research and development of bipedal and quadrupedal robotics with a primary focus on military applications because of major financial investment being provided by The Defense Advanced Research Projects Agency (DARPA). Although, the directional focus of Boston Dynamics is the market of autonomous robotics as opposed to wearable assistive devices, it is important to acknowledge that along with Honda Robotics they have both pioneered the development and direction of robotics. Both physically manufactured robots from Boston Dynamics and Honda respectively, can be seen in figure 1-1 and 1-2.



Figure 1-1. Atlas Robot by Boston Dynamic USA (2022)



Figure 1-2. ASIMO Robot by American Honda Motor Co, INC (2022)

Exoskeletal systems are devices that have long been idealised and popularised within various mediums of science fiction. The visual design of exoskeletal systems previously aimed to incorporate features given in science fiction but are now understood not to necessarily be a practical basis. Furthermore, with the significant advancements of computerised special effects of the past 20 years these visualised systems have become more complex but more importantly they have become more compact. A progressive development which has further increased the gap of what is created for entertainment and what is achievable for real world applications, increasingly demonstrating the limits of viable engineering solutions. Not limited to just these devices, below are some examples of fictionalised systems as follows.

It is abundantly clear that the current achievable level of science and engineering that can be utilised is limiting, and manufacturing any of these systems would pose expensive and complex challenges. Producing any of these systems in a commercially viable manner would also be extremely challenging, this is proven by the fact that both the Boston Dynamics Atlas (figure 1-1) and the Honda ASIMO (figure 1-2) systems are not commercially available; with Boston Dynamics making only one of their quadrupedal system commercially available at a price of \$75,000 as specified by Whitwam in the (2021) article "*Boston Dynamics Atlas Robot Ups Its Parkour Game*". Although, a recent project performed by the media/engineering company Hacksmith Industries succeeded in manufacturing a fully working power loader exoskeletal system. However, whilst this has been made physically possible a significant modification was enforced due to the inability to transpose what was imagined for cinema into a real-world prototype. This modification is the introduction of a Caterpillar track system in replacement of the original visualised bipedal design, this change was implemented due to the associated issues posed by both the transfer of force and the dynamic balance of a bipedal system at such a large scale. Furthermore, as with previously manufactured robotics, this system is also not yet a commercially viable product. Paleja (2021) provides an image of the system being tested as seen in figure 1-4.



Figure 1-3. Hacksmith Industries Power Loader Testing. (Paleja 2021)

1.1. Applications of Assistive Devices

Based on previous discussion focussing on fictitious devices, military applications, and manufactured systems currently not commercially available, understanding a new niche and applicability to the consumer market needs defining. Dr John Little is commonly recognised as the first individual to study cerebral palsy as far back as 1853, (Poinsett, 2020). Additionally, in 1869 neurologist Jean-Martin Charcot first identified another neurological condition affecting the muscles, commonly referred to as Amyotrophic lateral sclerosis (ALS), (ALS.org, 2022). The National Health Service Scotland (2021) informs that 2 in 100,000 people in the UK are affected by motor neurons disease (ALS) each year. Additionally, www.scope.org.uk (2022) also informs that 1 in 400 children within the UK are affected by cerebral palsy. Both these illnesses are irreparable degenerative neurological conditions, with a detrimental impact on the central nervous system which consecutively and severely affects multifidous aspects of an individual's muscular system. The dominant affliction of any illness of this kind is reduced mobility which in most cases slowly declines until the individual is the victim of paraplegia, which in most cases of ALS progresses to full body paralysis. In data published by The Department for Transport (2021) it was revealed that in 2019 aduly individuals with disabilities made around 26% fewer trips that those individuals without disabilities. Additionally, The Department for Transport (2021) have provided a graphical representation (figure 1-4) of the distribution of this data across different transport mediums which demonstrates that walking was the mode of transport with the biggest differential when compared to abled individuals, whilst the mode car passenger held the highest positive differential for disabled individuals.

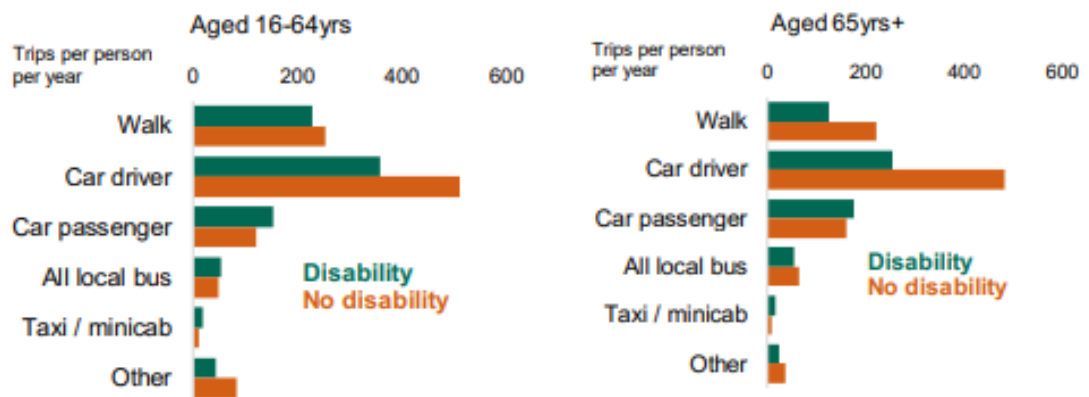


Figure 1-4 Number of trips per person per year, by main mode and disability status, The Department for Transport (2021)

Ailing to a physically impairing disability in the UK is financially detrimental, with it being estimated that a disabled individual can be responsible for up to £583 of additional living expenditure per month, (Scope.org.uk, 2022). When observing commonly available assistive mobility devices Jung and Ludden (2019) provide photographs of six typical devices, as seen in figure 1-8 with www.healthcarepro.co.uk (2022) providing a typical price range of these items as follows:

- Four-wheel walker – Price range £70.82 to £554.14
- Non wheeled Zimmer frame – Price range £16.38 – £107.49
- Walking stick – Price range £7.49 – £89.99
- Crutch (pair) – Price range £11.65 – £63.32
- Non-motorised wheelchair – Price range £126.67 - £3,200
- Motorised wheelchair – Price range £1,990 - £21,999
- Mobility scooter – Price range £600.82 - £2,864.16



Figure 1-5 (A) four-wheel walker, (B) non wheeled Zimmer frame, (C) walking stick, (D) Crutch, (E) Wheelchair, (F) motorised scooter. Provided by Jung and Ludden (2019)

However, recent attempts and developments have led to the introduction of an assistive exoskeletal system by the ReWalk Company, which has focussed its efforts on providing commercially viable assistive device that can be purchase both by an institution or individual. The exoskeletal assistive device for which an image is provided below in figure 1-5 by ReWalk USA (2022), is designed specifically for individuals with spinal cord injuries causing lower movement restrictions and provides the operator with the assistance required to perform a walking motion. Despite the fact this is a commercially available device, it is not an economically accessible device with Canada's Drug and Health Technology Agency (2021) informing that the ReWalk costs around US\$71,600 for personal use and up to US\$85,500 the device to be used by an institution such as a physiotherapy clinic, with additional annual service fees. Additionally, Health Technology Agency (2021) estimates the lifespan of the system to be around 5 years of service.



Figure 1-6 ReWalk 6.0 assistive exoskeleton provided by Rewalk.com (2022)

Observing robotics in its entirety it can be understood that since the first description of exoskeletal systems in 1937 and the creation of the first iteration of an exoskeletal system in 1965, over the last 50 years there has been exponential development in this field of which the velocity of these developments has significantly increased in the last 20 years. However, the development of commercially feasible, easily accessible assistive devices for the consumer market is an element of the robotics industries that appears to have been neglected. the majority of the robotic rehabilitation devices in existence are modifications of and developments of existing fitness equipment (Jobbágy et al, 2014). By further developing robotics and wearable robotic technologies not only can more integrative solutions to individuals daily living be created, but additionally the quantity of individual rehabilitated could be increased. This demonstrates a requirement to research and develop assistive devices from a practical engineered perspective utilising the plethora of developed robotic technologies to understand how these can be commercialised and made accessible to consumers.

When using a keyword search criterion such as: accelerometer muscle, artificial muscles, intelligent muscle sensors and intelligent assistive devices; few practical or commercially viable devices were found. The closest research found to that of the contents within this thesis, is that performed by Baraka, A. et al. (2019), where the use of both an accelerometer and surface electromyography (sEMG) were used to monitor muscular tremors to detect Parkinson's disease. Although similar to this research project in terms of using an accelerometer placed in different position on the forearm, the research performed by Baraka, A. et al. (2019), did not attempt to understand how the accelerometer can be used to monitor the position of the forearm as presented

within this research. Furthermore, no credence was given to understanding how this type of technology can be used in low-cost wearable robotics without devices such as sEMG's which require skin contact.

Another research article rendered from using the aforementioned search criteria is that performed by Peng, L. et al. (2013), where an accelerometer and surface electromyography (sEMG) were used to monitor rotation in the hand and forearm. Similar to the research discussed above, this too used sEMG which are skin contact devices and require a method of being attached to the user's skin. Whilst this research did demonstrate how the rotation of the hand and forearm can be monitored with an accelerometer, this research did not provide much in terms of practical research that can be introduced at commercial engineered level.

From the above a research gap can be identified, where accelerometer technology has been discussed in alternate application; but not strictly applied to the area of wearable robotics. With this knowledge, an argument can be made for the study and research of wearable robotics where the activation methodology is both reliable and non-invasive (or requires no set up from the user i.e., the sensor can be hidden within clothing that is easily applied to the user). Additionally, neither researcher provided any attempt to understand how the electrical signal for the sensor can be acquired in either a wireless or compact manner.

1.2. Objectives

Detailed below are the objectives designed for this research. These objectives are important to the outcome of the research, providing a directional goal to attain allowing the research to remain focused on a specific outcome. Objective 1 has been established to provide a suitable basis on which the outcomes of the research can be supported. The decision to work towards this objective has been developed based on the knowledge of the standard format of which research is performed. Objective 2 has been established to ensure that a practical engineered approach is applied to this thesis. Manufacturing a prototype will not only allow scientific data to be establish, but additionally from an engineering perspective a prototype will aid in understanding the feasibility and practicality of the outcomes of the developed research. Both project deliverables 1 and 2 have been established as a direct outcome of objectives 1 and 2.

Table 1-1. Objective 1

Reference:	Objective 1			
Description:	Identify areas of improvement based on current technologies			
Specific	Measurable	Attainable	Relevant	Time
Provide critical analysis of existing systems in addition to understanding basic muscle mechanics to understand where improvements are required.	By March 2022 this will be complete.	This can be easily achieved, based on the improvements already identified within the introduction.	This research is a fundamental element of this thesis.	March 2022

Table 1-2. Objective 2

Reference:	Objective 2			
Description:	Develop a prototype device with a suitable testing methodology			
Specific	Measurable	Attainable	Relevant	Time
Identify a method of monitoring an individual's struggle point during motion.	Physical testing and data can be attained to support this.	The development of prototype is attainable.	This device will be instrumental in providing scientific data for the thesis.	July 2022

1.3. Project Deliverables

The major deliverables for this thesis are:

- **Deliverable 1:** Prototype – a physical representation of the discussed suggestions will be manufactured. This will either be a full system or specific element identified for further development.
- **Deliverable 2:** Testing – original developed testing will be performed to evaluate the validity of the prototype(s) and establish objective to data to be analysed.
- **Deliverable 3:** Data Analysis – scrutinization of the collated data will be performed with statistical analysis such as a confidence interval being performed.

2. Literature Review

This chapter critically reviews the background and existing work relevant to this study. It covers the scientific and engineering technology currently available within the subject of artificial muscle technology and related ancillary technologies. It helps to identify opportunities for further research relating to artificial muscle technology.

2.1. Muscle Basics

Building an adequate knowledge pool to design artificial muscle technology requires a thorough comprehension of the operational principles of biological muscles. In the most basic form, a muscle is an anatomical actuator that is fixed in place via bonded tendons to the surrounding structure (i.e., skeleton) - these actuators are strategically placed throughout a biological specimen to allow manipulation of the entire structure. For example, Kerkman et al, (2018) indicates that the average human body consists of over 200 skeletal bones and over 300 skeletal muscles which are utilised to manipulate these bones and are termed as “voluntary movement muscles”. However, the research published by Campbell et al (2021) indicates that recent investigations reveal over 400 skeletal muscles. In addition to these skeletal muscles there are also two other categories of muscle types located within the human body; one of them, smooth muscles, are located in various organs and are specified as an involuntary muscle.

Contrary to skeletal muscles, smooth muscle tissues occur on a cellular level and can be understood to be in the billions when it comes to the quantity of them (Seladi-Schulman, 2020). The third and final muscle group is a singular muscle solitarily grouped as the cardiac muscle (the myocardium); this is also classed as an involuntary muscle type. Furthermore, this specific muscle has structure more akin to a skeletal muscle. To enable the cardiovascular system to circulate blood around the body a rapid involuntary contraction and relaxation of the muscle occurs, to enable this to happen involuntarily the cardiovascular muscles have distinct features within their structures (Saxton et al, 2021).

Regardless of classification all muscles can only contract – Oxford Cambridge and RSA (2019) specifies that skeletal muscles are uniaxial and only capable of contracting or relaxing. Therefore, muscles have to work in pairs to move a joint. One muscle will contract and pull a joint one way and another muscle will contract and pull it the other. As mentioned above this contraction can occur either actively or involuntary depending on whether this is a skeletal muscle or a smooth/cardiac muscle. Within the boundaries of the above muscle classifications there are two different types of muscular tissue structures: there are “striated” and “smooth” tissues. Striated muscle tissues which are typically found in skeletal muscles and the myocardium, encompass fibres that have sarcomeres attached to them to create muscular contraction. These types of muscles are constructed from striations which allow each muscle to be consciously controlled. Figure 2-1 illustrates the typical structure of the different muscles.

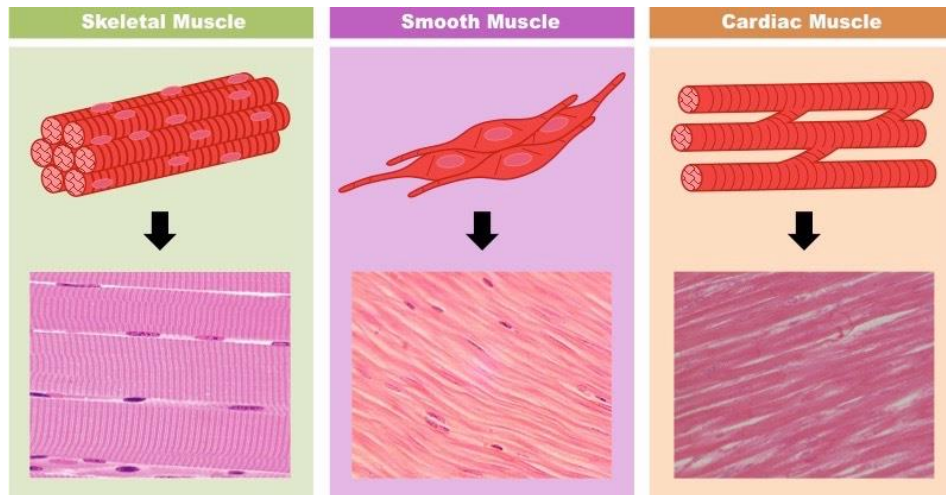


Figure 2-1. Muscular Structures provided by *ib.bioninja.au* (2022)

Smooth muscle tissues are located within the lining of internal organs rather than being attached to the skeletal structure and are stimulated involuntarily; these specific muscles are observed at a cellular level. The nervous system uses the smooth muscles to tightly and accurately regulate the bodies subsystems without thought or conscious input from the individual, all of which are important to sustain life, (Hafen and Burns, 2020). For example, during exercise an individual does not need to consciously consider an increase in blood pressure to accommodate the increasing oxygen demands. The nervous system uses a multitude of receptors such as hormones and neurotransmitters to control the spontaneity of the smooth muscles (Hafen and Burns, 2020). This explanation gives a clear understanding to the defined difference between the application of smooth muscles and skeletal muscles. Huxley and Niedergerke (1954) and Huxley and Hanson (1954) describe muscle contraction as a sliding filament theory. They discovered that within the sarcomeres, the thick myosin filament remains constant with minimal contraction and when the actin filament slides against this, it causes the muscle to contract. This is because the actin is secured to the lateral end of each sarcomere also known as “Z Bands”. This process is visually demonstrated in Figure 2-2.

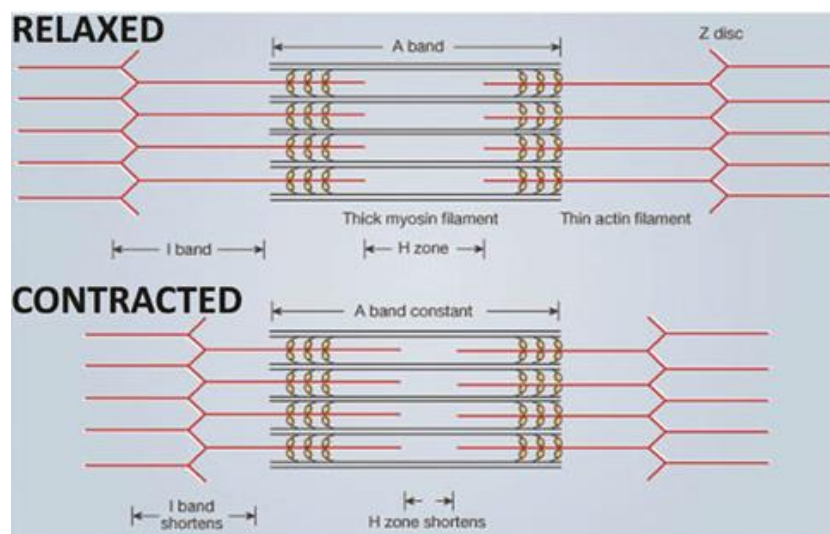


Figure 2-2. Filament muscle theory diagram provided by *Krans* (2012)

Krans (2012) stated an analogy to aid in understanding the mechanics of how this works. This is explained as follows: “Imagine that you are standing between two large bookcases loaded with books. These large bookcases are several meters apart and are positioned on rails so that they can be easily moved. You are given the task of bringing the two bookcases together, but you are limited to using only your arms and two ropes. Standing centred between the bookcases, you pull on the two ropes — one per arm — which are tied securely to each bookcase. In a repetitive fashion, you pull each rope toward you, regrasp it, and then pull again. Eventually, as you progress through the length of rope, the bookcases move together and approach you. In this example, your arms are similar to the myosin molecules, the ropes are the actin filaments, and the bookcases are the z discs to which the actin is secured, which make up the lateral ends of a sarcomere.” Figure 2-3 illustrates this explanation.

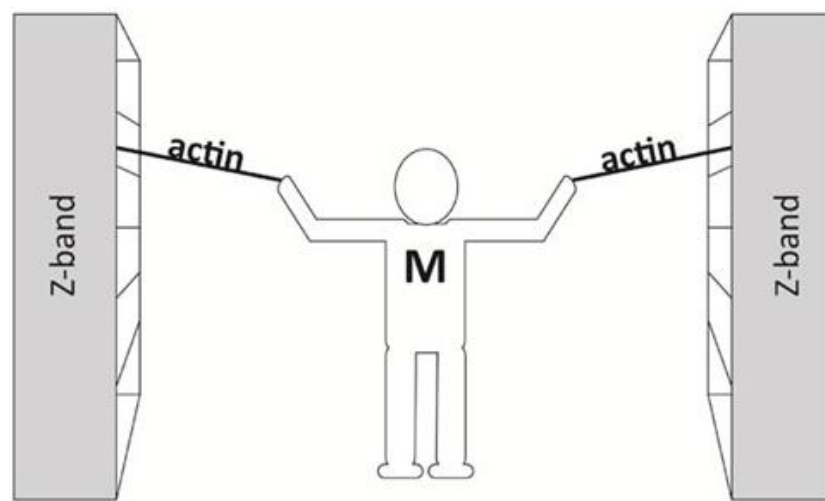


Figure 2-3. Z band illustration provided by Krans (2012)

Generally, there are only two types of muscles which have striated tissue: these are skeletal muscles which are attached to bone via tendons and used for movements - these muscles can be actively actuated by the motor neuron system; and cardiac muscles which aid in the operation of the cardiac muscles such as the heart - these muscles are involuntarily controlled. Smooth muscle tissues are constructed in an alternate way to striated muscles, utilising layered sheet mechanics rather than strands of fibres.

2.2. Control of muscles

Voluntary movements of muscles are controlled via the central nervous system (CNS) and the peripheral nervous systems (PNS) (Brigham Young University, 2022). When a conscious decision to move is made, it's the upper motor neurons (UMN) located in the cerebral cortex, this location in the nervous system is where the initiation, planning, and coordination of movement is calculated and actioned. The cranial nerve nuclei which is an aggregate of cells, or the anterior horn, which is the grey matter within the spinal cord, then allows the upper motor neurons to synapse with the lower motor neurons (LMN). The lower motor neurons then exit the central nervous system before transferring the signal via a chemical synapse to the muscle fibre at the neuromuscular junction. The voluntary nervous activation system detailed above is described as the somatic nervous system (SNS). Each lower motor neuron innervates muscle fibres within a skeletal muscle collectively making up what is called a motor unit. Whenever a motor neuron sends an action potential, this will cause an action potential in each muscle that it supplies, (Purves et al, 2001). It is important to note that reflex movements operate in the reverse of voluntary movement. Involuntary muscle movement mainly refers to the change in shape of internal organs to aid them in working i.e., the shape modification of the intestine to push food through the digestive system. These work via the autonomic nervous system (ANS) which is a part of the peripheral nervous systems (PNS); this nervous system is further split into three segments, cherry (2020) specifies these as the following:

- The autonomic nervous system which also includes the enteric nervous system within the gastrointestinal tract.
- The parasympathetic division within the autonomic nervous system which helps maintain the normal bodily functions. Furthermore, this division also controls the following: bladder, heart rate and eye pupils.
- The sympathetic division of the autonomic nervous system allows for the regulation of the impulsive "fight or flight" responses. Again, this also assists with the following: bladder, heart rate and eye pupils.

The sympathetic and parasympathetic divisions work in contrast to each other to help regulate the body for different scenarios - the sympathetic system works by stimulations whilst the parasympathetic system works from inhibitions. For example, the sympathetic system will work to increase the body's blood pressure in a situation where the body is required to respond to a situation; whilst the parasympathetic system will work to reduce the blood pressure to bring the organs back to a state of equilibrium. Both these systems utilise a chemical messenger/neurotransmitter - these are acetylcholine for the parasympathetic divisions and norepinephrine for the sympathetic divisions. The enteric nervous system works via the use of complex reflex circuits that detect and understand the physiological state of the gastrointestinal tract; this system can then relay information about the condition of the gastrointestinal tract back to the brain to give the outputs required to control the gut movement. This can be seen in figure 2-4, which has been sourced from Meenakshi and Gershon (2016).

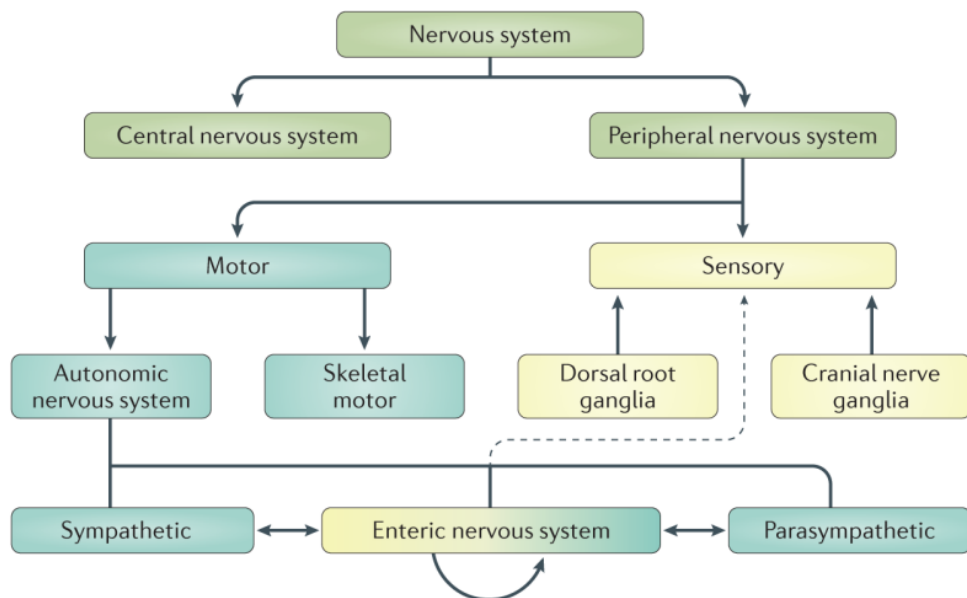


Figure 2-4. Nervous system Diagram – Meenakshi and Gershon (2016)

2.3. Neurological signals (neurons)

Signals within the nervous system are known as neurons - these cells are electrically excitable and transmit data throughout the body, especially within the CNS, PNS and ANS. These neurons are instrumental in transmitting electrical signals or action potentials around the body, enabling both autonomous and conscious muscular control, operating as small electrical pulses rather than continuous frequency driven signals. A microscopic image of a neuron provided by Woodruff (2019) can be seen in figure 2-5.

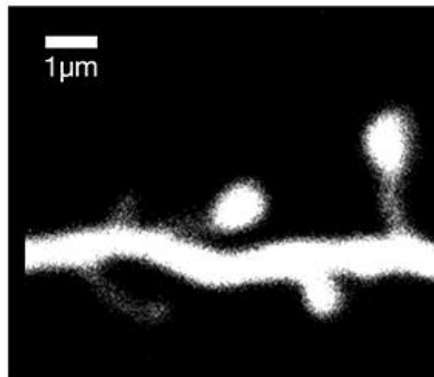


Figure 2-5. Confocal microscopy image of a Neuron - Woodruff (2019)

To ascertain a directive to the muscle, sensory input operations (somatosensation) such as Phototransduction (Purves et al, 2001) or touch (matosensation-transduction) transpose the absorbed information into an action potential (electrical pulse signal) via a chemical synapse within cells localised to the specific receptor and then transfer this data to various neurological systems such as the cerebral cortex and cerebellum for processing and distribution around the required control paths such as the central nervous system or the peripheral nervous system. A diagram image of the photoreceptor provided by Dubuc, B (2002) can be seen in figure 2-6.

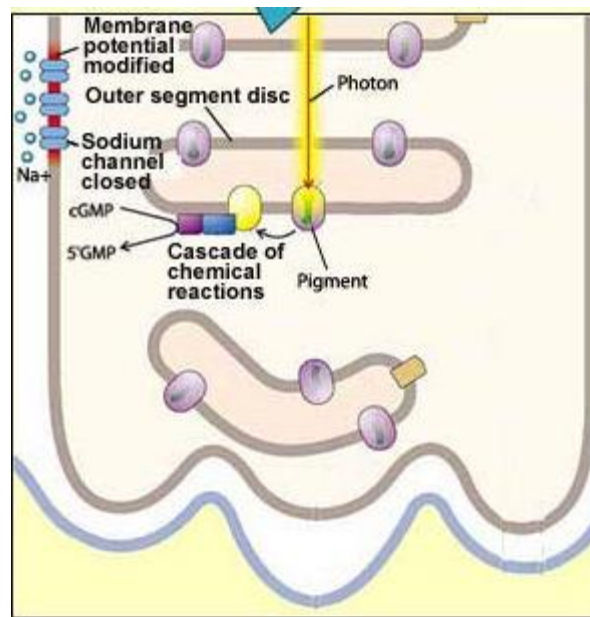


Figure 2-6. Photoreceptor Diagram - thebrain.mcgill.ca. (2022)

Multitudinous research scholars have debated the quantity of neurons located within the human brain, with Ullian et al., (2001); Doetsch, (2003); Nishiyama et al., (2005); Noctor et al., (2007); and Herculano-Houzel (2009) all giving an estimation of 100 billion neurons being contained within the human brain. Williams and Herrup (1988) estimated that a more accurate figure was 85 billion neurons with a neural distribution as follows: less than 1 billion located in the brain stem, 12 to 15 billion located in the telencephalon (Shariff, 1953) and around 70 billion neurons located in the cerebellum (Lange, 1975). However recent research performed by Pelvig et al., 2008 estimates around 21-26 billion neurons within the cerebral cortex. To allow the muscle directives to navigate the body, the over 70 billion neurons are interconnected in a vast network that is present throughout the CNS, PNS and ANS. Zhang whose research “Basic Neural Units of the Brain: Neurons, Synapses and Action Potential” (2019) estimates a total of 10,000 connections per neuron with as many as 1 quadrillion synapses.

A signal traveling through the CNS is transferred from the pre-synaptic neuron via the axon to the dendrite of the connected post-synaptic neuron above a specific threshold which activates an impulse known as an action potential - this action potential is generated via the collation of electrically charged atoms (ions) from calcium atoms which are located across the membrane of the axon in the sarcoplasmic reticulum. At the end of the axon the neuron synapses with the next required neuron in the network, allowing the signal to be passed from one neuron to the other. Examples of neurons detailed by Freudenrich and Boyd (2001) are listed below in addition to an image provided by Huang et al (2018) displayed in figure 2-7 which demonstrates not only the build-up of the neuron but also the point at which the synapse occurs.

- “Sensory neurons carry signals from the outer parts of your body (periphery) into the central nervous system.”
- “Motor neurons (motoneurons) carry signals from the central nervous system to the outer parts (muscles, skin, glands) of your body.”
- “Interneurons connect various neurons within the brain and spinal cord.”

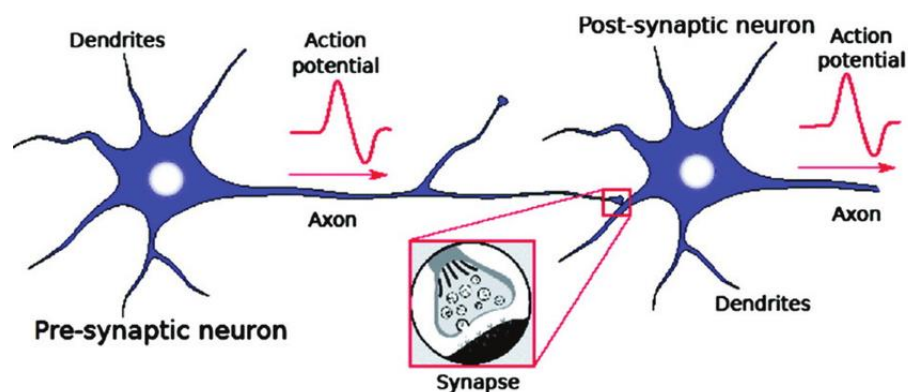


Figure 2-7. Neuron Diagram - Huang et al (2018)

2.4. Stopping contraction

Stopping a muscular contraction from the perspective of a conscious decision involves the redirection of calcium ions back into sarcoplasmic reticulum which then causes the actin and myosin to stop binding. By decreasing the intracellular concentration of the Ca^{2+} activator a smooth muscle relaxation can be elicited. Both the sarcoplasmic reticulum and plasma membrane are mechanics required in the removal of cytosolic Ca^{2+} , (Webb, 2003). In addition to conscious relaxation, there are also other factors that can stop a muscle contracting, provide by www.ptdirect.com (2022) these are listed below:

- Energy fatigue, where within the muscle cell the adenosine triphosphate (ATP) has been used up so the muscle can no longer contract.
- Nervous fatigue, where the nervous system cannot create impulses sufficiently or rapidly enough to create a calcium release.
- Voluntary nervous control, where the brain consciously informs the muscle to stop contracting by reducing the quantity of calcium ions.
- Sensory nervous control, where the sensory neurons identify an external stimulus such as pain and feed this back to the brain, which in turn prohibits the contraction from continuing.

2.5. Summation of muscle mechanics

Upon reviewing the above sections of muscle mechanics, a logical operation can be distinguished. As an example, the following process can be applied to the actuation of an individual's bicep:

1. Ocular observations establish a requirement for the bicep to contract.
2. Information is transferred to the brain for distribution around the central nervous system.
3. The upper motor neurons transfer the electrical impulse signal (action potential) containing the coordination information via the cerebral cortex.
4. Within the cranial nerve nuclei the upper motor neurons activate the action potential to travel down the axon until it reaches the synapse at which point the action potential is transferred to the lower motor neurons.
5. The lower motor neurons travel through the peripheral nervous system before reaching the neuromuscular junction, at which point a chemical synapse transfers the signal from the PNS to the muscle fibres.
6. After receiving this chemical signal within the sarcomeres, a reaction between myosin and actin takes place.
7. The sarcomeres' A band within the muscle fibres contracts.
8. Bicep actuates.

2.6. Artificial Muscles Currently Available

2.6.1. Festo Fluidic Muscle



Figure 2-8. Festo Fluidic Muscle - Festo Germany (2019)

One of the most popular artificial muscles available to the open market is the Festo fluidic muscle DMSP (figure 2-8), that Festo (2019) themselves describe as a fluidic muscle which is a tensile actuator that mimics the natural movement of a muscle. The muscle utilises a very elementary design principle to create the actuation required, by hermetically sealing pneumatic connectors to contractible tubing manufactured from rubber sheath which is used to seal the operating medium; additionally, to mimic the striations of a biological muscle, non-crimped aramid fibres are used internally to create a reinforced fabric that allows for power transition throughout the muscle. It is apparent that aramid fibres were selected for this device due to the high tensile properties they possess, being that they are composite fibres manufactured from both Kevlar and Twaron.

When researching aramid fibres, it was found that they have superior mechanical properties when compared to steel and glass, in addition to being heat and flame resistant which is supported by Ertekin (2017). Like the design of the device, the operational principle is also simplistic in approach - being that it is pneumatically powered. The muscle is mounted within a system where there is an equilibrium force acting on both connector ends i.e., a spring force making the device a single acting actuator - if the internal pressure of the device is increased, then the flexibility within the fabric and rubber sheathing allows for a circumferential expansion which in turn creates a linear contraction. Because of the tensile properties of the materials utilised, the contraction creates a tensile force in the linear plane. Festo Germany (2019) state that the maximum permissible tensile force available is at the start of a contraction with reduction over the course of the contracting stroke of the device. This muscle is what can be determined as a passive device rather than an active device - this is because for the muscle to be actuated, any signalling or control is performed remotely and not within the muscle. For example, to control this muscle a solenoid valve island must be installed which will direct the compressed air supply to the muscle when the software controlling the solenoids informs it of this decision. Alternatively, this muscle can be controlled via a conscious input such as a push button.

The practical implementation of the fluidic muscle DMSP within industry is multitudinous ranging from high-speed automation to advanced robotics, with applications such as:

- Production line conveyance (figure 2-9).

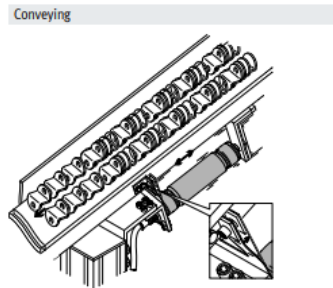


Figure 2-9. Conveyor Application diagram - Festo Germany (2019)

- Various work piece clamping methods (figure 2-10).

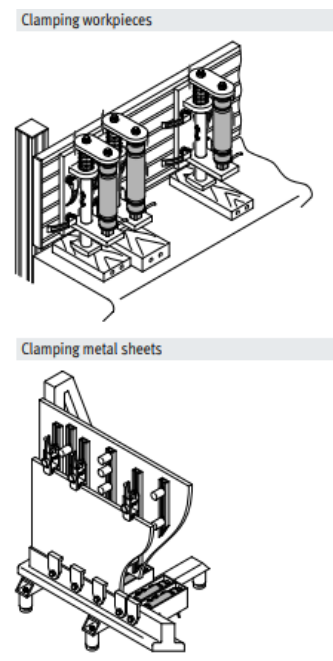


Figure 2-10. Clamping Applications Diagram - Festo Germany (2019)

- Advanced robotic movement (figure 2-11).



Figure 2-11. Robo Thespian - www.engineeredarts.co.uk. (2022).

The Festo fluidic muscle DMSP has one major benefit that surpasses the benefits of any other artificial muscles currently developed - this benefit is that it is currently commercially available. In the industry of pneumatics Festo are the only current provider of an actuator based around biological muscle design. Similar companies, such as SMC and Metalwork do not currently offer any kind of muscle technology. Additionally, the majority of artificial muscle technologies that exist are in their infancy and are not yet a commercially viable option. Another benefit to this technology is its lifting force capabilities - as seen in figure 2-12, at its peak operating force, the muscle can inflict around 6000N (dependant on model as illustrated below) of force due to the use of compressed air.

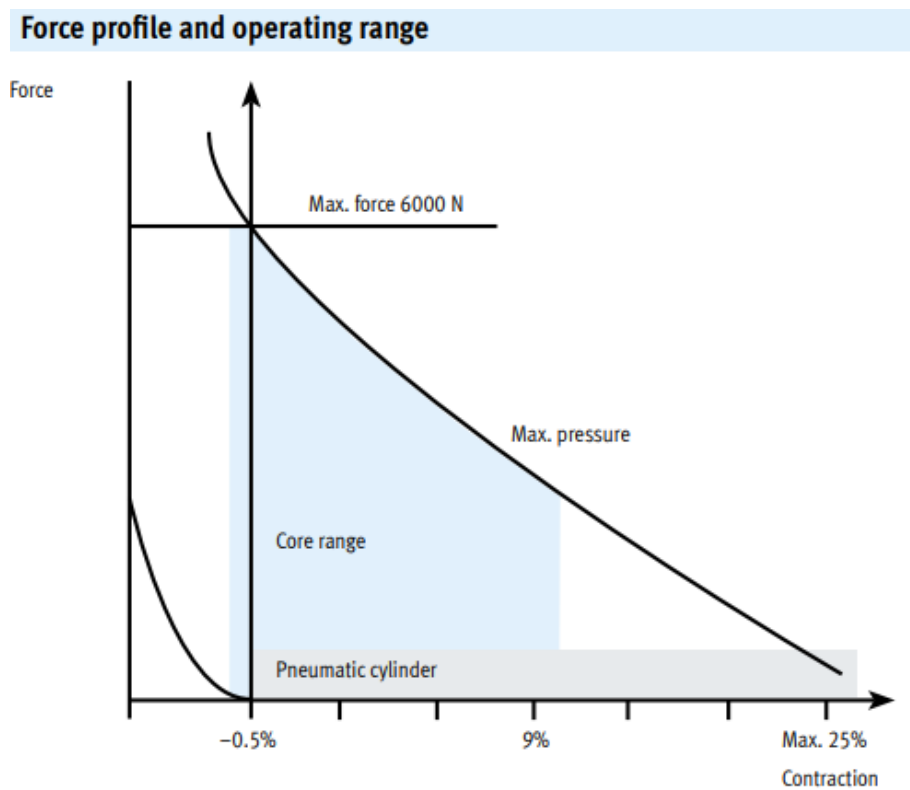


Figure 2-12. Force Profile and Operating Range Graphic - Festo Germany (2019)

Table 2-1. Fluidic Muscle Data - Festo (2019)

Internal Diameter (mm)	Nominal Length Range (mm)	Lifting Force (N)	Maximum permissible contraction	Mass Per Meter (g)
5	30-1000	0-140	20% of Nominal Length	27
10	40-9000	0-630	25% of Nominal Length	94
20	60-9000	0-1500	25% of Nominal Length	178
40	120-9000	0-6000	25% of Nominal Length	340

Although this device is in use within industry and is currently a commercially viable solution, there is one major drawback to the design and operation of the muscle, and that is the ratio of contraction to mass manipulation, as illustrated in both figure 2-12 and table 2-1 above. Similarly, to a biological muscle which loses its strength capabilities throughout its actuation, this is also the case for the Festo Fluidic muscle DSMP. However contrary to a biological muscle, the device is also limited in its linear displacement. When reviewing the data for this muscle, it becomes apparent that the diameter and length are key components to achieving the replication of muscle contraction. There appears to be a limitation around the circumferential increase that allows the muscle to contract. It can be seen in the captured data detailed in table 3 that there is also a link between the length of the device versus the displacement, this is illustrated below by utilising the reference points defined by the below formula with the exception of the first and last reference point which utilised the minimum and maximum lengths, this calculated data is visually represented in figure 2-13.

$L_1 = \text{Minimum Length}, L_2 = 25\%, L_3 = 50\%, L_4 = 75\%, L_5 = \text{Maximum Length}.$

$(L_5 - L_1) * L_x = \text{Displacement in mm}$

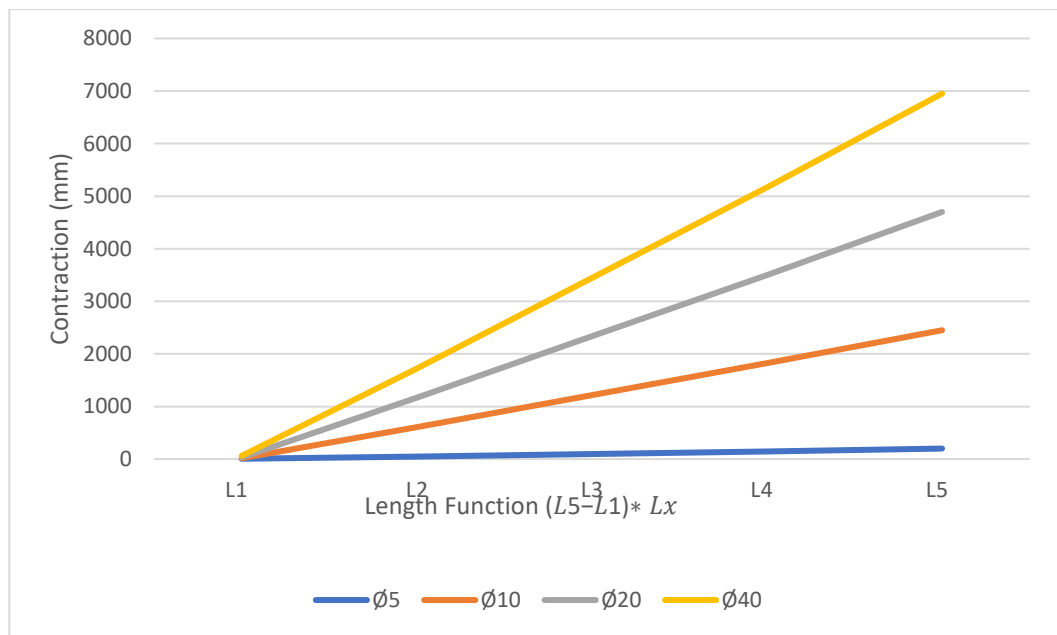


Figure 2-13. Linear Line graph of Muscle Contraction

2.6.2. MIT contracting fibres

A recent research project performed by Kanik et al (2019) at the Massachusetts Institute of Technology (MIT) explored the use of *strain programmable fibre-based artificial muscles* utilising the coiling affect – which in nature can be observed in cucumber plant tendrils as the plant begins to sprout, as illustrated below in figure 2-14. In its simplistic format, the actuator design utilised two materials of differing thermal conductivity properties bonded together and drawn into a coil; this actuator was then exposed to a heat source which would increase the heat of the actuator. As the materials have different coefficient values, when heat is applied the material of higher thermal conductance attempts to expand whilst the material with a lower thermal conductance co-efficient fix it in position causing the overall actuator to curl creating a strong linear contraction. This actuator can be seen in figure 2-15.

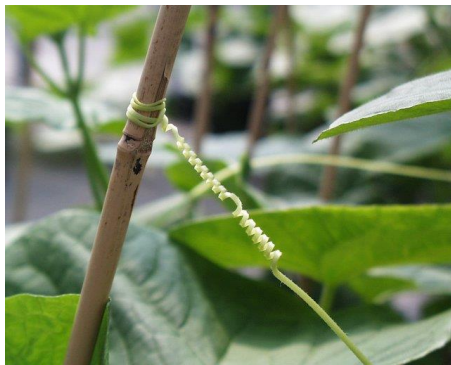


Figure 2-14. Cucumber Tendrils - davidrhodes124. (2018)



Figure 2-15, Strain Programmable Fibres – Chandler (2019)

Charles Darwin (1875) published a book entitled ‘On the Movements and Habits of Climbing Plants’ in which he studied many species of climbing plants, including the *cucumis sativus* (cucumber plant) and how these organisms have the ability to rise up and search for structure support before attaching and tensioning itself to the support. Understanding the experiments performed on cucumber tendrils by Gerbode et al, (2012), it can be concluded that the tendril coiling occurs via the asymmetric contraction of an internal fibre containing special cells. When under tension both fibres demonstrate a twist less of overwinding and more of underwinding.

This phenomenon is the underpinning methodology used for the study performed by MIT, focusing specifically on the differential swelling of fibres within the tendril compartments to aid in achieving a high power to mass ratio. Gerbode et al, (2012) further informs that whilst the hypothesis first poised by *C. Darwin (1875)* states that the tendrils operate like a ‘soft spring’ the full mechanical analysis of the tendrils’ behaviour remains unknown. With this understanding, the MIT study opted for utilising thermodynamics in attempt to replicate the tendrils behaviour in a more controlled manner. Using a bimorph polymer structure incorporating an elastomer and thermoplastic polymer, the differential in thermal expansion allowed for a tendril like spring geometry that could perform linear actuations (Kanik et al, 2019)

As the study was using a process known as thermal drawing, which is where a perform macro-structure is heated and drawn in extended lengths of fibre (Nicholas et al, 2011), both materials which would make up the bimorph would need to have similar viscosities at the thermal drawing temperature. Referring to the flow of two or more materials in a laminar direction thermal co drawing enables a continuous fibre structure. To allow the matching of two appropriate materials which can be combined into a single preform, often the glass transition temperature is used a guide. However, in actuality to ensure the materials co draw sufficiently the viscosity of the two materials is a better indicator of compatibility (Loke et al, 2019). With this knowledge the researchers opted for High-density polyethylene (PE, melting temperature $T_m = 120^\circ\text{C}$, $\alpha = 1.3 \times 10^{-4}, K^{-1}$) and cyclic olefin copolymer elastomer (COCE, melting temperature $T_m = 84^\circ\text{C}$, $\alpha = 2.6 \times 10^{-5}, K^{-1}$) to create the bimorph fibres.

To create this actuator the study team used identical PE and COCE blocks with a dimensional value of 25mm wide by 8mm high and 200mm long, annealed under the conditions of pressure = 50bar and temperature = 125°C . Additionally, a jointing material (poly (methyl methacrylate) PMMA) with a preform size of 35mm wide by 26 mm high was implemented. Throughout the drawing process the thermal drawing synthesis machine utilised the following settings: temperature = 290°C to 310°C , feed rate= 1mm/min and draw rate = 2 to 3m/min. By implementing this set up, the researchers were able to tune the fibre into dimensions between $50\mu\text{m}$ by $35\mu\text{m}$ and 5mm by 3.5mm with a length of 500m. Upon completion of the thermal drawing process the PMMA cladding was removed via a mechanical method, allowing the tension of 70Nm to 100Nm retained within the bimorph to create a coiled effect with coil diameters of 30 to 40 mm. In order to create the programmable strain bimorph, the fibre was then cold-drawn to strains of 50% to 1300% to induce PE plastic deformation; to create stress within the bimorph structure, the fibre was then released allowing the elastomeric properties of COCE to attempt to contract, increasing the internal stress on the fibre and thus creating a coiled tendril spring.

To prove the effectiveness of the manufactured bimorph coiled actuator, a simple test was devised and performed as seen in figure 2-16. Additionally, data recorded from a variety of tests performed is illustrated in figure 2-17 and 2-18.

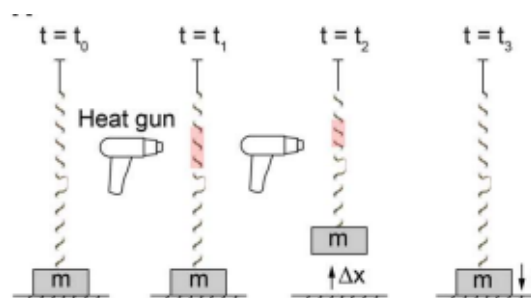


Figure 2-16. Thermal Coiling Test Diagram – Kanik et al (2019)

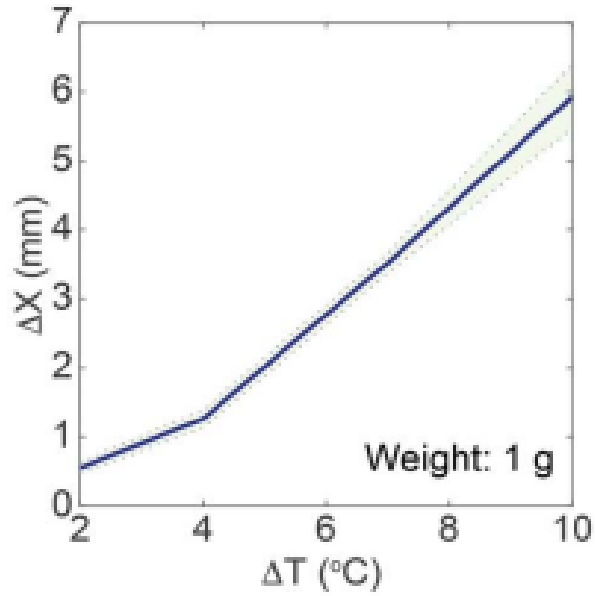


Figure 2-17. Vertical Displacement Graph - Kanik et al (2019)

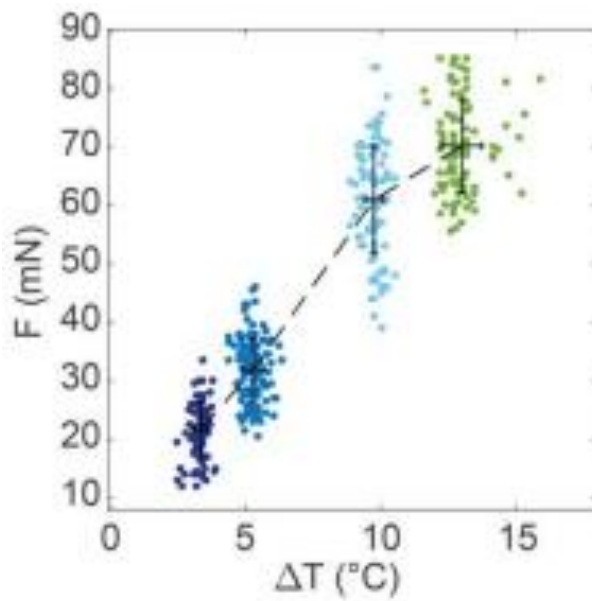


Figure 2-18. Generated Force vs Temperature Graph - Kanik et al (2019)

When transposing this actuator to the use of artificial muscle technology, the Massachusetts Institute of Technology (MIT) created an appropriate representation of a biological muscle based on the human bicep muscle, as detailed below in figure 2-19 and 2-20.

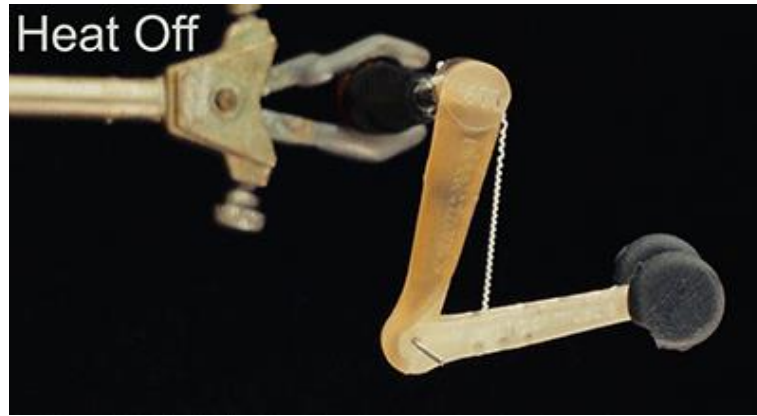


Figure 2-19. Programmable Fibre Bicep Actuation Test (on) – Chandler (2019)



Figure 2-20. Programmable Fibre Bicep Actuation Test (off) – Chandler (2019)

The strain programmable fibre based artificial muscle also has its limitations - the main one being the activation method. As described in the research and illustrated above in figure 2-16, to activate the muscle, sensible heat is required - in this case a heat gun was required to generate temperature differences of up to 14°C. With regards to this methodology of activation, a significant heat source is required to be used; if this type of activation is to be implemented in conjunction with the coiled fibre muscle for use with a practical task, then not only could there be issues with storing and powering the heat device locally to the user; but additionally various health and safety precautions would need to be considered to ensure no injury through heat could be caused.

These actuators are capable of lifting more the 650 times their own weight (Kanik et al, 2019). Although this value of 650 is impressive and proven through testing, this has yet to be scaled up to a larger size, more representative of biological muscles. Until this research is expanded and further explored, the technology remains a success only within a research laboratory and cannot yet be considered for practical applications.

2.6.3. Fluid-driven origami-inspired artificial muscles (FOAMs)

The fluid driven origami muscle is a new invention based on the materials fabricated in an origami like fashion, this can be seen in figure 2-21. The actuation methodology is contradictory to typical methods of actuation using a negative pressure (vacuum) regime to control the contraction of the muscle. Lang (2007) informs that whilst typically associated with the Japanese culture due to its renaissance in the 20th century by artist Akira Yoshizawa and taking its name from the Japanese language of “ori” which means “folded” and “Kami” which means paper. The methodology of paper folding into complex structures is estimated by Robinson (2021) to be over 1,000 thousand years old. Although often reduced to an elementary explanation of being just “folded paper” the practical applications for origami-derived components are still in the early stages of investigation and discovery. Lang (2007) additionally states that in the mid 1970’s mathematicians attempted to calculate the number of shapes that could be created from an uncut square piece of paper, with the results they conjured as endless. Additionally, methods of folding such as the “Miura-ori” (figure 2-22) have been extensively investigated for practical application due to the methodology allowing the final product to fold when compression at a specific single point is applied.

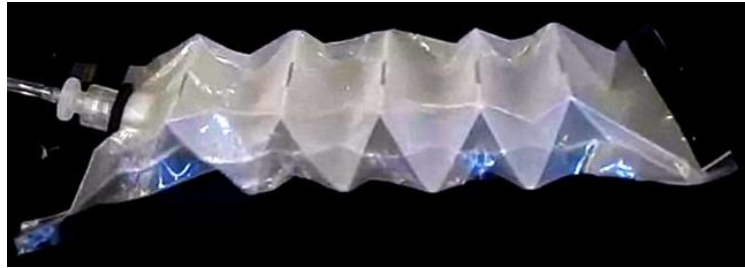


Figure 2-21. Fluid Driven Origami Muscle (FOAM) – Mandal (2017)

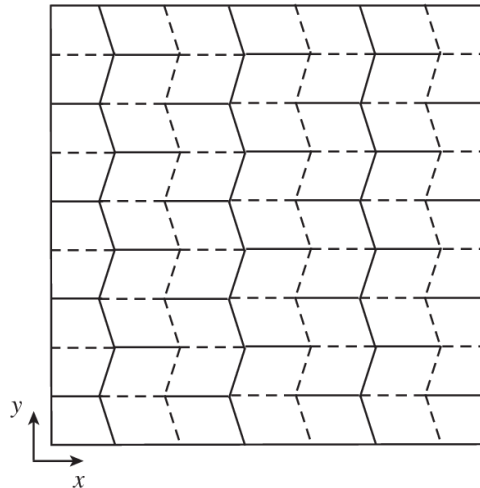


Figure 2-22. Miura-ori Fold - Magleby et al (2013)

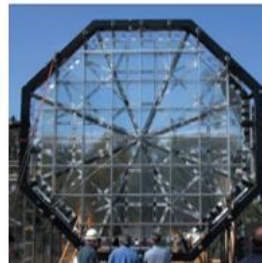
Examples of origami-derived technology displayed in figure 2-23 (Gent, 2018) include: artificial muscle technology, planetary explorers, collapsible telescope glass lens, foldable ballistic shield, deep sea grabber.



A



B



C



D



E

Figure 2-23. (A) artificial muscle technology, (B) planetary explorers, (C) collapsible telescope glass lens, (D) foldable ballistic shield, (E) deep sea grabber. (Gent, 2018)

Whilst origami in itself can be described as producing relatively strong and robust items, research by a team at Harvard University in collaboration with the Massachusetts Institute of Technology (MIT) investigated how the strength capabilities of origami-derived artificial muscles can be increased. To achieve this, a reverse hydraulic methodology was explored, implementing the use of non-compressible fluids. However, contradictory to conventional methods of hydraulic motion, this research used a negative pressure relative to ambient regime, rather than supplying a fluid to the muscle and relying on circumferential displacement similar to the pneumatic method employed with the Festo muscle discussed in 2.6.1 where in the equilibrium state the muscle was filled with the fluid to create an extended density. When actuation is required, a vacuum is generated, which will significantly reduce the volume of fluid stored within the muscle, causing the system to collapse in on itself, thus replicating a contraction. This vacuum-actuated muscle-inspired pneumatic structure (VAMPs) is illustrated in figure 2-24.

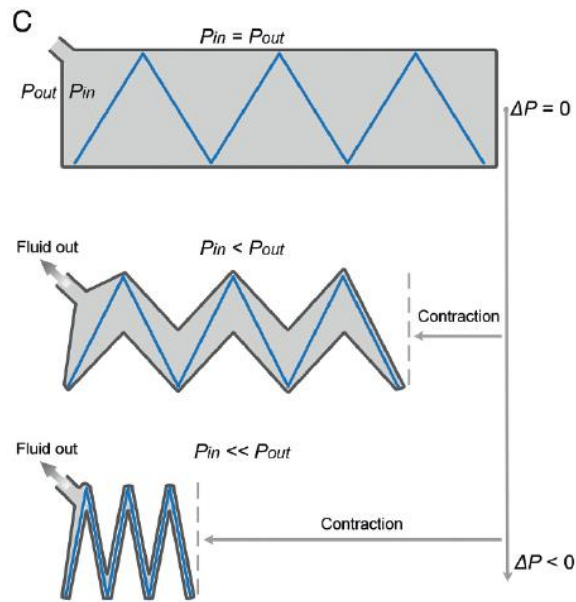


Figure 2-24. Principle of VAMP operation - Shuguang et al (2017)

To develop this type of muscle technology in addition to the structure strengthening via the implementation of origami, the design was also one in which the exo-structure was just as important. The muscle utilised an internal skeletal structure that was manufactured from a thin, stiff material that was not only strong enough to perform its designed task, but that was also malleable enough to be folded into the required origami structure. This skeletal structure was then enclosed within a hermetically sealed exo-skeletal skin, typically manufactured from thin film material to allow the deformation required to contract the muscle. Table 4 below details out the different combinations of skeletal materials (SKEM) and skin materials (SKIM) that were used. Finally, the fluid medium utilised was also an important aspect to consider when designing a muscle of this nature. Typically, with fluid motion devices hydraulics are the desired fluid medium due to their incompressibility, giving the system high strength capabilities. However, in this instance, because these research group used a vacuum rather than a positive pressure regime, hydraulic methodologies could hinder efficient operation of the muscle; this can be attributed to elements such as the increased co-efficient of friction making it hard to extract the fluid from the muscle. Additionally, the viscosity of hydraulic fluid versus gaseous fluids can also make it harder to extract the fluid in an efficient manner. However, this is not to say that fluids cannot be used as detailed in the row 4 of table 2-2, where water was used as the fluid medium. Fluids with low viscosity are ideal for uses within artificial muscle technologies due to their ability of being able to perform rapid energy efficient actuation. Compressed air is often the medium chosen due to its abundant availability (Shuguang, et al, 2017).

Table 2-2. VAMP Combination Table - Shuguang, et al (2017)

Combination	Skeletal Material (SKEM)	Skin Material (SKIM)	Fluid Medium
1	0.254mm polyester sheet	0.102mm thick polyvinylchloride (PVC)	Air
2	Silicone rubber (M4601)	0.24mm thick thermoplastic polyurethane (TPU)	Air
3	polyvinyl alcohol (PVA)	0.025mm PVA Film	Air
4	0.254mm thick 316 stainless steel	0.24mm thick thermoplastic polyurethane (TPU)	Water

Testing performed by the research group revealed results that not only demonstrated a high power to weight ratio, but also fast actuation due to the methodologies employed. Figure 2-25 demonstrates one of the tests performed where L, Shuguang et al (2017) indicates that the nylon linear zigzag actuators where exposed to a blocked force of 428 N via the use of a vacuum supply of -90 kPa, demonstrating that the actuation stress (600 kPa) is approximately six times higher than the capable stress of a mammal skeletal structure. Similarly, to the MIT coil muscle, the tests performed showed that a muscle with a weight of 2.6g could manipulate a load of 3kg, demonstrating the muscles capabilities to lift over 1,000 times its own weight with a vacuum of -80 kPa.

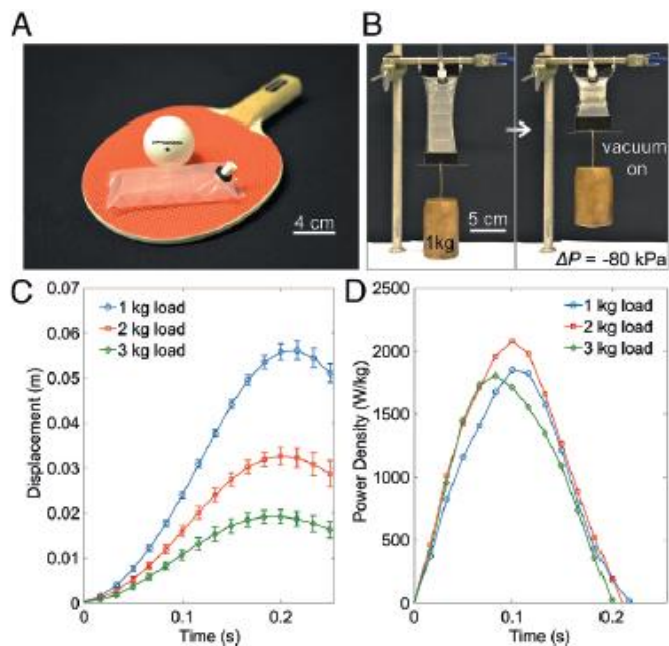


Figure 2-25. Experimental Test for Zig Zag Actuator - Shuguang, et al (2017)

As with the MIT coiled muscle, this piece of technology demonstrates an impressive capability to manipulate loads much higher than its own weight; as the actuator weighed 2.6g and was able to manipulate a load of 2kg. Additionally with the research the study also showed that this type of methodology could manipulate loads with a specific time threshold, with the 2kg load being raised to 5.5cm within 0.2 seconds. However, these FOAMs are also victim to the same limitations of technology as the artificial muscles explored above. The main issue appears to be the methodology of actuation - using a vacuum methodology provides great power but requires a vacuum pump to be located near the muscle, many of which are heavy and bulky. Additionally, this pump will need a power source and logic control. Furthermore, the actual method of signalling the actuation is not explored in this research, however if typical vacuum pump methodologies are explored then it can be understood that the implemented signalling device will be a dumb device requiring using operator input.

2.6.4. Knitted and weaving fabrics



Figure 2-26. Knitted Electronic Actuator - Puiu (2017)

A Linköping University research team (Edwin et al, 2017) explored the use of a fabric muscle constructed from a weaved and knitted structure as seen in figure 2-26; this muscle was then given an electrical power source to aid in actuation via the electroactive coating that laced the fabric. This specific device is designed in a way that accommodates for the operator, rather than designing an artificial muscle that possess strength or control in lab environment and then speculating on the development of the muscle for future applications - the research team have placed the operator at the centre of their consideration. With Edwin et al (2017) hypothesising that what can be considered as an ideal exoskeleton is a device that can be hidden under existing clothing, that would increase the user's mobility. To assume the appropriate balance of force versus strain, the muscle incorporated both a weaved structure to amplify the force output and a knitted structure to provide strain amplification as illustrated in figure 2-27.

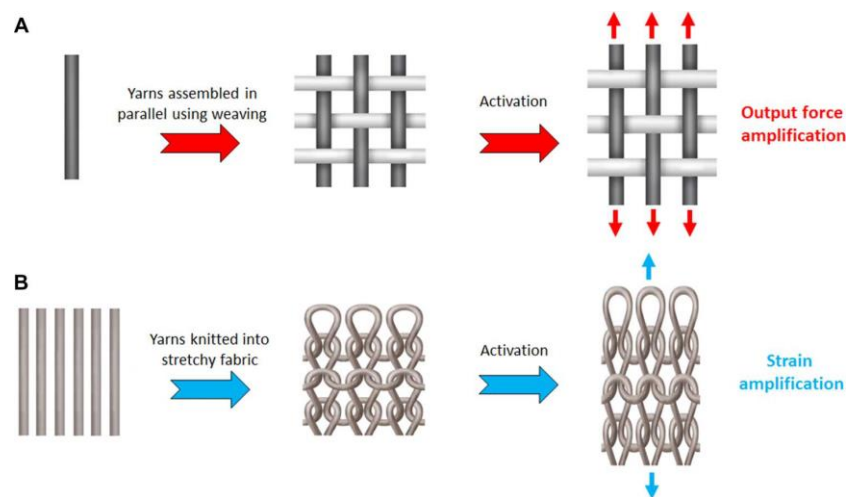


Figure 2-27. Knitted and Weaved Structures – Edwin et al (2017)

To develop this type of technology the Edwin et al (2017) used a conducting polymer (polypyrrole) that would deform from electrical stimulation; when a potential is applied to this polymer, there is a volume change within the polymer matrix due to either an ejection or insertion of ions. To fabricate the material, structure cellulose-based material (lyocell) was used due to its high compatibility with conducting polymers - in this case poly(3,4-ethylenedioxythiophene) or PEDOT, a two-ply twisted yarn was utilised with 4/4 twill weave pattern and a 2:1 ratio rib knit structure illustrated in figure 2-28. A twostep electrochemical synthesis was used to apply the electroactive polymers post fabrication. The overall manufacturing process of the muscle is indicative of typical methodologies employed within the textile industry, allowing the possibility of mass production of the fabric.

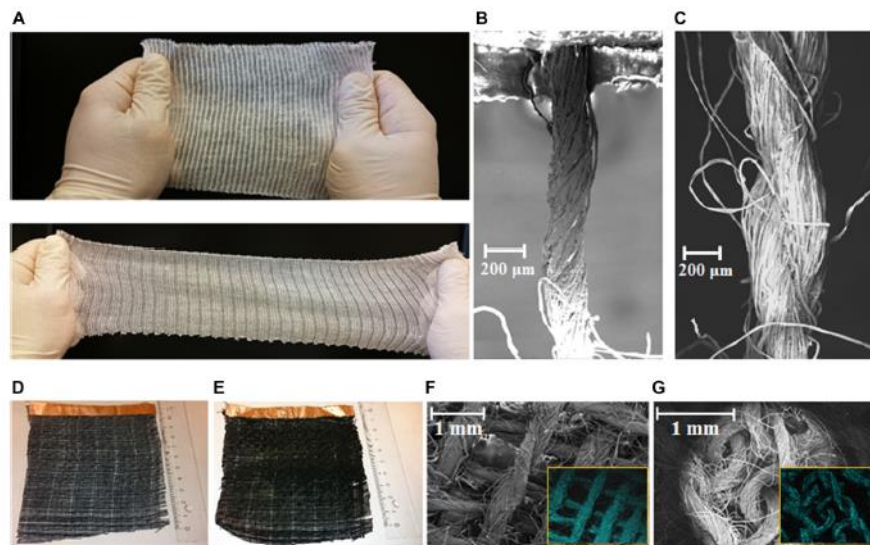


Figure 2-28. Fabric Structure - Edwin et al (2017)

This pioneers the use of knitted and weaved fabrics, combined with low voltage electrical signals to re-create the contraction experienced by biological muscles. The material was first constructed in a knitted manner before being woven to match the build-up of a biological muscle. It was found that the knitted construction gave the fabric the flexibility required to maintain a fluidic motion whilst the woven structure provides the strength when contracting. The fabric is then coated in an electroactive solution which - when energised - causes a contraction.

2.7. Critical Analysis of Current Technologies

Analysing the challenges associated with the aforementioned technologies is an important step to undertake when attempting to provide suggestion that will aid in advancing the speed at which these devices can become synergised with industrial applications in addition to being a commercially viable solution to artificial muscular assistance devices. To understand the direction of analysis it is first important to understand the requirements and applications of artificial muscles. Firstly, exploring the requirements for artificial muscle technologies means understanding both human illness and security applications.

Well known British Paralympians Sophia Warner (Warner, S, 2016) and Olivia Breen (Breen, O. 2021) are just two individuals who, like millions, suffer from cerebral palsy (CP) - with recent estimations stating that around 1 in 345 children in the USA has been diagnosed with cerebral palsy (Centres for Disease Controls and Prevention, 2020). This figure is further supported by scope.org.uk (2023) which also estimates that around 1 in every 400 children in the UK are diagnosed with cerebral palsy. Howard and Herzog (2021) informs that cerebral palsy is a condition affecting the cerebral cortex which effects the development and control of individual's movements. It is a condition that is attributed to loss of oxygen during birth and can cause shortening of an individual's muscles. Prenatal treatment for cerebral palsy can include: ensuring the expectant mother is fully vaccinated, alcohol and drugs are avoided and regular doctors' visits etc. Whilst these suggestions are fundamentals practises for prenatal care of a foetus, there is no proven link between these suggestions and preventing cerebral palsy (Proctor, 2023). Whilst a severe option, NHS.UK (2021) informs that invasive surgery is an option available to treat sufferers. Additionally, pharmacologic treatments are commonly utilised to treat the disability, NHS.UK (2021) informs that the following medicinal treatments can be administered for relative symptoms of cerebral palsy:

- Diazepam or Baclofen for muscle stiffness.
- Botulinum toxin injections for muscle relaxants.
- Melatonin for sleeping difficulties.
- Painkillers to reduce pain and discomfort.

As to date, cerebral palsy is an incurable disability; these abovementioned pharmacological treatments are utilised in conjunction with physiotherapy as this methodology allows the sufferer to continually aid development of their muscles thus reducing the debilitating effects of the illness. This is supported by Patel et al (2019) who informs that physiotherapy exercises aid in reducing joint contractures by using a passive range of motion exercise and stretches.

Whilst this condition most of the time has a negative impact on individual's life, it can be understood that in most cases the illness does not cause a serious risk to life. Both Paralympians referenced above have been able to compete in both the 2012 London Paralympics and the 2020 Tokyo Paralympics where bronze medals for track and field events were secured by them.

In 1963, the then PhD student Professor Stephen Hawking was diagnosed with Motor Neurone Disease (MND) also referred to as Amyotrophic Lateral Sclerosis (ALS). In 2019, the 39-year-old rugby league professional Rob Burrow also revealed to have been diagnosed with MND. ALS or MND is a condition that effects the motor neurone cells located in the central nervous system, to date the cause as to why these cells degrade is not fully understood, but speculation includes genetics and lifestyle. It is estimated by Motor Neurone Disease Association (2021) that around 1 in 300 people are at risk of being diagnosed with MND during their lifespan, whilst National Health Service Scotland (2021) states that at any one time, 5000 people in the UK are living with MND. As with cerebral palsy, this illness is a degenerative degrading illness which in most cause poses a serious risk to life; with National Health Service Scotland (2021) estimating that around 50% of individuals afflicted with the condition will have a life expectancy of around 3 years from the start symptoms. However, in some situations this can time period can be up to 10 years.

Similar to cerebral palsy, this illness can be treated with pharmacologic remedies, but as this illness is also incurable, physiotherapy is often employed to increase the sufferers' comfort; ultimately as the illness only progresses in its severity, the victim eventually becomes fully paralysed. All individuals discussed with reference to both cerebral palsy and motor neuron disease (with the exception of Rob Burrow) have continued to excel in their chosen career path, some of these in Olympic athletic sports. However, as previously stated both these illnesses are serious, incurable diseases that degrade a person's ability to perform conscious manipulation of the skeletal muscles over a multitude of time scales, rendering the sufferers non-autonomous (in a scale relative to the individual). With this consideration it is important to understand that each individual referenced here has/had a care team or person to support them, in some cases this team or person provided potential invasive 24-hour care.

Understanding the issues associated with these two diseases in addition to the awareness of multitudinous other paraplegic illnesses could be perceived as a great motivation to develop an initial application for artificial muscle technology. If the aforementioned artificial muscle can be further developed into standalone systems, then it can be hypothesised that with combined advancements in artificial intelligence, true artificial muscle technologies can be developed to assist with the day to day challenges that individual sufferers of paraplegic diseases encounter - in addition to aiding in achieving autonomy for these individuals. The hypothesis could suggest that if a cure cannot be found for these illnesses, then engineering may be able to develop technology that allows an individual with paraplegic-type illnesses to one day control their own skeletal structure via the use of external artificial muscles.

Understanding the security application side of the requirements for artificial muscle technologies mainly refers to military applications for exoskeletal systems. Recently a major advancement in military applications for artificial muscle technologies has been driven by US robotics company Boston Dynamics. Formally a part of the Massachusetts Institute of Technology (MIT) and funded

via the Defense Advanced Research Projects Agency (DARPA), Boston Dynamics is now owned by the Hyundai Group and focuses the applications for its research and products at the civilian markets. The company is predominantly known for their development of Spot®, their automated robotic canine illustrated below in figure 2-29. This product was initially designed for use within combat zones, searching for Improvised Explosive Devices (IED's) or for autonomous medical extraction of wounded soldiers. However, since Boston Dynamics have completed their contracts for DARPA the product is now sold to private sector companies in addition to government agencies and can be used for a multitude of operations. Unfortunately, there is not a lot of reliable sources that provide a full explanation to how the robot is designed and works, however it is apparent from the many test videos created by the company that the artificial muscle technology utilised is advanced and somewhat autonomous; the degree of autonomy is not understood - and neither is the aspect whether this could be transferred to a human operator. Nevertheless, what is apparent is that the muscle technology is compact and is not powered by pneumatics.



Figure 2-29. Spot the Dog - Boston Dynamics USA (2022)

If we consider the above artificial muscle technologies when referencing them to the discussed requirements and applications, an understanding can be gained into how these devices are both convergent and divergent in their applicability, suitability, and viability. It can be seen that due to the practical limitations of physics (how muscles operate in a simple mechanical way) the actual mechanics of each device is identical in that a contractional pulling method is employed to develop the actuation - no design utilises a methodology of pushing the skeletal frame. Analysed mechanically, it is apparent that the method of contraction that replicates typical biological muscle would be the most efficient and effective to utilise, however it can be posed that a method of extensional manipulation could be utilised for different muscles around.

When observing the way in which the different muscle contract, a difference can be seen in the design considerations of the mechanics of contraction. For example, the previously discussed FESTO Fluid Muscle requires circumferential space to allow the contracted muscle to offset the displacement of length, meaning that not only is the device limited in how much it can contract, but also there are limitation to where and how this type of artificial muscle can be fitted. In contrast, both the knitted fabric muscle and the MIT coiled muscle utilise have a design focused on the structure of the muscle, more replicative of biological structures (striated muscles and coiled tendrils); these structures allow for a more linear displacement within the contraction, meaning that contrary to the FESTO muscle, the resting positions of these muscles is a “nominally open” principle. These designs allow for a more compact device that can be integrated more easily into a working system. However, it is important to understand that the MIT coiled muscle does have a major drawback to its current design, in that the muscle is loose in its configuration making it susceptible to damage. To ensure the longevity of this muscle, the coiled polymer would need to be enclosed in a suitable skin-like material to provide additional strength. Finally, the fluid driven origami muscle is the only technology discussed that removes a majority percentage of its actuation medium to aid in the reduction of local space considerations required for muscle contraction, allowing for greater linear displacement of an object. However, whilst the medium (typically a fluid) is removed from the muscle it is stored remotely, meaning some method of vacuuming and storing the fluid needs to be considered for an operator; the required equipment will impact the usability of an artificial muscle system as a whole in addition to adding a large amount of weight to the device.

Strength is a typical measurement of how successful an artificial muscle design is - generally this is because the aim of the artificial muscle is to provide enhancement to typical human capabilities, and when referring to human muscular capabilities, strength is a key element that is often focussed on within the design. Observing the information displayed in section 2.6.1 it can be understood that the principles underpinning the design of the Festo fluidic muscle are indicative of an attempt to achieve high strength capabilities. Creating an artificial muscle with the anticipation of industrial use would require more consideration of strength than overall weight and agility of the muscle. Table 2-3 below demonstrates a metric often used to define the success of a device by comparing its

overall weight to the force output giving a force to weight ratio (FWR). Although a more scientific measurement to use would be *power to weight ratio* - as artificial muscle technology is generally considered for application requiring a small or wearable device - observing the overall *weight of the device vs the force output* is a suitable metric to which a muscle attempting to hold high strength capabilities can be scrutinised against. This can be attributed to the fact that the device is being considered in isolation from its power source with an assumed “isentropic” state, with the general design of artificial muscles utilising a remote source for power provided to the actuation - meaning that a *power to weight ratio* would be a less suitable metric due to weight of this specific part of the system been remotely located from the actual muscle. It is important to acknowledge that the data represented below displays each muscle in its lowest permissible length configuration and by increasing the length up to the muscle’s maximum permissible length will increase the overall weight of the device by a set value per meter thus, reducing the overall force to weight ratio.

Table 2-3. Festo Fluidic Muscle DMSP Model Data Table – Festo Germany (2019)

Description	*Weight (g)	Theoretical force at max operating pressure (N)	**FWR (N/g)
DMSP-5 (length = 30mm)	14	140	10
DMSP-10 (length = 40mm)	83	630	7.5
DMSP-20 (length = 60mm)	222	1500	6.7
DMSP-40 (length = 120mm)	827	6300	7.6
*Weight increases per additional meter of muscle added as follows 5=27g, 10=94g, 20=178g and 40=340g.			
** <i>FWR (newtons per gram)</i> = $\frac{Force}{Weight}$			

Although the *force to weight ratio* is relatively low with this device, the implementation of this technology is already accounted for with the muscle being utilised for a multitude of industrial applications, meaning that whilst the FWR is low, the practicality of the strength capabilities has been proven.

Similarly, the strain programable coiling muscle developed by MIT has demonstrated high *force to weight ratio* with the published article stating that the muscle tested can manipulate a mass 650 times its own weight. Additionally, the research states that a *power to mass ratio* for the muscle was calculated as 90 W/kg; this is 80% higher than what Kanik (2019) states as the average human muscle *power to mass ratio* which is stated as 50 W/kg. However, in the literature there is no detailed data, to support these claims - only a final value that is stated. In contrast, the fluid origami actuated muscle discussed in section 6 states that the device has a weight of 2.6g with a blocked force of 428N, this means the muscle force to weight ratio is around 165 N/g which places this at a higher rating than the FESTO muscle.

When evaluating the strength capabilities of the knitted and weaved CP fabric, the same methodology cannot be used; this is because the research (Edwin et al, 2017) for this specific muscle does not state an overall weight and a maximum weightlifting capability, and predominantly compares the strain rates of multiple configurations due to the design of the muscle being focussed on its stretch and return capabilities. However, the research does positively identify the strength of alternately sized fabrics, comparing the strength capabilities of different width woven fabrics utilising a ply twisted yarn (T) and a fluctuating voltage of between 0.5V and 1V in 800 second intervals; the information attained in this test is illustrated in figure 2-30.

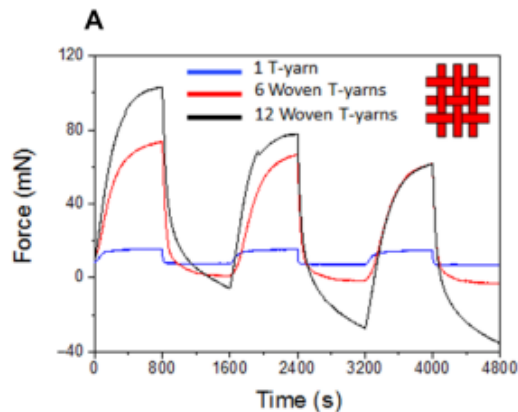


Figure 2-30. Measure Isometric Force Graph - Edwin et al (2017)

It can be seen that the research performed by Edwin et al. (2017) demonstrates that an increase in T-yarns does provide a significant increase in the strength capabilities of the overall fabric with the following results recorded: 1 yarn = $8\text{mN} \pm 0.5$, 6 yarns = $64\text{mN} \pm 4$ and 12 yarns = $99\text{mN} \pm 8$. In addition to this test being performed on woven structured fabrics, a single yarn (S) of $\text{Ø}200\mu\text{m}$ was also tested within a knitted structure, the results of which are displayed in figure 2-31. This type of structure demonstrated a lower strength capability than the woven fabrics tested but did demonstrate a moderate increase in isometric force when the singular yarn is compared with the knitted structure. However, it is also important to understand that whilst the knitted structure showed a lower force output, it did demonstrate more continuity in the actuations. It can be seen that the highest strength output of the woven structure's manifests during the first actuations, after this initial actuation the isometric force output decreases.

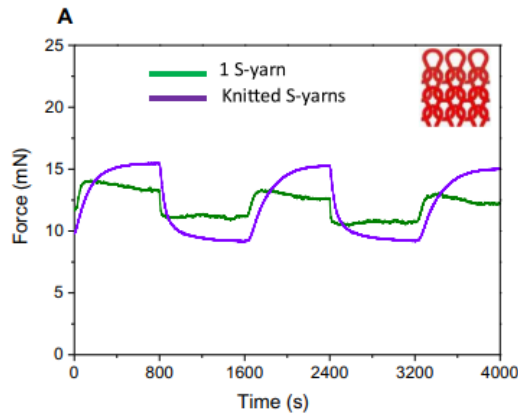


Figure 2-31. Isotonic Strain Graph - Edwin et al (2017)

Encouraging the development of artificial muscle technology into a commercially viable solution that is in line with compact user expectations means identifying critique that's has been established during the evaluations of the aforementioned technologies, this being the method of signalling the actuation. Throughout the literature reviewed for all the discussed devices, discussions with regards to how these muscles will be instructed to actuate have been completely neglected, scientific and engineering experience can allow an estimation of how these signals could be generated for each device and it is as follows. Reviewing the applications of the FESTO Fluidic muscle, it can be understood that this can be termed as a “dumb” device, as it holds no localised electrics or logic; this type of device would typically be activated via a physical push button/switch or a programmed software upload to a microchip or programmable logic controller (PLC). This controller would provide the logic behind how and when the muscle would actuate, either using a pre-programmed recipe, feedback provided from external sensors or human input. A signal actuation based on the requirement of the above hardware means additional storage for the componentry, which for a remote device designed to be worn by an operator means that space around the body would need to be allocated in addition to the possible integration of local sensors. Finally, if a PLC is required (this method of control is industry standard) then a power supply is required; using the Siemens LOGO 8 as an example, the technical manual provide by Siemens (2020) specifies a voltage input of 24V DC which would need to be supplied either by a stand 230V AC connection or on-board batteries which would either reduce mobility or add additional weight to the system respectively. Continuing with this line of critique, the MIT strain programmable muscle also provides no investigation into the long-term considerations for actuation. This system is activated by significant temperature increase, currently induced via a remote heat gun activated by a conscious human decision. Again, this method of signalling the actuations provides no artificial logic and relies on a conscious input from an individual in addition to an external heat source capable of providing the required heat differential. The requirement for an external heat source again reduces the compactness of an exoskeletal device which would incorporate this type of artificial muscle technology. Whilst there are a many of methods available to allow for a significant inducement of heat differential, due to the absence of research into the long-term applications and

signalling for the technology it is hard to speculate on how this muscle can be signalled to actuate via a more compact and intelligent methodology.

When the fluidic origami artificial muscle is considered, it is apparent that the medium of actuation (water or air) requires storage upon removal from the muscle, additionally as the medium is fluidic then it can be assumed that the methodology of signalling an actuation is identical to the FESTO fluidic muscle discussed above; the difference being that the FESTO muscle is pneumatically operated, requiring compressed air to be supplied to the muscle, whilst the FOAM is predominantly a hydraulic system which removes the medium via an induced vacuum. This indicates that this system also has little logic to the signalling of that actuation, whilst the origami structure allows for a programmable motion, instructing this motion to begin still relies on human intervention. Finally, the fourth technology being reviewed also makes no investigation into the long-term considerations for providing a true artificial muscle technology with smart method of signal actuation. However, Maziz et al (2017) states “We envision adding sensing yarns into the fabric to allow sensing displacement and thus allow better control through a feedback system, thus developing multifunctional textiles.” This statement does demonstrate an intention to develop the muscle technology into a more autonomous artificial-type-utilising smart-sensing technology. It can be suggested that with this development of smart sensing, a method of smart signalling could simultaneously be developed.

The absence of artificial intelligence considered for signalling the actuation within the aforementioned muscle technologies suggests that either this element has been completely neglected or displaced for research at a later date; with minimal discussions for signalling referenced within the research for each device this hypothesis is further supported. Whilst these muscles are classified as “artificial” it can be postulated that utilising this terminology is at this stage not fully appropriate as although these mechanical muscles are artificial and not biological, if the information discussed in section 2 is considered, then a true artificial muscle would also encompass an “intelligent” signalling system that would allow the muscle to provide assistance to the operator without conscious intent. Considering this hypothesis these devices provide less assistance to an operator but rather muscular enhancements due to the operator being required to input the logic required for signalling the actuation.

2.8. Smart Material Properties

Typically, the implementation of smart materials most applicable when referring to the modern methodology of manufacturing devices requires sensory input response. Organs are stimulated by nerve impulse that travel through the brain and spinal cord to the required as destination, (American Psychological Association, 2021). When referring to smart materials Rogers (1989) informs that these are materials which change their behaviour in a systematic way as a response to specific external stimuli. A practical example of this can be observed with the MIT coiled muscle, as the muscle is manufactured from PMMA encapsulated bimorph fibres due to their thermal coefficient properties; when heat is applied, the muscle undergoes an external thermal induction, resulting in a volumetric expansion as illustrated in figure 2-32. It can be understood that this phenomenon occurs as a result of external stimulus that will ultimately allow manipulation of a materials shape. One favoured and important aspect of smart materials properties is that these scientific principles allow for more autonomy within technology.

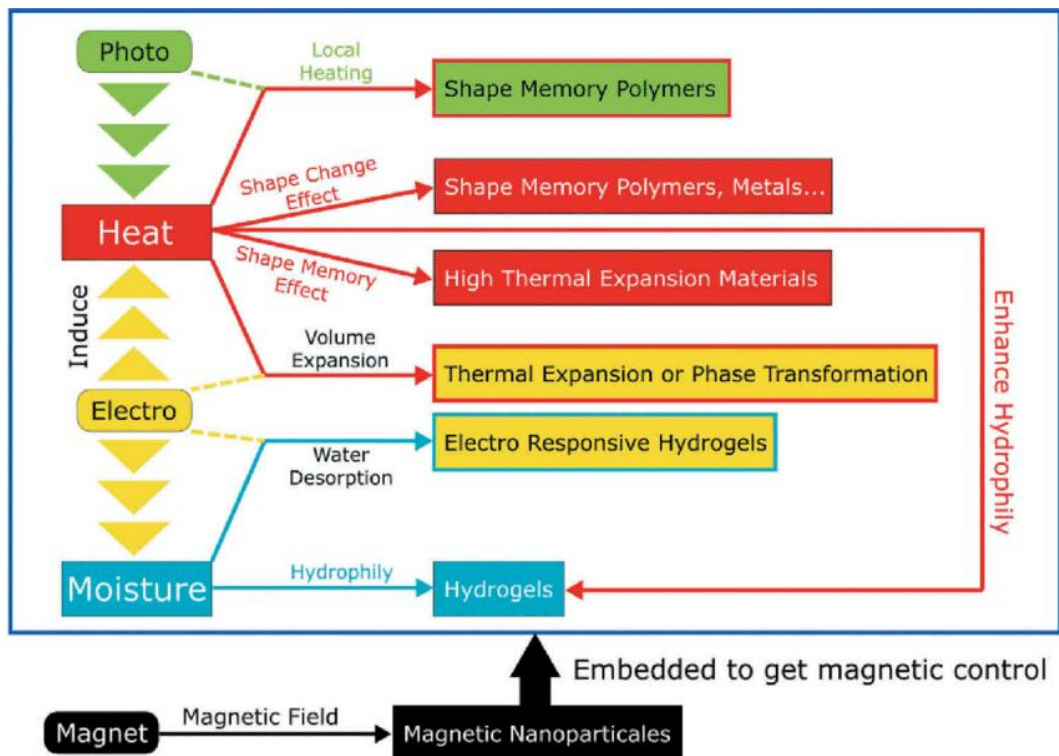


Figure 2-32. Smart Material Principles. Provided by Zhang (2019)

2.9. Shape Memory Effect

Currently there are two types of classifications to describe shape deformation materials: these are known as the shape memory effect (SME) or the shape change effect (SCE). Materials that fall under the SME category are commonly defined as shape memory materials (SMM) and can be sub-divided into the following categories:

- Shape memory alloys (SMA): the Institute of Making website by University College London (2021) informs that shape memory alloys are metallic materials which have the ability to be adapted from their original shape via external stimuli and then returned to their default geometrical shape. The two internal crystalline structures (martensite and austenite) are active at different temperature set points - when the material is exposed to high temperatures, it can be easily deformed and modified; this is also applicable to the cooling stage at which the martensite structure is favoured. Upon heating the deformed object, the phase shift in structure to austenite allows the atomic arrangement to return to its default programmed shape.
- Shape memory polymers (SMP): similar to SMA's, these polymer-based materials possess a two-phase state: the crystalline state and the amorphous state. The amorphous state can be described as a metastable state, where the free energy is larger in comparison with the crystalline structure, meaning the molecules in the material structure are no longer organised in a lattice pattern; this state can be produced via thermal induction (Cahn and Greer, 1996). The Archetypal shape memory polymer is polyurethane; SMP's like polyurethane have a third state known as the semi-crystalline state where both phases occur simultaneously. To enable the attainment of shape memory, SMP's have a two-stage temperature change. Rather than transforming from one phase state to the other at a defined temperature (typically referred to as the glass transition temperature T_g), SMP's remain in a bi-phase state at T_g with the amorphous state frozen defining the materials default shape. Once the material is heated, this then allows the amorphous state to become dominant allowing malleability of the material, after the material cools and reaches the defined T_g , then the default shape is retained.
- Shape memory ceramics (SMC): These are ceramic particles that utilise the same austenite and martensite crystalline structure as SMA's. SMCs are often used for the following properties they possess high strength, large recoverable strain, large energy damping, and light weight. An example of a SMC is zirconia.
- Shape memory gels (SMG): This category of smart materials is typically a material that is soft and malleable in all forms, it possesses high biocompatibility and is additionally highly biodegradable. SMGs are suitable for medical use with applications including bandages, optical lens and soft actuators (Kabir et al, 2014). SMG's (often termed as hydrogels) are predominantly polymer-based structures which contain a high quantity of water. Archetypal methods of manufacture for SMG material can be understood to be via reversible

interactions such as ionic interaction, host-guest inclusion, hydrogen bonding and dynamic covalent bond (Chen et al, 2018).

2.9.1. Thermo-responsive

Thermo-responsiveness is a property that is predominantly observed in polymer material - Teotia (2015) states that examples of thermo-responsive polymers include:

- “Poly (N-alkyl substituted acrylamides)”
- “Poly(N-vinyl-alkyl-amides)”
- “Poly (ethylene glycol)-poly (propylene glycol)-poly (ethylene glycol) copolymer (PEG–PPG–PEG)”
- “Poly (ethylene glycol)-poly (d, l-lactic acid)-poly (ethylene glycol) copolymer (PEG–PLLA/PDLA–PEG)”
- “Poly (ethylene glycol)-poly (lactic-co-glycolic acid) (PEG–PLGA)”

Typically, thermo-responsive materials are activated by the differential in bilayers, which have a differing co-efficient of thermal expansion (CTE). However, Teotia (2015) also informs that the polymers can be split into two categories: the first being polymers that are insoluble above a specific temperature, called the lower critical solution temperature (LCST) and the second being a polymer that will precipitate and perform a phase change below a set temperature called the upper critical solution temperature (UCST).

2.9.2. Moisture-responsive

Moisture-responsive smart materials (predominately hydrogels) have inspired high interest within the science community due to their ability to expand up to 200% in comparison to their original volume, their high biocompatibility making them suitable for the medical industry for applications such as broken bones, optical lenses, and soft actuators. The swelling within hydrogels is defined by the balance of free energy that will allow for a network expansion (Ionov, 2014), in addition to informing that hydrogels can be manufactured to respond to external stimuli such as:

- “pH-responsiveness”
- “Thermo-responsiveness”
- “Solvent-sensitive responsiveness”
- “Electro-responsiveness”
- “Photo-responsiveness”

These types of materials are relatively easy to manufacture through 3D and 4D printing methodologies - research performed by Chao (2017) provides a visual demonstration as shown in figure 2-33 of how they manufactured a hydrogel from PEG-DA (average Mn 700) and methylene blue (MB) utilising femtosecond laser direct writing (FsLDW) 3D printing methodologies.

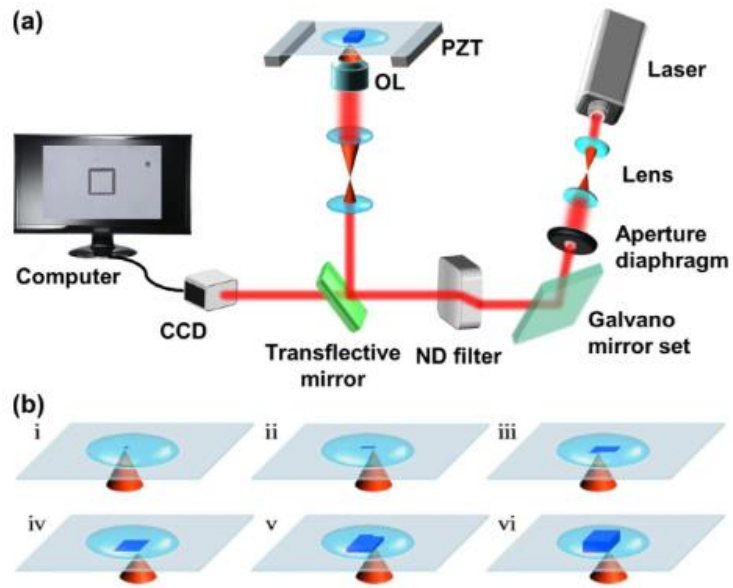


Figure 2-33. Hydrogel Manufacturing Process. Chao (2017)

However, one drawback identified is that hydrogels are predominantly for use with aqueous solutions - these actuators are not most efficient when being used in normal air conditions with the volume expansion in normal air being smaller than within water. Furthermore, this also effects the response time of the actuator (Ionov, 2014).

2.9.3. Photo-responsive

These types of materials which respond to photonic stimulus are created by implanting chromophores within the materials structure - these materials are typically a gel substance. One method of activation is via colour specific chromophores which will cause the smart material to respond to a specific value within the colour spectrum. Unlike other methods, photons are stimulus via proxy as the material uses the chromophores to attain what heat energy should be extracted. This allows for a light induced change at a molecular level, demonstrated in a macroscopic change of shape (Xion, et al, 2019). Zhaodi et al. (2022) also visually illustrates three alternate methodologies of activating phase change materials through photo sensitivity as illustrated in figure 2-34.

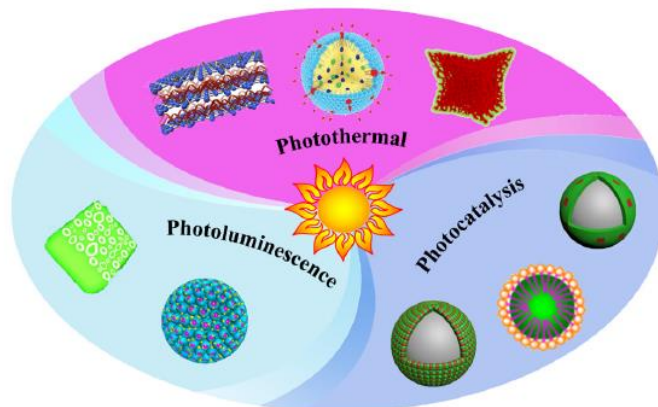


Figure 2-34. Photo responsive Categories. Zhaodi et al (2022)

2.9.4. Electro-responsive

Electro-responsive smart materials such as the knitted and weaved fabric discussed in section 2.6.4, reflect a change in response to an external electrical input. Similar to a photo-responsive material, electro responsive stimulus is indirect in its activation of a smart material. Electroactive polymers (EAPs) actuate based on a principle of two triggering mechanisms, ion migration and piezoelectric effect (Kim, 2017). Additionally, within the group of electro-responsive materials there is a sub process known as electrothermal actuation, where a bilayer structure within an internal electric to thermal layer interfaces with an external power source. The differing coefficients of thermal expansion are subject to increase in thermal heat as result of the conversion of the electrical energy (Yong-Lai, et al, 2021).

2.9.5. Magneto-responsive

Relatively simple when compared with the above methods, magneto-responsive materials are impregnated with ferritic oxide powders such as iron oxide Fe_3O_4 (Thevenot, et al, 2013). Additionally, this research further illustrates the applications of magneto-responsive materials as demonstrated in figure 2-35.

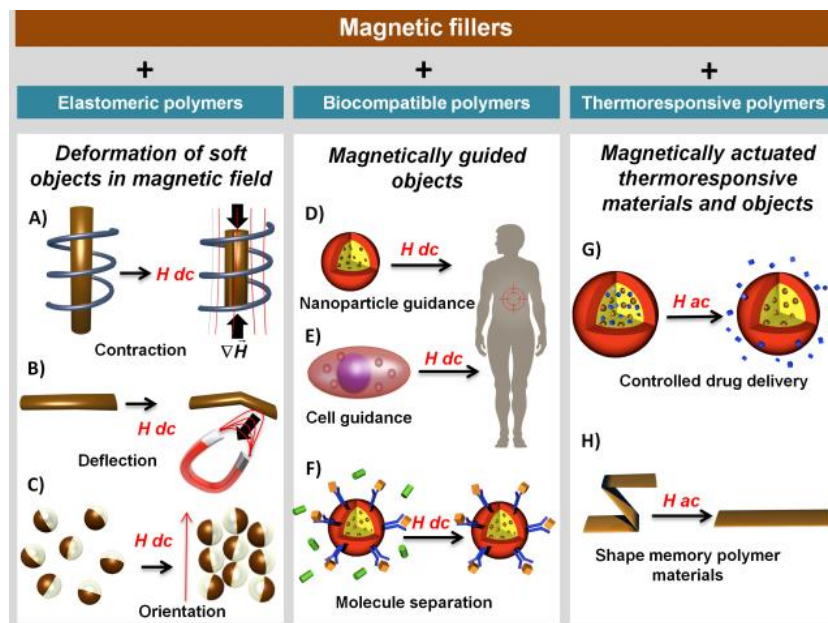


Figure 2-35. Magnetic Filler Types. Thevenot et al (2013)

However, there are a few drawbacks to this type of actuation such as: the total object size must be relatively small to ensure activation within a magnetic field, there must be a magnetic field generated through another device and finally the eddy current phenomena experienced with magnetics can cause instability with regards to control of the object.

2.10. Smart Textiles/Fibres

Smart textiles are yarns or fabrics that encompass properties discussed in 7.1, enabling advanced controllable systems to be developed with the intention of being compact and worn by a human operator. Celikel (2020) informs that smart textiles can be categorised into three sections as illustrated in figure 2-36.

	Sensing external conditions	Reacting	Responding and adopting
Passive smart textiles	√		
Active smart textiles	√	√	
Ultra smart textiles	√	√	√

Figure 2-36. Smart Textiles Categories. Celikel (2020)

2.11. Passive smart textiles

Often termed “passive smart textiles”, the first generation of smart textiles are materials that have functionally in advancement of traditional textiles, however, do not possess properties that allow them to change as a result of environmental conditions such as electrical charge. This is further supported by OTEX (2022) which informs of how these fabrics have functions beyond that of typical fabrics, however they do not use electrical stimulus. These types of fabrics purely really molecular change changes in material properties to perform smart processes. Example of passive smart textiles are materials that are used within sensing technology rather than dynamic control, as outlined by Çelikel (2020):

- UV Protective clothing
- Conductive fibres
- Plasma treated clothing
- Waterproof clothing

2.12. Active smart textiles

Active smart textiles commonly regarded as “second generation smart textiles” require external stimuli to encourage a reactionary change to the textile; these stimuli can be either a result of a user input or an environmental input. As discussed in section 7.2 these reactions are manifested in the shape change effect, phase change effect and the shape memory effect. This means that these materials can be programmed with a default setting (for example a default shape) and then be modified by external stimulus such as an electrical signal. Examples of active smart materials include are stated by Vogt (2019):

- Thermoregulation material such as cooling jackets
- Heat sensing systems such as heated car seats
- Shape memory system such as fabric muscles.

2.13. Ultra-smart textiles

Often named “the third generation” of smart textiles, ultra-smart textiles have the ability to not only sense and react but also adapt as a result of the external stimuli, meaning these smart textiles have the ability to evaluate and account for alternate conditions without previous programming of the materials’ shape. In addition to providing examples listed below Mikhailovsky (2017) informs that ultrasmart textiles work like a brain using an in-built microcomputer.

- Spacesuits
- Musical jackets
- Wearable computers.

2.14. Functions of Smart Textiles

It’s generally accepted that smart textiles can be categorised into five operational functionalities, as illustrated below in figure 2-37. Of these five categories only two are relevant for this research.



Figure 2-37. Smart Textile Categories. Celikel (2020)

2.14.1. Sensors

Smart textiles have been proven to be a highly successful component when manufacturing sensors which are required to be compact and functional. Leal-Junior, et al. (2020) informs that these developments in sensing technology utilising smart textiles will allow for further compactness of sensing system in addition to lower energy consumption and wireless connections.

Smart textiles have been extremely successful when utilised as sensors within systems. Çelikel, (2020) informs that examples of the types of sensors include:

- Thermal sensors - devices that can detect thermal differential. An example of this is a thermistor which senses an electrical resistance change due to a thermal change. An additional example of this is a hydrogel, which swell in response to a thermal change.
- Light sensors - devices such as photoresistors, that can convert light energy into a voltage output.
- Audio sensors - like the above, these are devices that can convert sound vibrations into an electrical signal. An example of this is piezoelectric materials.
- Humidity sensors - which can measure absolute or relative humidity. These devices typically use capacitance to perform this task, allowing the dielectric properties of the sensor to change with the absorption of moisture.
- Pressure sensors also convert contact pressure into an electrical signal, typically via the use of a strain gauge or diaphragm.
- Strain sensors use semiconducting materials or the piezoelectric effect to convert strain into an electrical signal.

2.14.2. Actuators

An actuator can be defined as method of converting external energy into controllable mechanical energy (Bellmunt and Campanile, 2010). Typically, this output motion is either a rotary or linear vector; additionally, the quantification of the output force of an actuator can be directly linked to the input media which can vary from electronic, hydraulic and pneumatic. An archetypal utilisation of smart materials is actuator technologies - to allow for the movement of objects in systems that required a more compact methodology of actuation. Person Et al (2018) explains that weaved textiles have an inherent x-y addressability which means that the columns and rows created by the warp and weft threads create an x-y grid system which will ultimately allow for a contraction of the fabric in either the X or Y plane of motion when a catalyst for actuation such as voltage is applied.

Person Et al (2018) additionally inform that the following are types of textile actuators:

- “Bladder type”
- “Piezoelectrical types”
- “Order change”
- “Thermal volume change”
- “Absorption volume change”
- “Distance change”

2.15. E-Fabrics

E-fabrics (or electronic fabrics) are similar to smart fabrics in that they can be actively manipulated, however these fabrics can also be used for electronic systems. In addition to figure 2-38 Maxey (2019) defines an E-textile as a textile which encompasses circuitry to allow electrical signalling. This is further supported by Wilson and Teverovsky (2012) who informs that E-textiles make up parts of electronic components that create systems which can provide sensing, heating and lighting.

Always Means an E-Textile	Can Mean an E-Textile	Can Be Used to Make an E-textile	Can Be Made of an E-Textile	Does Not Mean an E-Textile
Soft Circuit	Smart Textile	Printed Electronics	Smart Clothing	Wearable Clothing
E-Textile (Electronic Textile)	Functional Fabric	Conductive Ink	Wearable Technology	Wearable Fabric
	Smart Fabric	Conductive Thread		Wearable Fashion
	Ultraflexible Circuit			
	Technical Textiles			

Figure 2-38. E-textile Definitions. Maxey (2019)

E-fabrics are a separate classification of materials to that of the above smart materials discussed, specified by the American Society for Testing and Material (2020) in the ASTM D8248-20 standards smart materials can be defined as follows:

- “Smart Textile - Their definition of smart textile does not require an electrical function, but a response to stimuli, making thermochromic and non-electronic materials potentially a smart textile. Source”

Dias (2015) provides details into the main manufacturing methods of E-textiles, predominantly this these types of fabrics are constructed from a weaving technique with the both the plain weave and atlas weave provided as examples. Additionally, Dias (2015) also informs that embroidery is also a manufacturing method used to implant the active electric yarns into a fabric; with both chain stitch and standard embroidery being used as examples.

2.16. Heat-storing fabrics

A recent breakthrough in materials science has allowed the development of a dual mode temperature controlling fabric, which operates via self-endothemic regulation. The fabric operates by using a multilayer construction which consists of a bilayer thermal emitter for temperature control; this emitter is then coated in an Infrared transparent nanoPE textile, with an asymmetric thickness at either side. In his research, Po-Chun (2017) specifies that the bilayer emitter is manufactured from a 9 μm thick Carbon sheet and a 0.15 μm thick copper sheet. Carbon was implemented to allow the heating mode within the emitter, as carbon has a large IR absorption coefficient (IR rays in the same wavelength as human anatomy radiation). In contrast, to allow for cooling, copper was utilised due to its reflecting properties. Finally, the nanoPE, in addition to being transparent to mid-IR rays at a specific wavelength, is also porous, allowing for vapours and air to pass through the material. Peng Y, et al (2018) provides research which tests how transparent to mid-level infrared radiation nanoPE is via the use of a Fourier transform infrared spectrometer. Ultimately demonstrating that a nanoPE film of 12 μm thickness can allow for almost 100% transmittance while a nanoPE film of 450 μm thickness can achieve around 80% transmittance. Chandler, D (2014) explains that the reason a material such a silicone can be transparent or opaque to infrared radiation is due to the materials bandgap requiring more energy than what is required for the infrared photons.

Po-Chun (2017) provides an explanation with their research that informs the bilayer structure can control the emissivity of the material, whilst the nanoPE thickness allows the temperature to be controlled by providing distance between the hot side (human skin side) of the fabric. During cooling the layer of material with the high emissivity is facing towards the hot side where the nanoPE thickness is considerably less; this allows the heat to radiate through the fabric. During heating mode, the carbon emitter distance from the skin is increased decreasing thermal conductance of the fabric thus allow the heat to remain captured within the textile. This is visually demonstrated in figure 2-39. Additionally, the effectiveness of the material is demonstrated in figure 2-40 which gives a graphic indication of the capabilities of the textile.

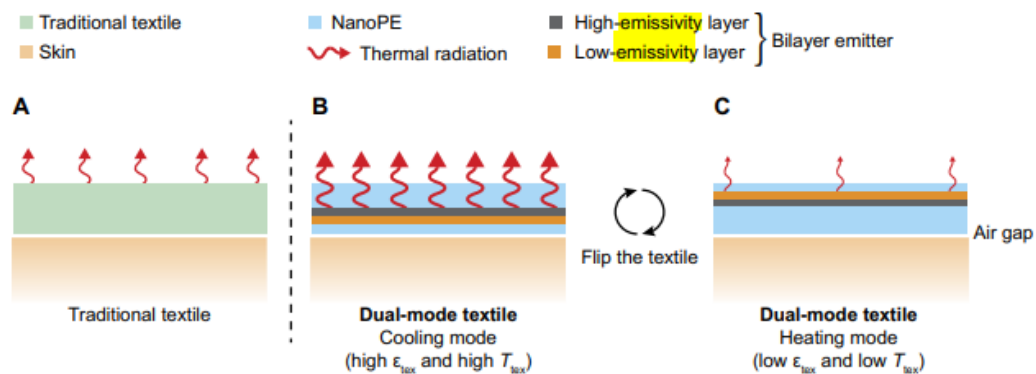


Figure 2-39. Schematic of Dual Mode Textile. Po-Chun et al (2017)

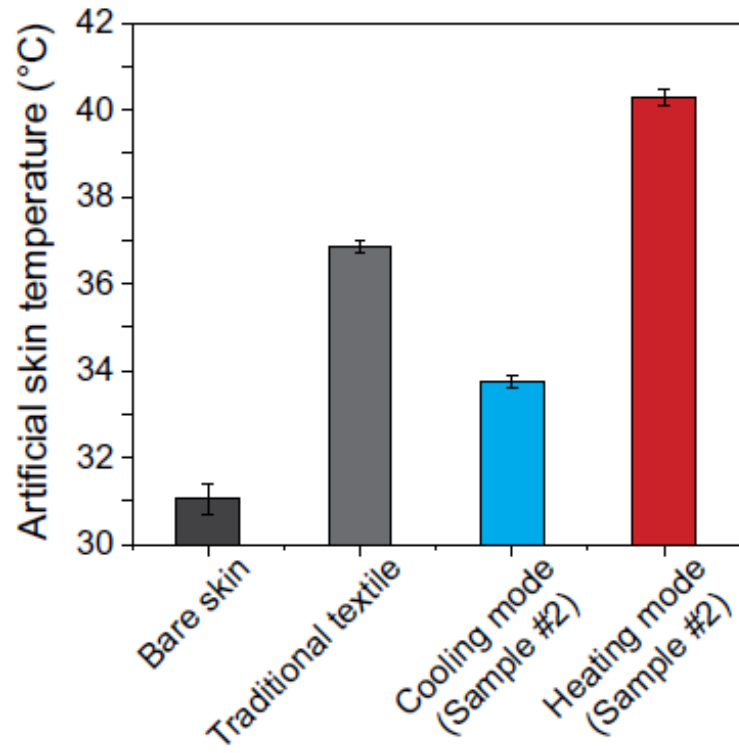


Figure 2-40. Artificial Skin Temperature Graph. Po-Chun et al (2017)

2.17. Monofilaments

Monofilaments are a type of material that consist of a singular solid material known as a filament - this is showcased by Tausif et al (2018) who states, "Monofilament yarn, as evident by its name, consist of a single solid filament." Monofilament yarns are utilised in everyday life for applications such as fishing line, dental floss, squash and tennis rackets etc. Tausif et al (2018) also informs that the typical diameter of a yarn monofilament is between 100-200 μ m. Monofilaments are noted for their high tensile strength, however most recently monofilaments have been used in a reverse sensory format due to dexterity. WEST monofilaments as seen in figure 2-41 are used in the health sciences to understand an individual's receptive response to touch; Occupational Medicine (2018) states that this is because when "Applied to the skin until they bend the monofilaments deliver the same force irrespective of any difference in observer or their degree of unsteadiness".



Figure 2-41. WEST Monofilaments Test Strip. performancehealth.co.uk (2022)

2.18. Graphene Textiles

The recent discovery and developments in graphene materials have had a profound effect on science and engineering. Graphene is an important and stand out material as a result of exceling at its basic characteristics, De La Fuente (2022) identifies three main properties of graphene to be: mechanical strength, electrical conductivity and optical absorption properties. The above discussed allows an understanding of graphene's versatility to be attained. Recent developments from the University of Manchester by Afroj et al (2019) has provided advancements with regards to graphene textile developments, demonstrating that cotton yarns can be coated in reduced graphene oxide (rGO) allowing for a conductive textile to be manufactured.

2.19. Thermoelectric materials

Self-powering systems can often use thermoelectric materials such as solar cells, piezoelectric materials and triboelectric materials, (Wu and Hu, 2018). Taking this into account thermoelectric materials can be utilised in the induction of heat that can then be transferred into an electrical signal similar to a Peltier module. Typically, thermoelectric technology will convert latent heat such as biological, geothermal, or residual heat directly to electrical energy. Fabric materials which can provide this type of conversion already exist and are termed thermoelectric generators (TEG); in short, these fabrics operate in exactly the same way a Peltier module does, just with alternate materials. These fabrics are constructed with multiple n-type and p-type semiconductors that are connected in a parallel circuit - this allows the Seebeck effect to take place within the material. A visual example of how a fabric TEG was constructed for testing by Lund (2020) can be seen in figure 2-42.

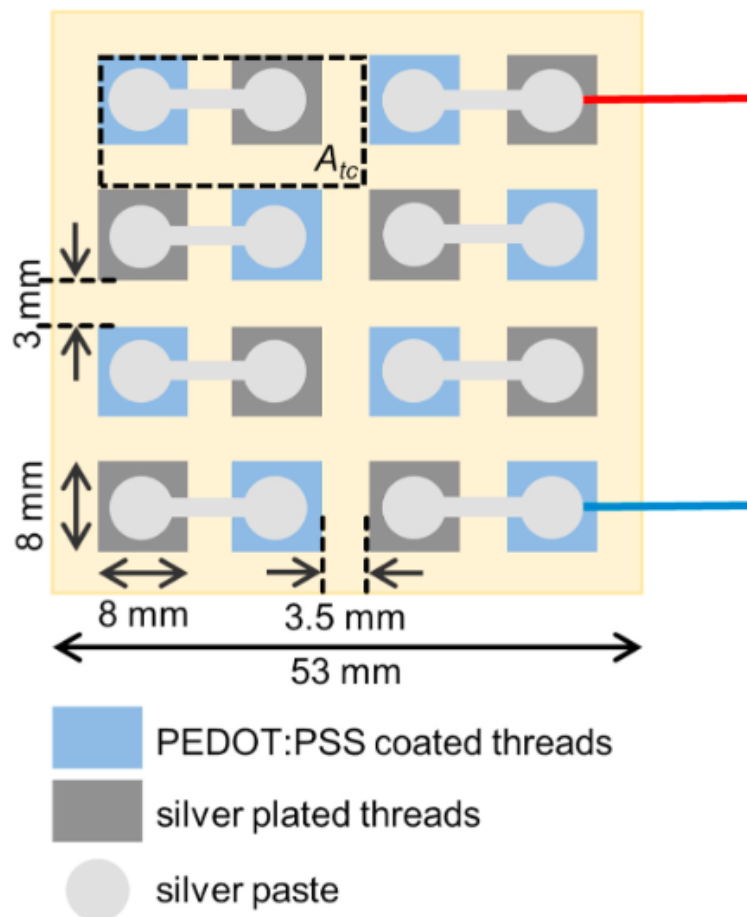


Figure 2-42. Fabric TEG. Lund (2020)

2.20. Seebeck Effect

Full understanding of thermoelectric materials requires a rudimentary understanding of the principle underlying their operation, this being the Seebeck effect. The Seebeck effect refers to the thermoelectric principle of generating electricity via free-flowing electrons which are acquired from a thermal source. Merck (2022) states the Seebeck co-efficient can be defined as $ZT = S^2\sigma T/K$. Snyder (2008) informs that within specific materials where the thermoelectric effect is occurring this will occur due to the charge carriers in metals and semiconductors being free to move like gas molecules, carrying both charge and heat. A temperature gradient applied to a material causes the mobile charge carriers at the hot side to diffuse the cold side. This build-up of charge carriers causes a net charge at the cold side, thus producing an electrostatic charge. These types of materials/systems are typically referred to as thermocouples and are manufactured from semiconductors of the N and P types; an illustration of a typical module for thermal conversion to electricity taken from Sault (2018) can be seen in figure 2-43.

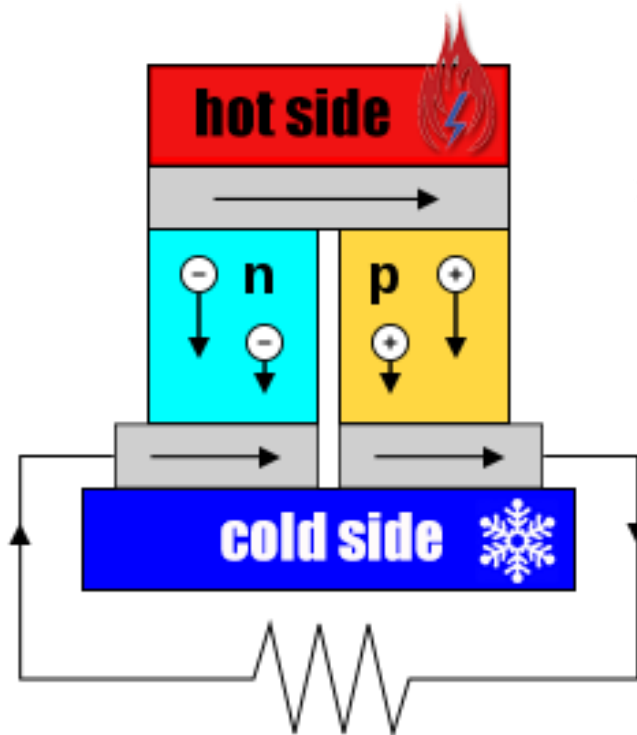


Figure 2-43. Thermal Conversion Generator Diagram. Sault (2018)

2.20.1. N-type semiconductors

Semiconductors of the N type are a silicon (Si) based semiconductors that are doped with arsenic (As) or phosphorus (P), both of which contain five electrons in their outer nuclei orbit allowing a covalent bond to occur with the crystalline structure of the silicon (Si). As the silicon (Si) has only four electrons, the fifth electron of either the arsenic (As) or phosphorus (P) is free moving allowing an electrical current to flow through the silicon (Si) semiconductor (James, 2020).

2.20.2. P-type Semiconductors

Semiconductors of the P type are also Si based; however these are doped with either B or Ga, both of which have three electrons in their outer nuclei orbits. When the covalent bond with the Si lattice takes place, the electrons from holes in the Si valence band, meaning the valance band electrons become active whilst the holes move in the opposite direction to the electrons. As the B or Ga is fixed in the crystalline structure of the Si, only the positive charges are free to move (James, 2020).

2.20.3. N-type and P-type semiconductors together

In a singular form these semiconductors hold no special qualities, however when N-type and P-type semiconductors are fused together, a PN junction is created. At this junction free electrons from the N-type and the holes from the P-type conductor interact to cancel each other out to create a neutral zone - Toshiba (2022) defines this zone as the “depletion layer”, which acts as an insulator allowing no current to flow. Atoms at either side of the depletion zone want to acquire electrons and get rid of the holes to attain neutrality; as there are no free charge carriers around the depletion zone, this cannot happen. If a power supply is connected to the semiconductor as P-type to +VE, and N-type to -VE then the holes in the P side are repelled, in addition to the electrons of the N side allowing an exchange of charge between atoms at the PN junction. A visual representation of a PN junction sourced from James (2020) is illustrated in figure 2-44.

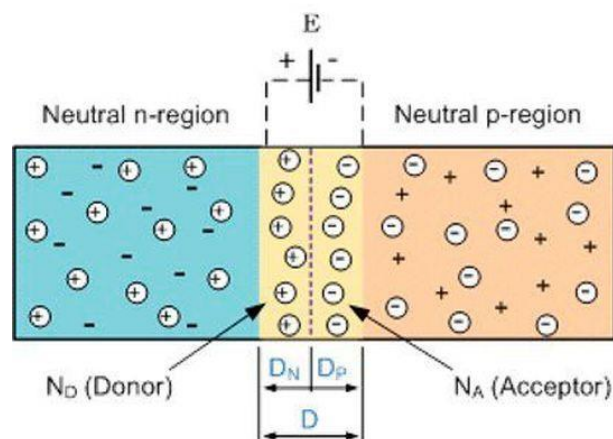


Figure 2-44. PN Junction Diagram. James (2020)

2.21. Critical Analysis

Thorough analysis of section 2.8 to 2.20 of the literature review provides an expanded understanding of smart materials' origins and properties. When reviewing the smart properties and smart materials it can be understood that these types of materials have a place in the development of a multitude of products, devices, and systems; materials with this naturally occurring "smart" phenomenon can be heavily utilised for artificial muscle technologies due to their compact and smart responsive properties. However, one major drawback to smart materials is that the activation of the smart property is in most cases indicated via an external input such as heat or electricity. This indicates that whilst the materials are labelled smart and can be pre-programmed, if they are implemented into an artificially controlled system then they are still either fixed to a specific program or require some other device or material to perform the logic required to control these smart properties.

With regards to the discussed materials, a conclusion could be drawn that polymerised materials would be the most appropriate to implement for a system desiring smart property outcomes from the base structure. Additionally, it can be understood from the research above that polymers are extremely versatile in their application, manufacturing method, and workability. The fundamental mechanical properties of these types of materials are close to or the equivalent of other harder materials such as steel wire rope – however, polymers tend to be lighter and more compact. This can be seen in products such as fishing lines which are manufactured from monofilament polymers and possess high tensile strength capabilities. Heat-absorbing materials discussed in show promise for their implementation into artificial muscle devices; based on reviewed research, these materials could have use for processes such as sensing, energy storage and energy transfer. Currently these materials are typically used for dual mode temperature-controlling clothing. An initial drawback that can be foreseen is that these materials - which use the Seebeck Effect to convert heat energy to electrical energy – require a large temperature differential to achieve high voltages. Farzana (2001) informs that human skin temperature is influenced by both the surrounding air temperature and its exposure to the surrounding environment, with normal skin temperature being around 33 °C or 91 °F. Taking this into account means that heat absorbing materials would need some method of creating a colder atmosphere to induce a high temperature differential in order to create a high voltage.

Analysing the literature review from a broad perspective, and understanding the discussions already performed in section 2.7, conclusions can be established which identify gaps in the existing technologies. Commercial viability of many of the technologies mentioned simply is not considered in the current research - many of the technologies require either expensive manufacturing methods or the materials themselves are expensive. As this thesis has been written from an industrial engineering perspective, any commercially considered technology must be compliant with the

time/cost triangle as illustrated in figure 2-45. If the cost is not realistically achievable for a consumer type user, then commercial applications of the technology could be seriously hindered.



Figure 2-45. Time/Cost/Scope Quality Triangle. Jacob, U & Ksenia, M. (2023)

Throughout this literature review the quantity of lab-based technologies presented far outweighs the quantity of commercially available technologies - this includes many of the smart materials discussed. Understanding this demonstrates how and why commercially available assistive devices exist in small quantities at a very high unit cost, which in turn causes a gap in research which can be studied, by doing so suggested developments can be proposed. The advancements suggested because of this research will come from the perspective of a practical engineering approach with a commercial understanding. At this stage the only relevant material/device that would have value in investigating further as part of this research would be the thermoelectric generators, due to their compact size, availability and being a relatively low-cost electronic device.

As discussed in section 1, reviewing this thesis thus far has helped to identify a research gap. This being the study and development of intelligent sensing, where the sensing device used can interpret an individual's struggle point and inform an artificial muscle to actuate. Currently, the sensing devices used within artificial muscle technologies require human input such as the heat gun required to actuate the tendril muscle demonstrated by Kanik et al (2019), rely on complex

software algorithms such as that which is used within the onboard controller for spot the dog (Boston Dynamics USA. 2022), or simply need multiple sensors such as the accelerometers and surface electromyography (sEMG) used by both Baraka, A. et al. (2019) and Peng, L. et al. (2013); with the sMEG sensor requiring surface (skin contact). A further drawback to many of the technologies discussed is their commercial availability. This discussion infers a gap in research of integrated sensing technologies, where the study of a sensing device that can accurately map a user's movement in an intelligent manner, without being invasive or needing skin contact to operate is needed. The sensing device should not require the user to set up or interfere with the system, using a global constant as the datum for the sensors measurements will greatly aid the simplicity, integrability and useability of the device. Finally, this device should be low cost in nature, preventing significant cost increases to any system which it is integrated to; vastly improving the commercial availability of the device and/or system. Based on discussion in section 1 with information provided by www.healthcarepro.co.uk (2022), an attempt should be made to keep the sensor below £100 - this will assist with the device's integrability with other systems as the overall commercial value of the system will not be as severely impeded by the cost of the sensor.

In addition to the underdevelopment of sensing devices, an additional research gap has also been identified, this is the issue of powering artificial muscle in a remote manner. This is an important aspect of artificial muscle technologies not only for their mobility, but also for their compatibility with the global requirements of recyclability and renewable energy. Edwin et al (2017) provides the only artificial muscle that can be powered from low voltage electronics, however because of the low voltage there is a compromise in the muscle's strength capabilities. Based on this, to make the development of a renewable energy source a more manageable and achievable task, the focus should be placed on powering the aforementioned sensing device in a renewable manner. The Boston Dynamics (2022) technical document states that Spot the Dog is a battery powered device, which can be operational for around 90 minutes. Once the battery has been used up, then the unit is required to be powered down and charged for a minimum of 60 minutes. This clearly demonstrates the current limitations facing robotics and artificial muscle technologies.

However, when observing the materials research undertaken as part of this literature review, various materials which are influenced by heat have been discussed. Additionally, within this literature review discussions on the Seebeck effect, with referenced technologies such the fabric thermoelectric generator demonstrated by Lund (2020), and heat storing fabrics provided by Po-Chun (2017), provide a foundation from which the use of a renewable energy source can be studied.

3. Methodology

The following section applies knowledge acquired in section 2 to further develop artificial muscle technologies. Based on the findings in sections 2, it is apparent that a plethora of engineering devices, scientific devices, methodologies, materials, and manufacturing processes exist that can be used to aid in achieving the desired outcome of this research. Whilst a brief investigation into muscles and actuators is discussed in this section, what was established previously is that the specific element which requires development and focus is the sensing technologies, specifically the artificial element of this. This research aims to develop a method of sensing motion and an actuation strategy for assistive devices such as wearable artificial muscles. Additionally, this research aims to provide solutions for a renewable energy source local to the wearer. To achieve these aims firstly an evaluation of available devices for sensing and renewable electrical generations will be undertaken, to identify the most appropriate approach to be employed. Secondly, physical prototypes incorporating the adopted devices will be manufactured. Finally, practical testing of these prototypes will be performed, and the data analysed to acquire quantitative conclusions. The following sections provide detailed explanations of the methods and materials employed to facilitate the research aims.

3.1. Design Brief

To attain a guided avenue of pursuit, an established design brief was created. A design brief is a document which outlines the core objectives and details of a design (Team Asana, 2021). Additionally, it explains that the following statements can be considered as key areas of definition and exploration:

- Overview
- Project Scope
- Design Goals
- Target Audience
- Budget and Timeline

Focusing specifically on this thesis, key guidelines of current issues associated with wearable robotic technologies already uncovered within this research needed affirming. It has already been established that limitations relating to the user's comfort in addition to cost have hindered the commercialisation and widespread use of wearable robotics (Babič et al, 2021). Additionally, Martinez-Hernandez et al (2021) provides an insight into the current issues associated with wearable assistive devices; two stand out statements as follows demonstrate the need for an engineered approach to the subject:

- "In wearable assistive devices, there are elements such as low-weight, low-power consumption, battery lifespan and calibration that remain a challenge".
- "The need for personalised and adaptive assistive devices is widely recognised. Adaptivity refers to how devices adapt to changes within their operating environment, such changes might include: user habits, situations, individual preferences, and exogenous changes".

If inspiration is to be taken from discussions in section 5, a design criterion can further be developed based on the existing assistive mobility devices. Observing existing products such as the four-wheeled walker and Zimmer frame, it can be seen that these devices - whilst extremely practical in their design - are not concealable or aesthetically pleasing, in addition to still requiring the operator to have specific level of mobility to manipulate the device. Additionally, whilst foldable versions are available at an additional cost, these products are rather bulky. Observing products such as non-motorised/motorised wheelchairs and mobility scooters these products are typically large units that can also require the assistance of another individual. Furthermore, the retail prices of such items are some the highest out of the available assistance devices discussed. Finally, whilst this critique adds value to the design brief, it is important to understand that these devices are predominantly aimed at older individuals and/or people suffering from waist-down mobility restriction or paraplegia. With the above understanding attained, a visual representation of the overall project intentions was developed utilising the Lucidchart online software, this graphic can be seen in figure 3-1.

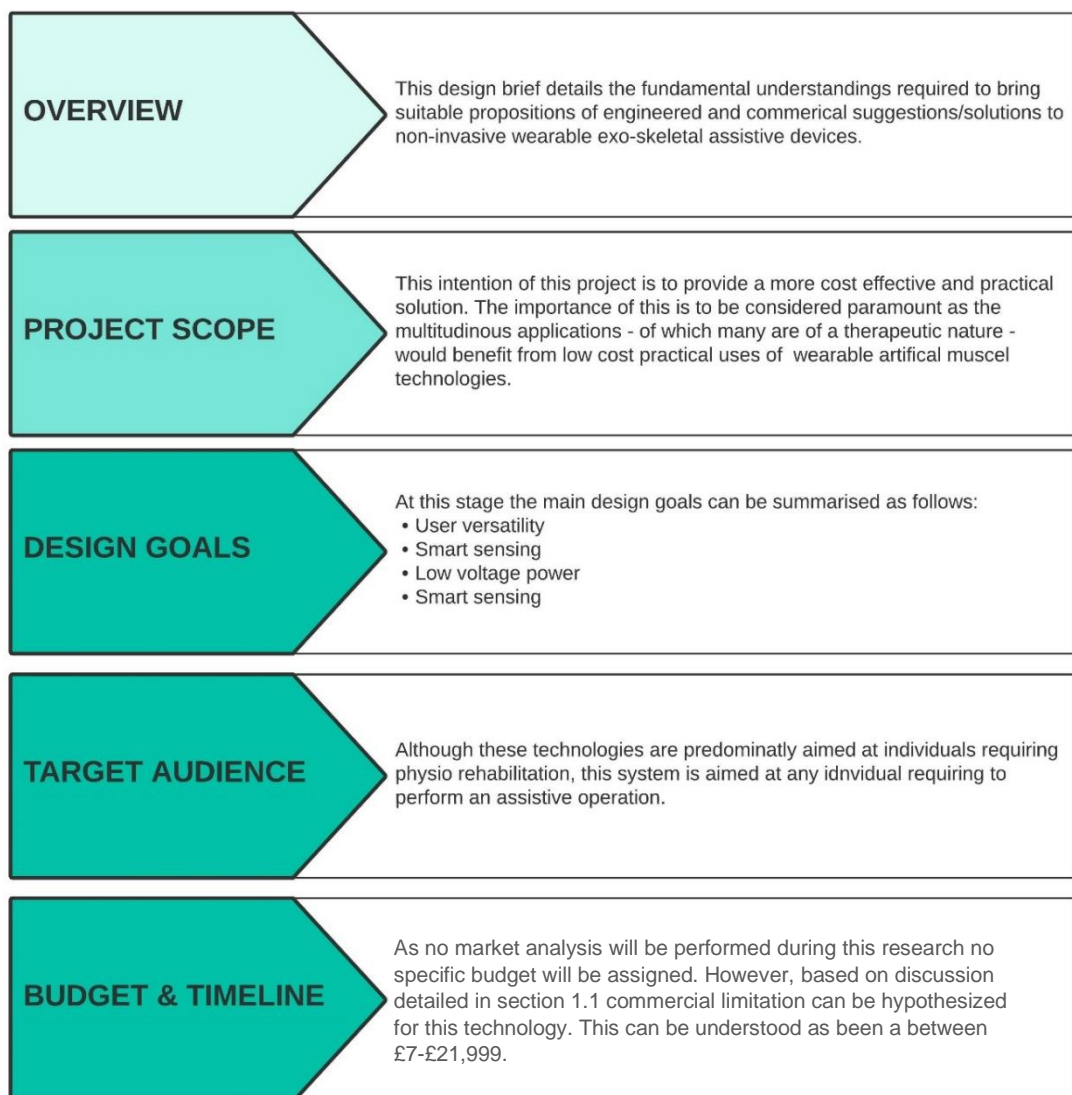


Figure 3-1. Project Design Requirements Graphic

Additionally, using the Lucidchart online software a visual mind map was created to provide a simplistic overview of the ideal development requirements that could aid in achieving the thesis aim; this can be seen below in figure 3-2 with a brief explanation of the defining characteristics listed.



Figure 3-2. Project Mind Map

- Intelligent Sensing** – to enable the maximisation of the assistive elements of the device, the sensing system should incorporate a high level of artificial intelligence which will allow for instructions to be outputted based on circumstances surrounding the operator’s situation. As the potential operations being undertaken by the operator can vary significantly and be performed randomly, the integration of machine learning is not a priority; although each individual will have specific habits, a proposition can be made that the system would gain little benefit from an overcomplicated software system. The design and integration of such a sensing system for muscular assistive device would be extremely beneficial.

- **Compact** – a key design feature of such a device would be the integration of itself with its operator in a non-intrusive or non-invasive manner, with an emphasis on the overall size of the unit. Based on results rendered from section 2, it can be understood that the implementation of newly developed fabrics such as E-fabrics can be utilised. This would allow for circuitry that cannot be wireless to be manufactured in a way that allows interconnection to be integrated into the wearable device. For example, electronic power still remains an element of any circuit that is most reliable when hard-wired; however, if the fabric material discussed in section 2 is considered, then a postulation can be made that low voltage inputs for devices such as sensors can be generated locally from body heat. Finally, such fabrics would allow for the device to be manufactured into a styled wearable garment such as a sleeve.
- **Operator versatility** – as previously identified within this section, the importance of operator versatility is still an underdeveloped element of wearable assistive devices. With this understanding, it is important to focus on a universal design that can attain monitorable information that is common to all operators. However, it is important to understand that a certain level of commissioning may be required, similar to the level of set up required for other smart devices.
- **Commercially viable** – computers can be classed as one of the most important technological developments of the last 50 years, becoming so accessible and integrated into everyday life that human reliance on these devices could be described as detrimental. However, these devices were not always as accessible as they are today; with Comen (2022) informing that the cost of a basic HP 3000 in 1972 was around \$95,000 compared the cost of an Apple MacBook in 2015 being \$1,299. This demonstrates not only how technology can potentially become more cost effective as its developed, but additionally how consumer demand plays heavily into this. Wearable robotics are no different and to date locating information on the cost value of such products is scarce, due to little of these devices being commercially available. This demonstrates a clear need for the utilisation of low-cost components in addition to creating a device that can be produced through lean manufacturing techniques at either a batch or mass production level. If the product can become more cost effective, then there is an opportunity to increase market demand.
- **Low/sustainably powered** – as previously discussed in this section, the implementation of a low/sustainable power source is highly desirable feature to be considered where possible. Developing this element will greatly improve the autonomy and mobility of such assistive devices. Furthermore, if this power source is that of a sustainable type, then this will aid in future proofing the technology.

3.2. Biological Muscle and Skeletal structure

What has been established within this research is that due to current technological restraints - such as the size and mobility of power sources - the underpinning principles for artificial muscle technologies are relatively similar and common across different technologies. A clear example of why the setup of a biological muscle provides the human structure with much more power to weight ratio than what can be comfortably and compactly achieved through engineered devices is discussed below. Considering the lifting operation represented in figure 3-3 and seen in figure 3-4 below, if a load of 215N (22kg) – which Jackson (2022) inform is what is considered an appropriate load for an average healthy adult male - is required to be manipulated from 0° to 150°, at a length of 0.460m which Swisstech (2016) informs is the 50th percentile adult male ergonomic reach dimension), then utilising the horizontal planar value of 90° (point of maximum mass excursion), the minimum torque value required can be calculated as $0.460 \times 215 \sin(90)$ by using the radial torque calculation of $\tau = rF \sin\theta$ which gives a required torque of 98.9 N/m at $\theta = 90^\circ$ to achieve an equilibrium state.

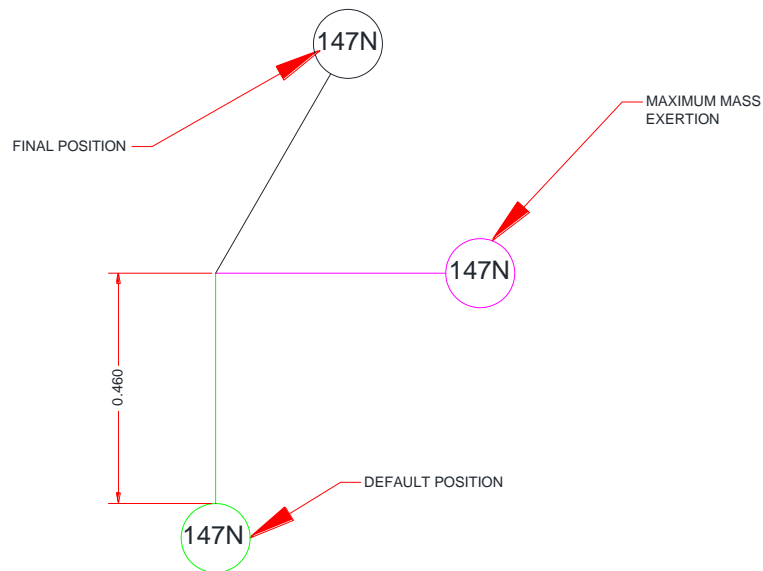


Figure 3-3. Schematic Bicep Curl Analysis

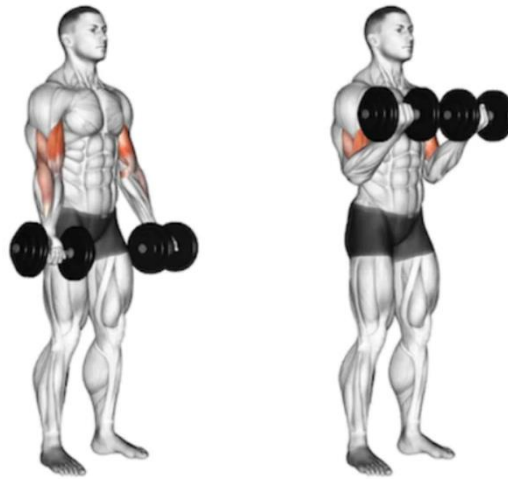


Figure 3-4. Bicep Operation Graphic

Understanding the above example, it is clear to see that the tendon connecting the muscle to the bone is located close to the elbow joint and far away from the load bearing point. It is archetypal that when systems of this nature are designed by engineering methods it is done in a different manner. For example, on closer analysis of figures 3-5 and 3-6, one can observe that the point of reaction or “shackle point” between the horizontal structure and angular structure is placed either closer to the loading point or distributed across the horizontal structure. However, Jackson et al (2019) provided a sourced image (figure 3-7) which slightly contradicts this understanding by visually demonstrating the use of the brachioradialis (forearm muscle) providing additional support to the lifting operation.

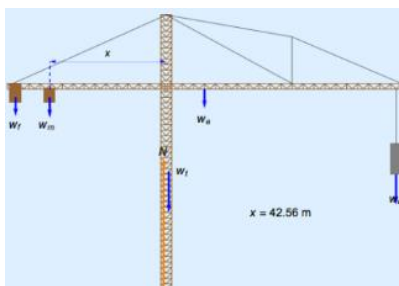


Figure 3-5. Tower Crane Schematic. Zeleny (2011)

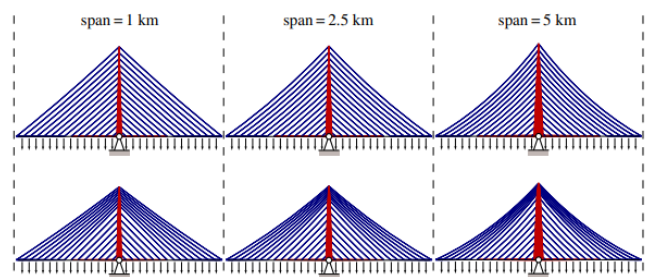


Figure 3-6. Suspension Bridge Graphic. Fairclough, et al (2018)

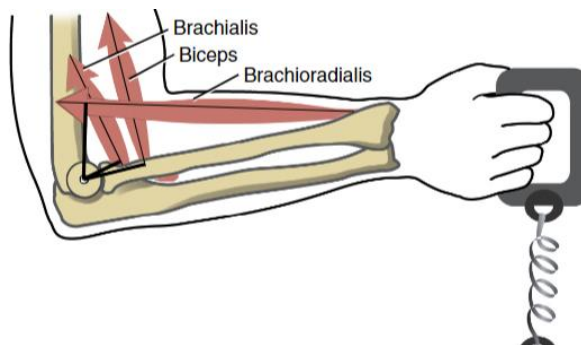


Figure 3-7. Tendon Schematic. Jackson et al (2019)

3.2.1. Mathematical Analysis Methodology

A mechanical evaluation of the radioulnar system can be understood by using the formulas detailed within table 3-1.

Table 3-1. Bending Moments Formula Table

Description	Formula/Parameter	Citation
Bending Moment	$M = WL$	C Matthews (2012)
Second Moment of Area (inertia)	$I_{NA} = \frac{\pi D^4}{64}$	C Matthews (2012)
Deflection	$\delta = \frac{WL^3}{3EI}$	C Matthews (2012)
Elastic modulus of Ulna and Radius	Ulna 4.5GPa and Radius 3.67GPa	D Singh (2019)
Anteroposterior radioulnar mean average (standard deviated) diameter	18.626 ±1.78 mm	P Puchwein, et al (2013)
<small>W=Applied load, L=Suspension length, D= Diameter, I=Second moment of area, E=Youngs modulus of elasticity</small>		

It is important to understand that for this evaluation specific assumptions have been made - the first being that the operation of the radioulnar joint system is based on a “cantilevered” beam, with a point load analysis approach as illustrated by mechanicalc.com (2022) in the form of a free body diagram (as seen in figure 3-8). Additionally, due to a specific thickness of the ulna and radius being difficult to attain, the second moment of area has been based around a circular beam section calculation rather than a thin-walled tube section. Finally, although within the system being observed, there are two individual bones the radius and the ulna, these two bones are joined at what is known as the anteroposterior radioulnar joint and therefore the following mathematical analysis is based on understanding this specific joint not the individual bones.

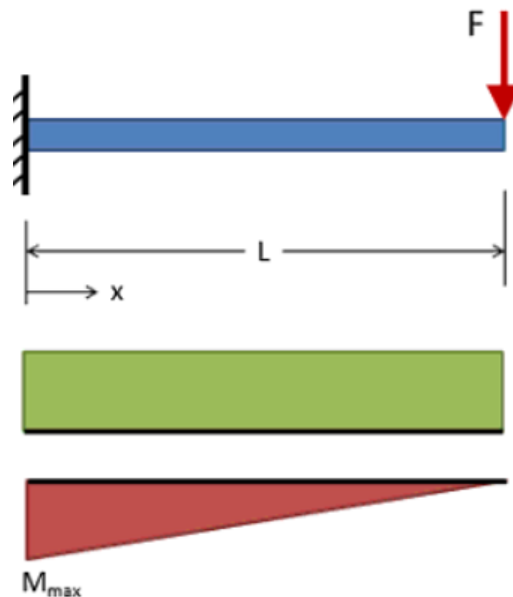


Figure 3-8. Cantilever Beam Free Body Diagram. Mechanicalc (2022)

To gain a brief understanding of the effects of torque on the anteroposterior radioulnar joint, four points were selected over the specified length of the arm to imitate moving the equilibrium point or “muscle support” from left to right - this point can be understood as the point at which the maximum force is being applied and balanced. Additionally, this analysis has been modelled at a period when the forearm would be perpendicular to the bicep. The points specified at ¼ of total length, ½ of total length, ¾ of total length and total length. This has been visually demonstrated in figure 3-9.

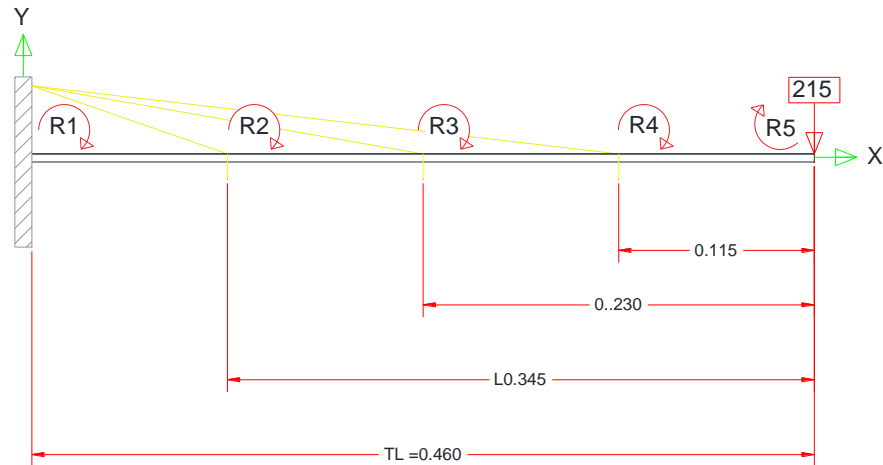


Figure 3-9. Bicep Free Body Diagram

3.2.2. Mathematical Analysis Results

The results rendered from the analysis can be seen in Table 3-2, with a visual force map provided in figures 3-10, 3-11, 3-12 and 3-13. The mathematics performed was done with the assistance of Microsoft Excel software, hand calculations and further checks with online beam calculators; the process of the calculation can be seen in appendix A.

Table 3-2. Bending Moments Results Table

Mechanical Evaluation								
REF	Bending Moment					Deflection		
	W (N)	L (M)	M (N/M)					δMax (M)
			R1	R2	R3	R4	R5	
R1	-215	0.460	0				-98.9	-0.14451747
R2	-215	0.345		0			-74.175	-0.060968308
R3	-215	0.230			0		-49.45	-0.018064684
R4	-215	0.115				0	-24.725	-0.002258085

*R1 Length = Total Length, R2 Length = Total Length - ¼,
 R3 Length = Total Length - ½, R4 Length = Total Length - ¾,*

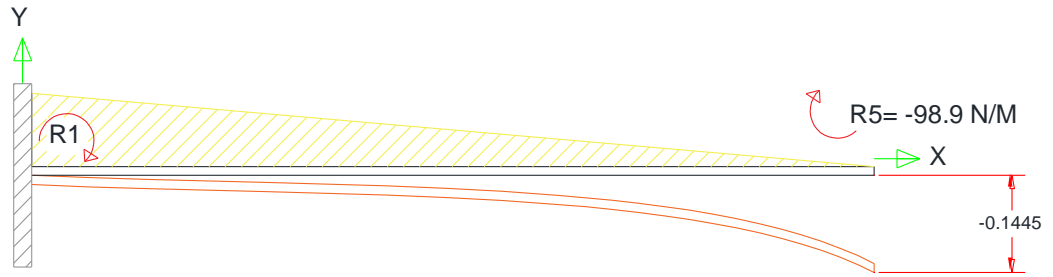


Figure 3-10. Point R1 Bending Moment Force Map

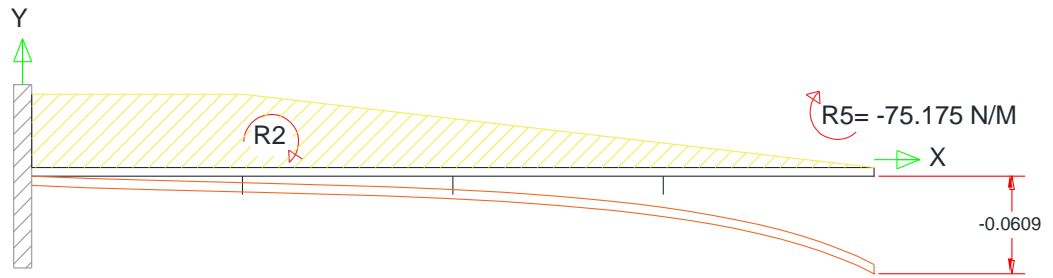


Figure 3-11. Point R2 Bending Moment Force

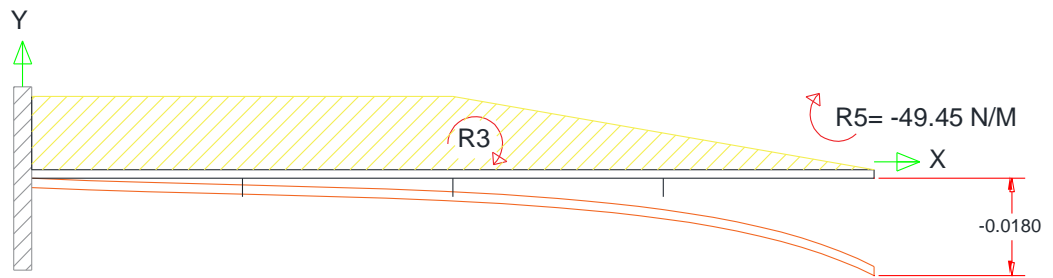


Figure 3-12. Point R3 Bending Moment Force

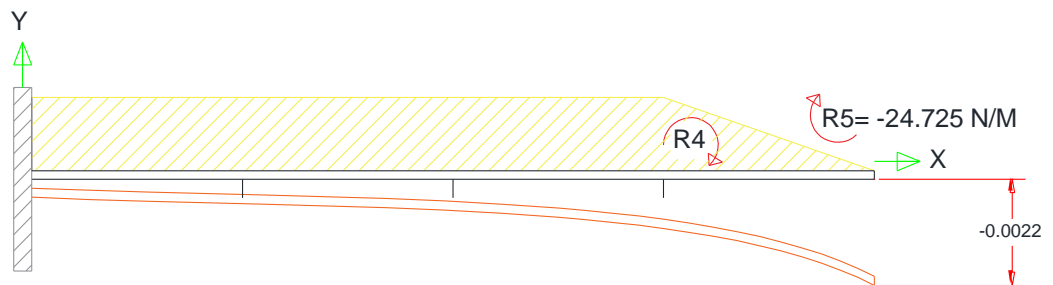


Figure 3-13. Point R4 Bending Moment Force

From the data displayed above, a conclusion as to the distinctive nature of biological muscles and the skeletal structure can be attained. Whilst a definitive location for the tendon to bone joint for the bicep cannot be accurately placed, based on the example Jackson et al (2019) provides above in figure 3-7, what can be speculated is that the location is between 0.460m and 0.345m from load the point region.

Firstly, if the bending moment is considered, it can be understood that as expected, the longer the distance from the point of $R_x = W$ where the reaction point is equal to zero and the system is cantilevered, then the higher the point loading force impacts the system, thus requiring more upward force to achieve an equilibrium state. By moving the contact point of the tendon to skeleton, then the force exerted by the same point load is reduced; furthermore, this reduction in force directly relates to, and is proportional to the distance. For example, R4 which is a total of 0.115m from the point of load, is 25% of the total length; the force exerted at this length is -24.725n/m which is also 25% of the maximum force of -98.9n/m. What is clear from the force diagrams represented in figures 3-10, 3-11, 3-12 and 3-13 is that when the point of tendon connection is moved, then the reaction force around R_x will remain at zero, however the force is now evenly distributed between R_x and the pivot point.

Observing the deflection of the system is where the mathematics appears to become unreliable - this is due to the deflection figures rendered. It is visible that at $L=0.460m$ the maximum deflection will be 0.144m - this value is extremely high. Additionally, a reasonable assumption can be postulated that in practical terms this does not happen as in no cases does an individual's radioulnar deflect by such a value without shearing completely. The results rendered are interesting because of these high values, it can be interpreted that this is where the advanced mechanics of biology are demonstrated, providing an understanding the mechanics and properties of biological muscles are difficult to achieve with the current technological limitations. However, these high values could also be attributed to the lack of accurate information available surrounding the human anatomy, specifically the mechanical evaluation of it. Finally, this could also be attributed to mathematical errors.

Based on the muscle mechanics information collated and discussed thus far in the research, it is clear that the information has deduced that the development of exoskeletal artificial muscles is at a point where the quantity of technologies is increasing rapidly in small scale settings, demonstrating the difficulty in bringing a commercially viable solution to the market. Additionally, after performing the research above it can be understood that a paradigm shift in the research will now focus on the development of sensing technologies.

3.3. Sensing Systems

As discussed previously in this thesis, the methodology associated with informing each artificial muscle to signal is an aspect that is not prioritised due to many of the artificial muscles being relatively new technology that is still in the small-scale testing phase. This is with the exception of the FESTO fluidic muscle which, as discussed earlier, operates via the use of large signalling systems incorporating external sensors and a PLC. With this discussion considered it can be proposed that an effective avenue of research to pursue would be the development of the signalling system to increase the autonomy of the current muscle technologies available. Table 3-3 illustrates a GROW model constructed to surmise the current state and progression plan.

Table 3-3. Sensing System GROW Model

Goal	Reality	Options	Way Forward
<p>True artificial muscle technology, incorporating a control system indicative of the biological central nervous system (CNS). The signal required to inform the muscle activation should incorporate some basic level of “artificial Intelligence” where there is no requirement for the operator to make a conscious decision for the muscle to actuate.</p>	<p>The current reviewed artificial muscle technology does not inform of any locally mounted feedback sensors or any kind of artificial intelligence to enable the muscle to work independently of the operator. This means the muscle is not truly artificial due to the conscious input required.</p>	<p>The use of smart textiles to enable an autonomous electrical signalling system capable of instructing an actuation. Utilisation of onboard sensors to provide feedback to a small controls system providing a turnkey controls solution to the muscle.</p>	<p>To perform further research into the use of a newly developed textile which can store heat from human skin.</p>

3.3.1. Sensing, signalling and logic

So far what has been derived from this research is what appears to be the most neglected element of artificial muscle technologies - the methodology of sensing and signalling an actuation with the use of independent assistive logic which is indicative of biological muscles and helps to support the adjective “assistive” in the description of assistive artificial muscle systems. As found in section 2, many currently available systems require human input to provide the logic required to initiate an actuation, meaning that there seems to be minimal artificial logic within these systems. It is important to recognise that this is not necessarily a drawback, as this does allow human control over the movement, preventing false actuations - something which is important when it is to be considered that typically the intention behind these systems is to provide additional strength capabilities. If these systems were to accidentally activate, then there is a serious risk of injury to the operator, both empty and with a laden load.

However, if the critical analysis of section 2 is viable, then autonomous artificial muscle technologies are not only applicable but also extremely important for providing assistance to individuals with debilitating illness. In these cases, it can be postulated that rather than enhanced strength capabilities, the individual would better benefit from autonomy. Although the critical analysis in section 2 discusses serious illness such as cerebral palsy (CP) and motor neurons disease (MND), if a system were to be designed for an individual with either advanced CP or MND, then the artificial control would need to be significantly advanced and most importantly autonomous. It can be hypothesised that a system of this nature would require invasive integration into the operator using advanced and currently experimental technologies such as the brain interface technology designed by the Elon Musk-owned company, Neuralink.

Remarks by Ashraf (2018) hypothesises that the implementation of more robotic exoskeletons would be a useful tool not only for rehabilitation but additionally for the improvement of physical activity. If this statement is considered then there appears to be a clear application for a compact muscle technology that is non-invasive but remains autonomous and artificial in the use of signalling logic, allowing for a rehabilitative and assistive approach.

In addition to illness rehabilitation, a system like this could also be used in the space sector, allowing for earth gravity replicative resistance to be simulated, aiding in maintaining the working order of an individual’s muscles on a day-to-day basis. To suitably design a system like this, these two key parameters must be developed as follows: specific sensing technology, and an understanding of when the sensor should signal an actuation. It is important to understand that whilst the aim is to develop an autonomous artificial operational system, commissioning activities specific to each individual operator would be required to ensure efficient operation of such system.

Understanding when an actuation is required requires an understanding of how the human cognitive systems operate, which is both complex and still speculative in places. It can be described that volitions are not within the chain of causation, that volition is not the cause of voluntary actions as support by Huxley (1874) and republished by Anger (2009).

In 1985 American scientist Benjamin Libet appeared to have provided evidential proof of Huxley's statement with a free will experiment test. Subjects were asked to press a button and note down the time at which they believed they were consciously aware of this activity; these participants were also being monitored via EEG electrodes. The results consistently demonstrated unconscious brain activity associated with the task around half a second before the task took place - Libet called this the "readiness potential". Willing an act can be associated with interpreting though as the cause of the act as informed by Wegner and Wheatley (1999)

This statement is something that the Libet experiment appears to support. However, whilst being widely acknowledged within the scientific community, there is no unanimous acceptance of the outcomes of Libet experiment. Taylor (2019) discussed many of the issues relating to the experiment such as the fact that the participants were required to record their own response, stating noting that there may be a delay between the impulse of action and the actual documentation of it. For this research, what the aforementioned experiments provide, is a brief understanding of the complexities associated with developing an artificial autonomous sensing system.

3.4. Development Test 1 - Heart Rate and Blood Oxygen Level monitoring

It is common understanding that when an individual performs physical activities such as running, swimming, or weightlifting; the individual's heart rate will increase from the resting rate of between 60-100Bpm as specified by National Health Service UK (2021) to a target illustrated by the American Heart Association (2021) in figure 3-14. Additionally, it can be understood that a chemical change in oxyhaemoglobin during exercise does take place; Hüseyin et al (2018) provides an image (figure 3-15) that not only supports a change in oxyhaemoglobin during exercise but also illustrates the changes in heart rate.

Age	Target HR Zone 50-85%	Average Maximum Heart Rate, 100%
20 years	100-170 beats per minute (bpm)	200 bpm
30 years	95-162 bpm	190 bpm
35 years	93-157 bpm	185 bpm
40 years	90-153 bpm	180 bpm
45 years	88-149 bpm	175 bpm
50 years	85-145 bpm	170 bpm
55 years	83-140 bpm	165 bpm
60 years	80-136 bpm	160 bpm
65 years	78-132 bpm	155 bpm
70 years	75-128 bpm	150 bpm

Figure 3-14. Recommended age/maximum heart rate. American Heart Association (2021)

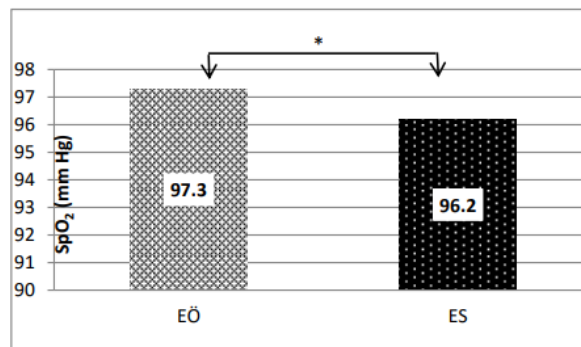


Chart 1. Pre-exercise and Post-exercise SpO₂ Values

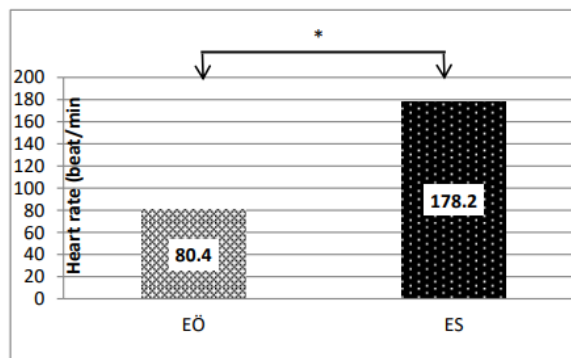


Chart 2. Pre-exercise and Post-exercise Heart Rate Values

Figure 3-15. Oxyhaemoglobin and heart rate during exercise. Hüseyin et al (2018)

With the above considered, it was decided that a test would be performed to understand the viability of whether the oxyhaemoglobin saturation level (SpO2) could be monitored to understand a change which would correspond with the effort of the individual's muscle. Typical blood oxygen saturation should be between 95-100% as stated by Asthma and Lung (2020).

3.4.1.Heart Rate and Blood Oxygen Level Monitoring Methodology

Recording of the oxyhaemoglobin saturation level (SpO2) was executed via the use of a Contec CMS50D pulse oximeter as seen in figure 3-16. The weighted equipment used was a mixture of Matrixfitness and Jordanfitness gym equipment located at the Huddersfield branch of TruGym. To attain this data a simple protocol was established, which is detailed out and illustrated below with figure 3-17 demonstrating the data capture form to be completed as part of the testing.



Figure 3-16. Contec CMS50D pulse oximeter

BLOOD OXYGEN TEST DATA CAPTURE SHEET									
Participant No.:			Date:			Age Range:			0-15, 16-24, 25-34, 35-44, 45-54, 55-64, 65-74, 75-84, 85+
Heart Rate at Rest (BPM):					Blood Oxygen Level at Rest (SpO2):		95% -		
Exercise	Muscle Actuated	Mass (Kg)	Set No.	Rep QTY	Start Heart Rate (BPM)	Finish Heart Rate (BPM)	Start Blood Oxygen Level (SpO2)	Finish Blood Oxygen Level (SpO2)	

Figure 3-17. Testing Procedure Data Capture Sheet



3.4.2. Testing procedure


To ensure the test is performed in a controlled and organised manner, the following procedure was adhered to:

1. Fill in required information located on Blood Oxygen Test Data Capture Sheet.
2. Measure and record SpO2 and heart rate on index finger of left hand before exercise is performed. Do not remove pulse oximeter.
3. Record muscle(s) being exercised, mass being manipulated, the set and repetition quantity.
4. Perform exercise and perform visual inspection of pulse oximeter during exercise.
5. Measure and record SpO2 and heartrate on index finger of left hand immediately after exercise is performed.

As this was a viability test to understand whether the discussed would be a suitable avenue of investigation, the testing was simplistic in its nature and tight control conditions were not a priority. The testing was also performed during a weekly exercise regime that was undertaken on Sunday the 24th of April 2022; this specific session focused on the following muscle groups: bicep muscles, major and minor pectoralis. The data collated was not recorded over a time weighted average but rather task based, focusing on specific muscle operations. The exercise operations specific to this research performed are listed below in table 3-4.

Table 3-4. Exercise Operation Table

Exercise	Focussed Muscle	Image
Dumbbell Bicep Curl	Bicep	 <p><i>Figure 3-18. Bicep Curl. Yeung (2022)</i></p>
Dumbbell Hammer Curl	Bicep	 <p><i>Figure 3-19. Hammer Curl. Yeung (2022)</i></p>

<p>Seated Barbell Preacher Curl</p>	<p>Bicep</p>	 <p><i>Figure 3-20. Seated Preacher Curl (Barbell). Yeung (2022)</i></p>
---	--------------	---

3.5. Development Test 2 – Radiative (Wireless) Power Generation

One identified issue with existing actuation systems as previously discussed is the power supply methodologies. With the exception of the actuation device, controlling elements of the system can be powered from a low voltage source. For example, if specific componentry such as accelerometers and raspberry pi logic controllers are used then these require little power, as demonstrated in table 3-5.

Table 3-5. Power Requirement Table

Description	Power max (V)	Current max (A)
Accelerometer	3.6	0.00035
Raspberry Pi Pico	5.5	0.3
Total	9.1	0.30035

From this information It can be considered that low power battery technology can be utilised for powering the sensing system such as a standard +9VDC battery. However, to further increase wearability and reduce the environmental implications of the sensing system; a hypothesis developed earlier in the research suggested the use of body heat to power the unit. Typically, heat can be converted from heat energy to electrical energy via a thermoelectric generator (TEG) or Peltier module via the seebeck effect, and example of a TEG can be seen in figure 3-21.

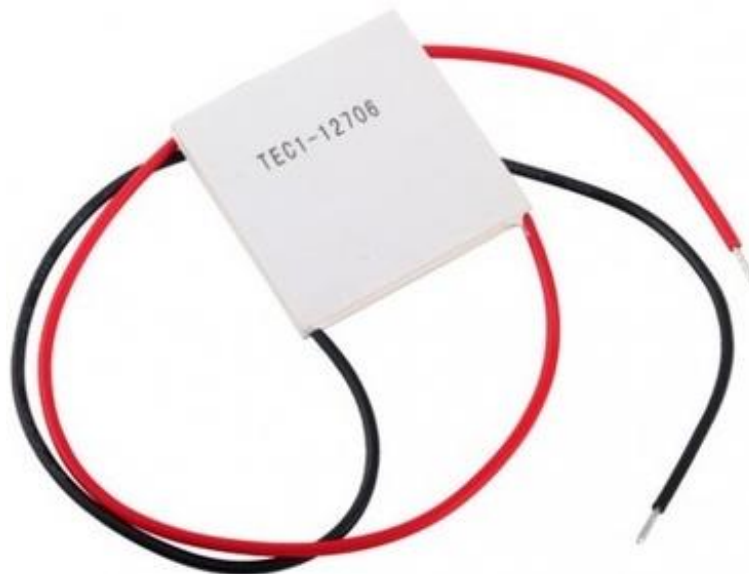


Figure 3-21. TEG Peltier Module. theplantbot.com (2019)

However, based on the research performed for section 2 with the development of new materials such as the dual-mode textile for human body radiative heating and cooling, a postulation can be made that further studies into the utilisation of this material as a thermoelectric generator could be performed. With advancements in E-fabrics that can facilitate the medium to which a printed circuit can be applied, then it could be a possibility that the semiconductors used for to assist the Seebeck effect could be applied direct to the fabric.

Additionally, it can be proposed that fabric could be a garment style such as a sleeve or clothing item that draws the heat from multiple places at once, alternately this could be a specific piece of fabric that is strategically located in a “hot spot”. It can be seen in figure 3-22 from the research performed by Lee et al (2019) that the body does have specific areas where the radiative heat is higher. To understand whether this methodology of signal generation is a viable solution that could be developed through further research, a brief bench top test was performed.

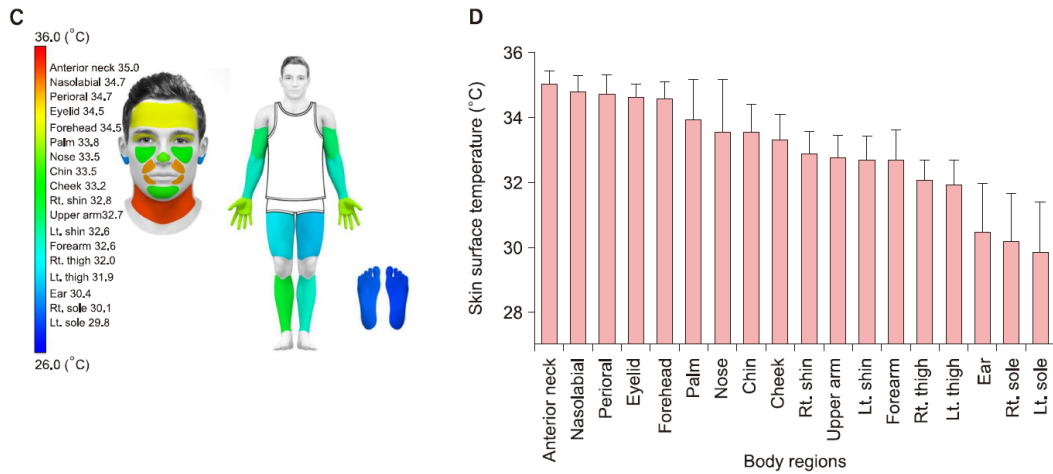


Figure 3-22. Body Heat Hot Spots. Lee (2019)

3.5.1. Radiative (Wireless) Power Supply Viability Testing

A total of six test variants were created and performed to attain a small but varied collection of data, utilising two different wiring principles in addition to increasing the temperature differential in line with the Seebeck principle with cold frozen granite blocks. The test variants are detailed in table 3-6 below and were performed three times.

Table 3-6. Test Variant Table

Test No.	TEG Qty	Wiring = Series	Wiring = Parallel	Granite Block
1	1	N/A	N/A	No
2	3	✓	✗	✗
3	3	✗	✓	✗
4	1	N/A	N/A	✓
5	3	✓	✗	✓
6	3	✗	✓	✓

The TEGs were applied to the inside of the left forearm in a linear pattern, no specific spacing was applied, the TEGs were simply placed as left middle and right with the datum being taken from the elbow joint. The TEGs were held in place by microporous medical tape, which was wrapped once around the forearm perpendicular to the connecting wires, this can be seen in figure 3-23.



Figure 3-23. Fitted TEGs

To understand the most beneficial methodology of connecting the TEG's together two wiring techniques were tested, these being the series wiring method and the parallel wiring method. A Schematic example of both methods are illustrated in figure 3-24 and 3.25.

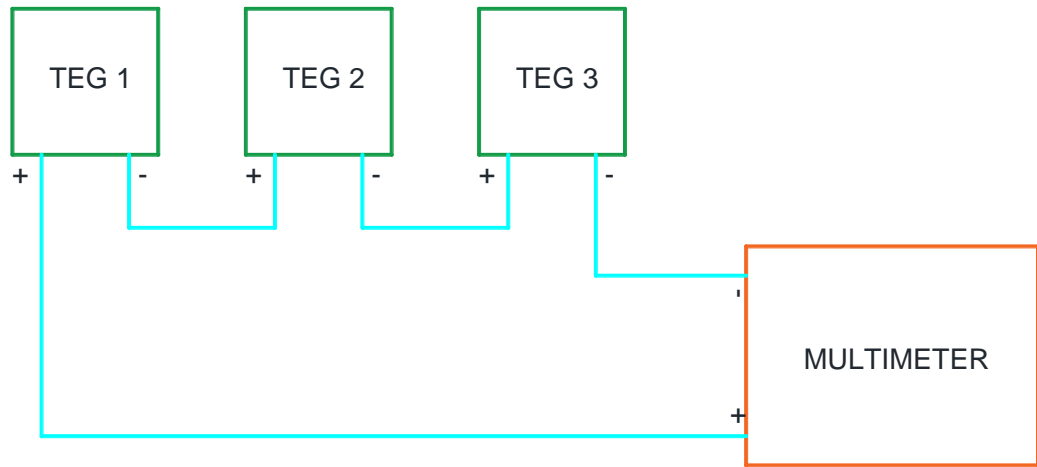


Figure 3-24. TEG Series Wiring Schematic

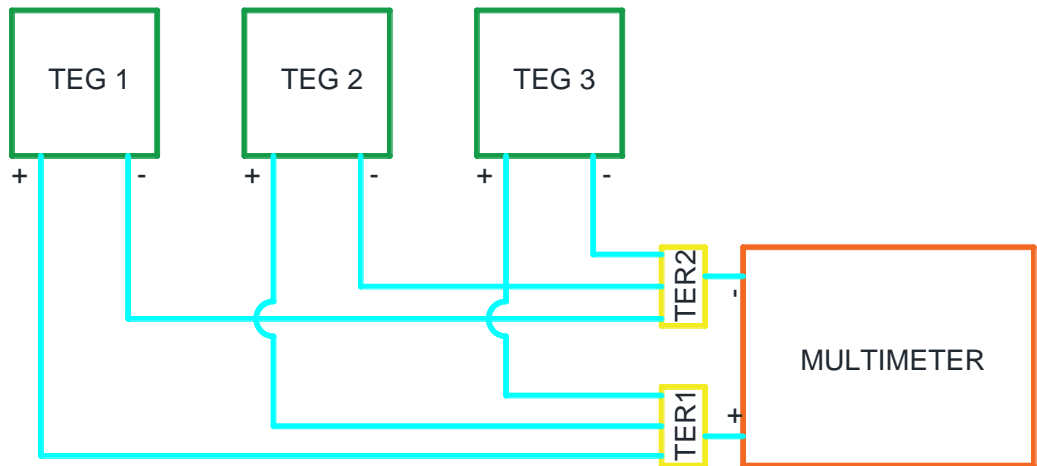


Figure 3-25. TEG Parallel Wiring Schematic

An attempt to control the ambient temperature was done via ensuring the test room heating radiator was turned off, additionally all windows and doors remained closed throughout the testing to prevent turbulent movement of air or accidental induction of external air. As the ambient temperature is a monitorable variable the temperature was noted at the beginning and end of each test and can be considered as having a small influence on the voltage output of the TEG. The ambient temperature was monitored via the room thermostat (figure 3-26). However, during this testing no live temperature monitoring of the skin surface temperature was recorded.

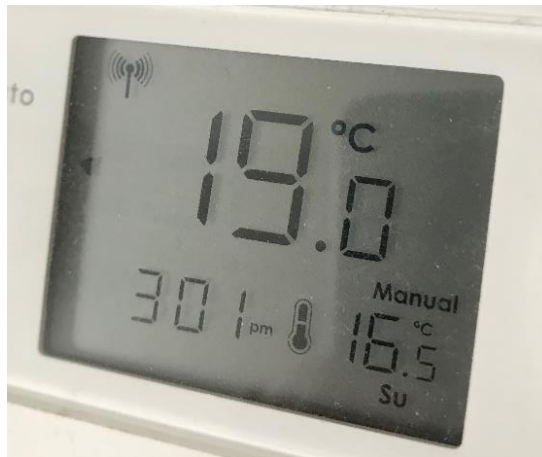


Figure 3-26. Room Temperature Monitoring Unit

To create a severe temperature differential, which would allow an understanding of the implications of implementing external cooling to the TEG, it was decided that frozen granite blocks would be used. These blocks would aid in preventing a quick and unstable temperature rise from that would occur when using ice, in addition, the phase change back to a fluid could potentially cause electrical issues. These were the factors guiding the decision to use cooled granite rather than ice as a method of providing a substantial temperature differential. The block which measured 20mm (W) x 20mm (D) x 20mm (H). The blocks were stored at -19°C for 24 hours, during transportation they were stored in an ice filled thermal contained to aid in reducing heat gain from external sources. Each TEG was fitted with a single block that was centrally located within the area of the TEG, and then secured in place with masking tape, this can be seen in figure (3-27).

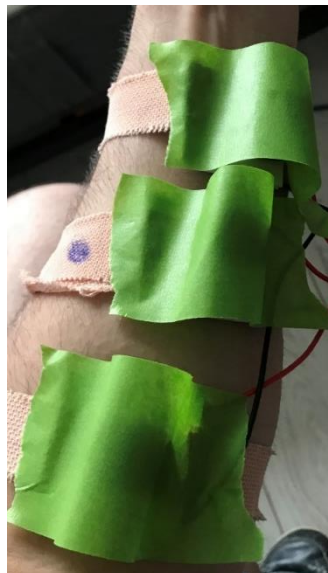


Figure 3-27. Granite Blocks Fixed in Place

In an attempt to establish a foundation from which further research can be build it was important to not only understand the outputted voltage and how the changeable parameters affected this, but it was also important to gain an understanding of the continuity of the signal, if the signal recorded was unreliable with large fluctuations, then this could pose sever challenges. With this understanding each test was performed over a five-minute time period, this specific duration was selected to keep the testing small scale as its intention was to understand the viability.

3.5.2. Testing Procedure

To ensure the test is performed in a controlled and organised manner, the following procedure was adhered to:

1. Turn multi-meter 2 V⁻. (Figure 3-28)
2. Start stopwatch at 5 minutes.
3. Record output voltage and ambient temperature.
4. After 1 minute Record output voltage in capture spreadsheet. (Figure 3-29)
5. After 1 minute Record output voltage in capture spreadsheet.
6. After 1 minute Record output voltage in capture spreadsheet.
7. After 1 minute Record output voltage in capture spreadsheet.
8. Record output voltage and ambient temperature.



Figure 3-28. Multi-meter

Title								
Test Number	Min 0 (V)	Min 1 (V)	Min 2 (V)	Min 3 (V)	Min 4 (V)	Min 5 (V)	Start Amb Temp (°C)	End Amb Temp (°C)
1								
2								
3								
4								
5								
6								

Figure 3-29. Data Capture spreadsheet

It is important to understand that the tests performed were not done under strict laboratory conditions where temperature and humidity are controlled to highly accurate levels, however as discussed above there were specific restrictions enforced to aid the reduction of deviating variables such as the ambient temperature. One additional restriction was the reduction of movement, to attain a default radiance understanding the subject was in a standing position with their forearm extended vertically downwards in a relaxed manner. Keeping the arm in this position would prevent operator fatigue and aid in reducing heat gain due to movement, this can be seen in figure 3-30. Nevertheless, it can be postulated that as the intention is to understand the viability for the technology being investigated to be used within wearable devices, this testing is almost

representative of real-world applications and thus the results rendered could be considered an almost worst-case scenario.



Figure 3-28. Arm Position During Testing

3.6. Development Test 3 – Accelerometer Motion Sensing

Based on the literature establish in section 2, it can be understood that to design a device which will not only allow any operator to use it but will also have a accuracy and repeatability, a monitorable change during muscle actuation - that is universally applicable to all operators, in addition to being reliable and non-fluctuating - needs to be established. Whilst there are many methods that could be used from a biological perspective, for the purpose of this research the decision has been made - based on the research showcased in section 3.5 to pursue the use of an external variable, in this case Newton's second law of motion expressed as $f = ma$. With the understanding of research direction being clarified as that of using motion to attain the relevant required data, the starting point for development was to understand existing devices that apply similar technology. Smart technology can be traced as far back as 1975 with the release of the X10 home automation platform informs Stanley (2021). However, over the last 20 years the commercialisation of smart devices has allowed for items such a smart phones, interactive tables, fitness trackers etc. Commonly smart phones and fitness trackers such as the Apple Watch or Fitbit devices are used during activities of motion and have the ability to perform data monitoring based on feedback from an internal sensor, typically an accelerometer.

This information is confirmed by Apple Inc (2022) which states that all iOS devices have a three-axis accelerometer, this is further supported by Fitbit (2022) who also inform that all Fitbit devices use a 3-axis accelerometer which allows the device to determine the frequency, duration, intensity, and patterns of the wearer's movement. From the above information, it can be understood that current devices use accelerometers to monitor the three axes of which in turn can be used to track and monitor motion. A hypothesis conceived during the initial design stages of this research suggested the use of motion to provide live monitoring feedback during actuation. This proposed system is illustrated in the schematic figure 3-31.

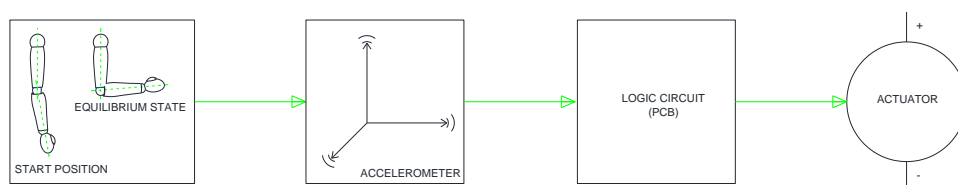


Figure 3-29. Basic Motion Monitoring Schematic

By using the motion created as a result of the actuation, the monitorable variables that can be recorded can be limited to values that are simple to interpret in addition to being repeatable with different operators. A logic process flow can be seen in figure 3-32 which provides a detailed overview of not only how the system works but additionally where specific components are required to perform. To fully understand the operational process of the hypothesised system, a brief overview of the anticipated hardware components which will be required has been listed and described in table 3-7.

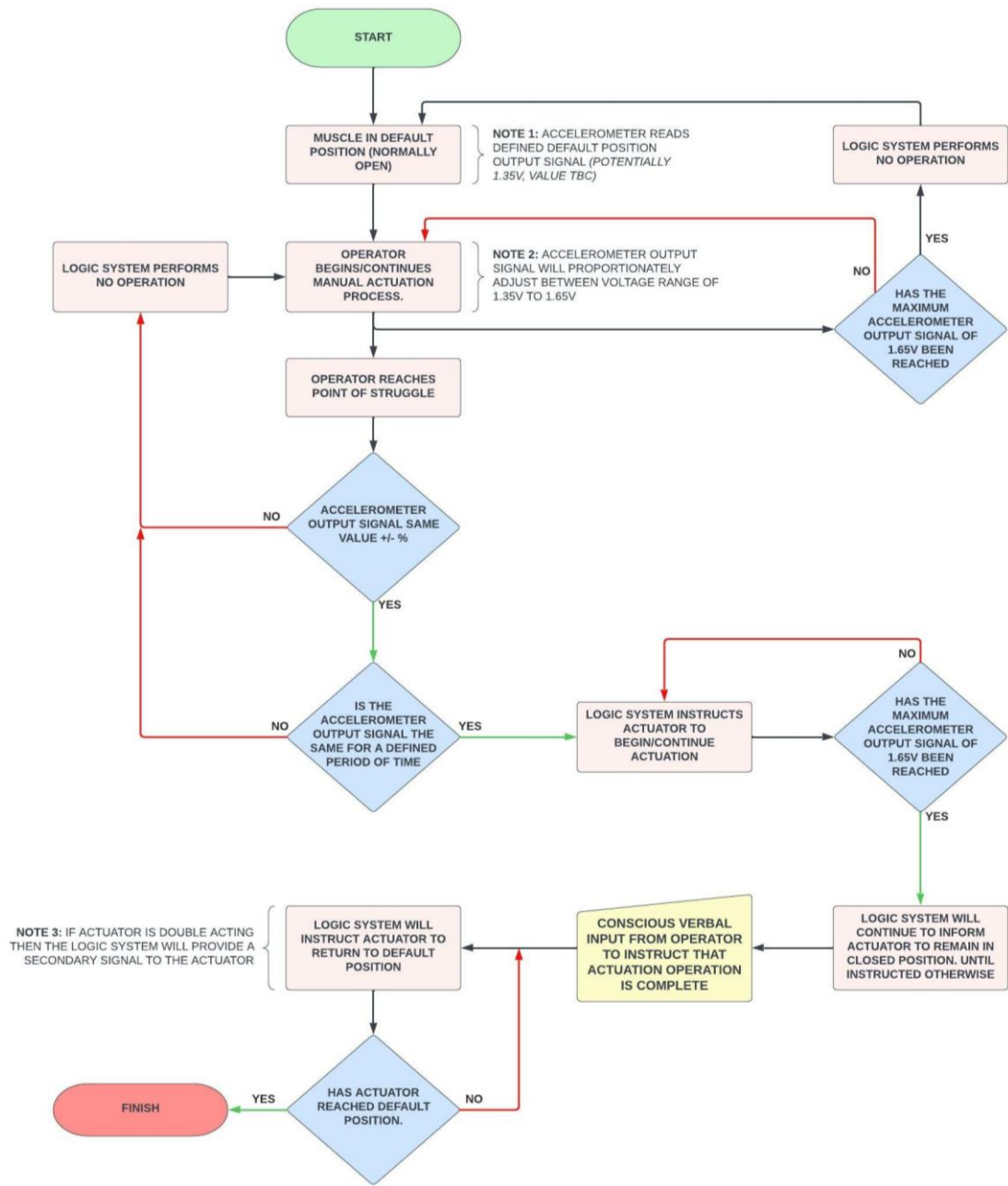
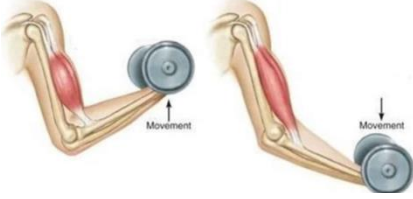
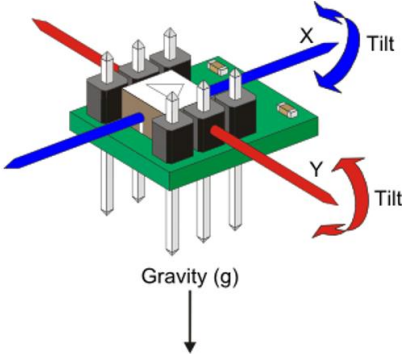
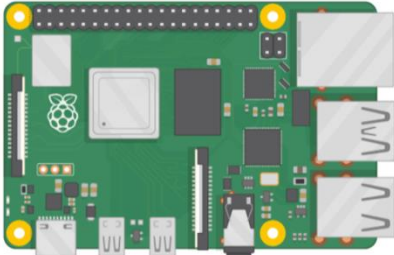
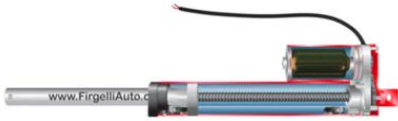
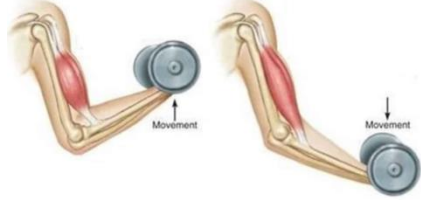
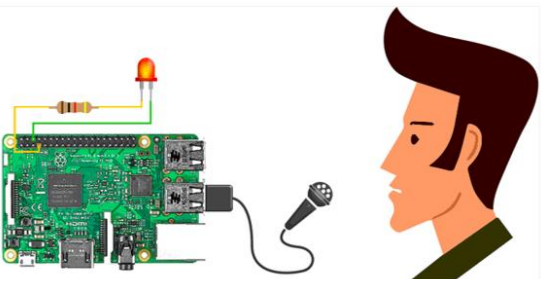


Figure 3-30. Motion Monitoring Process Flow

Table 3-7. Hardware Description Table

No.	Comments	Image
1	<p>During the actuation operation the user will reach a point of struggle at which the determined motion variable being monitored will equate to either 0 and or a specified \pm tolerance. A time delay may be required to prevent accidental actuation.</p>	 <p><i>Figure 3-31. Bicep Actuation Direction of Movement. Campbell (2022)</i></p>
2	<p>The accelerometer will be remotely located from the printed circuit board (PCB) in a suitable defined location, this location must allow for the most accurate results to be attained providing either a continuous linear or tangential motion to be performed in the vector of the muscular actuation. The output of the accelerometer will be an electrical signal which will vary in proportion with the motion applied.</p>	 <p><i>Figure 3-32. Accelerometer Graphic. Papoutsidakis (2016)</i></p>
3	<p>The outputted signal from the accelerometer can be evaluated by a logic system. The controls hardware printed circuit board can be located away from the operating muscle and be interconnected with other componentry through routed cabling.</p>	 <p><i>Figure 3-33. Raspberry Pi Graphic. Raspberrypi.org (2022)</i></p>
4	<p>The input/output module of the logic system will then inform the actuation device to perform a contraction or extension to the point of its dimensional limit, at which point it will stop. This sensing system can provide accommodation for a multitude of actuation devices.</p>	 <p><i>Figure 3-34. Linear Actuator Graphic. Fircelli Automations Team (2020)</i></p>

5	<p>Once the actuation has taken place and the manipulated mass in its secondary position, the system will require operator input to provide the release instruction. This is to allow the operator to hold the mass in place for a time which suites their discretion.</p>	 <p><i>Figure 3-35. Bicep Actuation Direction of Movement. Campbell (2022)</i></p>
6	<p>A device that would provide the least amount of concentrated effort for an operator would be a voice command module. This would allow any operator to vocally inform the system that the lifting operation is complete, and all components can be returned to their default state.</p>	 <p><i>Figure 3-36. Raspberry Pi Voice Module Graphic. Mahesh (2016)</i></p>

3.6.1.Existing Technologies

Similar to the procedure performed within the literature review, to understand what technologies already incorporate this method of sensing, a research review was performed which did indeed render results utilising accelerometers to detect motion for assistive devices. These technologies are briefly explained below.

a) Applications of Wireless Sensor Networks in Fall Detection for Senior People

The technology demonstrated in figure 3-39 was developed by Wernhuar, C and Hsin, H (2011) and features a wearable unit housing circuitry system which is inclusive of an accelerometer; this then allows geometrical position of the operator to be continuously monitored. In contrast to this thesis, this technology is utilised for fall detection.

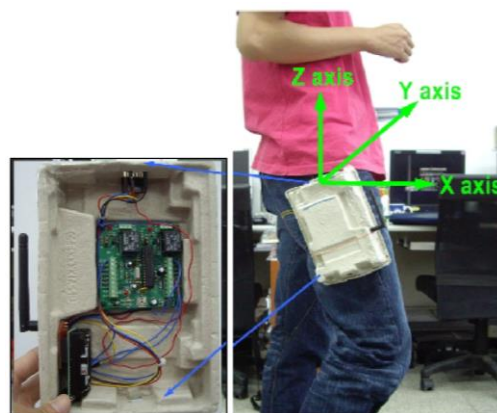


Figure 3-37. Fall Detection. Wernhuar, Chia-Hwei and Hsin-Hun (2011)

b) Wearable Power Assist Device for Standing Up Motion Using Pneumatic Rubber Artificial Muscles

A wearable assistive device that is demonstrated in figure 3-40 that was developed in 2007 by T Noritsugu (2007); this technology uses both a force sensor and an inclination angle sensor. This technology does require extensive mathematics to be programmed within the control system making it a complex piece of equipment.

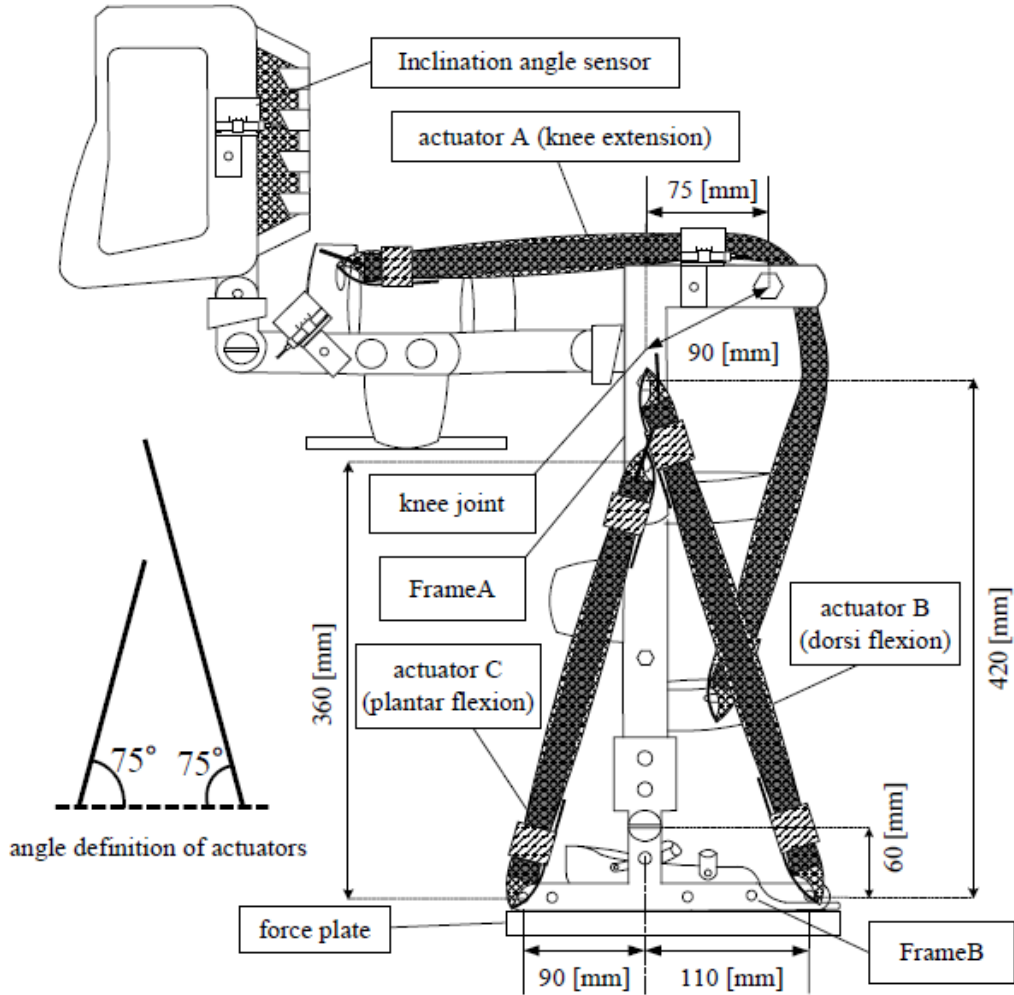


Figure 3-38. Assistive Standing Device Schematic. Noritsugu et al (2007)

c) Robotic arm with artificial muscles in rehabilitation

Figure 3-41 demonstrates a device that is modelled around the bicep muscle and uses an integrated accelerometer located on the forearm to monitor the motion created by the operator - this technology was created by Jobbágy et al (2014). The purpose behind this device is to aid in physiotherapeutic activities, the device itself is not a mobile device or easily wearable by an operator. Additionally, it can be understood that a key distinction between this thesis and the work produced is the intended application. This research project aims to provide a versatile commercial solution to non-invasive assistive exo-muscular enhancement; whilst the purpose of the device discussed is specific to physiotherapeutic applications. The research performed by Jobbágy et al (2014) is of paramount importance to this research as it provides a base of knowledge from which further development can be achieved - such as proving that a forearm mounted accelerometer can be used for motion monitoring on this type of technology.

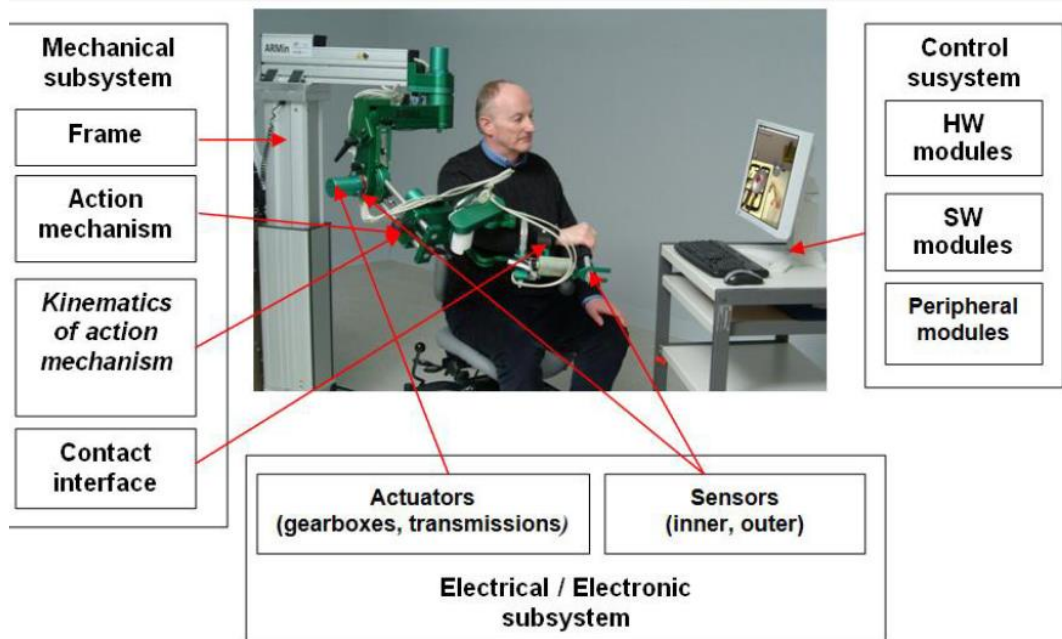


Figure 3-39. Robotic Arm. Jobbágy et al (2014)

3.6.2. Motion Detection System Prototype

To enable testing of the proposed hypothesis, a prototype was manufactured to allow sufficient data to be acquired. This was a crude wearable device that encompasses two major components, as detailed below. An original schematic of the prototype circuit design can be seen in figure 3-42.

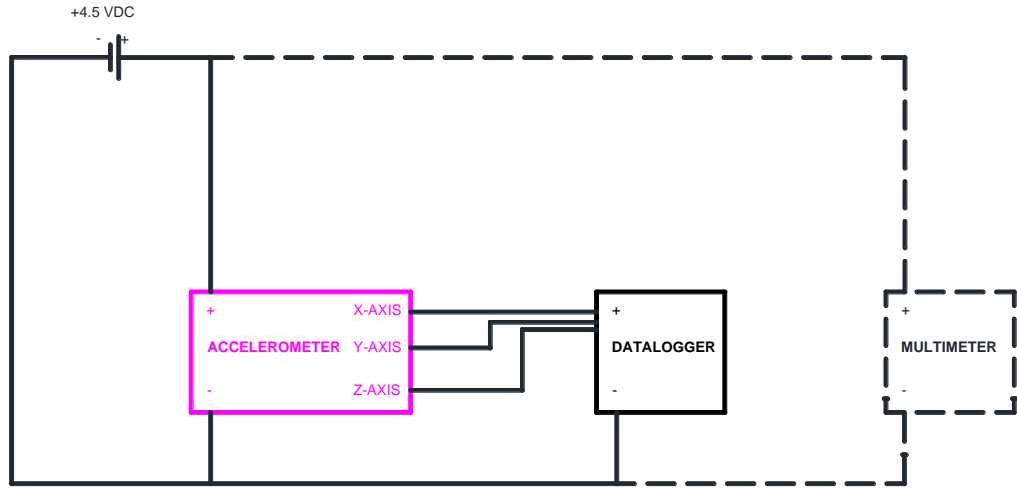


Figure 3-40. Prototype Circuit Design

3.6.3. Accelerometer

Accelerometers utilise a Newtonian constant, the value of gravity at 9.81m/s^2 as a basis for assigning a monitorable value to the device's location within Euclidian space. When no external acceleration is applied to the device the accelerometer will only measure the standard free fall value of gravity, TME (2020). Typically, there are two types of accelerometers: piezoelectric effect devices which contain two microcrystal structures that will generate a voltage when subjected to a force, and the second type which is a capacitance device with two internal structures where the variance in capacitance can be monitored. Montalvao (2015) provides a section diagram of a triaxial piezoelectric accelerometer as seen in figure 3-43, with Venkatanarayanan and Spain (2014) providing a microscopic image of a capacitance accelerometer as seen in figure 3-44.

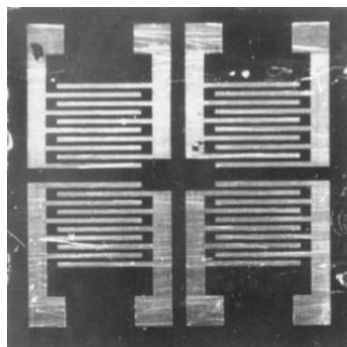


Figure 3-41. Capacitance Accelerometer. Venkatanarayanan and Spain (2014)

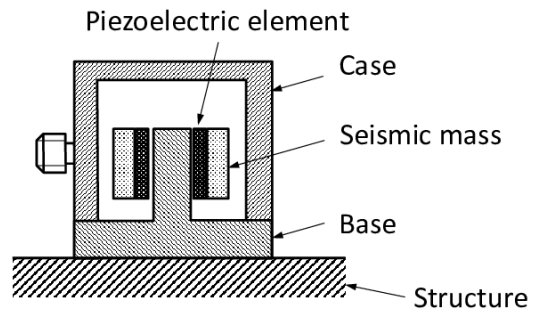


Figure 3-42. triaxial piezoelectric accelerometer. Montalvao (2015)

A capacitive accelerometer will monitor the acceleration by using the re-arranged formula of Newton's second law of motion to express acceleration as a result of force, as illustrated in the following formula $a = \frac{F}{m}$. Accelerometers are commissioned with a central zero value where the axes planes X, Y and Z are in a state of equilibrium, where upon the only force acting is gravity with a value of 9.81m/s^2 giving them a value of zero within the reference frame of the accelerometer. This value is linked to a signal output value which is typically central within the voltage requirements of the device. If motion is provided to anyone of the 3-dimensional planes then the device can interpret this change in g-force; due to the movement associated with the asserted force there is a change in capacitance which is again linked to the output voltage. A graphical representation of the typical relationship between a g-force input and a voltage output is provided by Analog Devices (2022) and can be seen in figure 3-45.

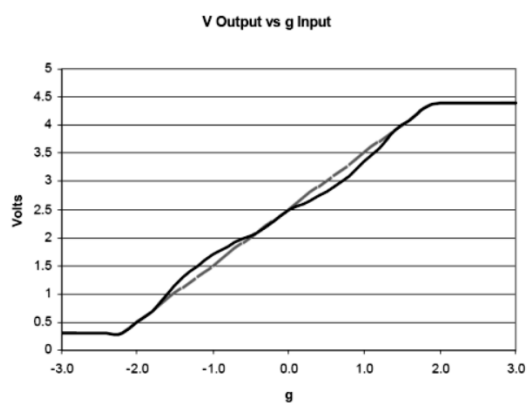


Figure 3-43. G Force to Gravity Line Graph. Analog Devices (2022).

Due to its usability, applicability, and compact size, for the purpose of this research it was decided that a capacitive accelerometer would be used within the prototype circuit. Specifically, the ADXL335 -BB, which is an accelerometer break out board that's simple to integrate into a circuit. The application of this sensor within the circuit will be to detect acceleration from movement generated by the operator actuating their arm. A physical photograph of the unit can be seen in figure 3-46.

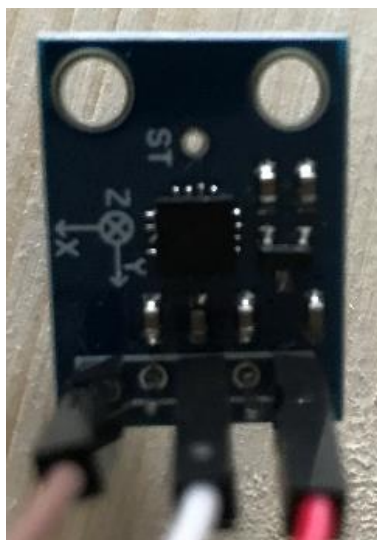


Figure 3-44. ADXL335-BB Accelerometer

3.6.4. Data Logger

To enable the voltage output of the accelerometer to be recorded in a CFR 21 Part 1 compliant manner where the data cannot not be manipulated once recorded, a Lascar Electronics EasyLog EL-USB-3 voltage data logger was incorporated into the circuit design. The device allows for monitoring of a singular voltage signal and the captured data is stored locally on the device before it is transferred to a computer via its USB connection. Using the free EasyLog software, the data is then transferred onto the computer and stored as un-editable text file, which displays the data in a line graph form plotting the voltage (Y-axis) against time (X-axis). The data sheet provided by EasyLog (2021), states the following as key features of the unit; additionally, an image is provided below in figure 3-47.

- *0 to 30V dc. measurement range*
- *Stores over 32,000 readings*
- *Logging rates between 1 second and 12 hours*
- *Connection via two screw terminals*
- *Immediate and delayed logging start*
- *User-programmable alarm thresholds*
- *Status indication via red and green LEDs*
- *EasyLog software available as a free download*

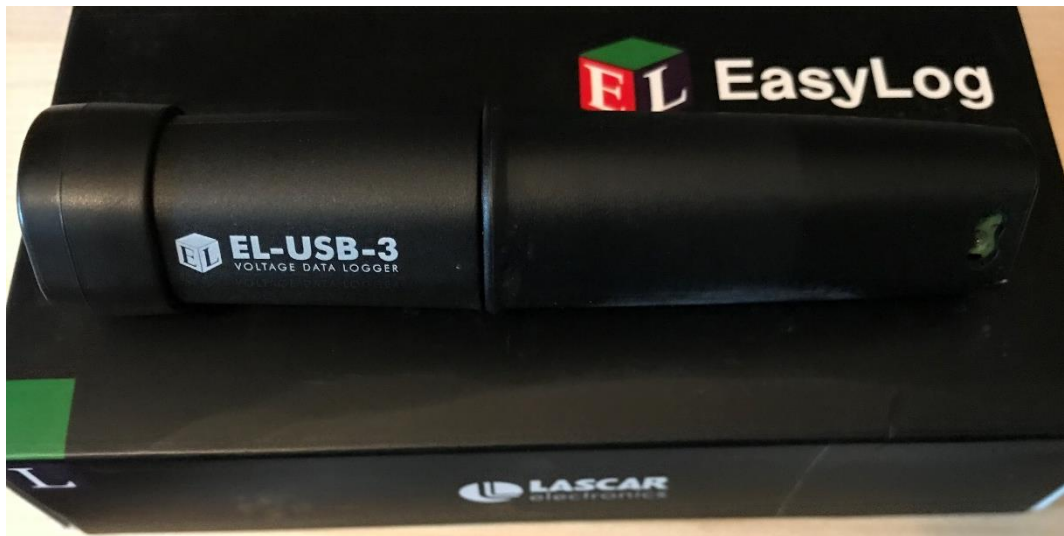


Figure 3-45. EasyLog EL-USB-3 Voltage Data Logger

3.6.5. Additional Items

To enable a prototype that was wearable and functional, additional items were required - these items are listed below:

- 3 x 1.5 zinc chloride Panasonic batteries (AA type).
- 2 x WAGO 221 terminal connectors.
- Elasticated fabric banding.

3.6.6. Motion Detection System Final Prototype

Upon completion of the various design stages discussed above, a final prototype consisting of three components was constructed as shown in figure 3-48.

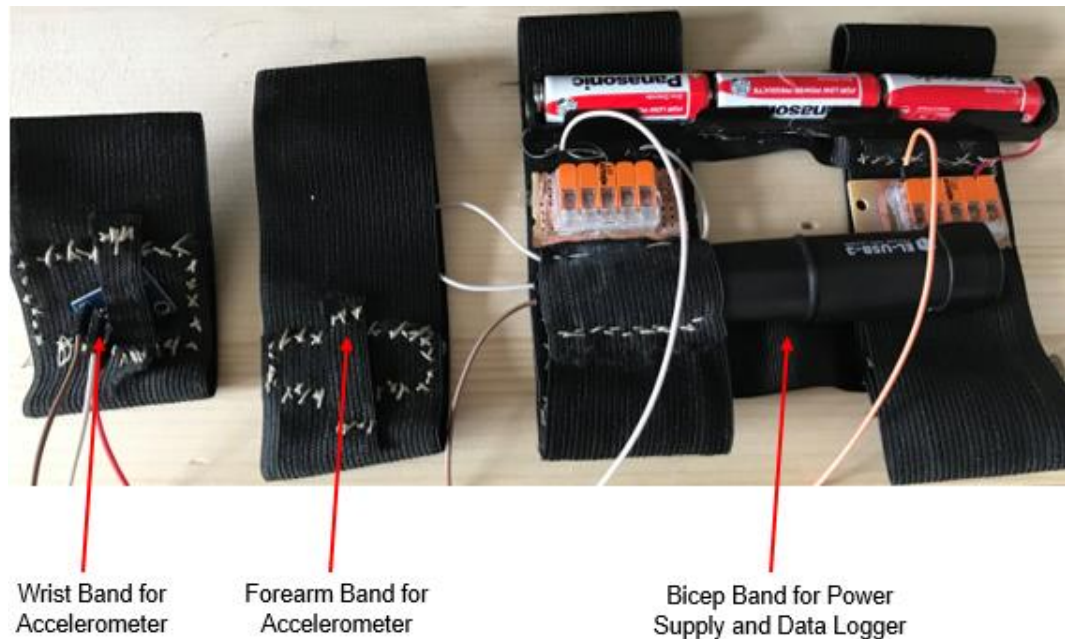


Figure 3-46. Motion Sensing Prototype

3.6.7. System Setup

Before the prototype could be used for testing, there was an element of set up that was required; the details behind this set up are discussed below.

3.6.8. Voltage Offset

During preliminary testing it was observed that the output voltage values – as specified in the ADXL335-BB data sheet (appendix C) - were not being achieved in the data logging software. When in an equilibrium state, the recorded voltage recorded should be 1.5v for the X, Y and Z axes. When in a motion that its negative the centre zero point of the device, then the voltage should read 1.35v for the X and Y axes and 1.2v for the Z axis. When in a motion that is positive to the centre zero point, the outputted voltage should be 1.65v for the X and Y axes and 1.8v for the Z axis. When observing the data recorded on the data logger, the peak value achieved at the point in which the bicep actuation was complete, was never higher than 1v. However, when the accelerometer was connected directly to a multi-meter, the aforementioned voltage values were achieved. As the input impedance of the multi-meter is high than the impedance of the circuit the

measure device will have no influence over the results as informed by Espinosa et al (2022). Meaning that to enable a device to not affect a circuit, the impedance of the device would need to be higher than that of the circuit. As the data logger has a lower impedance - which measured at 60.3k Ω as opposed to the circuit's 95.0k Ω - this would allow for a drop of voltage over the device. As an alternative to adding a resistor to the circuit, within the settings screen of the datalogger software a voltage offset can be applied, which will add the specified offset value to the recorded voltage. To understand what this offset value needs to be, a simple test was performed - this is detailed below.

- Fix accelerometer to flat surface (Equilibrium state) [figure 3-49]
- Apply voltage
- Measure with multi-meter
- Add data logger to circuit
- Measure with multi-meter

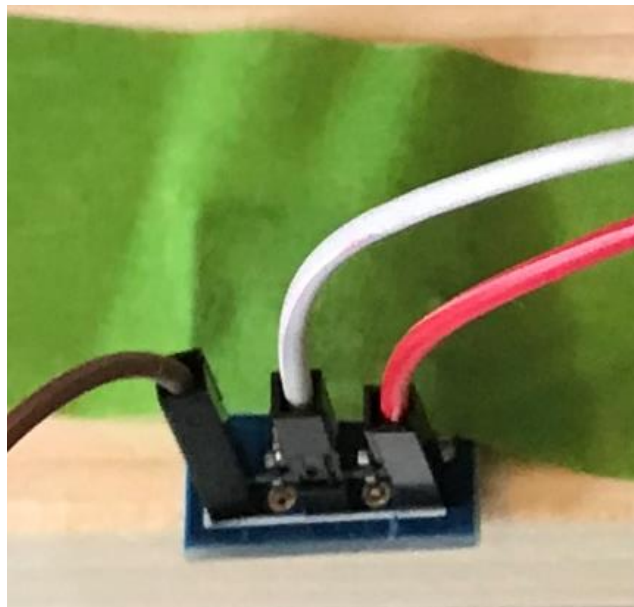


Figure 3-47. Accelerometer Place in Equilibrium State

The recorded data was then tabularised allowing for the deviation to be clearly illustrated; an average value or “offset” figure was then attained and can be seen in table 3-8.

Table 3-8. Voltage Offset Value

Axis	Direct To Multi-meter (V)	Through Data Logger (V)	Deviation (V)
X	1.59	1.05	0.54
Y	1.57	1.04	0.53
Z	2.00	1.33	0.67
Average Deviation in volts (offset value)			0.58

3.6.9. Voltage Recording Parameters

The EL-USB-3 data logger utilises an external software titled EasyLog to download and format the captured data - in this case the outputted voltage from the accelerometer. This software provides the attained results in an anti-tamper format and allows for specific interrogation of the results such as: average results, tabularisation and marking nodes. Additionally, this software allows the data logger to be set up specific to experimental requirements; this is done by connecting the data logger to the computer USB drive and navigating through the five set up screens. Below is a step-by-step description of how the data logger was set up for this research.

1. Select "Set up and start the USB data logger". (Figure 3-50)

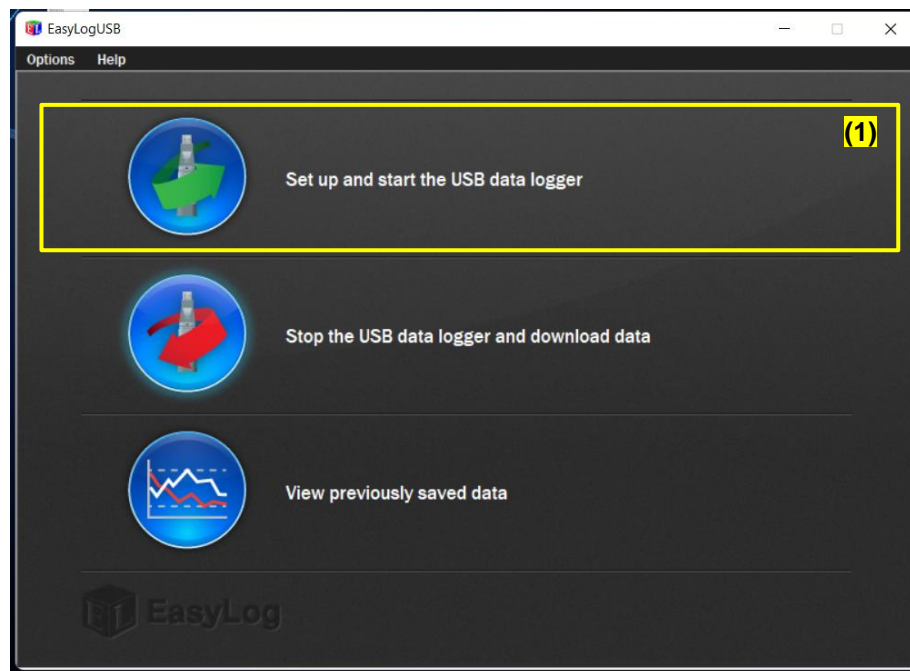


Figure 3-48. EasyLog Home Page

2. Enter “logger name” as UOM Data Log [add specific test number]. (Figure 3-51)
3. Set frequency to 2 Secs for 18 Hours. (Figure 3-51)
4. Select custom calibration for “The USB Voltage Data Logger is set to”. (Figure 3-51)

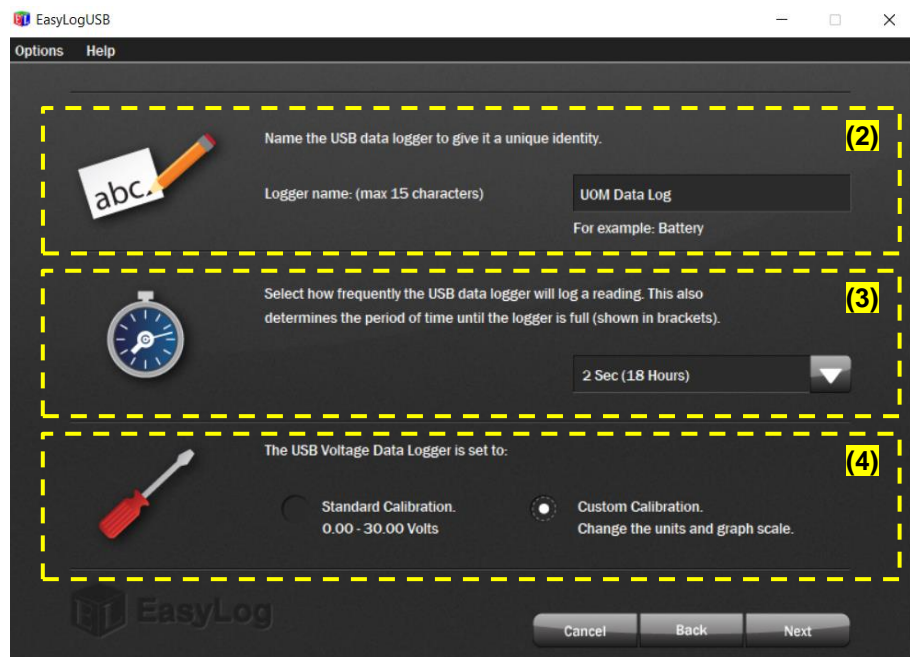


Figure 3-49. EasyLog Set up Page 1

5. For unit measurement select “Volts” from the drop down box. (Figure 3.52)
6. For offset value change “Graph Output” to 0.58 and 30.58 respectively. (Figure 3.52)

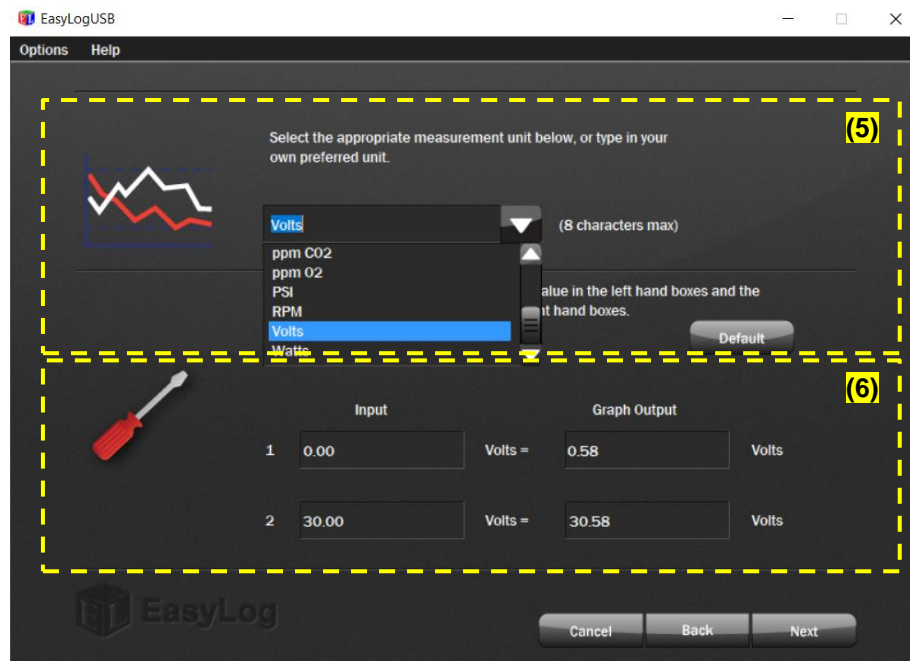


Figure 3-50. EasyLog Set up Page 2

7. To provide a visual banding within the outputted graph, tick active both the high and the low alarm. (Figure 3-53)
8. Set high alarm as 1.8v and the low alarm as 1.2v, as per the ADXL335-BB datasheet. (Figure 3-53)

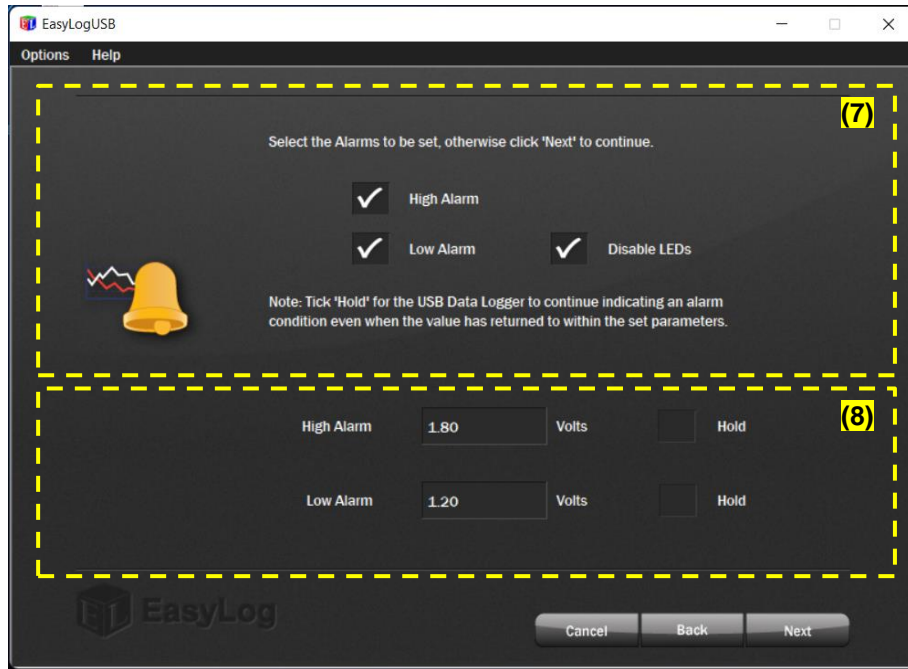


Figure 3-51. EasyLog Set up Page 3

9. To prevent spurious readings and to allow the operator sufficient time to attach the data logger, select “delay the start of the data logger”. (Figure 3-54)
10. Enter desired time delay.

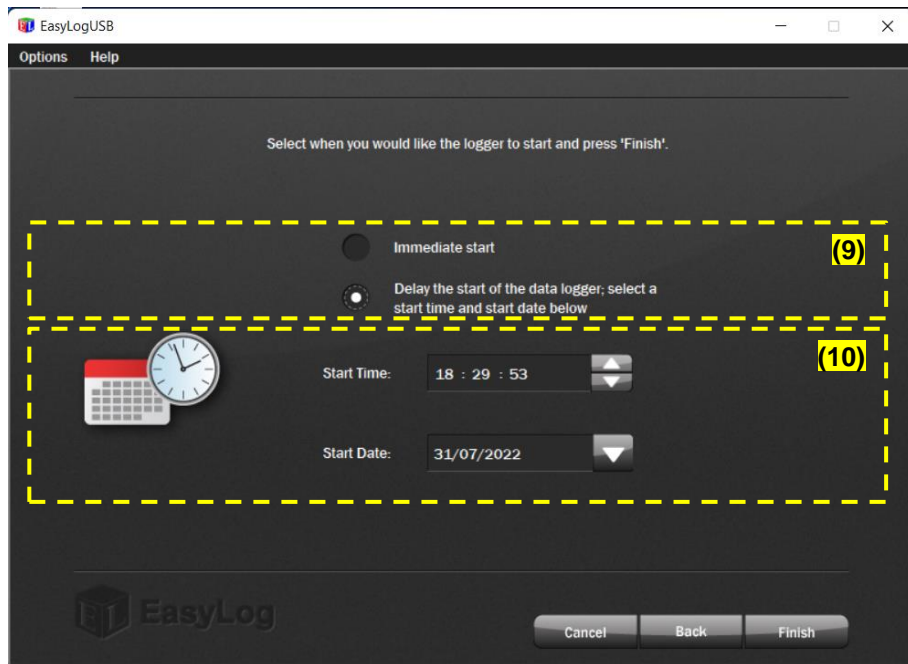


Figure 3-52. EasyLog Set up Page 4

3.6.10. Experiment design

As certain technologies already discussed, such as the Fitbit and Apple Watch use this type of technology, it was important for the testing to provide more than just data on the effectiveness of an accelerometer. Therefore, it was decided that in addition to data logging the voltage from the accelerometer, the device would be strategically located around the forearm to aid in providing information on the most effective place the sensor should be mounted. Furthermore, to simplify the testing, the motion utilised in the procedure would be what is titled a “Hammer Curl”; this involves actuation of the bicep in an upward motion with any applied force acting vertically through the palm of the hand. Stuart (2019) provides a graphic illustration of the “Hammer Curl” in figure 3-55.

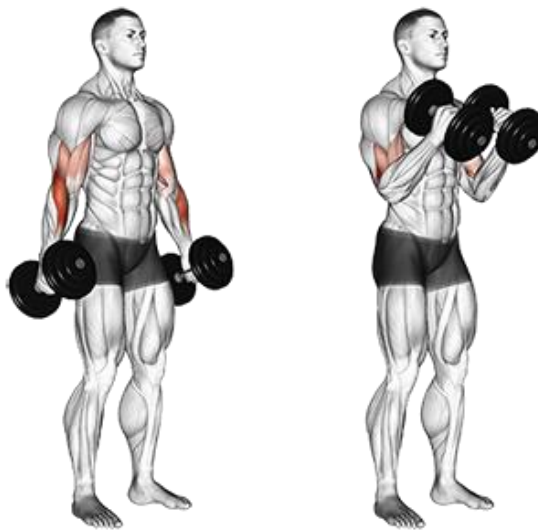


Figure 3-53. Hammer Curl. Stuart (2019)

A total of 12 locations around the forearm were selected as seen in figure 3-56, additionally the testing procedure is listed below with the testing matrix detailed in table 3-9.

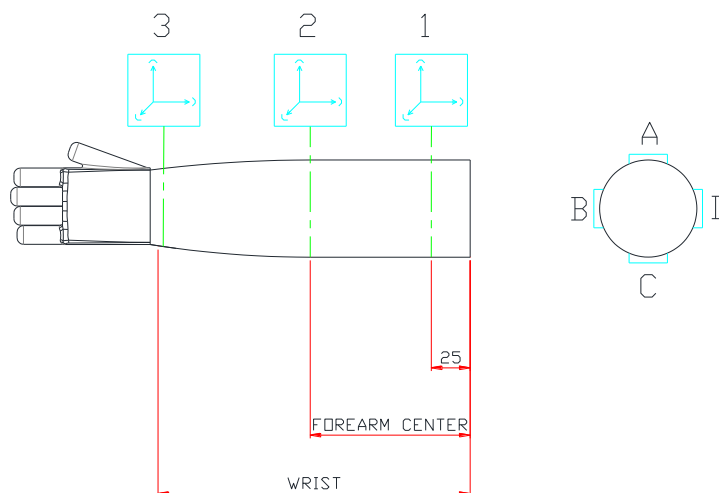


Figure 3-54. Accelerometer Position Schematic

3.6.11. Testing procedure

To ensure the test is performed in a controlled and organised manner, the following procedure was adhered to:

1. Apply prototype component band to bicep.
2. Utilising either the forearm or wrist band, set accelerometer in desired position. (Figure 3-57)



Figure 3-55. Wrist Mounted Accelerometer in position 3A

3. Perform data logger set up and mount to prototype.
4. Hold arm vertically downward, with fist clenched and knuckles perpendicular to the floor. Keep this position until delay timer ends; delay timer is observed by using a GMT zone clock as the delay is set as specific time to activate the data logger (Figure 3-58)

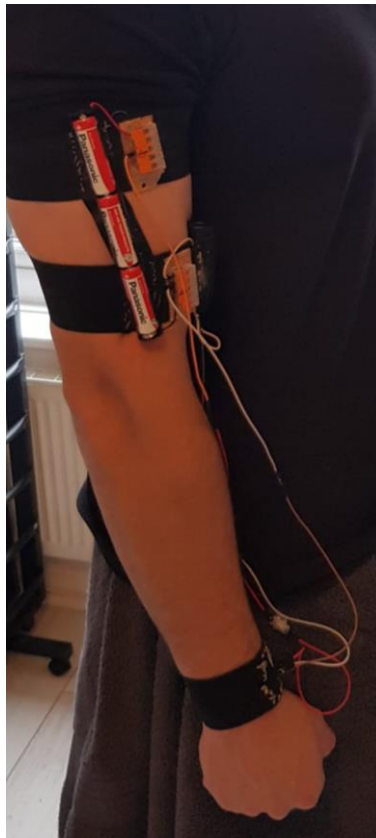


Figure 3-56. Arm in Default Position

5. After start time is reached, activate stopwatch; once five seconds has passed, slowly raise forearm over a period of ten seconds from default position (figure 3-59) to final position (Figure 3-59).



Figure 3-57. Arm in Final Position

6. Hold in place for ten seconds.
7. After ten seconds release slowly over a period of ten seconds.
8. Once default position is reached, hold for ten seconds.
9. After ten seconds, slowly raise the arm, stopping after three seconds and holding in position for ten seconds to simulate a struggle point. (Figure 3-60)



Figure 3-58 Arm in Simulated Struggle Point Position

10. After a ten second period, continue to raise arm from struggle point position (figure 3-60) to final position (figure 3-59). Hold for ten seconds.
11. Slowly release arm over ten seconds until in default position. (Figure 3-58)
12. Repeat consecutively three times to understand repeatability.
13. Test complete, re-perform for test variation as specified in table 3-9.

Table 3-9. Motion Test Variations

Test No.	Position (As per figure 162)	Accelerometer Axis		
MT-00	1A	X	Y	Z
MT-01	1B			
MT-02	1C			
MT-03	1D			
MT-04	2A			
MT-05	2B			
MT-06	2C			
MT-07	2D			
MT-08	3A			
MT-09	3B			
MT-10	3C			
MT-11	3D			
<i>Note: Test ID tag will be MT-00- (X, Y or Z).</i>				

4. Results and Discussions

4.1. Test 1 - Heart Rate and Blood Oxygen Level Monitoring discussions

Ultimately the testing performed did not progress to that of a larger sample group due to the results rendered from individual testing which indicated that interrogation of spO2 and heart rate was not a reliable methodology of signalling an actuation. The data captured demonstrated that whilst there were changes in the spO2 level, this change was not quick or significant enough in its response to enable the extraction of reliable data. Furthermore, it can be understood from the data displayed in figure 4-1 that the standard deviation of 0.5210 demonstrates an extremely small variance over a multitude of activities. This small variance can be attributed to how human physiology uses oxygen in the blood system and that oxyhaemoglobin is a relatively stable chemical in the body. All of this allows for the understanding that if monitored on a task-based basis, the variation in SP02 levels would be too small to gain reliable information to instruct an actuation. Additionally, the monitored heart rate proved too volatile to use as a source of information from the muscle, as seen in figures 4-2 to 4.8. Furthermore, the heartrate cannot only be specific to an individual, but also during period of high velocity exercise could provide the exo-muscles logic system with inaccurate information based on cardiovascular exercise.

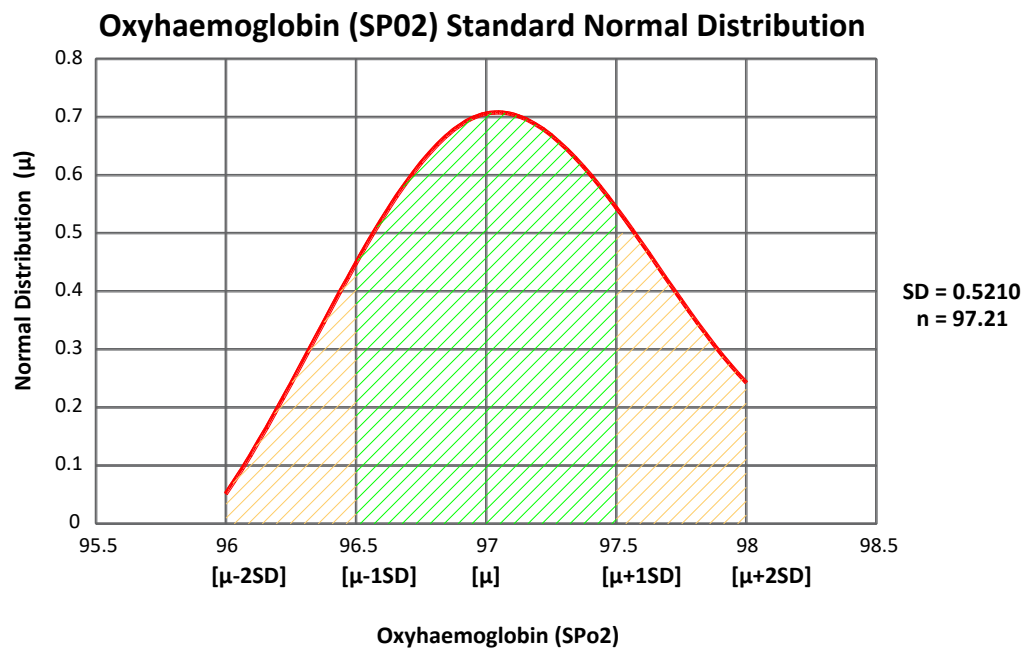


Figure 4-1. Oxyhaemoglobin Standard Normal Distribution Graph

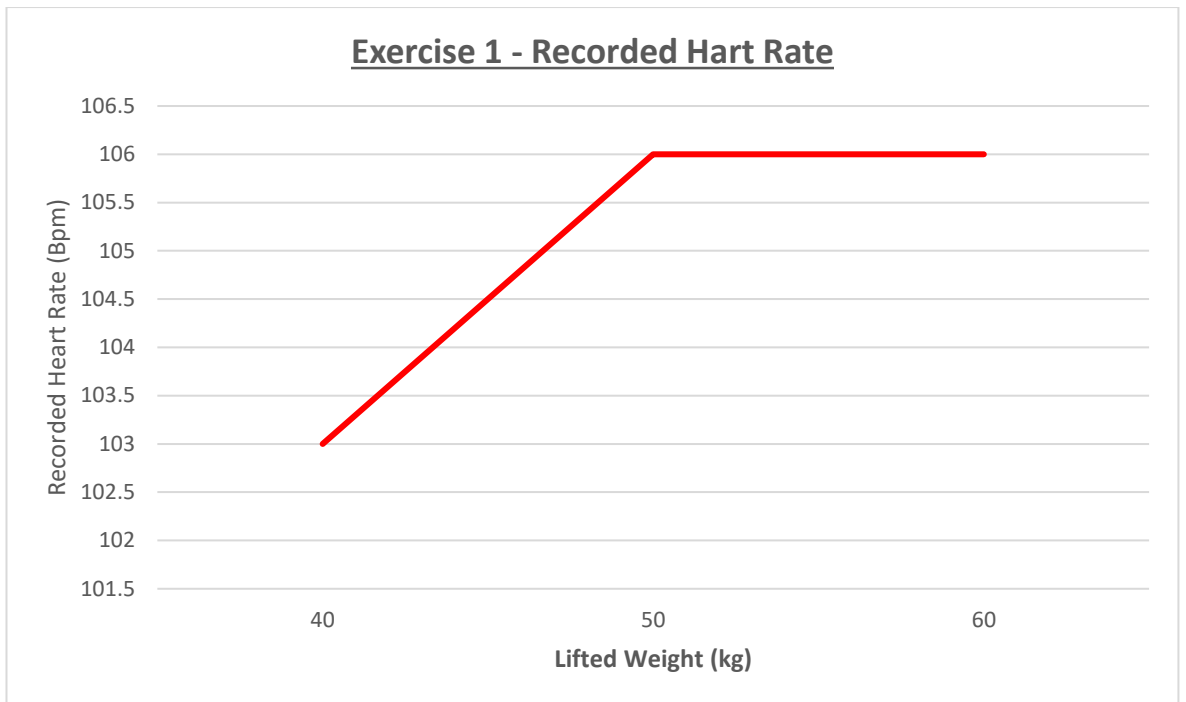


Figure 4-2. Exercise 1 – Recorded Heart Rate Graph

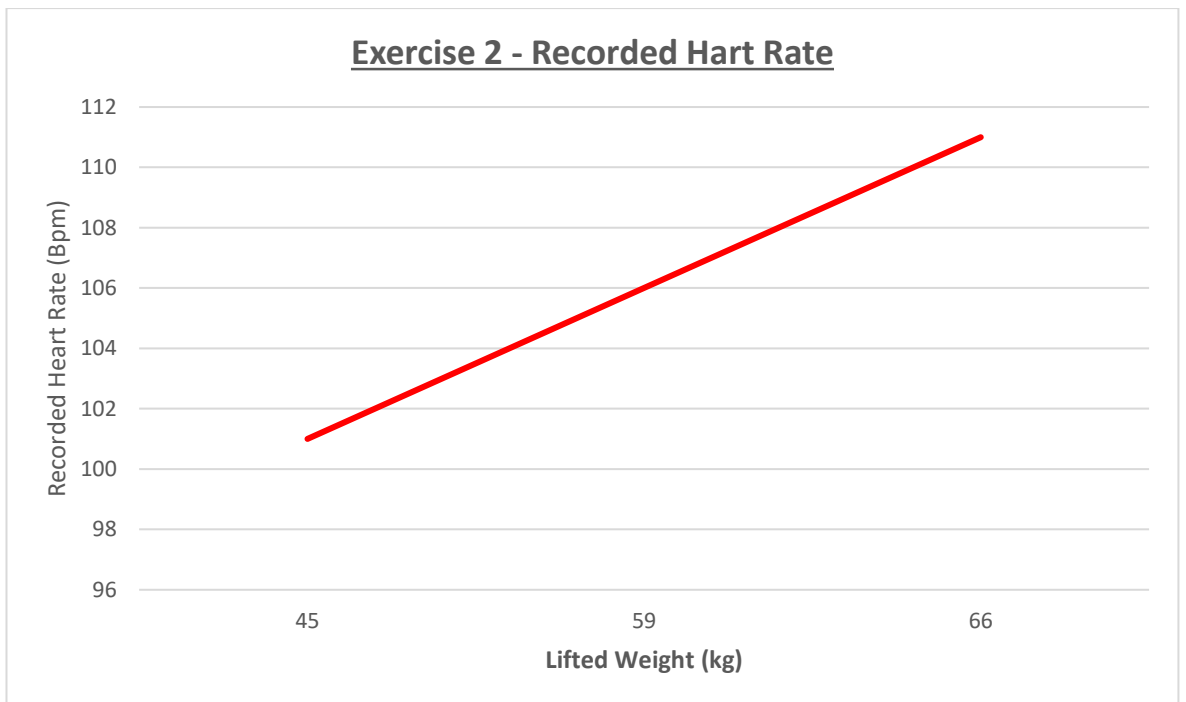


Figure 4-3. Exercise 2 – Recorded Heart Rate Graph

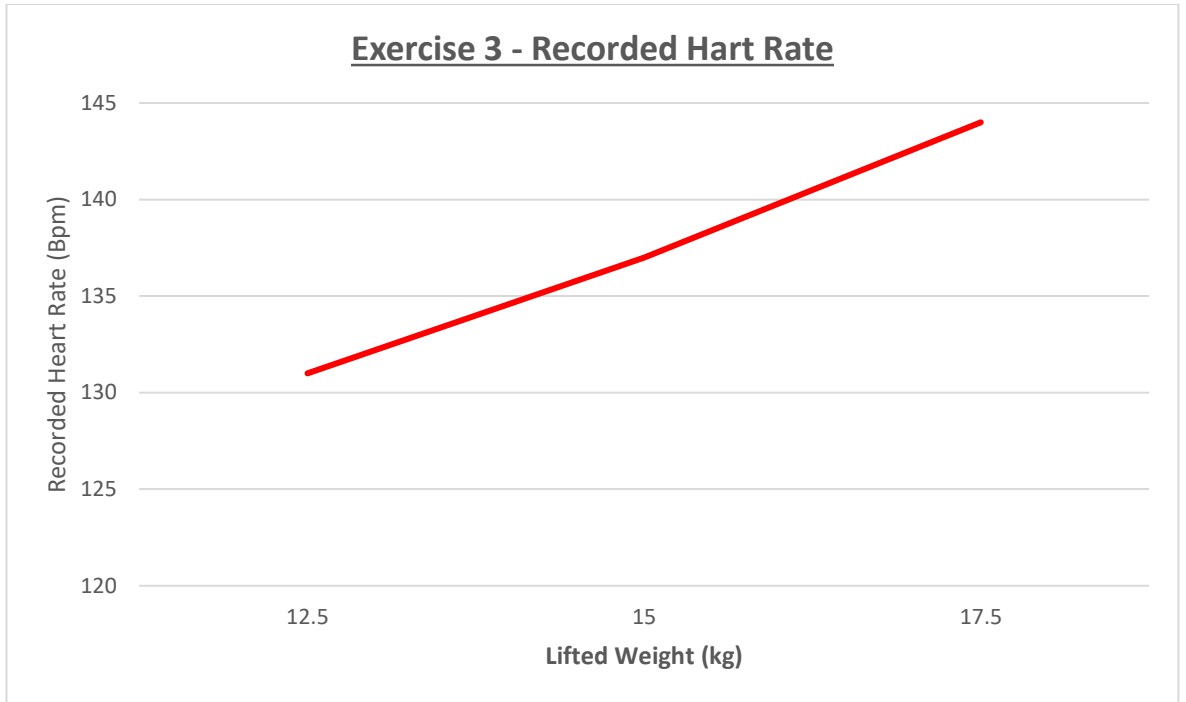


Figure 4-4. Exercise 3 – Recorded Heart Rate Graph

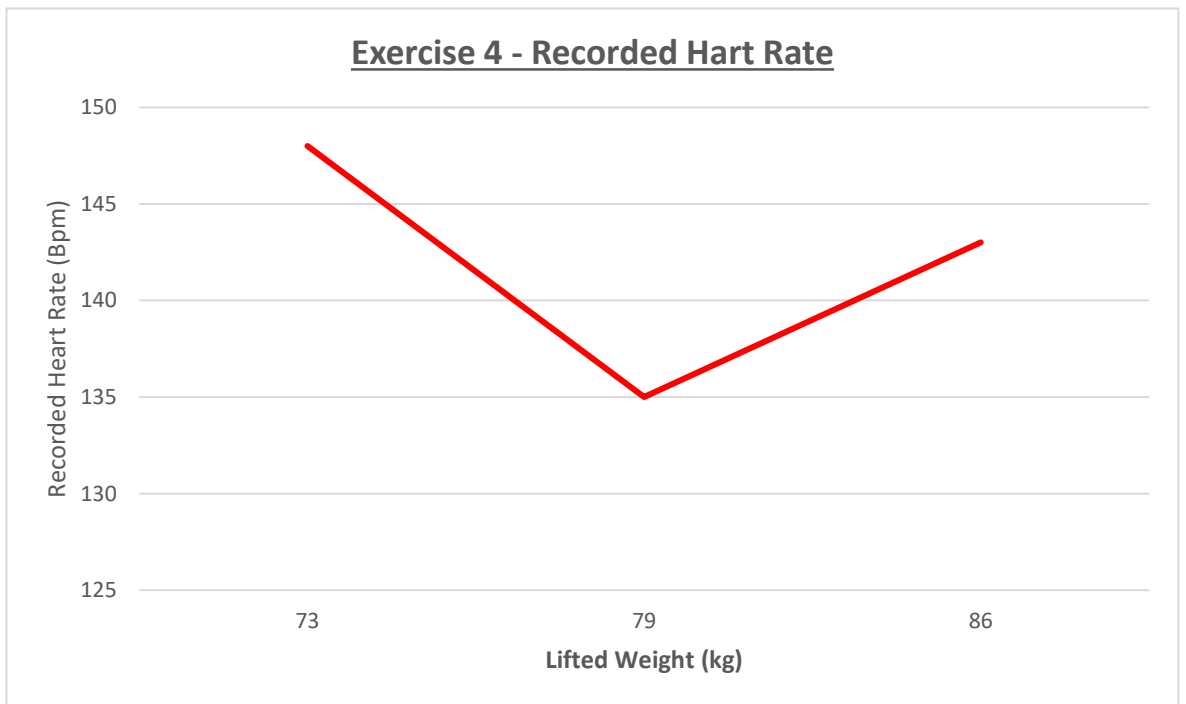


Figure 4-5. Exercise 4 – Recorded Heart Rate Graph

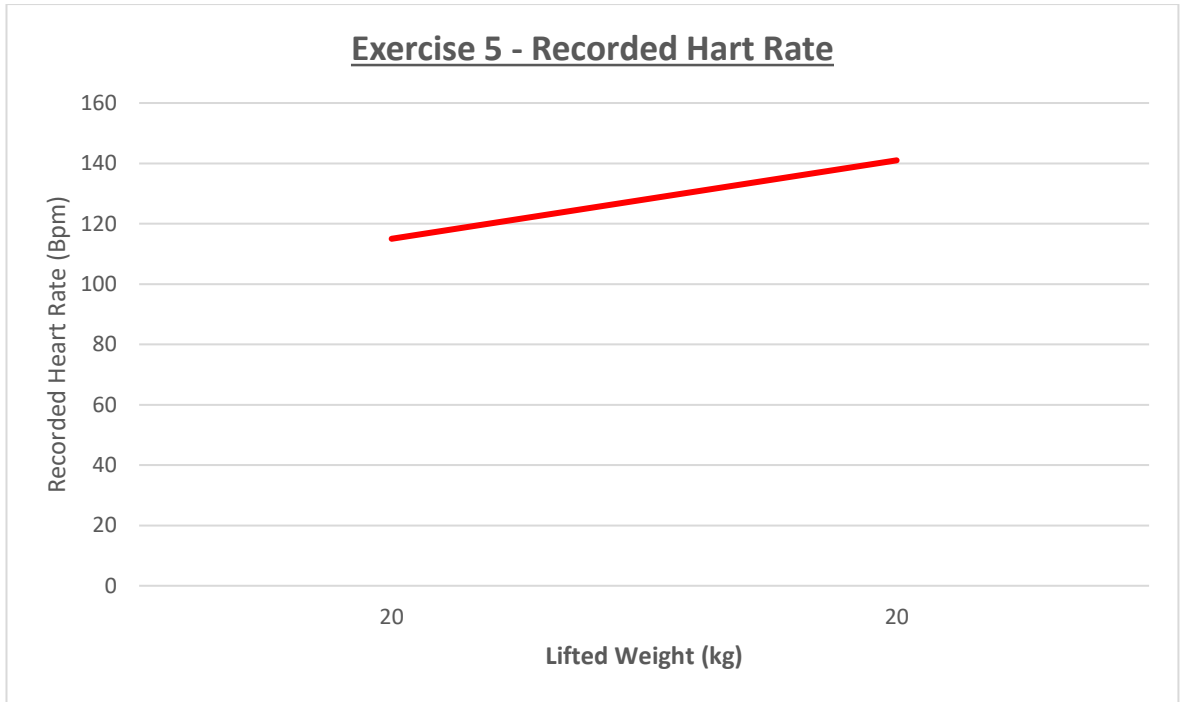


Figure 4-6. Exercise 5 – Recorded Heart Rate Graph

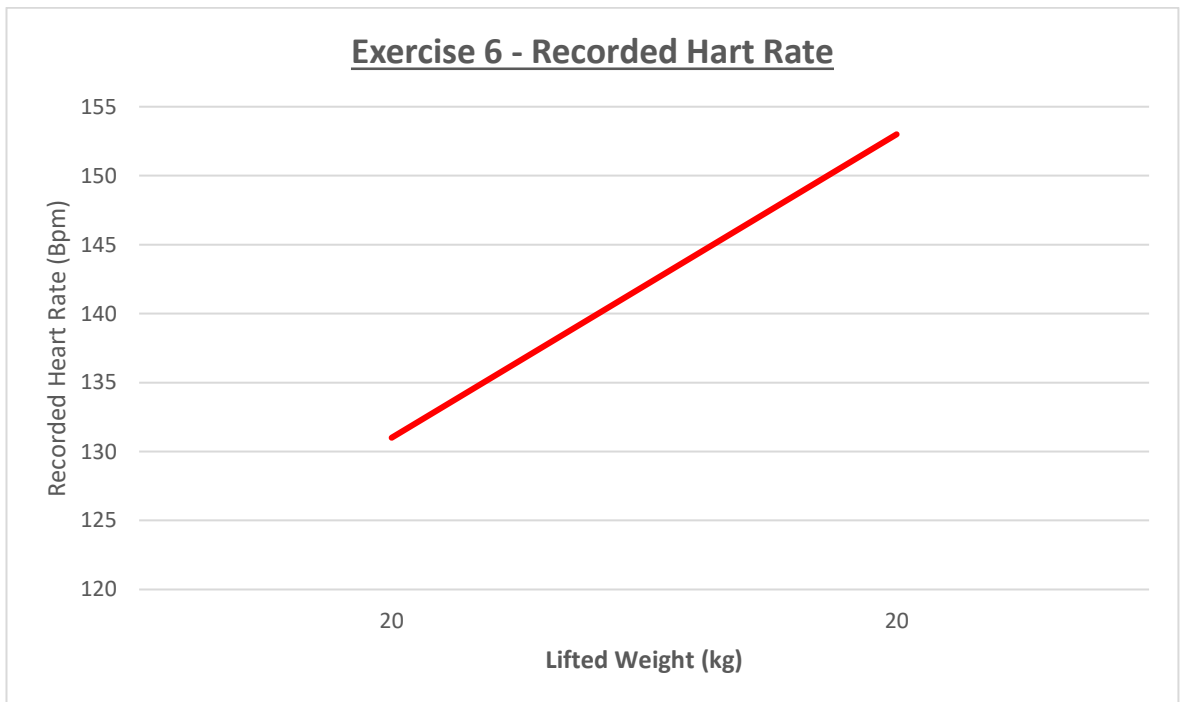


Figure 4-7. Exercise 6 – Recorded Heart Rate Graph

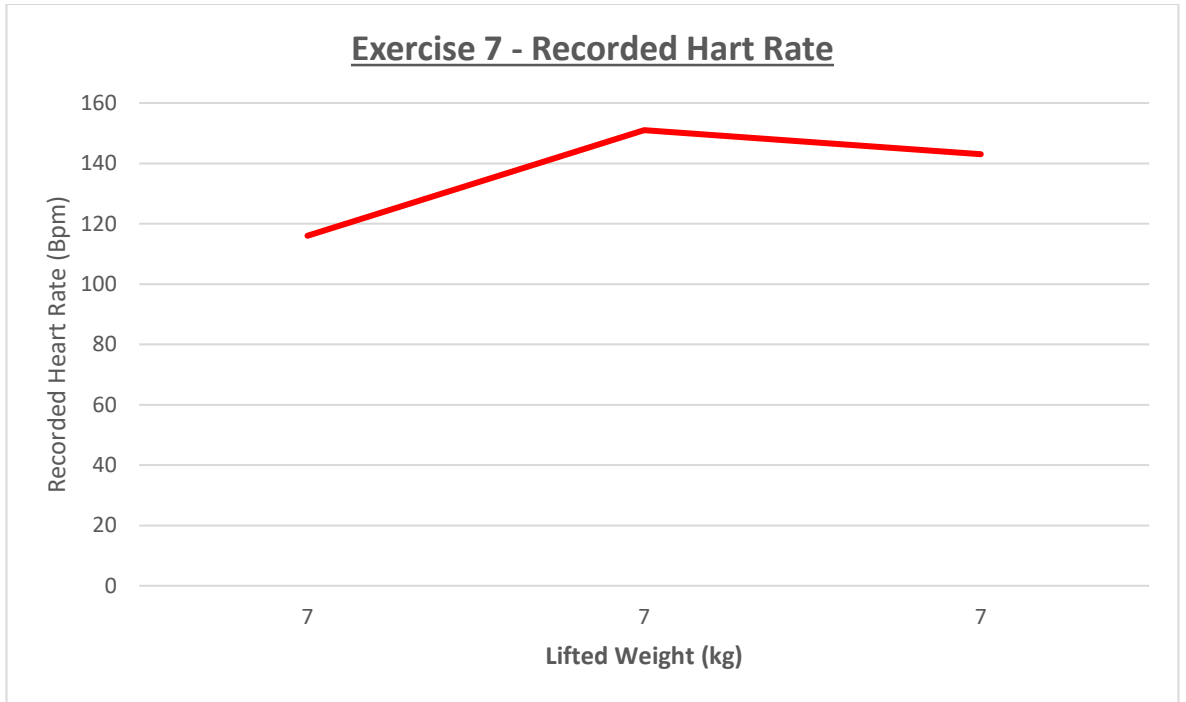


Figure 4-8. Exercise 7 – Recorded Heart Rate Graph

With this considered, it was decided that this methodology of monitoring was not an appropriate method to continue pursuing. The data established can be found in table 4-1 below with an example of the data being recorded demonstrated in figure 4-9 and 4-10, with the completed form found in appendix B.



Figure 4-9. Measure Heart rate and SP02 level before activity



Figure 4-10. Measure Heart rate and SP02 level after activity

Table 4-1. Raw Data Table 1

Exercise	Weight	Set	Reps	Starting Heart Rate	Finish Heart Rate	Start BPM	Finish BPM
1	40	1	10	103	106	97	97
1	50	2	6	106	106	97	97
1	60	3	6	106	106	97	97
2	45	1	10	101	106	97	98
2	59	2	10	106	111	98	98
2	66	3	6	111	110	98	98
3	12.5	1	10	131	137	97	97
3	15	2	10	137	144	97	96
3	17.5	3	10	144	149	96	98
4	73	1	10	148	135	98	97
4	79	2	8	135	143	97	97
4	86	3	6	143	134	97	98
5	20	1	6	115	141	97	98
5	20	2	6	141	131	98	97
6	20	1	6	131	153	97	97
6	20	2	6	153	160	97	98
7	25	1	4	116	151	97	97
7	20	2	6	151	143	97	98
7	20	3	6	143	135	98	98

4.2. Test 2 - Radiative (Wireless) Power Supply Results and discussions

The recorded raw data from test 2 can be found in tables 4-2, 4-3 and 4-4; with the processed data being displayed graphically in figures 4-11 to 4-16. The ideal outcome of this testing would be a consistent voltage signal of more than 2V which as discussed in 3.6.8 is the required voltage to power an accelerometer.

The collected data infers that the use of both an “in series” and “parallel” wiring methodology vastly benefits the collation of an electrical voltage signal from body heat energy. Observing figures 4-12, 4-13, 4-15 and 4-16, it can be seen that the repeat “parallel” and “series” wiring of multiple TEG’s render results which were close in value. If figure 4-11 is observed in conjunction with figures 4-12, then it can be clearly observed the voltage output is higher in value for a test parameter where three TEG’s are wired in series, compared to a single TEG. What can be concluded from this observation is that the increase of covered surface area plays an important role in the value of the outputted voltage - tests 1 and 2 are the easiest to compare due to them both being an “in series” wiring method; the only variable factor is the quantity of TEG’s used in the circuit. This clearly demonstrates that just by increasing the surface area covered by the TEG’s, the output voltage signal can be increased by as much as 50% across all tests performed. However, when viewing figure 4-11 with figure 4-13, the results show that the voltage output from three TEG’s wired in parallel is less than that of a single TEG by around 16%. By viewing figure 4-13, it can be seen that the outputted voltage from the set up used for test 3 allowed for a consistent voltage to be attained.

To develop an understanding of how the TEG will perform when exposed to an extreme temperature differential, tests 4,5 and 6 replicated the experiments undertaken for test 1,2 and 3; however, to induce the difference in temperature between the hot side (skin side) and cold side of the TEG, frozen granite blocks were mounted to the surface. When reviewing the data for tests 4,5 and 6 displayed in tables 4-2, 4-3 and 4-4; in addition to the graphical representation of this data in figures 4-14, 4-13 and 4-16, it can be seen with clarity that the increase in temperature differential vastly improves the voltage strength of the output signal from the TEG. If test 4 is compared with its counterpart test 1 in all performances of the testing, a 75% increase in voltage is acquired; with the highest recorded value being 0.168v. This percentage value increase of 75% is the same when test 6 is compared with test 3, with test 6 having a maximum voltage output of 0.91v. Although significantly lower than the tests discussed above, when test 5 is compared to test 2 there is a still a 50% increase in the output voltage signal, with test 5 achieving 0.110v as its highest output. Similar to the graphical data representation for test 1,2 and 3; when figures 4-14, 4-13 and 4-16 are viewed, a declining slope for tests 4,5 and 6 can be seen; illustrating that the instability of the surrounding environment causes the voltage signal to become weaker over the duration of the test. Whilst the above discussion unequivocally demonstrates the importance of creating a high temperature differential to increase the output voltage, what has been identified is the instability in the signal due to the change of circumstance with the surrounding environment. This provides

insight into an area of development, where a method of stabilising the cold side (non-skin contact side) requires further study.

Viewing all testing data as a whole by observing figures 4-11 to 4-16, one common trait that all the performed tests have, is a decline in output voltage over the time period. As the TEG absorbs the radiative heat being emitted from the body, the semiconductors themselves retain some of the heat, which reduces the efficiency of the TEG. This fundamental issue with the TEG's does provide an additional avenue of research that is required to understand how this fault can be resolved and the TEG efficiency be improved.

It is important to note that there does appear to be disparity between the results attained during the first test and the ones gained in the two-repeat test, specifically when observing figures 4-14 and 4-15. This differential could be as a result of the first test taking place on a different day to the two repeat test which were performed on the same day. Looking at the ambient temperature readings it can be seen that there is a substantial difference of around 5 degrees Celsius, which can have an impact on the operational efficiency of a TEG. Because the temperature differential between the surface skin temperature and the external side of the TEG is larger than that of the two repeat tests, the TEG operates at a higher efficiency due to the increased flow of electrons from the n-type semiconductor through the PN junction. The represented data for the initial test when viewed with the data acquired from the two repeat tests demonstrates that the TEG will operate better in a colder climate vs a warmer climate; this is further supported by the data attained for tests 4,5 and 6 which features a method of increasing the temperature differential by decreasing the temperature of the n-type or "cold" side of the TEG.

From the above research it can be inferred that using thermoelectric generators in conjunction with body heat could be a viable option for generator small electrical signals - such signals that could be used for communicating with logic controllers. But the use of this type of technology does require further experimental research to alleviate several key issues. The collected data infers that the use of both an "in series" and "parallel" wiring methodology vastly benefits the collation of an electrical voltage signal from body heat energy. However, the acquired data did demonstrate a draw back to the use of TEG's, this being their inefficiencies over a time period. The data clearly showed that the peak outputted voltage for a TEG is at the time period of 0 minutes, where in all cases (with the exception of test 2 repeat 1, test 4 repeat 1, test 6 repeat 1 and test 2 repeat 2) the voltage would degrade over the full duration of the test. Furthermore, the stability of electrical signal did appear inconsistent over the performed test, with degradation of the signal being discussed previously. However, adding a simple device such as capacitor to the circuit could aid in smoothing the voltage flow. Positioning the TEG in different areas of the body where heat is more radiant could also render a higher voltage output. This testing provided data analysis from an area of the body which is not a noticeably warm area in addition to being continuously open to atmosphere, allowing less heat to be stored. Finally, as has been discussed above, the stability of the surrounding

environment does create an impedance on the output voltage, detrimentally effective in its reliability and repeatability. Overall, this testing demonstrated how the voltage signal acquired from thermoelectric generators can be significantly increased – however, whilst creating a substantial temperature difference did in fact significantly increase the output voltage, the methodology of how this was done did not assist the continuity of signal. Thus, presenting a new research gap where the stability of the signal requires further study.

Table 4-2. Radiative Power Supply Initial Testing data

Initial Test								
Test Number	Min 0 (V)	Min 1 (V)	Min 2 (V)	Min 3 (V)	Min 4 (V)	Min 5 (V)	Start Ambient Temp (°C)	End Ambient Temp (°C)
1	0.017	0.016	0.015	0.014	0.013	0.012	18.5	18.5
2	0.051	0.039	0.040	0.041	0.041	0.038	17.5	18.5
3	0.014	0.015	0.013	0.013	0.012	0.011	18.5	19
4	0.039	0.045	0.040	0.039	0.035	0.032	18.5	18.5
5	0.207	0.200	0.181	0.165	0.130	0.111	19	19
6	0.053	0.050	0.046	0.041	0.038	0.034	19	18.5

Table 4-3. Radiative Power Supply Repeat 1 Testing data

Repeat 1								
Test Number	Min 0 (V)	Min 1 (V)	Min 2 (V)	Min 3 (V)	Min 4 (V)	Min 5 (V)	Start Ambient Temp (°C)	End Ambient Temp (°C)
1	0.027	0.019	0.016	0.016	0.015	0.014	20	21
2	0.042	0.038	0.035	0.035	0.036	0.033	23.5	23.5
3	0.019	0.014	0.014	0.013	0.013	0.012	23	23
4	0.141	0.168	0.131	0.114	0.086	0.069	20.5	20.5
5	0.110	0.083	0.066	0.052	0.041	0.036	21	21
6	0.075	0.070	0.073	0.062	0.053	0.047	20.5	20.5

Table 4-4. Radiative Power Supply Repeat 2 Testing data

Repeat 2								
Test Number	Min 0 (V)	Min 1 (V)	Min 2 (V)	Min 3 (V)	Min 4 (V)	Min 5 (V)	Start Ambient Temp (°C)	End Ambient Temp (°C)
1	0.022	0.018	0.016	0.016	0.016	0.014	21.5	22
2	0.038	0.037	0.034	0.035	0.036	0.027	24	24
3	0.023	0.015	0.013	0.013	0.014	0.013	23	24
4	0.138	0.116	0.108	0.081	0.064	0.052	20.5	20.5
5	0.102	0.077	0.060	0.052	0.045	0.041	21	21
6	0.091	0.083	0.073	0.067	0.058	0.048	21	21

To understand the validity of this data a 95% confidence level was used to calculate the confidence interval based on a total sample size of 18 data points for each test. Because this sample size was below 30 the T-distribution table was used, to calculate a 95% confidence level a T value of 2.110 acquired. The calculated confidence level for each test can be found in table 4-5 below. Observing this data it can be understood that whilst multiple test were performed, test 4,5 and 6 show a larger confidence interval that what was calculated for tests 1,2 and 3.

Table 4-5. Radiance Testing Error Treatment Table

Test Number	Average Output Signal	Confidence Interval (Z)
1	0.016V	±0.0017V
2	0.038V	±0.0024V
3	0.014V	±0.0013V
4	0.083V	±0.021V
5	0.097V	±0.027V
6	0.097V	±0.025V

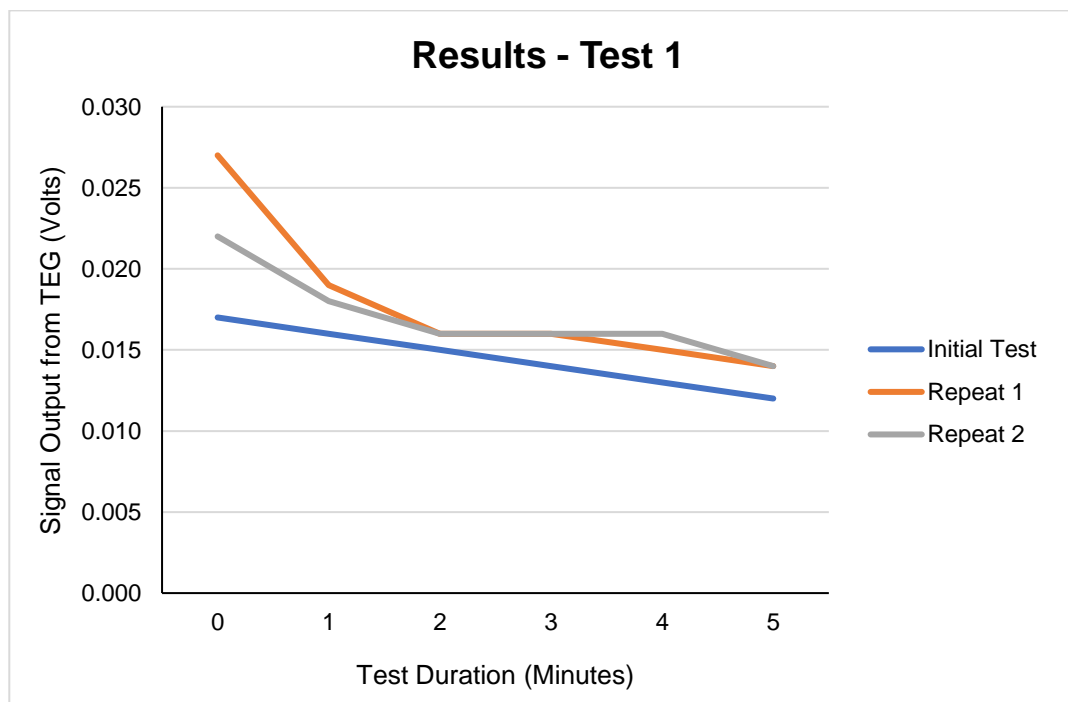


Figure 4-11. Results Graph Test 1 – Single TEG (No Granite Block)

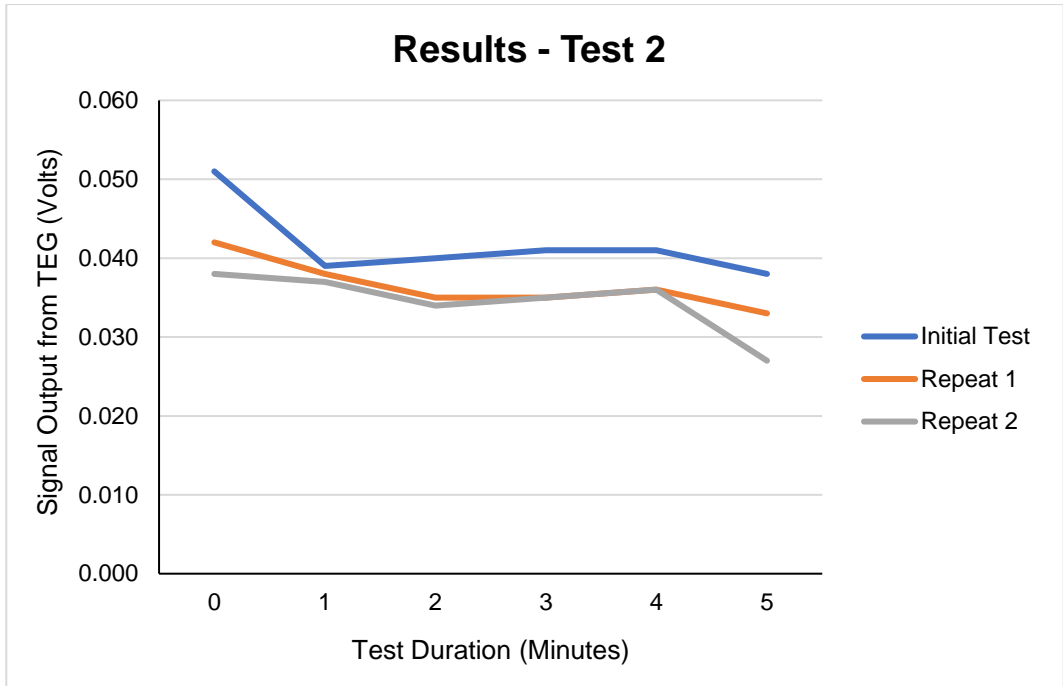


Figure 4-12. Results Graph Test 2 – Three TEG's, Series Wiring Method (No Granite Block)

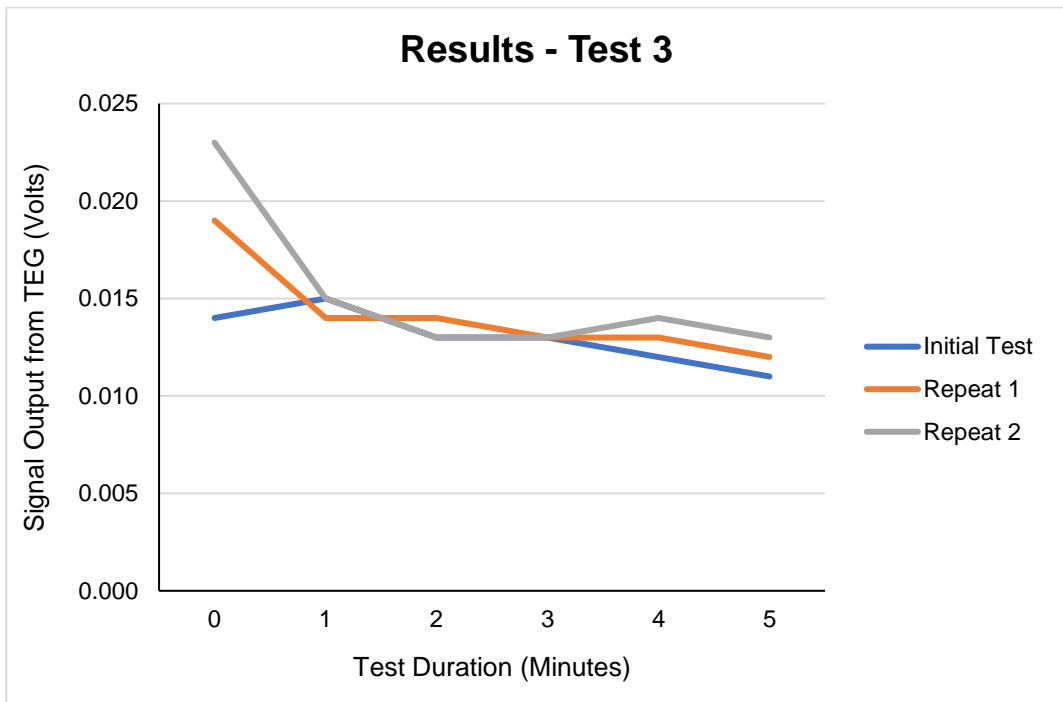


Figure 4-13. Results Graph Test 3 – Three TEG's, Parallel Wiring Method (No Granite Block)

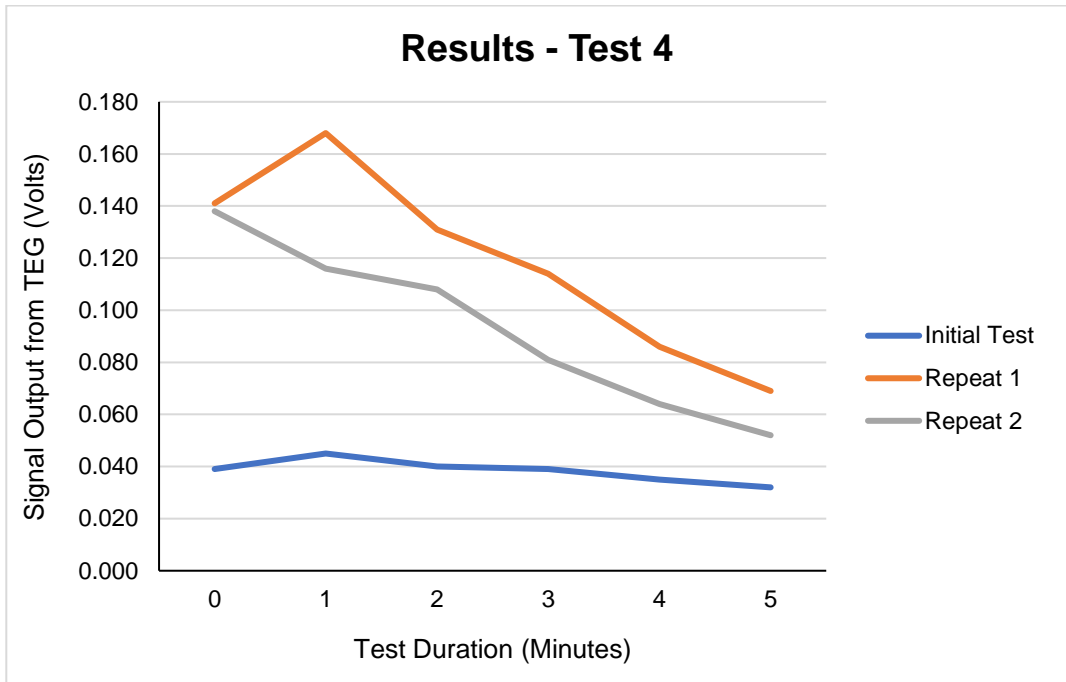


Figure 4-14. Results Graph Test 4 – Single TEG, with Granite Block

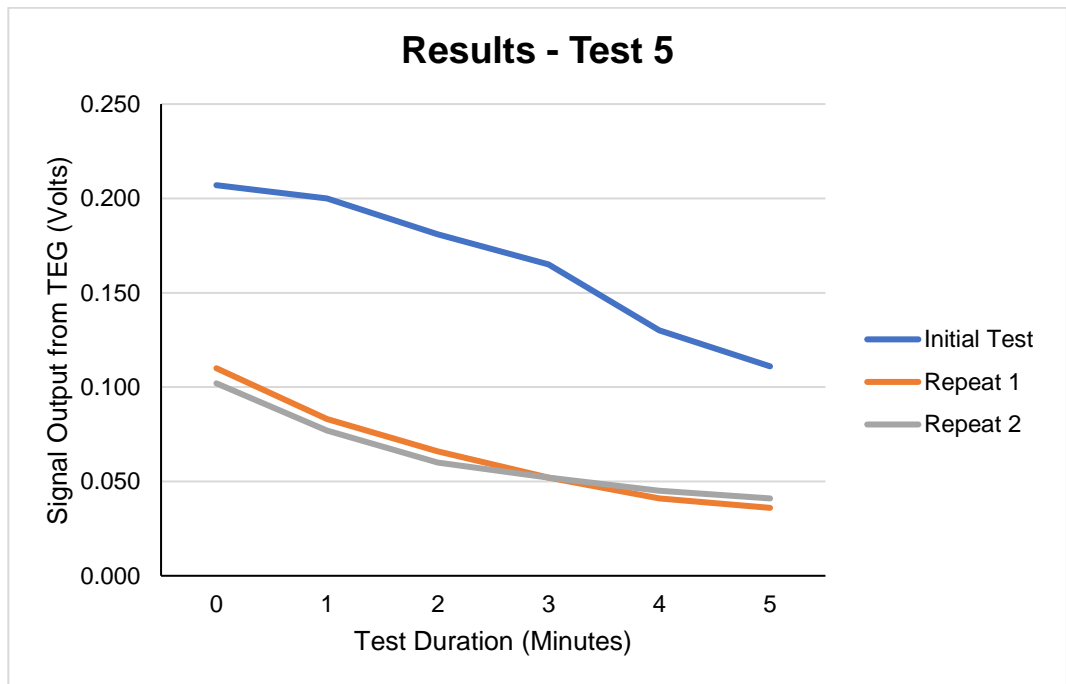


Figure 4-15. Results Graph Test 5 – Three TEG's, Series Wiring Method, with Granite Block

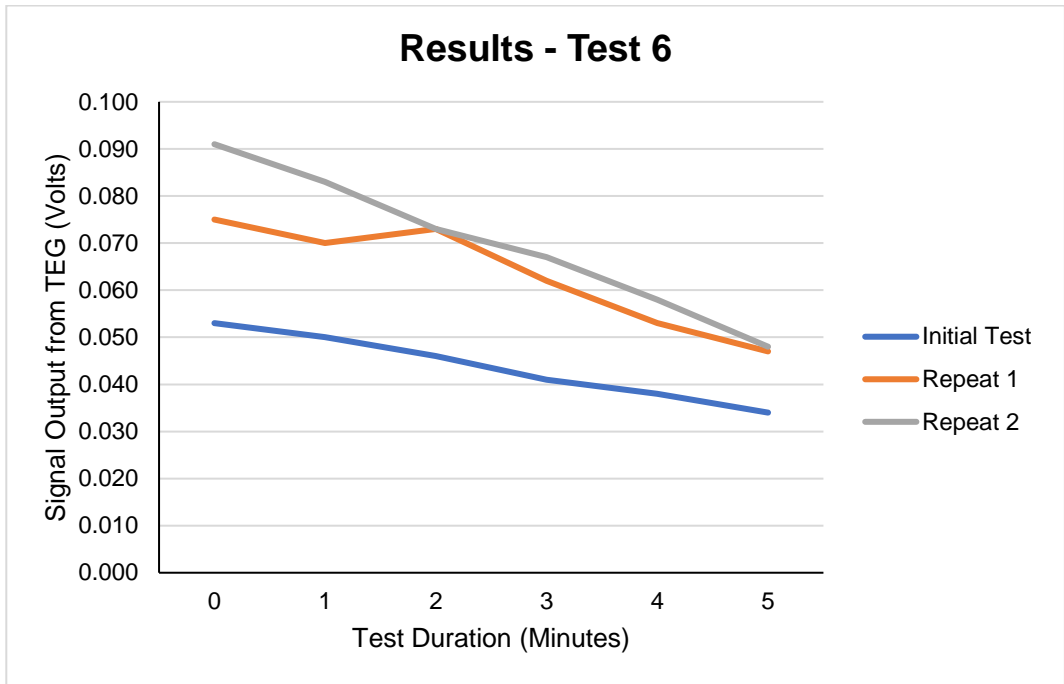


Figure 4-16. Results Graph Test 6 – Three TEG's, Parallel Wiring Method, with Granite Block

4.3. Test 3 – Motion Sensing Results and Discussions

This test was performed on 7th of August 2022. Each performed test took between 250 to 260 seconds to execute, with an average test time of 84 seconds. Overall, the testing yielded positive results. Upon completion of each individual test, the data logger was connected to the computer and the recorded data was downloaded into the EasyLog software; after all tests were complete, the outputted data chart and graphs were converted to PDF file format. The data logger output format is that of a non-modifiable nature, the represented graphs do not have suitably named axis; for these tests performed the Y axis represents the out voltage recorded from the accelerometer whilst the X axis is the time recorded as minutes from the specific time of recording. As the data logger continuously takes readings until the connection with the circuit is broken, the specific data range can be understood as being viewed from the very beginning of the graph up until 84 seconds. When observing the graphically displayed data, two horizontal red dotted lines were applied, these lines show the maximum and minimum voltage inputs as specified in the ADXL335-BB. Whilst all the data should fall in between these two lines, there are instances where the maximum limit is exceeded - this is as a result of the voltage offset applied. When noting periodic voltage measurements taken with a multi-meter, it can be understood that there is a tolerance of $\pm 0.05V$. Although the data logger was recording the output voltage of the accelerometer in volts and attaining numerical data, for the purpose of this research, the predominant interest is the graph shape. Observing figure 4-17, it can be understood that there are two desired profiles, as discussed below.

- The “Full Bicep Actuation” shape, which can be interpreted by a positive slope from the lowest voltage value to the highest value. This is then followed by a straight run where the motion was held for the ten second timer period. After this there is an inverse slope returning from the highest value to the lowest value.

- The “Simulated Struggle Point”, where the profile again begins with a positive slope, however where the simulated struggle was performed, a straight run halfway through the positive slope should be seen. Once the ten second time interval is complete, then the actuation continues, and a positive slope should continue until the highest voltage value is again achieved. Again, after the ten second time interval, a continuous inverse slope back to default should appear.

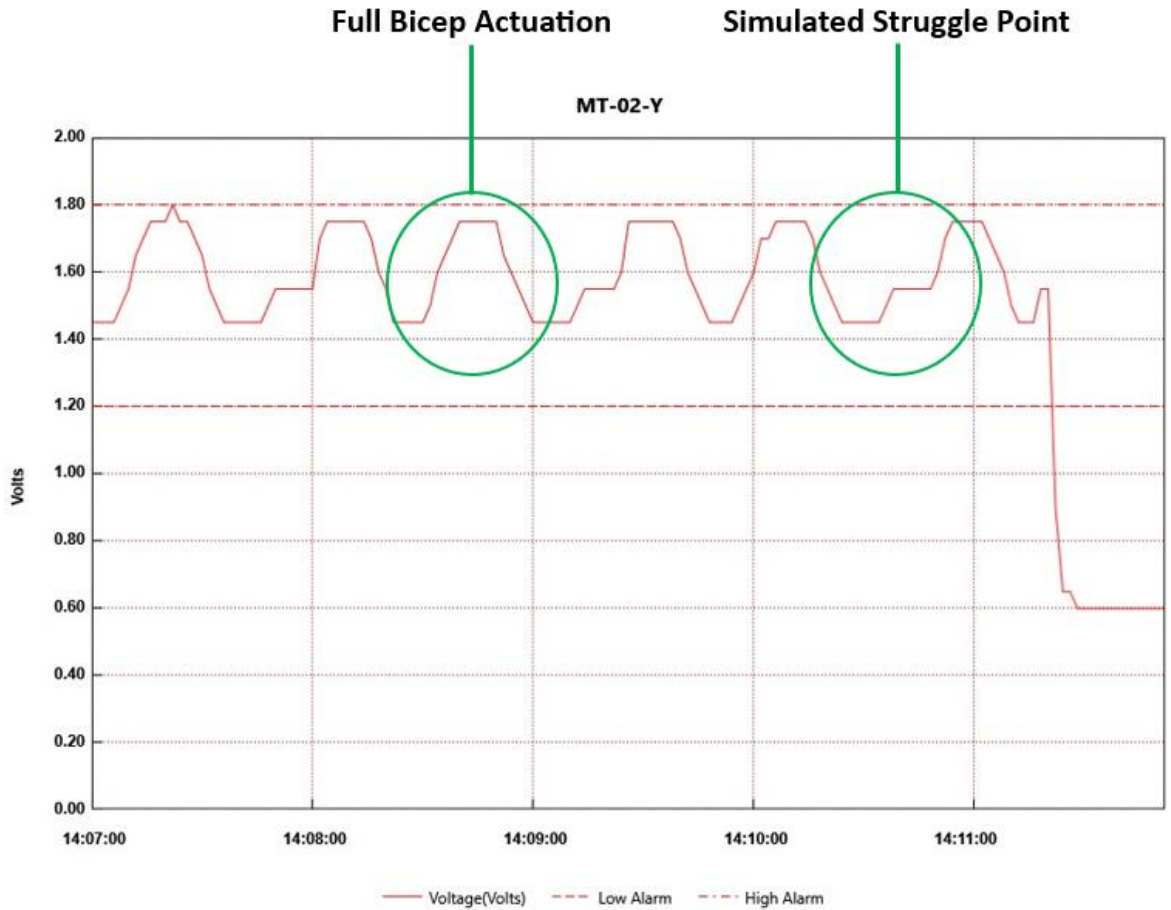


Figure 4-17. Image Illustrating the Desired Graphical Shape

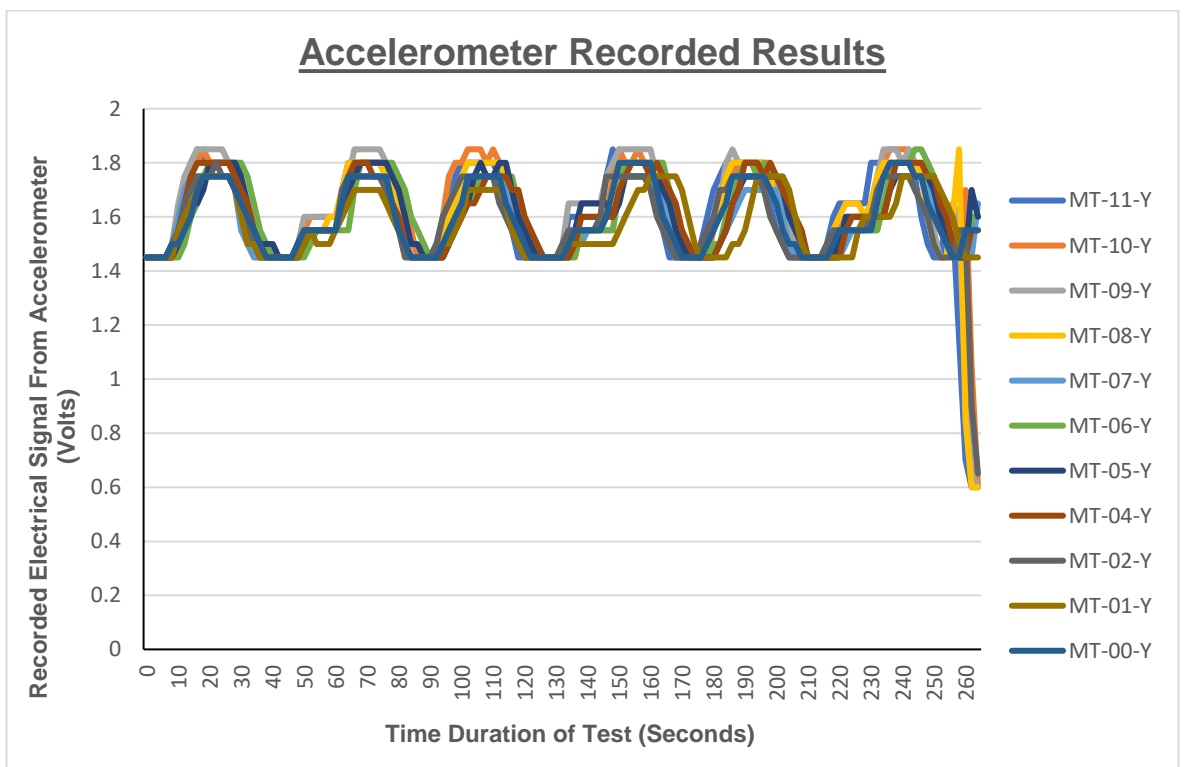


Figure 4-18. Processed Results of Accelerometer Testing

If the discussion above in section 4.3 in addition to figure 4-17 is understood when reviewing the generated line graphs visually, it can be seen that 11 of the 36 tests almost perfectly replicated the desired line profile. Figure 4-18 illustrates the combined 11 successful test clearly demonstrating the accuracy of the accelerometer output signal with relation to time and position. Figures 4-20 to 4-30 provide a more detailed view of the data recorded for each test. When observing these graphical representations, the results rendered clearly demonstrate the success of the accelerometer, the clarity in which the device provided an electrical feedback signal in relation to the movement performed and the struggle point simulated; shows promise for the implementation of the device into wearable robotics.

When looking closely at the electrical output signal, it can be seen that for each test the signal fluctuates between 1.45v and 1.85v which is in line with the manufacturer's specification of the accelerometer. This demonstrates that the accelerometer is not only operating correctly but also that it is tracking the actuation movement efficiency. Additionally, credence can be given to the test data by looking at the centre point (equilibrium point) reading of the device, which the manufacturer states is 1.65v at 0 degrees of movement in the Y axis. In figure 4-18 at the start of the actuation, the electrical output signal is at around 1.45v, showing that the accelerometer was in a negative angular position to the centre point; as the device is raised during the actuation, the electrical output signal rises to around 1.85v passing the centre point.

When specifically examining the 1.65v value detailed on the Y axis of figure 4-18, it is clear that this value is positioned in at the middle of the actuation. As discussed in section 3.6.11, the actuation methodology starts with the arm extended fully with the fingertips being parallel to the floor, before rising upward, arcing around the elbow joint. Observing the electrical output signal starting at 1.45v rising past 1.65v, peaking at 1.85v before returning to 1.45v. This unequivocally supports the actuation methodology described, showing the accelerometer being located in a negative degree of movement with relation to its central set point value of 1.65v before rising to a positive value (1.85v).

Understanding whether the device can accurately track a point at which a "struggle" occurs, requires interrogation of the data displayed between 40 to 80 seconds, 130 to 170 seconds and 210 to 250 seconds demonstrated in figure 4-6. When this data is reviewed, it can be understood that - in line within the testing methodology - a "flat line" occurs when the user holds their arm in a stationary position for the specified time period. The electrical output signal from the accelerometer records a voltage of between 1.5 and 1.65v, a variation that can be attributed to the nature of the test being performed; being that the timings of each movement were reliant on human operator. These results clearly demonstrate an accurate, real time and repeatable electrical output signal that can graphically mimic an individual's movement.

It is also important to review the actual device used for capturing this data, and how it is compliant with the objectives of this research. The ADXL335 accelerometer that was used in this study can be purchased for £14.10 as listed on The PiHut (2023) website, demonstrating the cost-effective nature of this sensory device. Additionally, this device can interface with, and be controlled by, a Raspberry Pi 4 Model B computer, which is listed as costing £45 on The PiHut (2023) website. By using this device within the testing performed for this research and evaluating it in conjunction with the test data returned, it can be distinctly seen that a method of monitoring and assisting an individual with movement, costing sub £100 has been identified.

Based on the discussions above it can be affirmed that this testing identified three optimum positions for recording the desired movement performed; these positions can be observed below in figure 4-19 and are as follows: MT-00-Y (position 1A), MT-02-Y (position 1C) and MT-07-Y (position 2D).

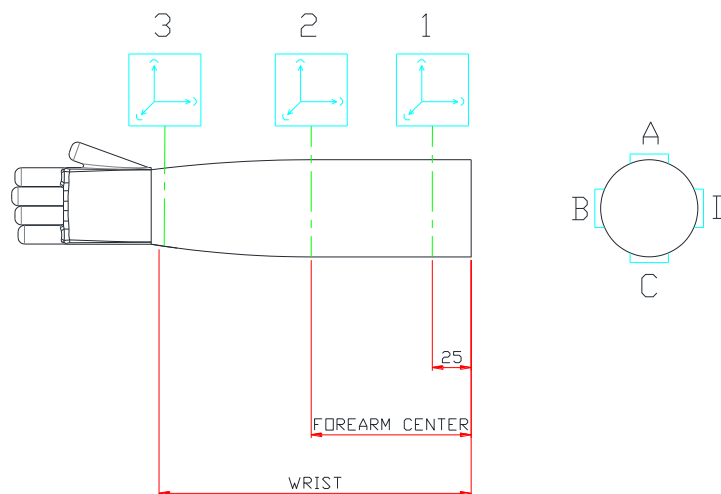


Figure 4-19 Accelerometer Position Schemati

To understand the validity of this data a 95% confidence level was used to calculate the confidence interval based on a total sample size of 134 data points for each test. Because this sample size was over 30 the Z-distribution table was used, to calculate a 95% confidence level a Z value of 1,96 acquired. The calculated confidence level for each test can be found in table 4-6 below. When reviewing this data, it can be seen that there is minimal fluctuations between each test when observing the average output voltage. Although for test MT-06-Y, MT-05-Y and MT-04-Y the average is the same value, the confidence interval does vary.

Table 4-6. Accelerometer Testing Error Treatment Table

Test Number	Average Output Signal	Confidence Interval (Z)
MT-11-Y	1.60V	±0.037V
MT-10-Y	1.63V	±0.032V
MT-09-Y	1.62V	±0.035V
MT-08-Y	1.60V	±0.035V
MT-07-Y	1.58V	±0.021V
MT-06-Y	1.61V	±0.024V
MT-05-Y	1.61V	±0.022V
MT-04-Y	1.61V	±0.023V
MT-02-Y	1.58V	±0.027V
MT-01-Y	1.57V	±0.020V
MT-00-Y	1.60V	±0.022V

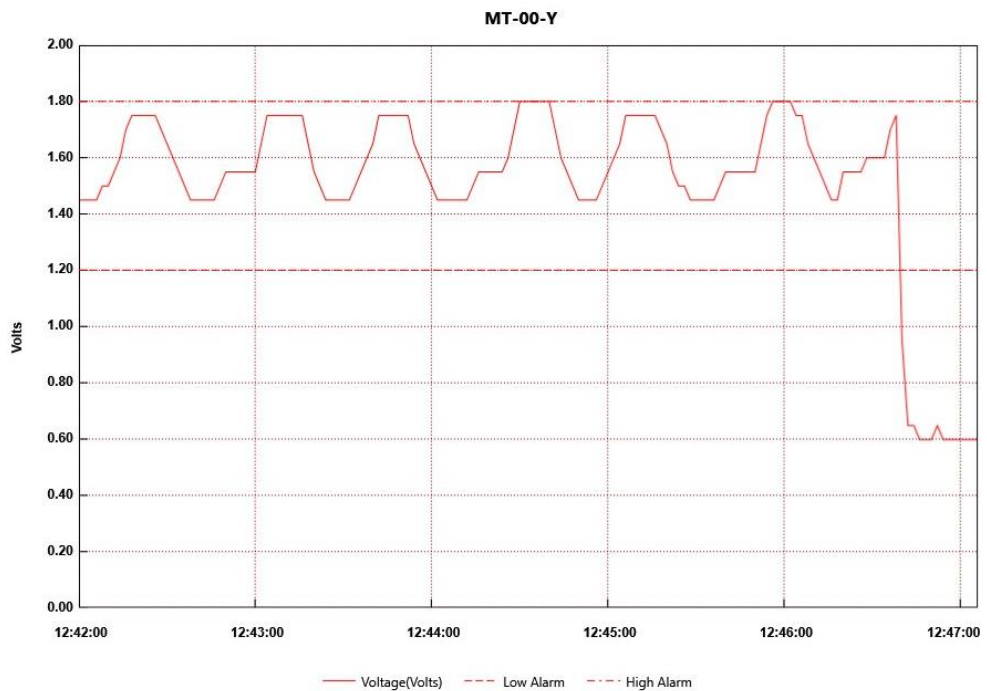


Figure 4-20. Test MT-00-Y (Position 1A)
 [Y axis = electrical output signal in Volts, X Axis = test duration in minutes]

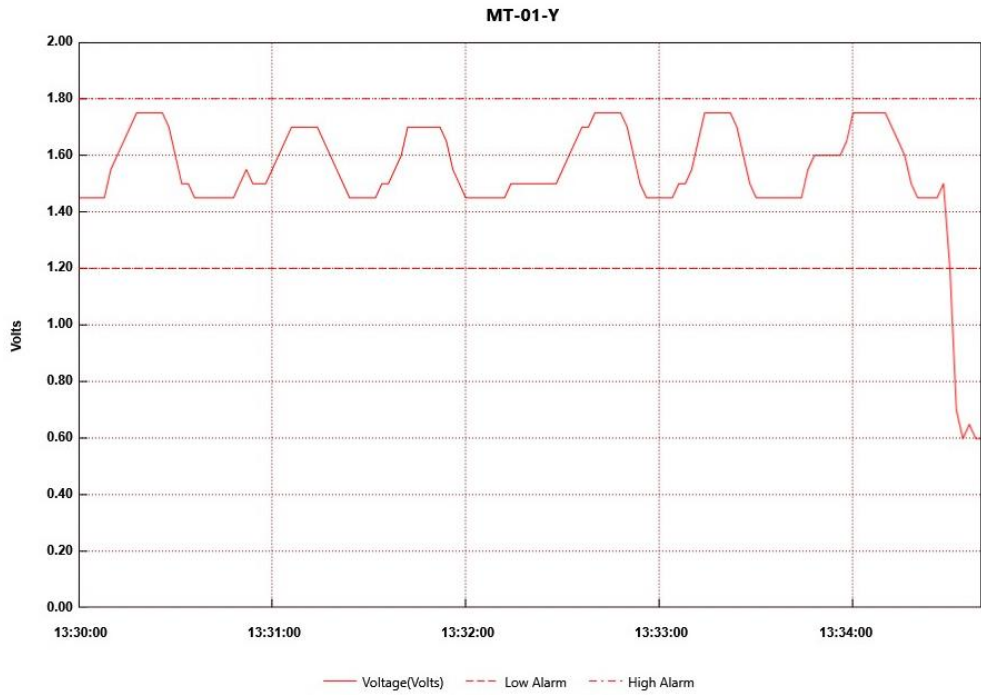


Figure 4-21. Test MT-01-Y (Position 1B)
[Y axis = electrical output signal in Volts, X Axis = test duration in minutes]

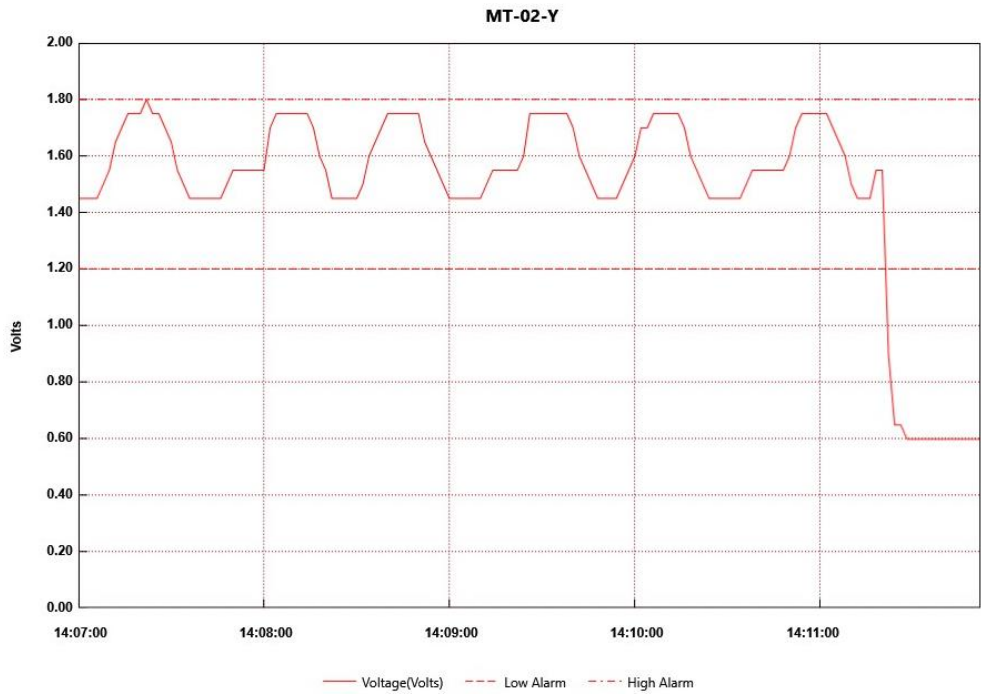


Figure 4-22. Test MT-02-Y (Position 1C)
[Y axis = electrical output signal in Volts, X Axis = test duration in minutes]

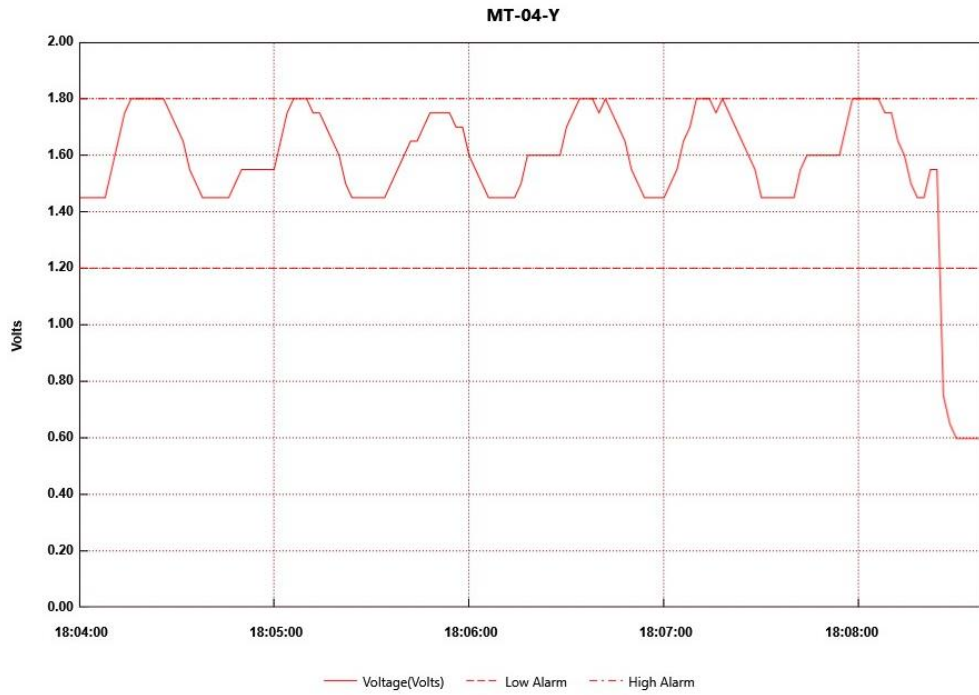


Figure 4-23. Test MT-04-Y (Position 2A)
 [Y axis = electrical output signal in Volts, X Axis = test duration in minutes]

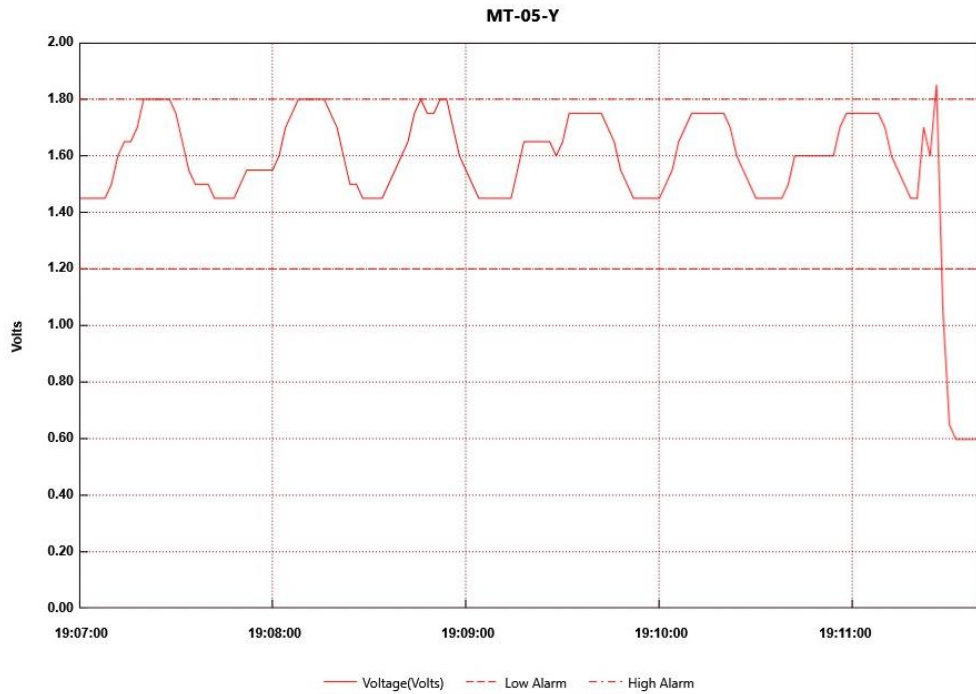


Figure 4-24. Test MT-05-Y (Position 2B)
 [Y axis = electrical output signal in Volts, X Axis = test duration in minutes]

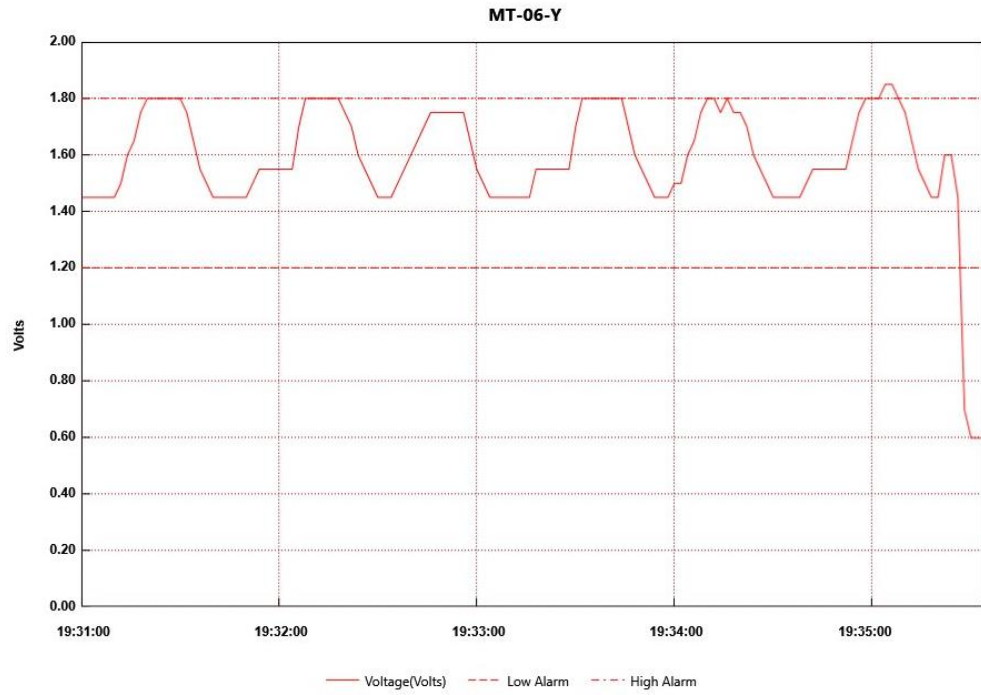


Figure 4-25. Test MT-06-Y (Position 2C)
 [Y axis = electrical output signal in Volts, X Axis = test duration in minutes]

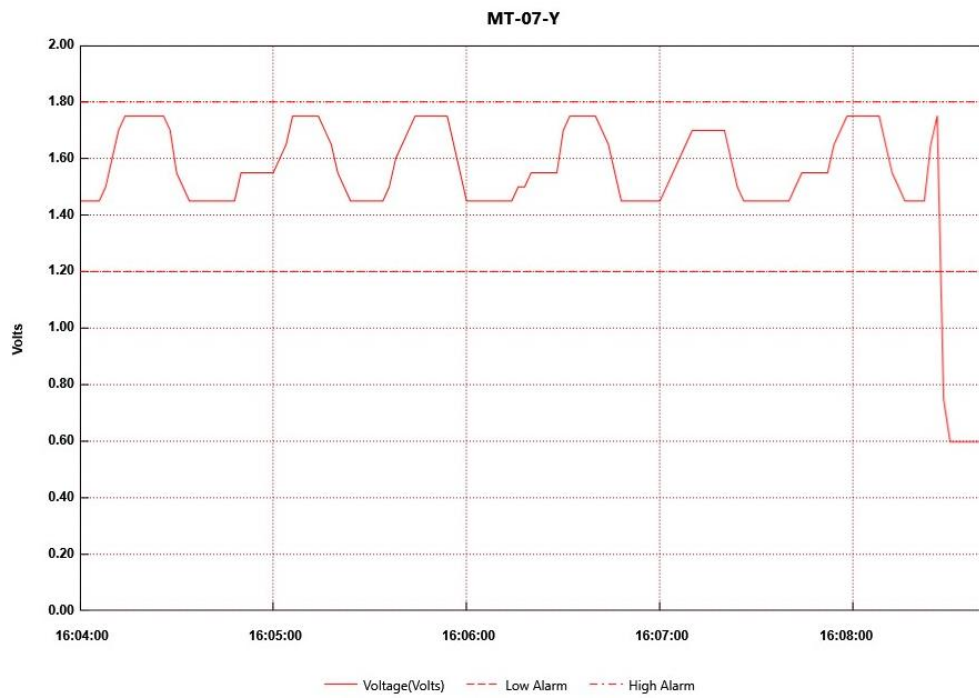


Figure 4-26. Test MT-07-Y (Position 2D)
 [Y axis = electrical output signal in Volts, X Axis = test duration in minutes]

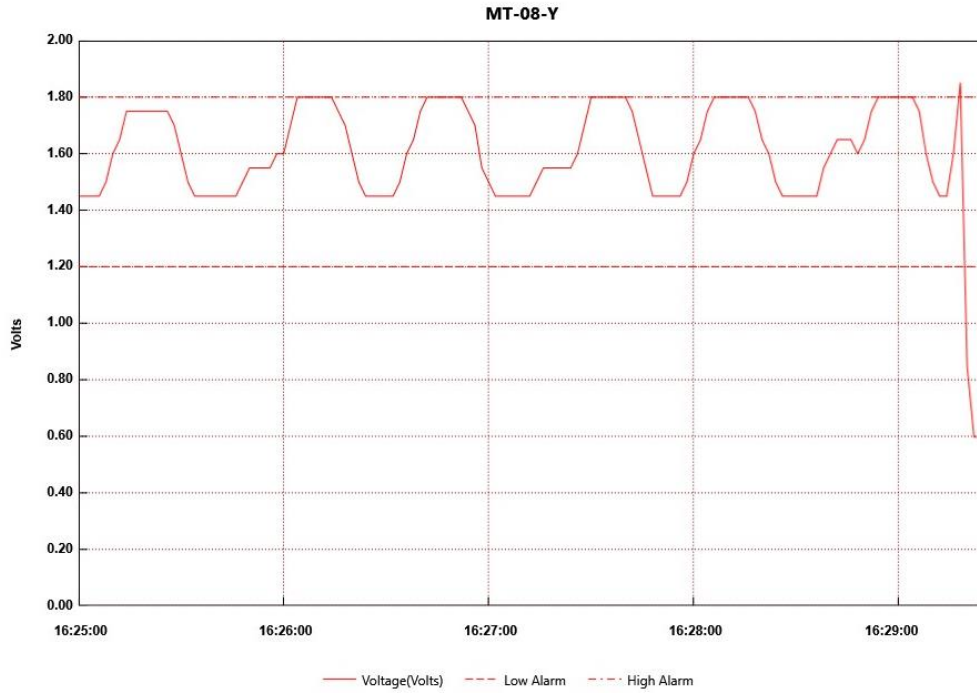


Figure 4-27. Test MT-08-Y (Position 3A)
 [Y axis = electrical output signal in Volts, X Axis = test duration in minutes]

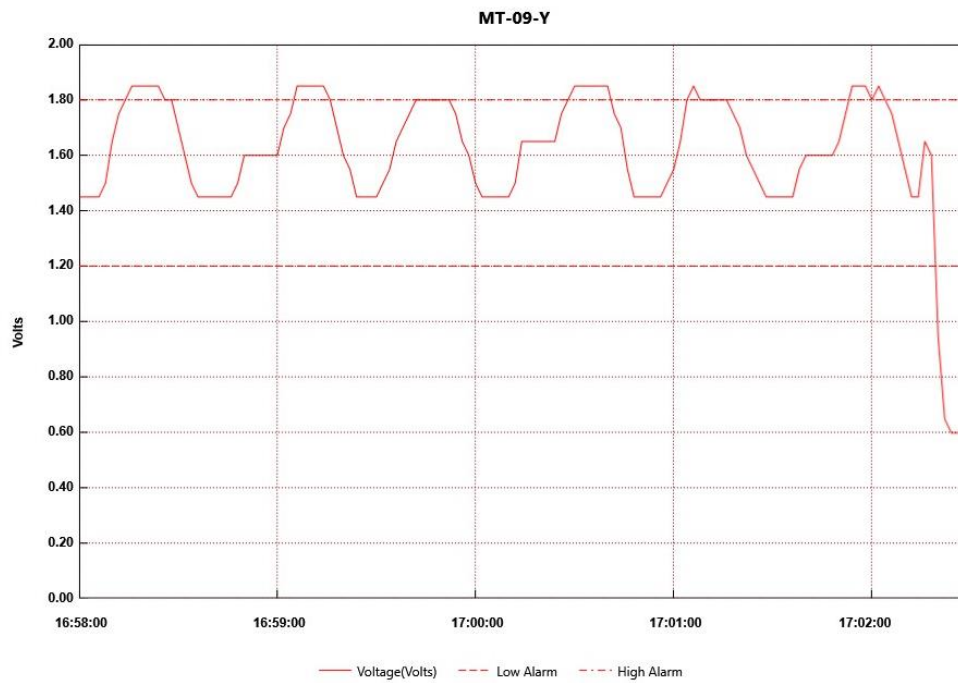


Figure 4-28. Test MT-09-Y (Position 3B)
 [Y axis = electrical output signal in Volts, X Axis = test duration in minutes]

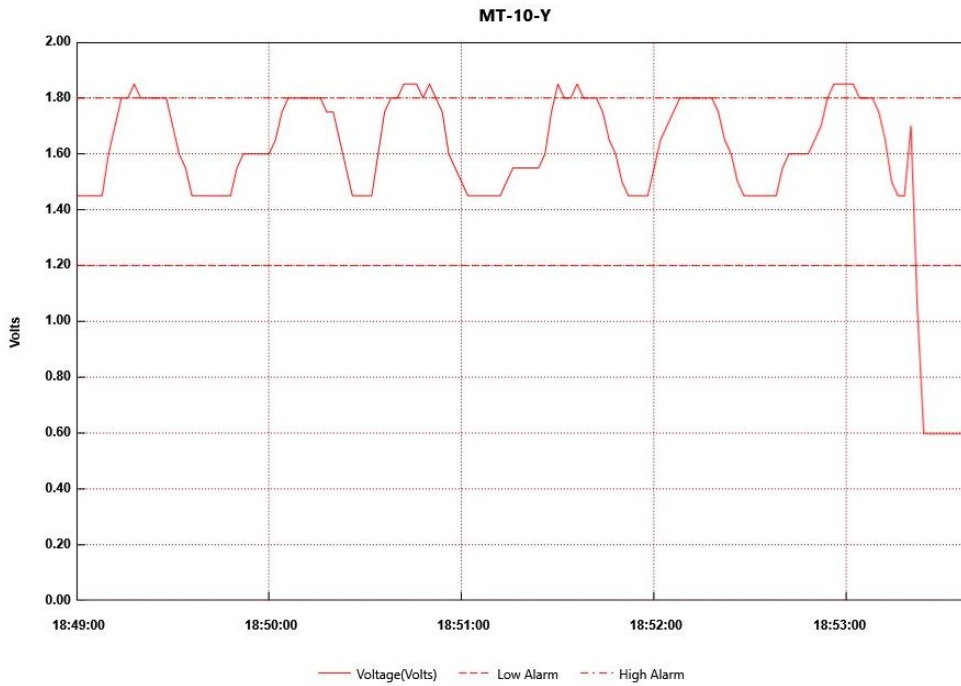


Figure 4-29. Test MT-10-Y (Position 3C)
 [Y axis = electrical output signal in Volts, X Axis = test duration in minutes]

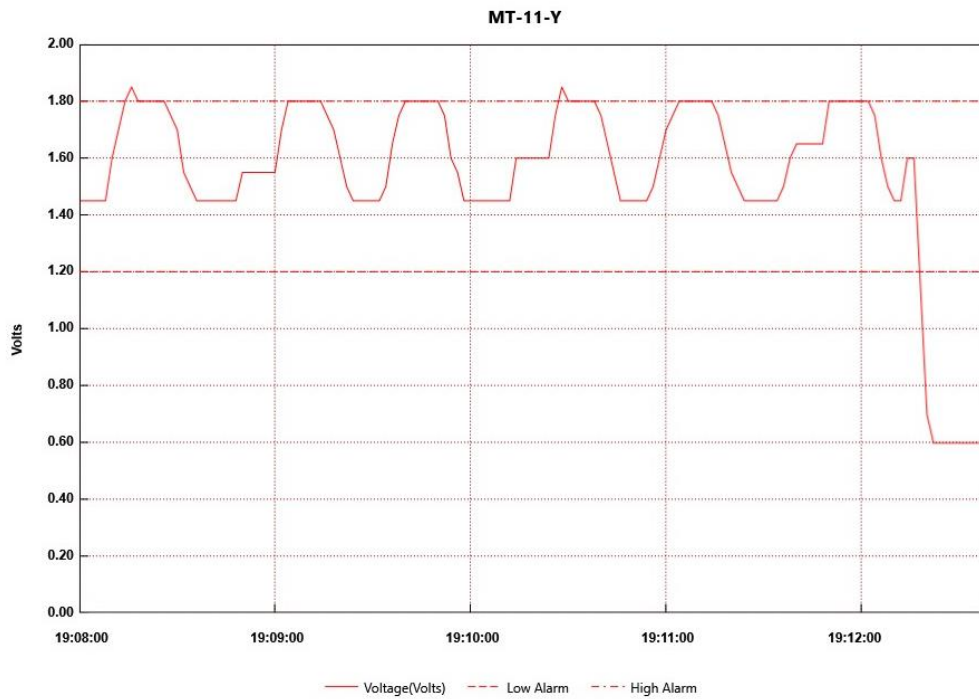


Figure 4-30. Test MT-11-Y (Position 3D)
 [Y axis = electrical output signal in Volts, X Axis = test duration in minutes]

5. Conclusion

The literature review of this thesis identified two key research gaps that required studying, the first being the development of a low-cost motion sensing device that had the criterion of being: easy to integrate into an assistive muscle device, non-invasive (or requiring being fixed to an individual's physiology directly), accurate in its data acquisition of the user's movement and having the ability to monitor an individual's struggle point. The second being a method of powering this device in a mobile and renewable manner, which was identified through the literature review as being done so via human thermal radiance (body heat). A cross-referenced overview of the introduction and literature review identifies a fundamental lack of viable engineered solutions that can be classed as non-invasive exo-muscular devices, with many technologies falling victim to the current limitations of this field of study; these limitations being the commercial viability of these devices where they are too expensive for general consumer use, the impracticality of the systems where they are not easily integrated into a person daily life and in many cases where they are underdeveloped and remain at lab scale testing. Through both the introduction and the literature review's critical analysis, a neglected potential user can be presumed - these being individuals inflicted with debilitating muscular illnesses, where the current assisting technology is relatively inaccessible to these individuals. This not only affirmed the research gap previously discussed, but also provided an additional reason as to why this research was undertaken.

A key aspect of this research was to provide an industrial engineered approach to the research, where both commercial viability and technical practicality overlapped to provide sufficient outcome. Analysing the experiments designed for this research, it can be observed that a balanced engineered approach has been employed, which attempts to not only provide suggestion on technological advancements but also considers commercial implications; in some cases, these benefits can be considered as indirect. Three pivotal experiments were performed within the scope of this research to provide suggestion on further development to the subject matter. Summarising the desired outcomes, the research aimed to provide two main contributions. The first being that of a sensing device which would employ a global constant that can be monitored for change when muscle actuation takes place allowing for more accurate data to be analysed during operation and used in conjunction with simplified logic controllers. This device would need to be able to map the data efficiently, specifically during a point of struggle within an individual's motion. The second outcome needed to provide suggestion on how the reliance on plugged power such as mains electric or large batteries could be reduced – e.g., by using a more natural power source such as natural body radiance (body heat).

The first test that was performed investigated whether a biological constant within human physiology could be used, this being either heart rate and/or oxyhaemoglobin saturation levels (SpO₂). When reviewing the results and discussions from the performed test in section 4.1, there is a clear understanding that this methodology of sensing movement and struggle is not adequate to provide sufficient and consistent data. Reviewing the data displayed in section 4.1, it is clear that

the heart rate recorded during movement fluctuated in large quantities, the graphical slopes represented in figures 4-2 to 4-8 have no consistency and demonstrate somewhat erratic data sets. Furthermore, the individual used during this test was a 27-year-old male who suffered from asthma but had no existing heart conditions; this parameter (heart rate) is variable from individual to individual which could further exacerbate issues with attaining reliable data. This captured data and the above discussion unequivocally rule out the heart rate being used as method of monitoring an individual's movement with the intention of identifying a struggle point. If the second data set within this test is observed, this being the monitoring of oxyhaemoglobin saturation levels, it can be understood that this methodology performs in a manner that's opposite to the heart rate. The lack of tangible change in the oxyhaemoglobin saturation levels provides no clear basis for data to be drawn and interrogated for the purpose of signalling an artificial muscle actuation. Observing figure 4-1, and by using a Gaussian function, the normal distribution of the data set is 97.21 with a standard deviation of 0.5210; this data processing informs that through the testing the recorded data remained stable and was relatively non-reactive to the motion and simulated struggle. Additionally, similar to the heart rate, as this is a biological value that is being monitored, the reliability of this could be affected from individual to individual. Simply explained the oxyhaemoglobin saturation levels provided such little deviation from which tangible data could be extrapolated and processed, whilst the heart rate was too volatile to provide consistent data which could be interrogated. This allows a conclusion to be firmly drawn which states that neither the heart rate nor oxyhaemoglobin saturation levels are a sufficient method of sensing motion for use within artificial muscle technologies.

The second test developed and performed investigated how a renewable energy source could be attained and utilised within an artificial muscle system, this being the use of natural human thermal radiance (body heat) and its conversion via the Seebeck effect to electrical power. The conversion methodology was done by employing a simple thermoelectric generator (TEG) device. A total of eighteen test were performed, this being six tests original in their design and two repeats of each test, meaning each test was performed a total of three times. The tests were split into two main subcategories exploring the effects of the TEG devices both with and without assistive cooling. Within these two subcategories the tests were then divided by both quantity and wiring methodology.

When first observing the tests at their most sub level (the differences between each test being the quantity and wiring method), the results displayed in tables 4-2 to 4-4 and figures 4-11 to 4-13 provide an interesting insight into the development of power generation specifically for sensing devices. As discussed in section 4.2 the wiring methodology used for multiple TEG's does affect the output signal, with the research demonstrating a 62% increase in power when using the series wiring methodology. However, the parallel wiring method provided a slightly more consistent electrical signal, with test 3 having an average normal distribution of 0.014V with a standard deviation of 0.002 across all tests; whilst test 2 had an average normal distribution of 0.037 with a

standard derivation of 0.003 across all tests. This data does demonstrate the benefits to both wiring techniques, however, this does not provide a definitive conclusion as to which wiring methodology is preferred for the application of powering sensing devices. Whilst a higher voltage output is required than what can be achieved with parallel wiring, the signal constancy is important to ensure the device that is being powered is working efficiently. In both case additional electrical devices can be added to circuit to assist with this, to increase the voltage a DC power step up device can be added, whilst a capacitor can be added to series circuit to assist with smoothing the signal.

Observing the second subcategory of testing, demonstrates how the first data set is affected when the temperature differential between the hot and cold side of the TEG is increased. Reviewing all this data definitively illustrates that significantly increasing the opposing temperatures at either side of the TEG can have an enormous impact on the outputted voltage. As discussed in section 4.1 by applying a cold temperature differential to the outside surface of the TEG, an increase of voltage out value by 75% can be gained. This testing and the data acquired informs that if body heat is to be considered for use in this application, then relying on the surrounding environmental temperature is not enough to ensure the maximum efficiency of the TEG. If a significant and consistent temperature differential is not maintained, then this could have a detrimental impact on the functionality of the TEG's. One limitation of this specific testing performed within this research is the method of how the temperature differential was created. This was done in a simple manner with granite blocks which had been stored at -19°C - the surface temperature of the blocks was not recorded before or after the testing was performed.

Reviewing figures 4-11 to 4-13, one common trait that is visible across all testing scenarios, is the correlation of signal degradation over the test duration. It can be seen in all cases that over the period of the test the electrical output signal significantly declined, with an average decline of around 60%. Although the results are promising, one limitation of this thesis is that lack of additional testing. As discussed in section 4.2 the required voltage to power a sensor such as an accelerometer requires a voltage of around 2 Volts, with the maximum outputted voltage recorded being 0.2 Volts. During this research no attempt was made to perform testing with the TEG's directly powering an accelerometer during its operation. However, understanding all the discussion above it can be concluded that this test was successful in demonstrating the suitability of using human thermal radiance (body heat) as method of generating low voltage electrical signals.

The final experiment performed rendered positive and informative results from the testing undertaken. Demonstrating the applicability and useability of a low-cost electric sensor to monitor an individual's motion and struggle point when actuating their bicep, in addition to defining three optimum locations for the sensor as per the detailed graphic in figure 4-19 within section 4.3. The optimum positions are as follows:

- Position 1A - in line with the user's thumb and close to the elbow joint.

- Position 1C - in line with the user's small finger and close to the elbow joint.
- Position 2D - located 90° clockwise to the user's thumb and in the centre of the forearm.

Whilst all the performed tests provided some manner of graphical feedback that mimicked the operator's movement, eleven of the thirty-three tests provided the most tangible and clear data; with the remaining twenty five test providing visibly skewed data. In each test a total of three bicep actuations were performed to understand the repeatability of the device. Observing figures 4-20 to 4-30, visually the represented line shows the movement undertaken during the testing, at each struggle point this is demonstrated by a flat line where the device was held stationary, and then a continuation of the line as the actuation was completed.

The conclusion that can be drawn from the discussions and acquired data for this test, can confidently confirm the useability, repeatability, and reliability of using an accelerometer for the purpose of not only monitoring motion, but also providing sufficient and accurate analysis of the user's movement for a logic controller to interpret. As no existing research currently provides details of the expected graphical outcome of an individual's struggle point being monitored by an accelerometer, the originality of this testing not only provides credence to the outcomes of this research thesis, but additionally has provided a graphical line shape that can be used in future projects as datum reference. By using low-cost devices such as accelerometers, the overall complexity of the controlling system for artificial muscle technologies can be reduced; as suggested in section 3.6, the use of low-cost controllers such as the Raspberry Pi Pico is a possibility when using accelerometers.

The research performed was undertaken during the 2020 global pandemic and subsequent years, and as a result of this, the experimentation was undertaken in a home environment rather than a strict controlled lab-based environment. However, this is not necessarily detrimental to the outcomes of the research - attempting to provide an engineered approach to the subject field does by definition require an element of "real world" condition testing, where variables such as environmental conditions cannot be controlled. Additionally, to provide a focused approach to the research, the experiments were limited to the arm only.

Overall, the research performed within this thesis has demonstrated an original approach to advancing the study area of non-invasive exo-muscular assistive devices. Adopting an industrial engineering perspective and approach to the testing performed, the research has been undertaken with the practical and commercial viability of intelligent sensing for use within assistive muscular devices at the forefront of the objective outcomes. Through practical experimentation and prototyping, this research has not only clearly demonstrated where developments of the topic are required but also how these developments can be achieved. This thesis provided details and in-depth analysis of three original experiments specifically developed for this subject matter, with two out of the three test rendering positive and informative results. The research demonstrated how a

low-cost electronic sensor such as accelerometer can be integrated into assistive devices, with the purpose of accurately analysing the user's movement and mapping struggle points within their movement. Additionally, the testing undertaken has shown how such devices can be powered in a mobile and renewable way, by developing a method of testing which enabled an understanding of how an individual's body heat can be used to provide power via the conversion of a TEG. Finally, in keeping with the industrial engineering perspective of the research, this thesis also provided insight into why further developments in non-invasive exo-muscular assistive devices is important and must be continued. Observing individuals afflicted with illnesses such as ALS and cerebral palsy, the literature review endeavoured to understand the "how" and "why" this technology is needed, in an attempt to make this research further applicable.

5.1. Suggested Future Works

Based on the findings attained and the experiments performed within this research, it is clear that this thesis is the start of a larger research project. Aspects of this research, whilst studied, do require further advancements to ensure that the subject field does not remain underdeveloped. Furthermore, as the aim of this research was to assist with providing commercially viable solutions, if under researched then the discussed technologies may never make it beyond the lab. Therefore, to ensure a consistent and efficient development in the field of study of wearable robotics, additional future works must be performed, based on the suggestions discussed below.

When observing the future use of thermo-electric generators, research into methods of improving not only the value of the outputted voltage, but also its stability when using these devices will greatly aid the compactness of the overall system in addition to its green carbon footprint effect by using a renewable energy source. Further developments of soft TEG's in addition to the implementation of fabric developed by developed by Po-Chun (2017) and Wu and Hu (2018) must be considered to provide advancement to this field of study. Based on the confidence interval calculated and displayed in table 4.5 within section 4.2, there is a clear need further repeat tests to be performed to further study the reliability of using thermoelectric generators.

The use of an accelerometer device has been proven successful, further research into not only how this device can be made more compact but additionally how a device like this can be integrated into wearable robotics should be explored. Furthermore, additional position testing of the accelerometer on other areas of the body such as the legs, should be undertaken to aid in developing the versatility of artificial muscle technologies. The device should be tested in alternate scenarios, such as performing everyday tasks and running, to further expand the use and reliability that the device could have within wearable muscle technologies. To further ensure the repeatability of the accelerometer additional repeats of the tests performed in this thesis should be performed.

Developments into the actual muscle actuation devices must further be studied to aid in developing a full compact wearable assistive device. Exploration using some of the materials discussed in this thesis in addition to new manufacturing methods such as 3D printing needs undertaking, to further develop this field of study. However, this research must take into account commercial viability of the material.

6. References

- Als.org. (2022). Understanding ALS.
Available: <https://www.als.org/understanding-als#:~:text=ALS%20was%20identified%20in%201869,known%20as%20Lou%20Gehrig's%20Disease>. Last accessed 19th Apr 2022.
- Afroj, S. Karim, N. Wang, Z. Tan, S. He, P. Holwill, M. Ghazaryan, D. Fernando, A. Novoselov, K. Engineering Graphene Flakes for Wearable Textile Sensors via Highly Scalable and Ultrafast Yarn Dyeing Technique. *ACS Nano* **2019** 13 (4), 3847-3857.
Available DOI: 10.1021/acsnano.9b00319
- American Heart Association editorial staff. (2021).
Target Heart Rates Chart. Available: <https://www.heart.org/en/healthy-living/fitness/fitness-basics/target-heart-rates>. Last accessed 19th Mar 2022.
- American Honda Motor Co. Inc. (2022). High Quality Photos.
Available: <https://asimo.honda.com/gallery/>. Last accessed 31st May 2022.
- Analog Devices. (2022). Accelerometer Specifications - Quick Definitions.
Available: <https://www.analog.com/en/products/landing-pages/001/accelerometer-specifications-definitions.html>. Last accessed 12th May 2022.
- Analog Devices. (2010). Small, Low Power, 3-Axis ± 3 g Accelerometer.
Available: <https://www.analog.com/en/products/adxl335.html#product-evaluationkit>. Last accessed 24th Jul 2022.
- Anger S. (2009). Thomas Huxley, "On the Hypothesis that Animals are Automata" (1874).
Victorian Review. 35 (1), 50-52.
- Apple. (2022). Getting Raw Accelerometer Events.
Available: https://developer.apple.com/documentation/coremotion/getting_raw_accelerometer_events. Last accessed 12th May 2022.
- Artificialhumanoid. (2013). Festo fluidic muscle.
Available: <http://artificialhumanoid.blogspot.com/2013/09/festo-fluidic-muscle.html>. Last accessed 18th May 2022.
- Ashraf, G. (2018). Robotic exoskeletons: The current pros and cons.
World Journal of Orthopaedics. 18 (9), 112-119.
- Asthma and Lung (2020). Tests to measure your oxygen levels.
Available: <https://www.asthmaandlung.org.uk/symptoms-tests-treatments/tests/oxygen-level-tests> Last accessed 19th Apr 2022.
- ASTM. (2020). Standard Terminology for Smart Textiles.
Available: <https://www.astm.org/d8248-20.html>. Last accessed 6th Mar 2022.

- Azom.com. (2001). Chlorinated Polyethylene - CPE.
Available: <https://www.azom.com/article.aspx?ArticleID=346>. Last accessed 5th Jul 2022.
- Babic, J. Laffranchi, M. Tessari, F. Verstraten, T. Novak, D. Sarabon, N. Veneman, J. (2012).
Challenges and Solutions for Application and Wider Adoption of Wearable Robots.
Wearable Technologies, 2, E14. Doi:10.1017/wtc.2021.13
- Baraka, A. et al. (2019). Wearable Accelerometer and sEMG-Based Upper Limb BSN for Tele-Rehabilitation. Applied Sciences, 9(14), p.2795. [online].
Available from: <http://dx.doi.org/10.3390/app9142795>
- BBC.co.uk. (2022). How do your muscles work?
Available: <https://www.bbc.co.uk/bitesize/topics/z7x78xs/articles/zpbxb82#:~:text=Muscles%20are%20attached%20to%20bones,back%20to%20its%20normal%20size>. Last accessed 21st Apr 2022.
- Bellis, M. (2019). Exoskeletons For Experimentation.
Available: <https://www.thoughtco.com/exoskeleton-for-humans-1991602#:~:text=General%20Electric%20developed%20the%20first,to%20be%20of%20military%20use>. Last accessed 19th Apr 2022
- Bellmunt, G O. Campanile, F L (2010) Actuator Principles and Classification.
In: Design Rules for Actuators in Active Mechanical Systems. Springer, London.
https://doi.org/10.1007/978-1-84882-614-4_1
- Boston Dynamics USA. (2022). ATLAS™.
Available: <https://www.bostondynamics.com/atlas>. Last accessed 31st May 2022
- Boston Dynamic USA. (2022). Payloads.
Available: https://shop.bostondynamics.com/spot?cclcl=en_US&pid=aDI6g000000XdpZCAS.
Last accessed 18th May 2022
- Breen, O. (2021). ABOUT OLIVIA. [Online]. www.oliviabreen.co.uk.
Available at: <https://www.oliviabreen.co.uk/biography> [Accessed 23 July 2023].
- Brigham Young University. (2022). Control of Body Movement.
Available: https://content.byui.edu/file/a236934c-3c60-4fe9-90aa-d343b3e3a640/1/module9/readings/voluntary_control.html. Last accessed 21st Apr 2022.
- Campbell NJ, Maani CV. Histology, Muscle. [Updated 2021 May 10]. In: StatPearls [Internet].
Treasure Island (FL): StatPearls Publishing; 2022 Jan-.
Available from: <https://www.ncbi.nlm.nih.gov/books/NBK537195/>
- Campbell, T. (2022). It's Eccentric!
Available: <https://thegolfperformancecenter.com/physical-performance/its-eccentric/>. Last accessed 11th May 2022.

- Canada's Drug and Health Technology Agency. (2021). Copied to clipboard ReWalk: Robotic Exoskeletons for Spinal Cord Injury.
Available: <https://www.cadth.ca/rewalk-robotic-exoskeletons-spinal-cordinjury#:~:text=ReWalk%20costs%20US%2471%2C600%20for,with%20additional%20annual%20service%20fees>. Last accessed 30th May 2022.
- Cahn, R W. Geer, A L (1996). Physical Metallurgy (Fourth, Revised and Enhanced Edition). 4th ed. UK: Elsevier. 1764-1765.
- Çelikel, D. C., 2020, 'Smart E-Textile Materials', in N. Tasaltin, P. S. Nnamchi, S. Saud (eds.), Advanced Functional Materials, IntechOpen, London. 10.5772/intechopen.92439.
- Centers for Disease Controls and Prevention. (2022). Data and Statistics for Cerebral Palsy.
Available: <https://www.cdc.gov/ncbddd/cp/data.html>. Last accessed 18th May 2022.
- Chandler, D. (2014). Making silicon devices responsive to infrared light. MIT News. [Online]. 2nd January 2014.
Available at <https://news.mit.edu/2013/making-silicon-devices-responsive-to-infrared-light-0102#:~:text=Silicon%2C%20which%20forms%20>. Last accessed 03rd August 2023.
- Chandler, D. (2019). Artificial “muscles” achieve powerful pulling force.
Available: <https://news.mit.edu/2019/artificial-fiber-muscles-0711>. Last accessed 18th May 2022.
- Chao, Lv. Et al. (2017). Humidity-responsive actuation of programmable hydrogel microstructures based on 3D printing.
Sensors and Actuators B: Chemical. 259 (B), 736-744.
- Chen, J. Et al. (2018). Rigid and Strong Thermoresponsive Shape Memory Hydrogels Transformed from Poly (vinylpyrrolidone-co-acryloxy acetophenone) Organogels.
Applied Materials and Interfaces. N/A (N/A), 32707-32708.
- Cherry, K. (2020). What Is the Autonomic Nervous System?
Available: <https://www.verywellmind.com/what-is-the-autonomic-nervous-system-2794823>. Last accessed 22nd Apr 2022.
- Comen, E. (2022). Check out how much a computer cost the year you were born.
Available: <https://eu.usatoday.com/story/tech/2018/06/22/cost-of-a-computer-the-year-you-were-born/36156373/>. Last accessed 25th May 2022.
- Darwin, C. (1875). INSECTIVOROUS PLANTS. London: JOHN MURRAY.
- Davidrhodes124. (2018). Cucumber tendrils.
Available: <https://steemit.com/steemstem/@davidrhodes124/cucumber-tendrils>. Last accessed 18th May 2022.

- De La Fuente, J. (2022). Properties Of Graphene. [Online]. www.graphenea.com.
Available at: <https://www.graphenea.com/pages/graphene-properties#.YxTqp3bMJEZ>
[Accessed 4 September 2022].
- Department for Transport. (2021). Transport: Disability and Accessibility Statistics, England 2019/20.
Available:https://assets.publishing.service.gov.uk/government/uploads/system/uploads/attachment_data/file/972438/transport-disability-and-accessibility-statistics-england-2019-to-2020.pdf. Last accessed 27th May 2022.
- Dias, T. (2015). Electronic Textiles Smart Fabrics and Wearable Technology. Cambridge: Woodhead Publishing. pp.76-104.
- Doetsch, F. (2003). The glial identity of neural stem cells.
Natural Science. 11 (6), 112-1134.
- Dubuc, B (2002). Photoreceptors.
Available: https://thebrain.mcgill.ca/flash/d/d_02/d_02_m/d_02_m_vis/d_02_m_vis.html. Last accessed 22nd Apr 2022.
- EasyLog. (2021). EL-USB-3 Voltage Data Logger.
Available: https://www.lascarelectronics.com/media/7276/package-easylog-data-logger-el-usb-3-iss18_02-21.pdf. Last accessed 24th Jul 2022.
- Edwin, J. et al. (2017). Knitting and weaving artificial muscles. Science Advances. 3(1), pp.1-11. [Online].
Available at: DOI: 10.1126/sciadv.1600327 [Accessed 23 July 2023].
- Ertekin, M. (2017). 7 - Aramid fibres. In: Seydibeyoğlu, M. Mohanty, A. Misra, M
Fibre Technology for Fibre-Reinforced Composites. UK: Woodhead Publishing. 153-167.
- Espinosa, J. et al. (2022). Multi-meter. [Online]. web.ua.es.
Available at: <https://web.ua.es/docivis/magnet/multi-meter.html> [Accessed 31 July 2022].
- Fab-ent. (2022). WEST Monofilaments.
Available: <https://www.fab-ent.com/evaluation/sensation/west-monofilaments/>. Last accessed 21st Mar 2022.
- Fairclough HE, Gilbert M, Pichugin AV, Tyas A, Firth I. (2018) Theoretically optimal forms for very long-span bridges under gravity loading. Proc. R. Soc. A 474: 20170726. <http://dx.doi.org/10.1098/rspa.2017.0726>
- Farzana, A. (2001). Temperature of a Healthy Human (Skin Temperature).
Available: <https://hypertextbook.com/facts/2001/AbantyFarzana.shtml>. Last accessed 4th Apr 2022.

- Festo Germany. (2019). Fluidic muscle DMSP.
Available: https://www.festo.com/cat/en_gb/data/doc_engb/PDF/EN/DMSP_EN.PDF. Last accessed 18th May 2022.
- Firgelli Automations Team. (2020). Want to know how does a Linear Actuator work?
Available: <https://www.firgelliauto.com/blogs/actuators/how-does-a-linear-actuator-work-1>.
Last accessed 11th May 2022
- Fitbit. (2022). How does my Fitbit device calculate my daily activity?
Available: https://help.fitbit.com/articles/en_US/Help_article/1141.htm. Last accessed 12th May 2022.
- Freudenrich, C and Boyd, R. (2001). How Your Brain Works.
Available: <https://science.howstuffworks.com/life/inside-the-mind/human-brain/brain2.htm#:~:text=Sensory%20neurons%20carry%20signals%20from,the%20brain%20and%20spinal%20cord>. Last accessed 18th May 2022.
- Gent, E. (2018). 6 ways the centuries-old art of origami is bringing us the future.
Available: <https://www.nbcnews.com/mach/science/6-ways-ancient-art-origami-bringing-us-future-ncna898731>. Last accessed 18th May 2022.
- Gerbode, S. Et al. (2012). How the Cucumber Tendril Coils and Overwinds.
Science. 337 (6098), 1087-1091.
- Hafen BB, Burns B. Physiology, Smooth Muscle. [Updated 2021 Aug 30]. In: StatPearls [Internet]. Treasure Island (FL): StatPearls Publishing; 2022 Jan-.
Available from: <https://www.ncbi.nlm.nih.gov/books/NBK526125/>
- Herculano-Houzel, S. (2009). The Human Brain in Numbers: A Linearly Scaled-up Primate Brain.
Frontiers in Human Neuroscience. 3 (31), 1-11.
- Hüseyin, E. Et al. (2018). The Effect of Acute Aerobical Exercise on Arterial Blood Oxygen Saturation of Athletes.
Journal of Education and Training Studies. 6 (9), 74-79.
- Huxley, F and Niedergerke, R. (1954). Structural Changes in Muscle During Contraction
Interference Microscopy of Living Muscle Fibres.
Nature. 173 (1), 917-973.
- ib.bioninja.com.au. (2022). Types of Muscles.
Available: <https://ib.bioninja.com.au/higher-level/topic-11-animal-physiology/112-movement/types-of-muscles.html>. Last accessed 21st Apr 2022.
- Ionov, L. (2014). Hydrogel-based actuators: possibilities and limitations.
Materials Today. 17 (10), 494-504.

- Jackson, J. (2022). What is the average bicep curl weight for men and women? (Dumbbell and barbell curl strength standards).
Available: [https://criticalbody.com/average-curl-weight/#:~:text=With%20that%20in%20mind%2C%20the,and%2025%20lbs%20\(dumbbells\)..](https://criticalbody.com/average-curl-weight/#:~:text=With%20that%20in%20mind%2C%20the,and%2025%20lbs%20(dumbbells)..)
Last accessed 7th Apr 2022.
- Jackson, P. Et al. (2019). Structure and Function of the Elbow and Forearm Complex.
In: Essentials of Kinesiology for the Physical Therapist Assistant (Third Edition). 3rd ed. USA: Elsevier In. 91-119.
- Jacob, U & Ksenia, M. (2023). Project Management Triangle. [Online]. bordio.com. Last Updated: 10 August 2023.
Available at: <https://bordio.com/blog/project-management-triangle/> [Accessed 24 August 2023].
- James, L. (2020). Understanding the difference between n- and p-type semiconductors.
Available: <https://www.power-and-beyond.com/understanding-the-difference-between-n-and-p-type-semiconductors-a-905805/>. Last accessed 27th Mar 2022.
- Jin, C and Bai, Z (2022). MXene-Based Textile Sensors for Wearable Applications ACS Sensors 2022 7 (4), 929-950
Available: DOI: 10.1021/acssensors.2c00097
- Jobbágy, B. Šimšík, D. Karchnák, J and Onofrejevová, D. (2014). Robotic Arm with Artificial Muscles in Rehabilitation. Procedia Engineering. 94 (25), 195-202.
- Jung, M and Ludden, G. (2019). What Do Older Adults and Clinicians Think About Traditional Mobility Aids and Exoskeleton Technology?
ACM Transactions on Human-Robot Interaction. 8 (2), 1-17.
- Kabir, H. Et al. (2014). The Applications of Shape Memory Gel as a Smart Material.
The Physical Society of Japan. N/A (N/A), 1-5.
- Kanik, M. Orguc, S. Varnavides, V. Kim, J. Benavides, T. Gonzalez, D. Akintilo, T. Tasan, C. Chandrakasan, A. Fink, Y and Anikeeva, P. (2019).
Strain-programmable fiber-based artificial muscle. Science. 365 (6449), 145-150.
- Kenler, M. (2020). The Supinated Dumbbell Curl 101 | How to Build Bigger Biceps.
Available: <https://anobolicaliens.com/blogs/the-signal/supinated-dumbbell-curl>. Last accessed 17th Jul 2022.
- Kerkman, J. Et al. (2018). Network structure of the human musculoskeletal system shapes neural interactions on multiple time scales.
Science Advances. 4 (6), 1-10.

- Kermavnar T, de Vries AW, de Looze MP and O'Sullivan LW (2021) Effects of industrial back-support exoskeletons on body loading and user experience:
An updated systematic review. *Ergonomics* 64, 685–711. <https://doi.org/10.1080/00140139.2020.1870162>
- Kim, J. (2017). Multifunctional Smart Biopolymer Composites as Actuators.
In: *Biopolymer Composites in Electronics*. UK: Elsevier. 311-331.
- Krans, J. (2012). The sliding filament theory of muscle contraction.
Nature Education. Natural Science. 4 (4), 3-66.
- Lang, R. (2007). The science of origami.
Physics World. 20 (2), 30-31.
- Lange, W. (1975). Cell number and cell density in the cerebellar cortex of man and some other mammals. *Cell and Tissue Research*. 157 (1), 115-124.
- Leal-junior, A. et al. (2020) Smart textiles for multimodal wearable sensing using highly stretchable multiplexed optical fiber system. 10 (13687), 1-12
- Lee CM, Jin SP, Doh EJ, Lee DH, Chung JH. Regional Variation of Human Skin Surface Temperature.
Ann Dermatol. 2019 Jun;31(3):349-352. <https://doi.org/10.5021/ad.2019.31.3.349>
- Lund, A. Et al. (2020). A polymer-based textile thermoelectric generator for wearable energy harvesting.
Journal of Power Sources journal. 480 (1), 1-11.
- Magleby, S. Thmson, M. Zirbel, S and Sigel, D. (2013). Accommodating Thickness in Origami-Based Deployable Arrays.
Journal of Mechanical Design. 135 (11), 1-25.
- Mahesh. (2016). Voice recognition using Raspberry Pi 3.
Available: <https://www.rhydolabz.com/wiki/?p=16234>. Last accessed 11th May 2022.
- Mandal, A. (2017). Origami-inspired artificial muscles can lift 1,000 times their weight.
Available: <https://www.news-medical.net/news/20171127/Origami-inspired-artificial-muscles-can-lift-1000-times-their-weight.aspx>. Last accessed 18th May 2022.
- Martinez-Hernandez, U.; Metcalfe, B.; Assaf, T.; Jabban, L.; Male, J.; Zhang, D. (2021). D. Wearable Assistive Robotics: A Perspective on Current Challenges and Future Trends.
Sensors. 21 (6751), 1-19.
- Matthews, C. (2012). 6.3 Simple Stress and Strain.
In: *Matthews, C Engineers Data Book*. 4th ed. UK: A John Wiley & Sons, Ltd, Publication. 138-141.
- Matthews, C. (2012). Section 3. Engineering Design – Process and Principles.
In: *IMECH E Engineers Data Book*. 4th ed. London: John Wiley & Sons LTD. 54-55.

Maxey, M. (2019). What's the Difference between an E-Textile, Smart Fabric, Functional Fabrics and Smart Textiles?

Available: <https://www.loomia.com/blog/2019/9/2/zl70axxzv913ajm64vm1rbdvrrfhgu>. Last accessed 6th Mar 2022.

Meenakshi, R and Gershon, M. (2016). The bowel and beyond: the enteric nervous system in neurological disorders.

Nature Reviews Gastroenterology & Hepatology. 13 (1), 517-528

Merck. (2022). Materials for Advanced Thermoelectrics.

Available: <https://www.sigmaaldrich.com/GB/en/technical-documents/technical-article/materials-science-and-engineering/microelectronics-and-nanoelectronics/thermoelectrics>. Last accessed 27th Mar 2022

Mikhailovsky, A. (2017). Smart Clothing Classification.

Available: <https://teslasuit.io/blog/smart-clothing-classification/#:~:text=Such%20kind%20of%20textiles%20works,wearable%20computers%20and%20so%20on>. Last accessed 23rd Feb 2022

Mogahzy, Y. (2009). 10. Types of fabric for textile product design.

In: Mogahzy, Y Engineering Textiles Integrating the Design and Manufacture of Textile Products. UK: Woodhead Publishing. 271-299.

Montalvao, D. (2015). Sensors and Signal Processing - Draft version (unedited and before final revision) of Chapter 5 of the book "Mechatronics: Fundamentals and Applications".

In: Clarence W. de Silva, Farbod Khoshnoud, Maoqing Li, Saman K.

Halgamuge Mechatronics: Fundamentals and Applications. Boca Raton: CRC Press. 125-220.

Motor Neurone Disease Association. (2021). How many people are affected?. [Online]. www.mndassociation.org. Last Updated: 25 January 2021.

Available at: <https://www.mndassociation.org/about-mnd/mnd-explained/what-is-mnd> [Accessed 23 July 2021].

Mulatier, S Et al. (2018). Electronic Circuits Integration in Textiles for Data Processing in Wearable Technologies. Advanced Materials Technologies. 3 (10), 1-26.

National Health Service Scotland. (2021). Motor neurone disease (MND).

Available: <https://www.nhsinform.scot/illnesses-and-conditions/brain-nerves-and-spinal-cord/motor-neurone-disease-mnd>. Last accessed 18th May 2022.

National Health Service UK. (2022). Cerebral palsy.

Available: <https://www.nhs.uk/conditions/cerebral-palsy/treatment/>. Last accessed 18th May 2022.

- National Health Service UK. (2021). How do I check my pulse?
Available: <https://www.nhs.uk/common-health-questions/accidents-first-aid-and-treatments/how-do-i-check-my-pulse/>. Last accessed 19th Apr 2022.
- Nishiyama, A. Et al. (2005). Astrocytes and NG2-glia: what's in a name?
Journal of Anatomy. 207 (6), 687-693.
- Noctor SC, Martínez-Cerdeño V, Kriegstein AR. Contribution of Intermediate Progenitor Cells to Cortical Histogenesis.
Arch Neurol. 2007;64(5):639–642. doi:10.1001/archneur.64.5.639
- Noritsugu, T. Et al. (2007). Wearable Power Assist Device for Standing Up Motion Using Pneumatic Rubber Artificial Muscles.
Journal of Robotics and Mechatronics. 19 (6), 619-628.
- Otex. (2022). Passive vs. Active smart Textiles.
Available: <https://osnf.com/passive-vs-active-smart-textiles/>. Last accessed 21st Jan 2022.
- Oxford Cambridge and RSA (2019). Physical Education: Component 1-1.1.a. Skeletal And Muscular Systems
Available: <ocr.org.uk> > 559837-1.1.a.-skeletal-and-muscular-systems.pptx
- Paleja, A. (2021). Watch Mechanics Destroy an SUV With the Power Loader from Aliens They Built.
Available: <https://interestingengineering.com/mechanics-destroy-an-suv-with-the-power-loader-from-aliens>. Last accessed 23rd May 2022.
- Papoutsidakis, M. Et al. (2016). Motion Sensors and Transducers to Navigate an Intelligent Mechatronic Platform for Outdoor Applications.
Sensors and Transducer. 198 (3), 16-24.
- Patel, D. Et al. (2020). Cerebral palsy in children: a clinical overview.
Translational Paediatrics. 9 (1), 125-135.
- Peng, L. et al. (2013). Combined Use of sEMG and Accelerometer in Hand Motion Classification Considering Forearm Rotation. [Online]. ieeexplore.ieee.org. Last Updated: 7th July 2013.
Available at: <https://ieeexplore.ieee.org/stamp/stamp.jsp?tp=&arnumber=6610478> [Accessed 11 September 2023].
- Peng, Y. et al. (2018). Nanoporous polyethylene microfibrils for large-scale radiative cooling fabric. Nature Sustainability. 1(2), pp.105-112. [Online].
Available at: https://web.stanford.edu/group/cui_group/papers/Yucan_Cui_NATSUS_2018.pdf [Accessed 3 August 2023].
- Persson, N., Martinez Gil, J. G., Zhong, Y., Maziz, A., Jager, E., (2018), Actuating Textiles: Next Generation of Smart Textiles,
Advanced Materials Technologies, 3(10), 1700397. <https://doi.org/10.1002/admt.201700397>

- Plevig, D. et al. (2008). Neocortical glial cell numbers in human brains. *Neurobiology of Aging*. 29 (11), 1754-1762.
- Poinsett, P. (2020). Cerebral Palsy History.
Available: <https://www.cerebralpalsyguidance.com/cerebral-palsy/research/history/#:~:text=When%20Was%20Cerebral%20Palsy%20Discovered,and%20define%20it%20in%201853>. Last accessed 19th Apr 2022.
- Po-Chun, Hsu Et al. (2017). A dual-mode textile for human body radiative heating and cooling. *Science Advances*. 3 (1), 1-8.
- Proctor, K. (2023). Cerebral palsy prevention. [Online]. www.cerebralpalsyguide.com.
Available at: <https://www.cerebralpalsyguide.com/cerebral-palsy/prognosis/prevention/> [Accessed 23 July 2023].
- Puchwein, P. Et al. (2013). Computer-aided Analysis of Radial Head Morphometry. *Orthopedics* . 36 (1), 51-57.
- Puiu, T. (2017). Muscle-like fabric could turn regular clothes into 'Superman suits'.
Available: <https://www.zmescience.com/science/news-science/artificial-muscle-fabric/>. Last accessed 18th May 2022.
- Purves D, Augustine GJ, Fitzpatrick D, et al., editors. *Neuroscience*. 2nd edition. Sunderland (MA): Sinauer Associates; 2001. Phototransduction.
Available from: <https://www.ncbi.nlm.nih.gov/books/NBK10806/>
- raspberrypi.org. (2022). What you will make.
Available: <https://projects.raspberrypi.org/en/projects/raspberry-pi-getting-started>. Last accessed 11th May 2022.
- Rewalk.com. (2022). What is the ReWalk Exoskeleton?
Available: <https://rewalk.com/>. Last accessed 23rd May 2022.
- Robinson, N. (2021). History of origami.
Available: <https://www.britannica.com/art/origami/History-of-origami>. Last accessed 18th May 2022
- Rogers, C.A., 1989. US Army Research Office Workshop on Smart Materials, Structures and Mathematical Issues Held in Blacksburg, Virginia on 15-16 September 1988.
Virginia Polytechnic Institute and State University, Blacksburg.
- Sault, B. (2018). Scientific guide to understanding thermoelectric generators and teg products for converting heat to teg power!
Available: <https://www.tegmart.com/info/guide-to-understanding-and-using-teg-power-and-products/>. Last accessed 27th Mar 2022.

- Saxton A, Tariq MA, Bordoni B. Anatomy, Thorax, Cardiac Muscle. [Updated 2021 Aug 11].
In: StatPearls [Internet]. Treasure Island (FL): StatPearls Publishing; 2022 Jan-
Available from: <https://www.ncbi.nlm.nih.gov/books/NBK535355/>
- Seladi-Schulman, J. (2020). How Many Muscles Are in the Human Body?
Available: <https://www.healthline.com/health/how-many-muscles-are-in-the-human-body>. Last
accessed 21st Apr 2022.
- Shariff, G. (1953). Cell counts in the primate cerebral cortex.
The Journal of Comparative Neurology. 98 (3), 381-400.
- Shellabear, M. and Nyrhilä, O. (2016). ASME Historic Mechanical Engineering Landmark.
The American Society of Mechanical Engineers. 1 (1), 1-19.
- Shuguang, L. Et al. (2017). Fluid-driven origami-inspired artificial muscles.
PNAS. 114 (50), 13132-13137.
- Siemens. (2020). LOGO! System Manual. [Online]. Pages 14 -14.
Available at: <https://assets.new.siemens.com/siemens/assets/api/uuid:557e34c1-4111-4625-921a-0717d0053571/Manual-LOGO-2020.pdf> [Accessed 31 July 2023].
- Singh, D. Et al. (2019). Experimental assessment of biomechanical properties in human male
elbow bone subjected to bending and compression loads.
The Journal of Applied Biomaterials & Functional Materials (JABFM). 17 (2), 1-13.
- Snyder, G., Toberer, E. Complex thermoelectric materials.
Nature Mater 7, 105–114 (2008). <https://doi.org/10.1038/nmat2090>
- Sofge, E. (2010). A History of Iron Men: Science Fiction's 5 Most Iconic Exoskeletons.
Available: <https://www.popularmechanics.com/culture/movies/a5523/scifi-most-iconic-exoskeletons/#:~:text=The%20exoskeleton%20appears%20to%20have,wearing%20suits%20of%20powered%20armor>. Last accessed 19th Apr 2022.
- Stanley, J. (2021). The History of Smart Home Technology.
Available: <https://www.familyhandyman.com/article/the-history-of-smart-home-technology/>.
Last accessed 12th May 2022.
- Stuart, J. (2019). BICEPS - Standing Dumbbell Biceps Hammer Curls. [Online].
Available at: <http://www.jasestuart.com/standing-dumbbell-biceps-hammer-curls> [Accessed 2
August 2022].
- Stuart, M. A. C., Huck, W. T., Genzer, J., Müller, M., Ober, C., Stamm, M., et al. (2010). Emerging
applications of stimuli-responsive polymer materials.
Nat. Mater. 9:101. doi: 10.1038/nmat2614
- Swisstech (2016). Engineers Reference Book. 2nd ed. UK: Cromwell Group. 82-83.
- Tam, T and Bhatnagar, A. (2016). 1 - High-performance ballistic fibers and tapes.
Lightweight Ballistic Composites (Second Edition). 2 (1), 1-39.

- Tausif, M. Et al. (2018). Yarn and thread manufacturing methods for high-performance apparel. *High-Performance Apparel*. 1 (3), 33-73.
- Team Asana. (2021). How to create a design brief in 7 steps.
Available: <https://asana.com/resources/design-brief>. Last accessed 26th May 2022.
- Teotia, AK. Et al. (2015). Thermo-responsive polymers: structure and design of smart materials. In: Zhang, Z *Switchable and Responsive Surfaces and Materials for Biomedical Applications*. UK: Elsevier. 3-43.
- Thevenot, J. Et al. (2013). Magnetic responsive polymer composite materials. *Chemical Society Reviews*. 42 (1), 7099-7116.
- The American Psychological Association. (2021). Sensory Input.
Available: <https://dictionary.apa.org/sensory-input>. Last accessed 20th May 2022.
- The PiHut. (2023). ADXL335 - 5V ready triple-axis accelerometer (+-3g analog out). [Online]. thepihut.com. Last Updated: 2023.
Available at: <https://thepihut.com/products/adafruit-adxl335-5v-ready-triple-axis-accelerometer-3g-analog-out?vari> [Accessed 28 August 2023].
- The PiHut. (2023). Raspberry Pi 4 Model B. [Online]. thepihut.com. Last Updated: 2023.
Available at: <https://thepihut.com/products/raspberry-pi-4-model-b?variant=20064052674622&src=raspberrypi> [Accessed 28 August 2023].
- theplantbot.com. (2019). Thermoelectric cooling: peltier modules.
Available: <https://theplantbot.com/introduction-to-peltier-cooling/>. Last accessed 24th May 2022.
- The World Health Organisation. (2018). Assistive technology.
Available: <https://www.who.int/news-room/fact-sheets/detail/assistive-technology>. Last accessed 25th May 2022.
- TME. (2020). How does an accelerometer work and what is it used for?
Available: <https://www.tme.eu/en/news/library-articles/page/22568/how-does-an-accelerometer-work-and-what-is-it-used-for/>. Last accessed 12th May 2022.
- Toshiba (2022). What happens if a P-type semiconductor contacts an N-type?
Available: https://toshiba.semicon-storage.com/eu/semiconductor/knowledge/faq/common_common/what-happens-if-a-p-type-semiconductor-contacts-an-n-type.html. Last accessed 27th Mar 2022.
- Ullian, E. Et al. (2001). Control of Synapse Number by Glia. *Science*. 291 (5504), 657-661
- University College London (2021). Shape Memory Alloy.
Available: <https://www.instituteofmaking.org.uk/materials-library/material/shape-memory-alloy>. Last accessed 10 Jan 2021.

Venkatanarayanan, A and Spain, E. (2014). 13.03 - Review of Recent Developments in Sensing Materials.

In *Comprehensive Materials Processing*. 14th ed. London: Elsevier. 47-101.

Vogt, M. (2019). Passive vs. Active Smart Textiles.

Available: <https://www.loomia.com/blog/passive-vs-active-smart-textiles>. Last accessed 22nd Feb 2022.

Warner, S. (2016). What is the Superhero Series?. [Online]. superheroseries.co.uk.

Available at: <https://superheroseries.co.uk/about> [Accessed 23 July 2023].

Webb, R C. (2003). SMOOTH MUSCLE CONTR. ADVANCES IN PHYSIOLOGY EDUCATION. 27(4), pp.201-206. [Online].

Available at: <https://journals.physiology.org/doi/epdf/10.1152/advan.00025.2003> [Accessed 23 August 2023].

Wegner, D and Wheatley, T. (54). Apparent Mental Causation. *American Psychologist*. 1999 (7), 480-492.

Wernhuar, T. Chia-Hwei, L. Hsin-Hun, L. (2011). Applications of Wireless Sensor Networks in Fall Detection for Senior People.

International Journal of Computer Science and Information Technology. 4 (4), 79-95.

Whitwam, R. (2021). Boston Dynamics Atlas Robot Ups Its Parkour Game.

Available: <https://www.extremetech.com/extreme/325911-boston-dynamics-atlas-robot-ups-its-parkour-game>. Last accessed 31st May 2022.

Williams N (2018). *Occupational Medicine*, Volume 68, Issue 8, November 2018, Pages 559–561, <https://doi.org/10.1093/occmed/kqy116>

Williams, R and Herrup, K. (1988). The control of neuron number.

Annual Review of Neuroscience. 11 (0), 423-453.

Wilson, P and Teverovsky, J. (2012). experiences from the forefront of a new industry.

New Product Development in Textiles Innovation and Production. 1 (9), 156-174.

Woodruff, A. (2019). What is a neuron?

Available: <https://qbi.uq.edu.au/brain/brain-anatomy/what-neuron>. Last accessed 22nd Apr 2022.

Wu, Q and Hu, J (2018). *Bringing Thermoelectricity into Reality*. London: Intechopen. 386.

www.engineeredarts.co.uk. (2022). RoboThespian.

Available: <https://www.engineeredarts.co.uk/robot/robotthespian/>. Last accessed 24th May 2022.

www.healthcarepro.co.uk. (2022). Products.

Available: <https://www.healthcarepro.co.uk/search?query=four+wheel+walker&queryFromSuggest=true&userInput=four+wheel>. Last accessed 27th May 2022.

- www.mndassociation.org. (2022). What is MND?
Available: <https://www.mndassociation.org/about-mnd/what-is-mnd/>. Last accessed 18th May 2022.
- www.ptdirect.com. (2022). The Physiology of Skeletal Muscle Contraction.
Available: <https://www.ptdirect.com/training-design/anatomy-and-physiology/skeletal-muscle-the-physiology-of-contraction>. Last accessed 18th May 2022
- www.scope.org.uk. (2022). Cerebral palsy (CP).
Available: <https://www.scope.org.uk/advice-and-support/cerebral-palsy-introduction/>. Last accessed 23rd May 2022.
- www.scope.org.uk. (2022). Disability facts and figures.
Available: <https://www.scope.org.uk/media/disability-facts-figures/#:~:text=There%20are%2014.6%20million%20disabled%20people%20in%20the%20UK>. Last accessed 27th May 2022.
- Xiong, X. Et al. (2019). Chapter 4 - Photo responsive Polymers.
In Smart Polymers, and their Applications (Second Edition). UK: Elsevier. 87-153.
- Yeung, A. (2022). 10 Best Bicep Curl Variations To Build Muscle.
Available: <https://www.mensjournal.com/health-fitness/10-different-ways-do-curl/>. Last accessed 26 Apr 2022.
- Yixue, D. Gongchuan, Y. Kaien, S. Zhe, Z. Xiaoqiao, L. Linfeng, L. Hui, T. Bin, X. Liang, H. (2021).
Advances in wearable textile-based micro energy storage devices: structuring, application, and perspective.
Royal Society of Chemistry. 3 (3), 6271-6293.
- Yong-Lai, Z. Et al. (2021). Electro-responsive actuators based on graphene.
The Innovation. 2 (4), 1-17.
- Zeleny, E. (2011). Tower Crane.
Available: <https://demonstrations.wolfram.com/TowerCrane/>. Last accessed 17th Jul 2022.
- Zhang, J. (2019). Basic Neural Units of the Brain: Neurons, Synapses and Action Potentia. arXiv: Neurons and Cognition. 1 (1), 2-38.
- Zhang, Z. (2019). Developments in 4D-printing: a review on current smart materials, technologies, and applications.
International Journal of Smart and Nano Materials. 10 (10), 1-20.
- Zhaodi, T. Et al. (2022). Advanced multifunctional composite phase change materials based on photo-responsive materials.
Nano Energy. 80 (N/A), 1 - 21.

Sault, B. (2018). Scientific guide to understanding thermoelectric generators and teg products for converting heat to teg power!

Available: <https://www.tegmart.com/info/guide-to-understanding-and-using-teg-power-and-products/>. Last accessed 27th Mar 2022.

7. Appendix A

BENDING MOMENTS

$$M = WL$$

R1 $M = -215 \times 0.460 = -98.900 \text{ N/m}$
R2 $M = -215 \times 0.345 = -74.275 \text{ N/m}$
R3 $M = -215 \times 0.230 = -49.450 \text{ N/m}$
R4 $M = -215 \times 0.115 = -24.725 \text{ N/m}$

INERTIA

$$I_{NA} = \frac{J D^4}{64}$$
$$I_{NA} = \frac{J \times (0.018626^4)}{64}$$
$$I_{NA} = \frac{J \times 0.00000012}{64}$$
$$I_{NA} = \frac{3.7811 \times 10^{-7}}{64}$$
$$I_{NA} = \underline{5.9081 \times 10^{-9} \text{ M}^4}$$

Appendix A Figure 7-1. Hand Calculations for Bending Moments and Inertia

DEFLECTION

$$\delta = \frac{WL^3}{3EI}$$

$$E = 4.5 + 3.67 = 8.17 \text{ GPa}$$

$$I = 5.9081 \times 10^{-9} \text{ M}^4$$

$$R1. \quad \delta = \frac{-215 \times (0.460^3)}{3 \times 8.17 \times 10^9 \times 5.9081 \times 10^{-9}}$$

$$\delta = \frac{-215 \times 0.097336}{144.8}$$

$$\delta = \frac{-20.92724}{144.8}$$

$$\delta = \underline{\underline{-0.144 \text{ m}}}$$

$$R2. \quad \delta = \frac{-215 \times (0.345^3)}{3 \times 8.17 \times 10^9 \times 5.9081 \times 10^{-9}}$$

$$\delta = \frac{-215 \times 0.041063625}{144.8}$$

$$\delta = \frac{-8.828679375}{144.8}$$

$$\delta = \underline{\underline{-0.060 \text{ m}}}$$

Appendix A Figure 7-2. Hand Calculations for Deflection at Points R1 and R2

$$\begin{aligned}
 R3. \quad \delta &= \frac{-215 \times (0.230^3)}{3 \times 8.17 \times 10^9 \times 5.9081 \times 10^{-9}} \\
 \delta &= \frac{-215 \times 0.012167}{144.8} \\
 \delta &= \frac{-2.615905}{144.8} \\
 \delta &= \underline{\underline{-0.0180 \text{ M}}} \\
 \\
 R4. \quad \delta &= \frac{-215 \times (0.115^3)}{3 \times 8.17 \times 10^9 \times 5.9081 \times 10^{-9}} \\
 \delta &= \frac{-215 \times 0.001520875}{144.8} \\
 \delta &= \frac{-0.326988125}{144.8} \\
 \delta &= \underline{\underline{-2.2582 \text{ M}}}
 \end{aligned}$$

Appendix A Figure 7-3. Hand Calculations for Deflection at points R3 and R4

Input Values	
Span length, L	0.46 m ▾
Point load, P	-215 N ▾
Modulus of Elasticity, E	8.17 GPa ▾
Moment of Inertia, Ix	0.00000000590811 m⁴ ▾
Stiffness of the beam, Elx	48.27 Nm² ▾
Output value	
Maximum deflection, δ_{max}	-0.14452 m ▾

Appendix A Figure 7-4. Deflection Calculation at R1 checked via Omnicalculator.com

Input Values	
Span length, L	0.345 m ▾
Point load, P	-215 N ▾
Modulus of Elasticity, E	8.17 GPa ▾
Moment of Inertia, Ix	0.00000000590811 m⁴ ▾
Stiffness of the beam, Elx	48.27 Nm² ▾
Output value	
Maximum deflection, δ_{max}	-0.06097 m ▾

Appendix A Figure 7-5. Deflection Calculation at R2 checked via Omnicalculator.com

Input Values	
Span length, L	0.230 m ▾
Point load, P	-215 N ▾
Modulus of Elasticity, E	8.17 GPa ▾
Moment of Inertia, I _x	0.00000000590811 m⁴ ▾
Stiffness of the beam, E I _x	48.27 Nm² ▾
Output value	
Maximum deflection, δ _{max}	-0.01806 m ▾

Appendix A Figure 7-6. Deflection Calculation at R3 checked via Omnicalculator.com.

Input Values	
Span length, L	0.115 m ▾
Point load, P	-215 N ▾
Modulus of Elasticity, E	8.17 GPa ▾
Moment of Inertia, I _x	0.00000000590811 m⁴ ▾
Stiffness of the beam, E I _x	48.27 Nm² ▾
Output value	
Maximum deflection, δ _{max}	-0.00226 m ▾

Appendix A Figure 7-7. Deflection Calculation at R4 checked via Omnicalculator.com

8. Appendix B

BLOOD OXYGEN TEST DATA CAPTURE SHEET									
Participant No.:		1	Date:		26 APR 22	Age Range:			0-15, 16-24, <u>25-34</u> , 35-44, 45-54, 55-64, 65-74, 75-84, 85+
Heart Rate at Rest (BPM):				86	Blood Oxygen Level at Rest (SpO2):				95% - 97%
Exercise	Muscle Actuated	Mass (Kg)	Set No.	Rep QTY	Start Heart Rate (BPM)	Finish Heart Rate (BPM)	Start Blood Oxygen Level (SpO2)	Finish Blood Oxygen Level (SpO2)	
BARBELL CHEST PRESS	PECTORALIS MAJOR / MINOR	40	1	10	103	106	97	97	
"	"	50	2	6	106	106	97	97	
"	"	60	3	6	106	106	97	97	
CHEST PRESS MACHINE	PECTORALIS MAJOR / MINOR	45	1	10	101	106	97	98	
"	"	59	2	10	106	111	98	98	
"	"	66	3	6	111	110	98	98	
INCLINE DUMBBELL FLYE	PECTORALIS MAJOR / MINOR	12.5	1	10	131	137	97	97	
"	"	15	2	10	137	144	97	96	
"	"	17.5	3	10	144	149	96	98	
MACHINE CHEST FLYE	PECTORALIS MAJOR / MINOR	73	1	10	148	135	98	97	
"	"	79	2	8	135	143	97	97	
"	"	86	3	6	143	134	97	98	

Appendix B Figure 8-1. Blood Oxygen Test Data Capture Sheet (Page 1)

BLOOD OXYGEN TEST DATA CAPTURE SHEET									
Participant No.:		1	Date:		26 APR 22	Age Range:			0-15, 16-24, <u>25-34</u> , 35-44, 45-54, 55-64, 65-74, 75-84, 85+
Heart Rate at Rest (BPM):				N/A	Blood Oxygen Level at Rest (SpO2):				95% - N/A
Exercise	Muscle Actuated	Mass (Kg)	Set No.	Rep QTY	Start Heart Rate (BPM)	Finish Heart Rate (BPM)	Start Blood Oxygen Level (SpO2)	Finish Blood Oxygen Level (SpO2)	
DUMBBELL BICEP CURL	BICEP	20	1	6	115	141	97	98	
"	"	20	2	6	141	131	98	97	
"	"								
DUMBBELL HAMMER CURL	BICEP	20	1	6	131	153	97	97	
"	"	20	2	6	153	160	97	98	
"	"								
BARBELL PREACHER CURL	BICEP	25	1	4	116	151	97	97	
"	"	20	2	6	151	143	97	98	
"	"	20	3	6	143	135	98	98	

Appendix B Figure 8-2. Blood Oxygen Test Data Capture Sheet (Page 2)

9. Appendix C



Small, Low Power, 3-Axis $\pm 3 g$ Accelerometer

ADXL335

FEATURES

3-axis sensing
Small, low profile package
 4 mm \times 4 mm \times 1.45 mm LFCSP
Low power : 350 μ A (typical)
Single-supply operation: 1.8 V to 3.6 V
10,000 g shock survival
Excellent temperature stability
BW adjustment with a single capacitor per axis
RoHS/WEEE lead-free compliant

APPLICATIONS

Cost sensitive, low power, motion- and tilt-sensing applications
Mobile devices
Gaming systems
Disk drive protection
Image stabilization
Sports and health devices

GENERAL DESCRIPTION

The ADXL335 is a small, thin, low power, complete 3-axis accelerometer with signal conditioned voltage outputs. The product measures acceleration with a minimum full-scale range of $\pm 3 g$. It can measure the static acceleration of gravity in tilt-sensing applications, as well as dynamic acceleration resulting from motion, shock, or vibration.

The user selects the bandwidth of the accelerometer using the C_x , C_y , and C_z capacitors at the X_{OUT} , Y_{OUT} , and Z_{OUT} pins. Bandwidths can be selected to suit the application, with a range of 0.5 Hz to 1600 Hz for the X and Y axes, and a range of 0.5 Hz to 550 Hz for the Z axis.

The ADXL335 is available in a small, low profile, 4 mm \times 4 mm \times 1.45 mm, 16-lead, plastic lead frame chip scale package (LFCSP_LQ).

FUNCTIONAL BLOCK DIAGRAM

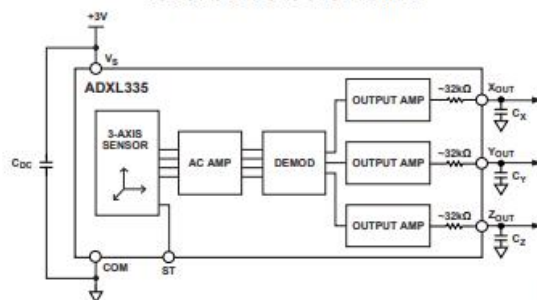


Figure 1.

Rev. B

Information furnished by Analog Devices is believed to be accurate and reliable. However, no responsibility is assumed by Analog Devices for its use, nor for any infringements of patents or other rights of third parties that may result from its use. Specifications subject to change without notice. No license is granted by implication or otherwise under any patent or patent rights of Analog Devices. Trademarks and registered trademarks are the property of their respective owners.

One Technology Way, P.O. Box 9106, Norwood, MA 02062-9106, U.S.A.
 Tel: 781.329.4700 www.analog.com
 Fax: 781.461.3113 ©2009–2010 Analog Devices, Inc. All rights reserved.

ADXL335

TABLE OF CONTENTS

Features	1	Performance	10
Applications.....	1	Applications Information	11
General Description	1	Power Supply Decoupling	11
Functional Block Diagram	1	Setting the Bandwidth Using C_x , C_y , and C_z	11
Revision History	2	Self-Test	11
Specifications.....	3	Design Trade-Offs for Selecting Filter Characteristics: The Noise/BW Trade-Off.....	11
Absolute Maximum Ratings.....	4	Use with Operating Voltages Other Than 3 V	12
ESD Caution.....	4	Axes of Acceleration Sensitivity	12
Pin Configuration and Function Descriptions.....	5	Layout and Design Recommendations	13
Typical Performance Characteristics	6	Outline Dimensions.....	14
Theory of Operation	10	Ordering Guide	14
Mechanical Sensor.....	10		

REVISION HISTORY

1/10—Rev. A to Rev. B	
Changes to Figure 21.....	9
7/09—Rev. 0 to Rev. A	
Changes to Figure 22.....	9
Changes to Outline Dimensions.....	14
1/09—Revision 0: Initial Version	

SPECIFICATIONS

$T_A = 25^\circ\text{C}$, $V_S = 3\text{ V}$, $C_X = C_Y = C_Z = 0.1\ \mu\text{F}$, acceleration = 0 g, unless otherwise noted. All minimum and maximum specifications are guaranteed. Typical specifications are not guaranteed.

Table 1.

Parameter	Conditions	Min	Typ	Max	Unit
SENSOR INPUT					
Measurement Range	Each axis	± 3	± 3.6		g
Nonlinearity	% of full scale		± 0.3		%
Package Alignment Error			± 1		Degrees
Interaxis Alignment Error			± 0.1		Degrees
Cross-Axis Sensitivity ¹			± 1		%
SENSITIVITY (RATIOMETRIC)²					
Sensitivity at X_{out} , Y_{out} , Z_{out}	Each axis $V_S = 3\text{ V}$	270	300	330	mV/g
Sensitivity Change Due to Temperature ³	$V_S = 3\text{ V}$		± 0.01		%/°C
ZERO g BIAS LEVEL (RATIOMETRIC)					
0 g Voltage at X_{out} , Y_{out}	$V_S = 3\text{ V}$	1.35	1.5	1.65	V
0 g Voltage at Z_{out}	$V_S = 3\text{ V}$	1.2	1.5	1.8	V
0 g Offset vs. Temperature			± 1		mg/°C
NOISE PERFORMANCE					
Noise Density X_{out} , Y_{out}			150		$\mu\text{g}/\sqrt{\text{Hz}}$ rms
Noise Density Z_{out}			300		$\mu\text{g}/\sqrt{\text{Hz}}$ rms
FREQUENCY RESPONSE⁴					
Bandwidth X_{out} , Y_{out} ⁵	No external filter		1600		Hz
Bandwidth Z_{out} ⁵	No external filter		550		Hz
R_{FLT} Tolerance			$32 \pm 15\%$		k Ω
Sensor Resonant Frequency			5.5		kHz
SELF-TEST⁶					
Logic Input Low			+0.6		V
Logic Input High			+2.4		V
ST Actuation Current			+60		μA
Output Change at X_{out}	Self-Test 0 to Self-Test 1	-150	-325	-600	mV
Output Change at Y_{out}	Self-Test 0 to Self-Test 1	+150	+325	+600	mV
Output Change at Z_{out}	Self-Test 0 to Self-Test 1	+150	+550	+1000	mV
OUTPUT AMPLIFIER					
Output Swing Low	No load		0.1		V
Output Swing High	No load		2.8		V
POWER SUPPLY					
Operating Voltage Range		1.8		3.6	V
Supply Current	$V_S = 3\text{ V}$		350		μA
Turn-On Time ⁷	No external filter		1		ms
TEMPERATURE					
Operating Temperature Range		-40		+85	°C

¹ Defined as coupling between any two axes.

² Sensitivity is essentially ratiometric to V_S .

³ Defined as the output change from ambient-to-maximum temperature or ambient-to-minimum temperature.

⁴ Actual frequency response controlled by user-supplied external filter capacitors (C_X , C_Y , C_Z).

⁵ Bandwidth with external capacitors = $1/(2 \times \pi \times 32\text{ k}\Omega \times C)$. For C_X , $C_Y = 0.003\ \mu\text{F}$, bandwidth = 1.6 kHz. For $C_Z = 0.01\ \mu\text{F}$, bandwidth = 500 Hz. For C_X , $C_Y = 10\ \mu\text{F}$,

bandwidth = 0.5 Hz.

⁶ Self-test response changes cubically with V_S .

⁷ Turn-on time is dependent on C_X , C_Y , C_Z and is approximately $160 \times C_X$ or C_Y or $C_Z + 1\text{ ms}$, where C_X , C_Y , C_Z are in microfarads (μF).

ADXL335

ABSOLUTE MAXIMUM RATINGS

Table 2.

Parameter	Rating
Acceleration (Any Axis, Unpowered)	10,000 g
Acceleration (Any Axis, Powered)	10,000 g
V _s	-0.3 V to +3.6 V
All Other Pins	(COM - 0.3 V) to (V _s + 0.3 V)
Output Short-Circuit Duration (Any Pin to Common)	Indefinite
Temperature Range (Powered)	-55°C to +125°C
Temperature Range (Storage)	-65°C to +150°C

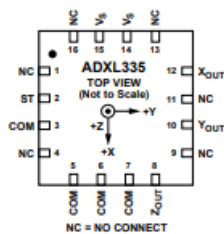
Stresses above those listed under Absolute Maximum Ratings may cause permanent damage to the device. This is a stress rating only; functional operation of the device at these or any other conditions above those indicated in the operational section of this specification is not implied. Exposure to absolute maximum rating conditions for extended periods may affect device reliability.

ESD CAUTION



ESD (electrostatic discharge) sensitive device. Charged devices and circuit boards can discharge without detection. Although this product features patented or proprietary protection circuitry, damage may occur on devices subjected to high energy ESD. Therefore, proper ESD precautions should be taken to avoid performance degradation or loss of functionality.

PIN CONFIGURATION AND FUNCTION DESCRIPTIONS



NOTES
 1. EXPOSED PAD IS NOT INTERNALLY CONNECTED BUT SHOULD BE SOLDERED FOR MECHANICAL INTEGRITY.

Figure 2. Pin Configuration

Table 3. Pin Function Descriptions

Pin No.	Mnemonic	Description
1	NC	No Connect. ¹
2	ST	Self-Test.
3	COM	Common.
4	NC	No Connect. ¹
5	COM	Common.
6	COM	Common.
7	COM	Common.
8	Z _{OUT}	Z Channel Output.
9	NC	No Connect. ¹
10	Y _{OUT}	Y Channel Output.
11	NC	No Connect. ¹
12	X _{OUT}	X Channel Output.
13	NC	No Connect. ¹
14	V _S	Supply Voltage (1.8 V to 3.6 V).
15	V _S	Supply Voltage (1.8 V to 3.6 V).
16	NC	No Connect. ¹
EP	Exposed Pad	Not internally connected. Solder for mechanical integrity.

¹ NC pins are not internally connected and can be tied to COM pins, unless otherwise noted.

ADXL335

TYPICAL PERFORMANCE CHARACTERISTICS

N > 1000 for all typical performance plots, unless otherwise noted.

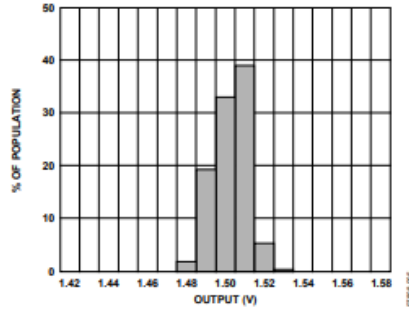


Figure 3. X-Axis Zero g Bias at 25°C, $V_S = 3 V$

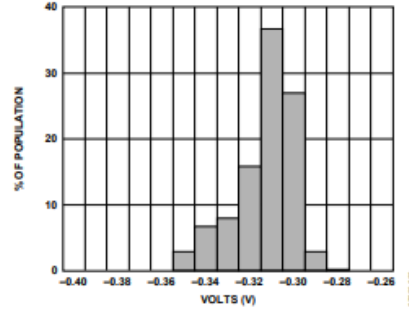


Figure 6. X-Axis Self-Test Response at 25°C, $V_S = 3 V$

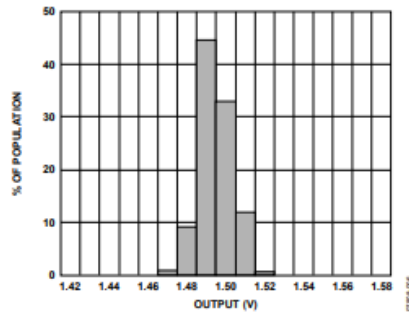


Figure 4. Y-Axis Zero g Bias at 25°C, $V_S = 3 V$

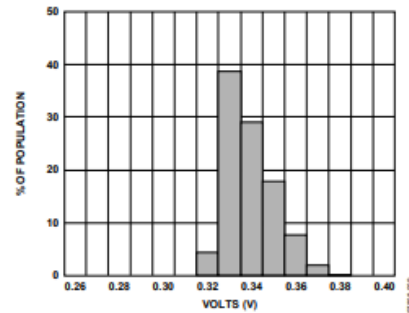


Figure 7. Y-Axis Self-Test Response at 25°C, $V_S = 3 V$

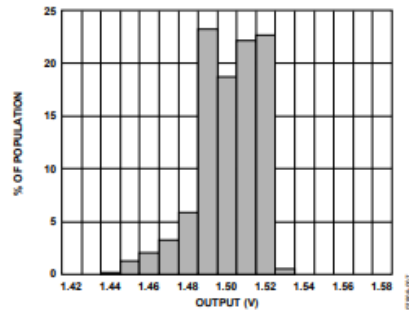


Figure 5. Z-Axis Zero g Bias at 25°C, $V_S = 3 V$

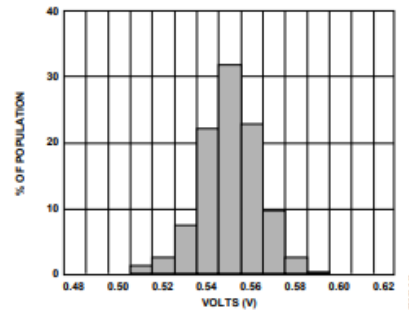


Figure 8. Z-Axis Self-Test Response at 25°C, $V_S = 3 V$

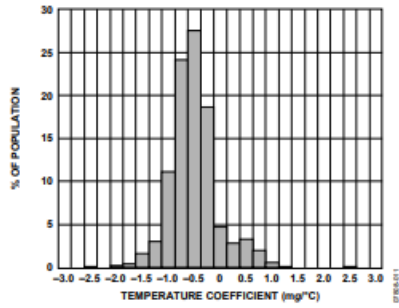


Figure 9. X-Axis Zero g Bias Temperature Coefficient, $V_s = 3\text{ V}$

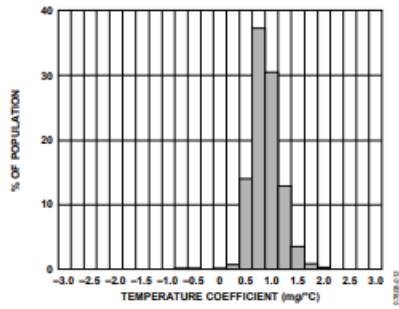


Figure 10. Y-Axis Zero g Bias Temperature Coefficient, $V_s = 3\text{ V}$

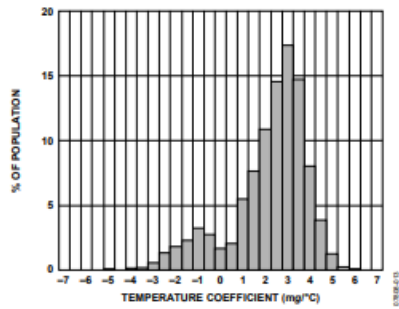


Figure 11. Z-Axis Zero g Bias Temperature Coefficient, $V_s = 3\text{ V}$

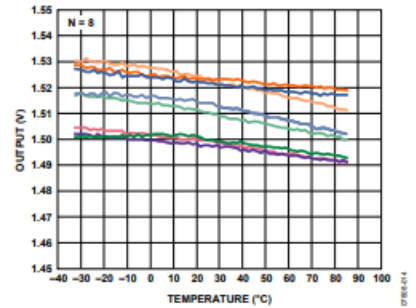


Figure 12. X-Axis Zero g Bias vs. Temperature—Eight Parts Soldered to PCB

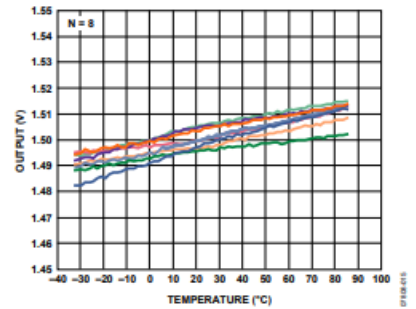


Figure 13. Y-Axis Zero g Bias vs. Temperature—Eight Parts Soldered to PCB

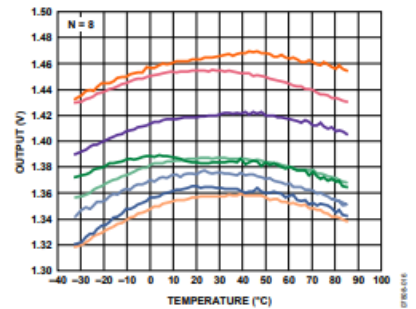


Figure 14. Z-Axis Zero g Bias vs. Temperature—Eight Parts Soldered to PCB

ADXL335

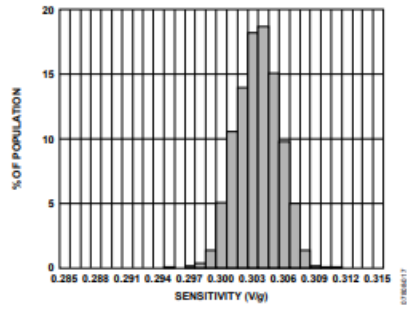


Figure 15. X-Axis Sensitivity at 25°C, $V_s = 3\text{ V}$

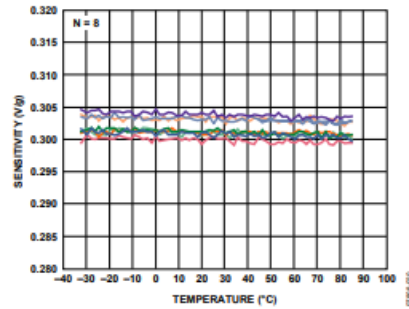


Figure 18. X-Axis Sensitivity vs. Temperature—
Eight Parts Soldered to PCB, $V_s = 3\text{ V}$

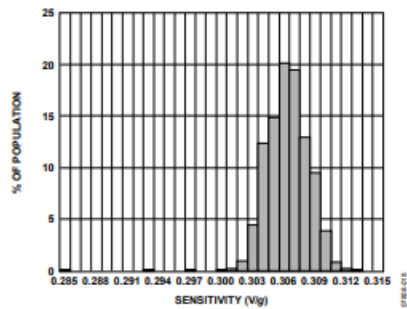


Figure 16. Y-Axis Sensitivity at 25°C, $V_s = 3\text{ V}$

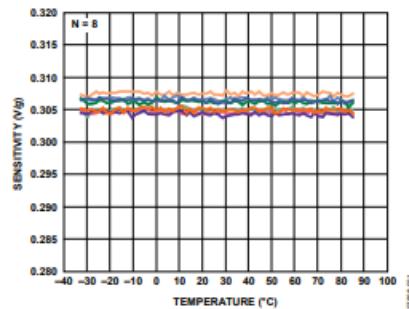


Figure 19. Y-Axis Sensitivity vs. Temperature—
Eight Parts Soldered to PCB, $V_s = 3\text{ V}$

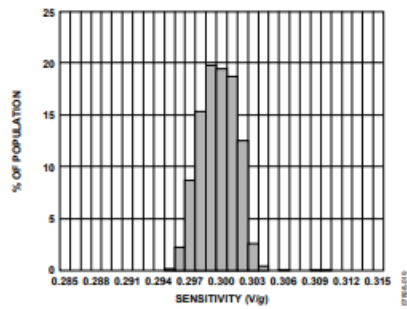


Figure 17. Z-Axis Sensitivity at 25°C, $V_s = 3\text{ V}$

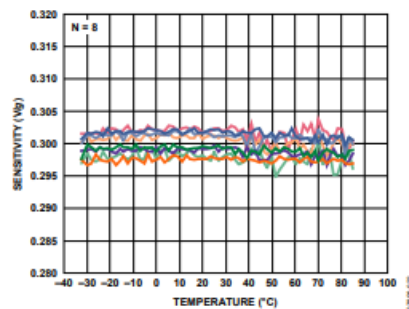


Figure 20. Z-Axis Sensitivity vs. Temperature—
Eight Parts Soldered to PCB, $V_s = 3\text{ V}$

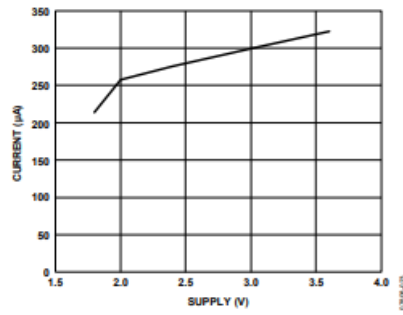


Figure 21. Typical Current Consumption vs. Supply Voltage

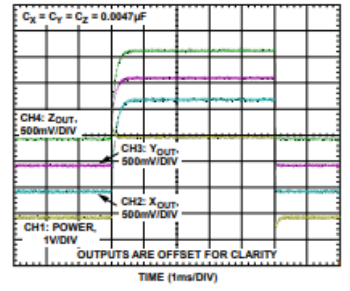


Figure 22. Typical Turn-On Time, $V_S = 3V$

ADXL335

THEORY OF OPERATION

The ADXL335 is a complete 3-axis acceleration measurement system. The ADXL335 has a measurement range of $\pm 3 g$ minimum. It contains a polysilicon surface-micromachined sensor and signal conditioning circuitry to implement an open-loop acceleration measurement architecture. The output signals are analog voltages that are proportional to acceleration. The accelerometer can measure the static acceleration of gravity in tilt-sensing applications as well as dynamic acceleration resulting from motion, shock, or vibration.

The sensor is a polysilicon surface-micromachined structure built on top of a silicon wafer. Polysilicon springs suspend the structure over the surface of the wafer and provide a resistance against acceleration forces. Deflection of the structure is measured using a differential capacitor that consists of independent fixed plates and plates attached to the moving mass. The fixed plates are driven by 180° out-of-phase square waves. Acceleration deflects the moving mass and unbalances the differential capacitor resulting in a sensor output whose amplitude is proportional to acceleration. Phase-sensitive demodulation techniques are then used to determine the magnitude and direction of the acceleration.

The demodulator output is amplified and brought off-chip through a $32 k\Omega$ resistor. The user then sets the signal bandwidth of the device by adding a capacitor. This filtering improves measurement resolution and helps prevent aliasing.

MECHANICAL SENSOR

The ADXL335 uses a single structure for sensing the X, Y, and Z axes. As a result, the three axes' sense directions are highly orthogonal and have little cross-axis sensitivity. Mechanical misalignment of the sensor die to the package is the chief source of cross-axis sensitivity. Mechanical misalignment can, of course, be calibrated out at the system level.

PERFORMANCE

Rather than using additional temperature compensation circuitry, innovative design techniques ensure that high performance is built in to the ADXL335. As a result, there is no quantization error or nonmonotonic behavior, and temperature hysteresis is very low (typically less than $3 mg$ over the $-25^\circ C$ to $+70^\circ C$ temperature range).

APPLICATIONS INFORMATION

POWER SUPPLY DECOUPLING

For most applications, a single 0.1 μF capacitor, C_{DC}, placed close to the ADXL335 supply pins adequately decouples the accelerometer from noise on the power supply. However, in applications where noise is present at the 50 kHz internal clock frequency (or any harmonic thereof), additional care in power supply bypassing is required because this noise can cause errors in acceleration measurement.

If additional decoupling is needed, a 100 Ω (or smaller) resistor or ferrite bead can be inserted in the supply line. Additionally, a larger bulk bypass capacitor (1 μF or greater) can be added in parallel to C_{DC}. Ensure that the connection from the ADXL335 ground to the power supply ground is low impedance because noise transmitted through ground has a similar effect to noise transmitted through V_S.

SETTING THE BANDWIDTH USING C_X, C_Y, AND C_Z

The ADXL335 has provisions for band limiting the X_{OUT}, Y_{OUT}, and Z_{OUT} pins. Capacitors must be added at these pins to implement low-pass filtering for antialiasing and noise reduction. The equation for the 3 dB bandwidth is

$$F_{3dB} = 1 / (2\pi(32 \text{ k}\Omega) \times C_{(X, Y, Z)})$$

or more simply

$$F_{3dB} = 5 \mu\text{F} / C_{(X, Y, Z)}$$

The tolerance of the internal resistor (R_{INT}) typically varies as much as ±15% of its nominal value (32 kΩ), and the bandwidth varies accordingly. A minimum capacitance of 0.0047 μF for C_X, C_Y, and C_Z is recommended in all cases.

Table 4. Filter Capacitor Selection, C_X, C_Y, and C_Z

Bandwidth (Hz)	Capacitor (μF)
1	4.7
10	0.47
50	0.10
100	0.05
200	0.027
500	0.01

SELF-TEST

The ST pin controls the self-test feature. When this pin is set to V_S, an electrostatic force is exerted on the accelerometer beam. The resulting movement of the beam allows the user to test if the accelerometer is functional. The typical change in output is -1.08 g (corresponding to -325 mV) in the X-axis, +1.08 g (or +325 mV) on the Y-axis, and +1.83 g (or +550 mV) on the Z-axis. This ST pin can be left open-circuit or connected to common (COM) in normal use.

Never expose the ST pin to voltages greater than V_S + 0.3 V. If this cannot be guaranteed due to the system design (for instance, if there are multiple supply voltages), then a low V_F clamping diode between ST and V_S is recommended.

DESIGN TRADE-OFFS FOR SELECTING FILTER CHARACTERISTICS: THE NOISE/BW TRADE-OFF

The selected accelerometer bandwidth ultimately determines the measurement resolution (smallest detectable acceleration). Filtering can be used to lower the noise floor to improve the resolution of the accelerometer. Resolution is dependent on the analog filter bandwidth at X_{OUT}, Y_{OUT}, and Z_{OUT}.

The output of the ADXL335 has a typical bandwidth of greater than 500 Hz. The user must filter the signal at this point to limit aliasing errors. The analog bandwidth must be no more than half the analog-to-digital sampling frequency to minimize aliasing. The analog bandwidth can be further decreased to reduce noise and improve resolution.

The ADXL335 noise has the characteristics of white Gaussian noise, which contributes equally at all frequencies and is described in terms of μg/√Hz (the noise is proportional to the square root of the accelerometer bandwidth). The user should limit bandwidth to the lowest frequency needed by the application to maximize the resolution and dynamic range of the accelerometer.

With the single-pole, roll-off characteristic, the typical noise of the ADXL335 is determined by

$$rms \text{ Noise} = \text{Noise Density} \times (\sqrt{BW \times 1.6})$$

It is often useful to know the peak value of the noise. Peak-to-peak noise can only be estimated by statistical methods. Table 5 is useful for estimating the probabilities of exceeding various peak values, given the rms value.

Table 5. Estimation of Peak-to-Peak Noise

Peak-to-Peak Value	% of Time That Noise Exceeds Nominal Peak-to-Peak Value
2 × rms	32
4 × rms	4.6
6 × rms	0.27
8 × rms	0.006

ADXL335

USE WITH OPERATING VOLTAGES OTHER THAN 3 V

The ADXL335 is tested and specified at $V_s = 3\text{ V}$; however, it can be powered with V_s as low as 1.8 V or as high as 3.6 V. Note that some performance parameters change as the supply voltage is varied.

The ADXL335 output is ratiometric, therefore, the output sensitivity (or scale factor) varies proportionally to the supply voltage. At $V_s = 3.6\text{ V}$, the output sensitivity is typically 360 mV/g. At $V_s = 2\text{ V}$, the output sensitivity is typically 195 mV/g.

The zero g bias output is also ratiometric, thus the zero g output is nominally equal to $V_s/2$ at all supply voltages.

The output noise is not ratiometric but is absolute in volts; therefore, the noise density decreases as the supply voltage increases. This is because the scale factor (mV/g) increases while the noise voltage remains constant. At $V_s = 3.6\text{ V}$, the X-axis and Y-axis noise density is typically $120\text{ }\mu\text{g}/\sqrt{\text{Hz}}$, whereas at $V_s = 2\text{ V}$, the X-axis and Y-axis noise density is typically $270\text{ }\mu\text{g}/\sqrt{\text{Hz}}$.

Self-test response in g is roughly proportional to the square of the supply voltage. However, when ratiometricity of sensitivity is factored in with supply voltage, the self-test response in volts is roughly proportional to the cube of the supply voltage. For example, at $V_s = 3.6\text{ V}$, the self-test response for the ADXL335 is approximately -560 mV for the X-axis, +560 mV for the Y-axis, and +950 mV for the Z-axis.

At $V_s = 2\text{ V}$, the self-test response is approximately -96 mV for the X-axis, +96 mV for the Y-axis, and -163 mV for the Z-axis.

The supply current decreases as the supply voltage decreases. Typical current consumption at $V_s = 3.6\text{ V}$ is 375 μA , and typical current consumption at $V_s = 2\text{ V}$ is 200 μA .

AXES OF ACCELERATION SENSITIVITY

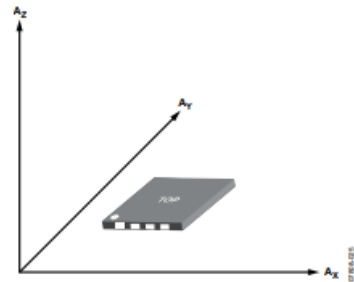


Figure 23. Axes of Acceleration Sensitivity; Corresponding Output Voltage Increases When Accelerated Along the Sensitive Axis.

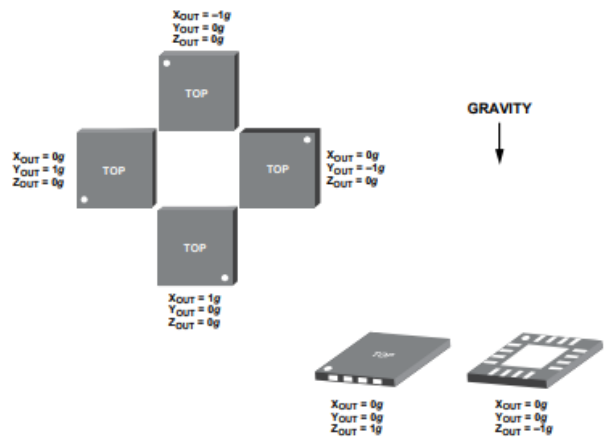


Figure 24. Output Response vs. Orientation to Gravity

LAYOUT AND DESIGN RECOMMENDATIONS

The recommended soldering profile is shown in Figure 25 followed by a description of the profile features in Table 6. The recommended PCB layout or solder land drawing is shown in Figure 26.

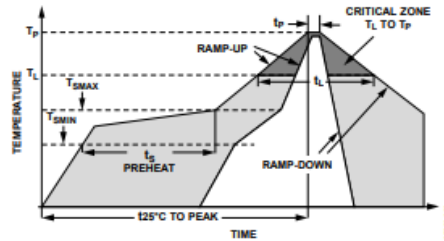


Figure 25. Recommended Soldering Profile

Table 6. Recommended Soldering Profile

Profile Feature	Sn63/Pb37	Pb-Free
Average Ramp Rate (T_L to T_P)	3°C/sec max	3°C/sec max
Preheat		
Minimum Temperature (T_{SMIN})	100°C	150°C
Maximum Temperature (T_{SMAX})	150°C	200°C
Time (T_{SMIN} to T_{SMAX})(t_p)	60 sec to 120 sec	60 sec to 180 sec
T_{SMAX} to T_L		
Ramp-Up Rate	3°C/sec max	3°C/sec max
Time Maintained Above Liquidous (T_L)		
Liquidous Temperature (T_L)	183°C	217°C
Time (t_L)	60 sec to 150 sec	60 sec to 150 sec
Peak Temperature (T_P)	240°C + 0°C/-5°C	260°C + 0°C/-5°C
Time Within 5°C of Actual Peak Temperature (t_p)	10 sec to 30 sec	20 sec to 40 sec
Ramp-Down Rate	6°C/sec max	6°C/sec max
Time 25°C to Peak Temperature	6 minutes max	8 minutes max

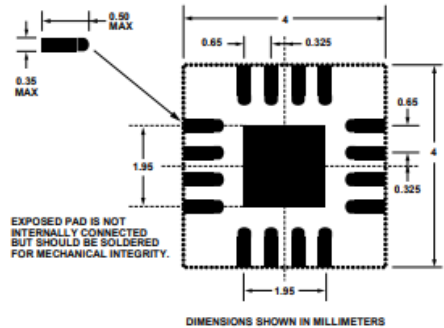
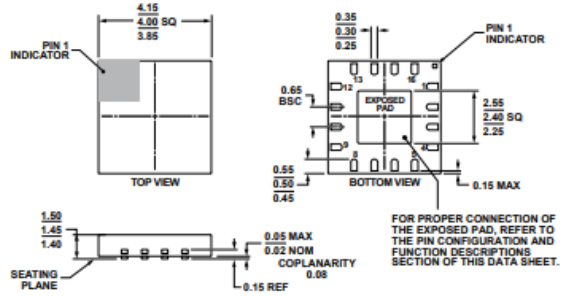


Figure 26. Recommended PCB Layout

ADXL335

OUTLINE DIMENSIONS



COMPLIANT TO JEDEC STANDARDS MO-220-WGGD.

Figure 27. 16-Lead Lead Frame Chip Scale Package [LFCS_P_LQ]
4 mm x 4 mm Body, 1.45 mm Thick Quad
(CP-16-14)
Dimensions shown in millimeters

ORDERING GUIDE

Model ¹	Measurement Range	Specified Voltage	Temperature Range	Package Description	Package Option
ADXL335BCPZ	±3 g	3 V	-40°C to +85°C	16-Lead LFCS_P_LQ	CP-16-14
ADXL335BCPZ-RL	±3 g	3 V	-40°C to +85°C	16-Lead LFCS_P_LQ	CP-16-14
ADXL335BCPZ-RL7	±3 g	3 V	-40°C to +85°C	16-Lead LFCS_P_LQ	CP-16-14
EVAL-ADXL335Z				Evaluation Board	

¹ Z = RoHS Compliant Part.

¹ Pages 15 to 16 are blank within the datasheet